



Dublin City University  
School of Chemical Sciences

# Physical and Chemical Sensing Applications of Polypyrrole-Coated Foams

By

Sarah Patricia Brady  
B.Sc. Analytical Science

A thesis submitted to DCU in part fulfilment for the degree of

**DOCTOR OF PHILOSOPHY**

Supervisor : Professor Dermot Diamond  
School of Chemical Sciences  
Submitted July 2006

## **DECLARATAION**

I hereby certify that this material, which I now submit for assessment on the programme of study leading to the award of Doctor of Philosophy is entirely my own work and has not been taken from the work of others save and to the extent that such work has been cited and acknowledged within the text of my work.

Signed: Gacle Bedy

(Candidate) ID No.: 98001035

Date: 25<sup>th</sup> Sept 2006

## **DEDICATION**

*For my family,  
Philip, Patricia, Bernadette, Philip, Peter & Anthony*

## ACKNOWLEDGEMENTS

Firstly, I would like to thank my supervisor, Prof. Dermot Diamond for his support and guidance over the last number of years, for allowing me the freedom to explore science both at home, abroad (in space and on the telly) and for encouraging me to apply for the IRCSET award all those years ago, without whose financial support I would not have been able to pursue my work, so thank you to the research council too.

Thanks to the chemistry department in DCU (I won't name names, for fear of forgetting someone) for all your friendship and support during my postgrad. Sincere thanks to all the technical staff of the chemistry department in the X-block and the NCSR for all their assistance. I must say a huge thanks to the past and present members of the BEST/ASG/NCSR group, especially to all the Dubs that once resided in SG03, and the luckier ones that weren't and to those in X152 for all the laughs and useful chemistry discussions (can cooking be classed as chemistry?). Thanks too to Nigel and Conor for being patient with my engineering teething problems! To the computer department in UCD; thanks a million to all, but especially Lucy Dunne for her ability to make my science stuff actually look like clothing and still work! Thanks too, to the department of sports science and health in DCU, especially Donal O'Gorman, Niall Moyna and Brian Carson for your invaluable help with the sports trials and for coercing the subjects into that very stylish breathing t-shirt!

I would also like to expression my appreciation to "the lads" from college for always being available for a laugh and for being just great friends.

Last but by no means least I would to thank my family, whom I'm indebted for all their encouragement and support while I've been in "school" all these years. I love you all very much. And to Anthony, thank you so much for your constant encouragement and belief that I could manage this mammoth journey and for not letting me do it alone.

*...The first will always have a path to pave,  
And older heads see pitfalls on the way,  
But hope, the tremulous makes less afraid,  
They see the pathway, and the falls evade....*

From Going Away, The Music of Humanity, Philip Brady, 1995, Alesbury Books

## TABLE OF CONTENTS

<b>DECLARATAION .....</b>	<b>II</b>
<b>DEDICATION.....</b>	<b>III</b>
<b>ACKNOWLEDGEMENTS.....</b>	<b>IV</b>
<b>TABLE OF CONTENTS.....</b>	<b>V</b>
<b>ABSTRACT .....</b>	<b>VII</b>
<b>LIST OF PUBLICATIONS &amp; PRESENTATIONS .....</b>	<b>VIII</b>
<b>ABBREVIATIONS .....</b>	<b>X</b>
<b>CHAPTER 1 LITERATURE.....</b>	<b>1</b>
1.1 AIM OF THIS THESIS .....	2
1.2 INTRODUCTION TO POLYMERIC MATERIALS .....	4
1.3 CONDUCTING POLYMERS .....	5
1.4 ELECTRONIC CONFIGURATION OF CONDUCTIVE ELECTROACTIVE POLYMERS.....	11
1.5 SYNTHESIS OF CONDUCTING POLYMERS.....	14
1.6 DOPING OF CONDUCTING POLYMERS.....	21
1.7 PROCESSIBILITY OF CONDUCTING POLYMERS .....	23
1.8 NON CONDUCTING POLYMERIC MATERIALS .....	26
1.9 COMPOSITE MATERIALS .....	32
1.10 APPLICATIONS FOR POLYMER COMPOSITE SYSTEMS.....	34
1.11 WEARABLE SENSORS .....	36
1.12 COMMUNICATION .....	42
1.13 MARKET POTENTIAL.....	45
1.14 CONCLUSION .....	47
1.15 REFERENCES .....	49
<b>CHAPTER 2 MATERIALS &amp; METHODS .....</b>	<b>58</b>
2.1 INTRODUCTION .....	59
2.2 MATERIALS.....	68
2.3 EXPERIMENTAL.....	71
2.4 RESULTS & DISCUSSION .....	82
2.5 CONCLUSION .....	124
2.6 FURTHER STUDIES .....	125
2.7 REFERENCES .....	127

<b>CHAPTER 3</b>	<b>APPLICATION OF PPY-COATED PU FOAM: CHEMO-SENSING.....</b>	<b>129</b>
3.1	INTRODUCTION .....	130
3.2	EXPERIMENTAL.....	131
3.3	RESULTS & DISCUSSION .....	136
3.4	CONCLUSION .....	151
3.5	REFERENCES .....	152
<b>CHAPTER 4</b>	<b>APPLICATION OF PPY-COATED PU FOAM: PLANTAR PRESSURE SENSING .....</b>	<b>154</b>
4.1	INTRODUCTION .....	155
4.2	WHY MONITOR PLANTAR PRESSURE? .....	155
4.3	INCORPORATION OF WIRELESS TECHNOLOGY .....	165
4.4	EXPERIMENTAL.....	167
4.5	RESULTS & DISCUSSION .....	175
4.6	CONCLUSION .....	189
4.7	REFERENCES .....	191
<b>CHAPTER 5</b>	<b>APPLICATION OF PPY-COATED PU FOAM: BIOMIMETIC SENSING ....</b>	<b>194</b>
5.1	INTRODUCTION .....	195
5.2	BACKGROUND STUDY .....	200
5.3	EXPERIMENTAL.....	202
5.4	RESULTS & DISCUSSION .....	212
5.5	FURTHER STUDIES: LIMB MOVEMENT .....	229
5.6	CONCLUSION .....	232
5.7	REFERENCES .....	234
<b>CHAPTER 6</b>	<b>GENERAL CONCLUSION .....</b>	<b>237</b>
6.1	SUMMARY OF THIS THESIS .....	238
6.2	SUMMARY OF RESULTS .....	239
6.3	COMPARISON WITH OTHER SENSING MATERIALS.....	240
6.4	FUTURE WORK: DEVELOPMENT AND INTEGRATION OF CHEMO- AND BIO-SENSORS.....	241
6.5	ISSUES ARISING FROM THE DEVELOPMENT OF WEARABLE SENSOR TECHNOLOGY.....	243
6.6	REFERENCES .....	245
<b>APPENDIX</b>	<b>.....</b>	<b>I</b>

## **ABSTRACT**

We live in a world of information, and emerging technologies, which compel us to look for new ways to collect, process, and distribute information. Today we are faced with an information overload problem as users struggle to locate the right information in the right way at the right time. In my view this is an “overload” of trivial information coupled with a gap in access to important information. Digitization of information and communications has seen the rise and rise of computers to a now ubiquitous position in our society. However, the problem remains as to how to merge the digital world with sensing, and respond to changes in the real world. Ubiquitous information systems are needed that will automatically sense and importantly, respond to changes in their environment and usage in order to deliver a more intelligent, proactive and personalized information service. These systems may be wearable, enabling them to disappear into our personal space, enhancing rather than burdening our daily activities. Conventional sensors are generally unsuitable for wearable body monitoring devices either due to their physical structure or their functional requirements. This thesis examines this area of wearable sensors, detailing the development and characterisation of novel sensing materials and outlines their performance in various on-body monitoring applications.

## **LIST OF PUBLICATIONS & PRESENTATIONS**

### **Poster Presentations**

*The Development and Characterisation of a Polymeric Sensing Device for Ammonia*, Sarah Brady, King-tong Lau, Dermot Diamond, 55<sup>th</sup> Irish Universities Chemistry Research Colloquium, Trinity, Ireland, **2003**

*The Development and Characterisation of Conducting Polymeric-based Sensing Devices*, Sarah Brady, King Tong Lau, Dermot Diamond, Progressive annual reports presented as posters for peer-reviewing at annual IRCSET National Research Symposia, Royal Hospital Kilmainham, Ireland, **2003**;  
Croke Park, Ireland, **2004 & 2005**.

*The Development and Characterisation of Conducting Polymer-based Sensing Devices*, Sarah Brady, Kim Lau, Gordon Wallace, Dermot Diamond, International Conference on Synthetic Metals, University of Wollongong, Australia, **2004**

*The Development and Characterisation of a Pressure Sensing Polymeric Device*, Sarah Brady, Kim Lau, Dermot Diamond, Adaptive Information Cluster Conference, DCU, Ireland, **2004**

*Wearable – Body Monitoring*, Sarah Brady, Dermot Diamond, Adaptive Information Cluster Conference, Santry, Ireland, **2005**

### **Oral Presentations**

“Discover Science, there’s no telling how far you can go...”  
Kennedy Space Centre, Florida, USA, **2003**

*The Development and Characterisation of Conducting –Polymer Based Sensing Devices*, Sarah Brady, Dermot Diamond, IRCSET National Research Symposium, Croke Park, Ireland, **2004**



*Combining Wireless with Wearable Technology for the Development of On-Body Networks*, S. Brady, B. Carson, D. O’Gorman, N. Moyna and D. Diamond, in *Proceedings for the International Workshop on Wearable and Implantable Body Sensor Networks*, Massachusetts Institute of Technology, Cambridge, Boston, USA, **2006**

## **Publications**

Inherently conducting polymer modified polyurethane smart foam for pressure sensing, *Sarah Brady, Dermot Diamond, King-Tong Lau, Sensors and Actuators A : Physical, Volume 119, Issue 2, 13 April (2005), Pages 398-404*

Initial Development and Testing of a Novel Foam-Based Pressure Sensor for Wearable Sensing, *Lucy E. Dunne, Sarah Brady, Barry Smyth, Dermot Diamond, J Neuroengineering Rehabil. (2005) Mar 1;2(1):4.*

Electrochemically Induced Fluid Movement Using Polypyrrole, *Jenny Causley, Shannon Stitzel, Sarah Brady, Dermot Diamond, Gordon Wallace, Synthetic Metals, Volume 151 (1), May (2005), Pages 60-64*

Coarse Sensing of Upper Arm Position Using Body-Garment Interactions, *Lucy E. Dunne, Richard Tynan, Gregory M.P. O’Hare, Barry Smyth, Sarah Brady, Dermot Diamond, in Proceeding of the International Forum on Applied Wearable Computing, Zurich, Switzerland, (2005).*

The Development and Characterisation of Conducting Polymeric-based Sensing Devices, *S. Brady, K.T. Lau, W. Megill, G.G. Wallace, D. Diamond, Synthetic Metals, Volume 154 (1-3), September (2005), Pages 25-28*

Wearable Sensors? What is there to sense? *Sarah Brady, Lucy E Dunne, Aogan Lynch, Barry Smyth, Dermot Diamond, Stud Health Technol Inform, (2005), Volume 117, Pages 80-88*

Garment-Based Body Sensing Using Foam Sensors *Dunne, L.E., Brady, S., Tynan, R., Lau, K., Smyth, B., Diamond, D. and O’Hare, G.M.P., Users Interfaces, In Proc. Seventh Australasian User Interface Conference (AUIC2006), Hobart, Australia. CRPIT, 50. Piekarski, W., Ed. ACS., January, (2006), Pages 165-171*

Combining Wireless with Wearable Technology for the Development of On-Body Networks, *S. Brady, B. Carson, D. O’Gorman, N. Moyna and D. Diamond, in Proceedings for the International Workshop on Wearable and Implantable Body Sensor Networks*, Massachusetts Institute of Technology, Cambridge, Boston, USA, (2006), *Pages 31-36*

Wireless-based monitoring of body movements using wearable sensors *Sarah P. Brady, Shirley Coyle and Dermot Diamond, in Proceedings for the MRS Spring Meeting, Symposium S, San Francisco. USA, April, 2006*

## ABBREVIATIONS

ICON	DESCRIPTION	ICON	DESCRIPTION
$\mu$	mobility of a charged particle	$iR$	current
$\mu l$	microlitre	$IT$	information technology
$A$	area	$ITO$	indium tin oxide
$A^+$	electron accepting species (anion)	$K$	Boltamann constant
$AAL$	Ambient Assisted Living	$K\Omega$	kilo Ohm
$Ag$	silver	$L$	litre
$AgCl$	silver chloride	$l$	length
$Au$	gold	$LDPE$	low density polyethylene
$BAN$	body area network	$LED$	light emitting diode
$BPM$	breaths per minute	$mM$	millimolar
$Br^-$	bromide ion	$Mm$	millimetre
$BSN$	body sensor network	$Ni$	nickel
$c$	concentration	$NIDDM$	non-insulin-dependent diabetes mellitus
$CEPs$	conducting electroactive polymers	$NIR$	near-infrared
$CF$	Cystic Fibrosis	$NMR$	nuclear magnetic resonance
$Cl^-$	chloride ion	$PANi$	polyaniline
$cm$	centimetre	$PC$	personal computer
$COM$	centre of mass	$PCB$	printed circuit board
$CPU$	central processing unit	$PE$	polyethylene
$csv$	comma separated values	$PF_6^-$	hexafluorophosphate ion
$Cu$	copper	$PIB$	polyisobutylene
$CV$	cyclic voltammetry	$PPy$	polypyrrole
$D^+$	electron donating species (cation)	$Pt$	platinum
$E$	electrical field	$PTh$	polythiophene
$e.m.f.$	electromotive force	$PU$	polyurethane
$E_a$	activation energy	$R$	resistance
$ECG$	electrocardiography	$R\&D$	research and development

<b>ECP</b>	electrochemical polymerisation	<b>RF</b>	radio frequency
<b>EDX</b>	energy dispersive x-ray analysis	<b>RH</b>	relative humidity
<b>E<sub>g</sub></b>	energy gap	<b>RR</b>	respiratory rate
<b>EL</b>	electroluminescence	<b>s</b>	seconds
<b>EMG</b>	electromyography	<b>SCE</b>	saturated/standard calomel electrode
<b>ESD</b>	electrostatic discharge	<b>SnO<sub>2</sub></b>	tin oxide
<b>e-textiles</b>	electronic textiles	<b>SpO<sub>2</sub></b>	oxygen saturation
<b>eV</b>	electron volts	<b>T</b>	temperature
<b>FeCl<sub>3</sub></b>	ferric chloride	<b>T<sub>g</sub></b>	glass transition temperature
<b>g/mol</b>	grams per mole	<b>UV-vis</b>	ultra-violet visible
<b>G-forces</b>	gravity forces	<b>V</b>	voltage
<b>GPRS</b>	general packet radion service	<b>V<sub>E</sub></b>	minute ventilation
<b>GSM</b>	global system for mobile communications	<b>X<sup>+</sup></b>	cation
<b>HDPE</b>	high density polyethylene	<b>Z</b>	charge of a particle
<b>HP</b>	Hewlett Packard	<b>ρ</b>	electrical resistivity
<b>i</b>	current	<b>σ</b>	electrical conductivity
<b>I</b>	iodide ion		
<b>IDDM</b>	insulin-dependent diabetes mellitus		
<b>IR</b>	infrared resonance		

## **Chapter 1   LITERATURE**

## 1.1 AIM OF THIS THESIS

The aim of this thesis has been to investigate the properties of conducting polymers, in particular polypyrrole, and to develop a sensing system using this material as the active sensing platform in a composite material. To begin the properties of polypyrrole and similar conducting polymers are presented, highlighting the benefits of these materials that have promoted the research that has begun in this area. For example polypyrrole has been used as a sensing platform to detect chemical targets such as ammonia. However, it has also been combined into composites, broadening the scope of applications for polypyrrole by enabling an electrically conductive pathway to be formed between different sensing materials.

This thesis investigated in detail the development of a sensing device using polypyrrole combined with polyurethane foam with the intention of applying it in wearable applications. In order for a sensor to be wearable it must essentially be comfortable to wear. This can mean that the material can be integrated comfortably into wearable garments, or that the garment itself is made to be the sensor. Depending on the application, the site and specifications of the sensor may change. If the aim of the sensor is to generate information about plantar pressure distribution or body movements which produce vertical forces, a material that is soft and compressible is desired. Or if the aim of the sensor is to develop of sensor of high surface area for sensitive gas detection, possibly for use as a wearable chemo-sensor, then a highly porous material is required. For these reasons, an open-celled foam was chosen as the base-substrate for the sensor. Further discussions of wearable sensors are also presented in the introduction of this thesis.

The polypyrrole layer, which is electroactive, coated the entire polyurethane matrix, thus rendering the whole material conductive. Being conductive, it was possible to measure its resistance. However it was found that the resistance of the material was dependent on the status of and environment surrounding the foam. Thus, by monitoring the resistance of the polypyrrole coated foam, aspects such as changes in forces applied to the material or the presence of chemical analytes close to the material could be identified. Thus a sensing system was established.

Throughout the research, certain aspects, outside the scope of the chemistry of the sensors, required modification, including the communication module. If the sensors could be wearable, then the communication module would also have to be wearable less the entire system would become redundant. Thus, these considerations had to be taken into account during the course of the studies. The aim of this thesis has been to present a material which could be used as a platform for further wearable sensors.

The work presented here represents an inter-disciplinary approach to tackling the topic of electronic (*e-*) or personalized (*p-*) health which is set to explode in the near future. The primary objective was to develop a successful wearable and wirelessly integrated body monitoring system. The results that will be presented within this thesis will confirm that the materials utilised throughout the thesis, a polypyrrole coated polyurethane (PPy-PU) foam, can be comfortable to wear but also generate accurate and meaningful results for the wearer.

## 1.2 INTRODUCTION TO POLYMERIC MATERIALS

The word “polymer” is derived from the Greek to mean “consisting of many parts”[1] and has evolved today to represent both natural and synthetic compounds constructed by the linking of millions of simpler repeated units. The first polymers that we came to know of were natural products. These included wood, bone, skin and fibres and have been used by man since prehistoric times. However the development of “polymer science” did not occur until the recent 20<sup>th</sup> century. Hermann Straudinger developed the concept of the macromolecule during the 1920s while later in 1935, Wallace Carothers invented nylon while carrying out polymerisation research in the DuPont Company [2]. Within a short time, Bakelite, a robust thermoset plastic that could be moulded to any desired shape was also commercially available [3]. This initial polymer research showed the great industrial potential of synthetic polymers; a potential that became a reality in a remarkably short time.

Different polymers may consist of similar chemical units but if they are of different molecular weight they will have diverse properties. This leads to differences in their aesthetic, tactile, physical and chemical characteristics. In the 1930s, distillation of crude oil (fossil fuel) revealed a number of by-products such as polypropylene (PP), polyethylene (PE) and polystyrene (PS) [4]. These high molecular weight polymers have been shown to be constructed by the repetition of smaller simpler, monomer units.

Polymer synthesis was dominated by Karl Ziegler and Giulio Natta during the 1950s, whose polymerisation catalysts were of great importance for the development of the modern “plastic” industry. In the 1970s a dramatic breakthrough occurred in the evolution of polymers with the discovery that some polymers could conduct electricity [5]. Up until then, it was assumed that polymers were saturated and non-conducting; hence their frequent use as insulators in electrical and electronic components. Since then, much research has been invested into deciphering the mechanisms of conductivity through the polymers [6-11] and also into the potential applications of such materials [12-16]. Such is the importance of these novel materials that Professor Bengt Rånby designated these electrically conducting polymers as the “fourth generation of polymeric materials” in a lecture at the Nobel Symposium (NS-81) in 1991 [17].

### 1.3 CONDUCTING POLYMERS

Conducting polymers are macromolecules that propagate charge along their structural format. There are two major classes of conducting polymers; (1) ion-containing polymers and (2) electroactive polymers.

#### 1.3.1 Ion-containing polymers

Ion-containing polymers (ionomers or polyelectrolytes), are polymers which contain charged ionic groups. They are copolymers, containing hydrophilic (ionic) portions and hydrophobic (non-ionic or nonpolar) sections and can bind ions from solution via an ion-exchange process. In ion-containing polymers, the current is transported by ions moving around. This movement or diffusion of ions is a random process but can be biased under the driving force of an applied electrical field ( $E$ ).

Examples of ionomers include poly(ethylene-co-methacrylic) acid and Nafion™, a perfluorinated polymer that contains small proportions of sulfonic or carboxylic ionic functional groups, see Fig. 1.1 for their respective structures. The presence of both negatively and positively charge groups within the polymeric structure result in electrostatic interactions which enable charge to propagate through the medium.

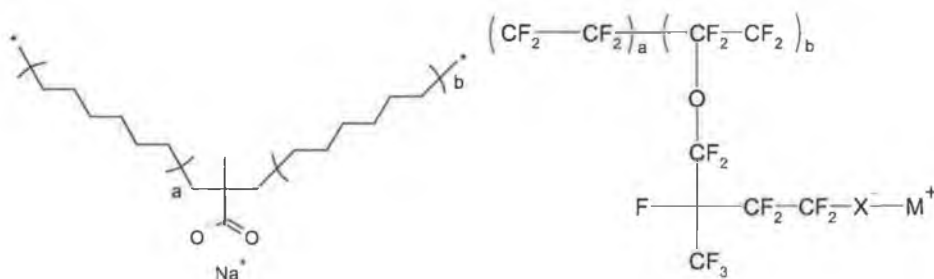


Fig. 1.1 Molecular structure of a) poly(ethylene-co-methacrylic) acid sodium salt and b) Nafion,  $\text{X}^-$  indicates a sulfonic or carboxylic group, while  $\text{M}^+$  represents a metal cation.

The electrostatic interactions in ionomers also cause the polar ionic groups to aggregate causing the polymer to behave similar to crosslinked polymers or block copolymers.



These thermoplastics exhibit reversible crosslinking since heating can reprocess them. Ionic conductivity is important for many products such as Type I and Type II (regular and rechargeable batteries), ion-selective membranes, such as proton exchange membranes, filters [18-20], mass transfer membranes [21] and catalysts [22-27]. For example, their function, in a proton exchange membrane fuel cell, is to conduct protons, or hydrogen ions, across the membrane, while being impermeable to gasses such as oxygen or hydrogen to maintain separation of the reactants.

### 1.3.2 Conducting Electroactive Polymers

Conducting electroactive polymers (CEPs), on the other hand are organic macromolecules. They do not contain ionic groups and so conduction of charge is mediated by a very different mechanism as described for ionomers. Instead, structural distortions and relaxation mechanism result in localisation of charge along the polymeric chain.

#### *The first conducting polymer – Polyacetylene*

The synthesis of the first conducting polymer, polyacetylene, was discovered surprisingly due to a communication breakdown when a visiting Korean researcher to Prof. Shirakawa's Tokyo Institute of Technology, mistakenly added too much Ziegler-Natta catalyst to his experiment while trying to synthesise the black powder, polyacetylene. However, instead it resulted in a conductive bright, glistening silvery film which puzzled Shirakawa [28]. Further investigations in collaborations with Prof. Alan MacDiarmid; and Prof. Alan Heeger, confirmed that this silver polyacetylene  $(CH)_x$  could also conduct charge. This opened up the prospect of cheap and lightweight electronic devices. In addition, conducting polyacetylene would present a new theoretical model for studying conduction mechanisms and the metal-insulator transition in organic materials. And so began the research and investigations of polyacetylene. This discovery of polyacetylene as a novel conducting polymer was recognised by the joint awarding of the Chemistry Nobel Prize in 2000 to each of these workers.

Investigations into the electronic properties of polyacetylene revealed that charge transport through this polymer is due to the structural conjugation of CH units [29].

The  $\pi$ -bonding, in which the carbon orbitals are in the  $sp^2p_z$  configuration, see Fig. 1.2, enable the orbitals of successive carbon atoms along the backbone to overlap, leading to electron delocalisation along the backbone of the polymer. This electronic delocalisation provides a pathway for charge mobility along the polymeric backbone [30].

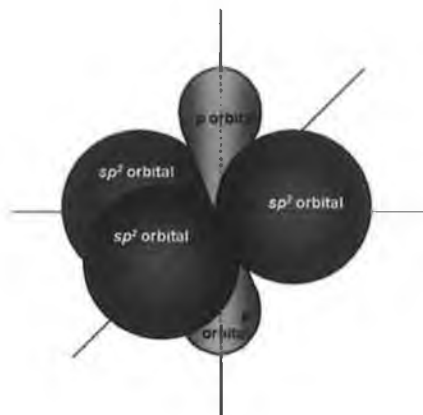


**Fig. 1.2 Outer shell orbitals of  $sp^2p_z$  configuration of carbon atoms.**

In 1977 it was discovered that dramatic changes in the electronic state of polyacetylene could be achieved by exposing the films to trace amounts of halogens [31]. This *doping* of the polymeric films resulted in increased conductivity of several orders of magnitude in only a few minutes. This ability to dope polyacetylene with a variety of dopants makes it significantly different from conventional covalent semiconductors. The electrical conductivity of polyacetylene can be increased by 12 orders of magnitude through chemical or electrochemical doping [32] thus making it an attractive material for photovoltaic and photoelectrochemical applications.

However, though polyacetylene revealed many secrets of conducting polymers it is not a practical material as it is environmentally unstable and insoluble in solvents. Thus, the focus shifts onto other conjugated polymers such as poly(p-phenylene), polypyrrole (PPy), polythiophene (PT), polyaniline (PANi) and their derivatives. The potential for these materials to impact on modern society is evidenced by the amount of research worldwide that has been invested in this area over the last 25 years. A huge variety of applications have benefited from this research from antistatic and electromagnetic shielding coatings to light-emitting diodes.

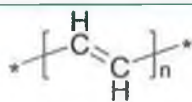
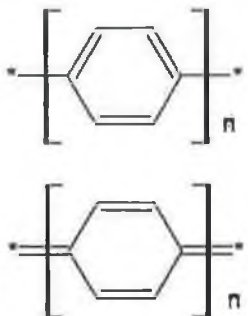
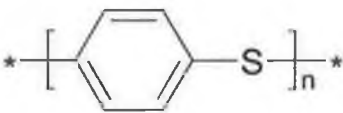
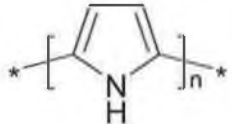
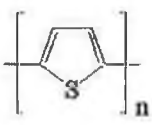
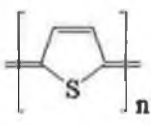
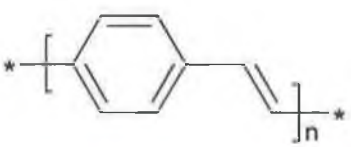
#### *Other conducting electroactive polymers*

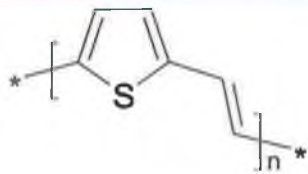
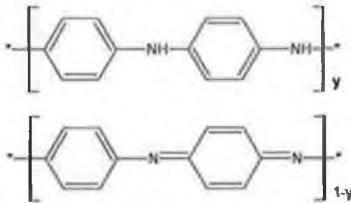
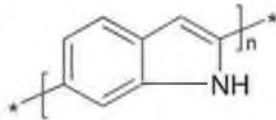
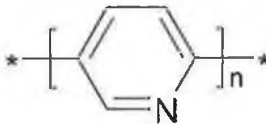
CEPs such the ones listed in Table 1.1 are at the fore-front of intelligent materials research as they can:

1. stimulate specificity at a molecular level;
2. facilitate the transduction of electrical information due to their inherent conductive nature;
3. be fabricated into specific design features
4. be electrically actuated to perform designated mechanical operations.

Many of these CEPs are poly(heterocycles) which can be viewed as carbon chains with the structure of polyacetylene stabilised by the heteroatom. For example, the nitrogen in pyrrole ring stabilises the polypyrrole chains with the result that polypyrrole is stable in ambient environments, whereas polyacetylene is not. These CEPs differ from polyacetylene by their no-degenerate ground state related to the non-energetic equivalence of their two limiting mesomeric forms, aromatic and quinoid (for example see Table 1.1 polyphenylene and polythiophene), their high environmental stability, and their structural versatility which allow modulation of their electronic and electrochemical properties by manipulation of the monomer structure [33].

**Table 1.1 Common Conducting Polymers.**

Polymer	Acronym	Structure
Polyacetylene	Pac	
Polyphenylene	PPP	
Poly(phenylene sulphide)	PPS	
Polypyrrole	PPy	
Polythiophene	PTh	<div style="display: flex; justify-content: space-around; align-items: flex-end;"> <div style="text-align: center;">  Benzoid form         </div> <div style="text-align: center;">  Quinoid form         </div> </div>
Poly(phenylene-vinylene)	PPV	

Polymer	Acronym	Structure
Poly(thienylene-vinylene)	PTV	
Polyaniline	PANi	 <p> <math>y=1</math> LEUCOEMERALDINE  <math>y=0.5</math> EMERALDINE  <math>y=0</math> PERNIGRANILINE </p>
Poly(indole)	PIn	
Polypyridine		

#### 1.4 ELECTRONIC CONFIGURATION OF CONDUCTIVE ELECTROACTIVE POLYMERS

As can be seen in the examples of CEPs listed in Table 1.1, all the molecules contain portions of unsaturated systems formed by the overlapping of adjacent  $p_z$ -atomic orbitals. According to the Huckel's  $\pi$ -electron theory for unsaturated systems [34], if the carbon-carbon bond lengths were of equal length then  $\pi$ -molecular orbitals would form a continuous band. Each carbon would contribute one  $\pi$ -electron, which would half-fill this continuous  $\pi$ -band. This would imply metallic conductivity for the polymer. However, distortions due to Peierls instability occur in these aromatic polymers causing adjacent CH groups to move towards each other, forming alternative shorter (double) and longer (single) bonds. Thus the  $\pi$ -band is split into two sub-bands,  $\pi$ - (the valence band in semiconductor terminology) and  $\pi^*$ - (the conduction band) separated by an energy gap,  $E_g$ . This idea is illustrated in Fig. 1.3

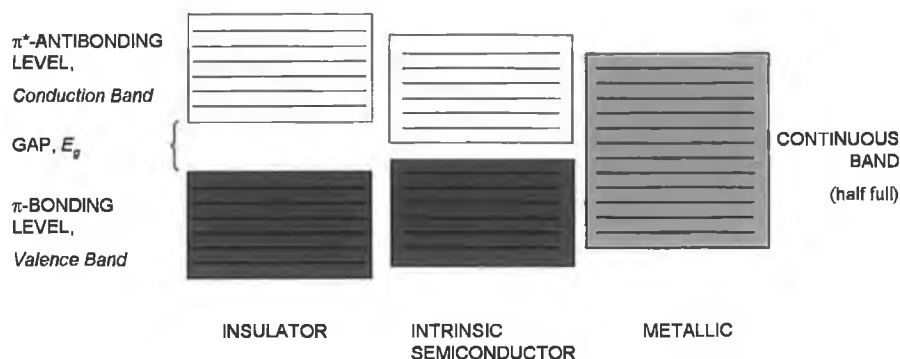


Fig. 1.3  $\pi$ -electronic band possibilities for undoped polyacetylene.

In order to promote electrons from the  $\pi$ - (valence) to the  $\pi^*$ -(conduction) band, energy equivalent or greater than the  $E_g$  must be supplied to the molecule. This may occur in the form of thermal or spectral energy. In conducting metals, the  $E_g$  can be overcome easily, enabling electrons to be promoted to the conduction band enabling conductivity. In contrast, the  $E_g$  of an insulator is so great, that it is difficult to promote electrons to the higher energy conduction band, thus resisting conductivity. The  $E_g$  of a semiconductor, thus as the name would suggest resides between that of a conductor and an insulator.

#### 1.4.1 Charge carriers

In traditional semiconductors, the coordination of each atom to its neighbours through covalent bonds, usually 4-6 adjacent atoms, leads to a rigid structure. In such systems the dominant charge carriers are considered to be electrons and holes.

In semi-conducting polymers, however, the arrangement of the atoms is not so rigid and so the polymer matrix is susceptible to structural distortions (Peierls dimerisation). Therefore, charge storage on the polymer chain leads to structural relaxation, which in turn localises the charge. Pople and Walmsley [35] first described these distortions as kinks in the bond length alteration pattern. Su, Schrieffer and Heeger (SSH) [36] considered these kinks were of finite width with an optimised geometry. These are the soliton (positively, negatively charged and neutral) states, Fig. 1.4A, B & C. The soliton electron describes those electrons that sit in the mid-gap region, the next region to the  $\pi$ -bonding level and describe solitary wave defects in the polymer. They are considered to be the major charge carrier in such conjugated polymeric systems. Removal of the soliton electron creates a delocalised cation, or positive soliton (Fig. 1.4C), whereas neutral solitons (Fig. 1.4B) are produced during isomerisation.

When a doped conjugated polymer is oxidised, additional charge carriers are included to enhance conductivity through the polymer. If an electron is removed from the top of the valence band the remaining hole does not delocalise completely as would be expected by the classical band theory. Instead the radical cation (polaron) is localised (Fig. 1.5B). This immobilisation of charge is in part due to the presence of doping agents, such as  $I_3^-$ , along the polymeric backbone. If a second electron is removed from an oxidised section of polymer, the one of two things can occur. Either a second independent polaron is created, or the unpaired electron of the first polaron is removed and a bipolaron is formed (Fig. 1.5C). The polaron, being a radical cation has a spin of  $\frac{1}{2}$  whereas the spins of the bipolarons, being paired, add to 0. These electronic states coalesce into bipolaron bands with further oxidation and doping [37]. This corresponds to approximately one charge for every three pyrrole monomer units. Another effect of this oxidation and doping is that the  $\pi$ - $\pi^*$  band gap will increase. [38]. While polarons are found in almost all conjugated polymers, solitons are not. This is because most CEPs have non-degenerate ground states and as such, the defects in these compounds

cause charge distortions [39] to be confined in pairs, thus giving rise to the presence of polarons and bipolarons.

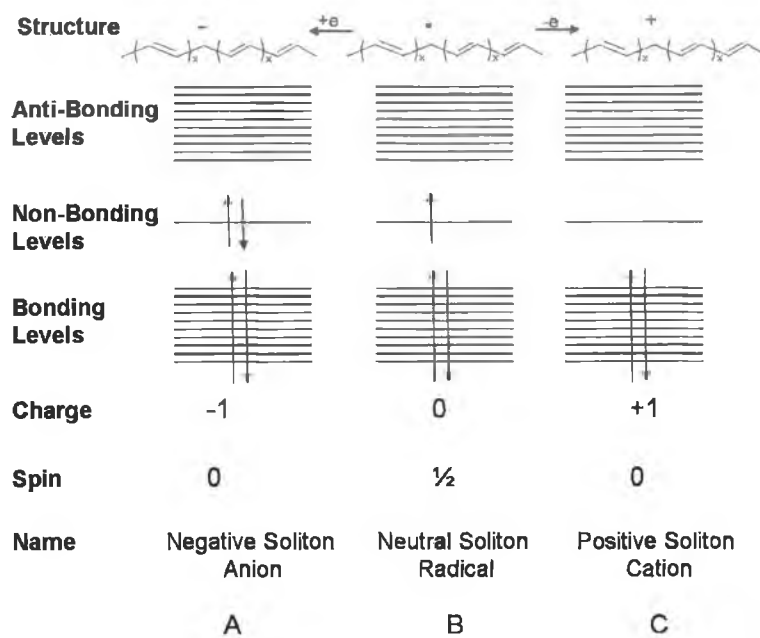


**Fig. 1.4** Band structure and electronic configuration for species implicated in conduction mechanisms in conjugated polymers, illustrated for polyacetylene. \*Negative analogues via electron addition [40].

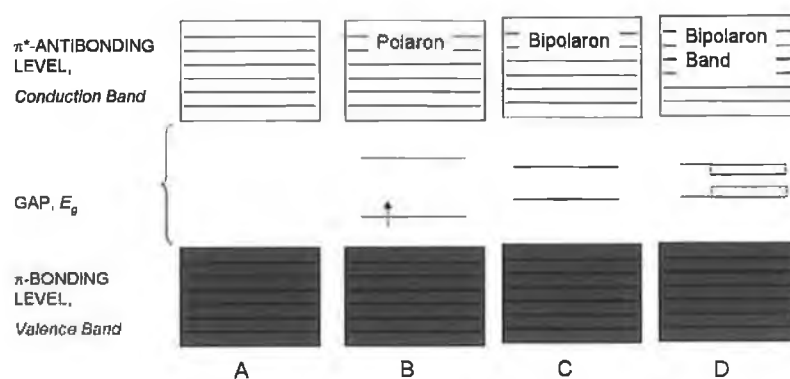


**Fig. 1.5** Electronic levels and bands for oxidised conducting polymers, such as polypyrrole.



## 1.5 SYNTHESIS OF CONDUCTING POLYMERS

Being electrically conductive, CEPs also have the additional practical benefit of enabling us to communicate with them through many of the electronic instruments we have become accustomed to in our scientific environment. The conductivity of CEPs are highly dependent on polymer morphology and chain symmetry. Hence, control of synthetic conditions is crucial for generating the desired product. The synthesis of CEPs is generally initiated by the oxidation of the monomer unit to generate a radical species, which propagates via chain reaction, yielding dimers, oligomers and finally polymers.

CEP synthesis can be facilitated by a number of methods;

1. electrochemical polymerisation at a conductive substrate (electrode) through the application of an external potential,
2. chemical polymerisation through the use of chemical oxidants,
3. photochemical polymerisation and
4. enzyme-catalysed polymerisation.

The various approaches produce CEP materials with different forms; chemical oxidations generally form powders and fibres whereas electrochemical polymerisations tend to yield films which adhere the electrode surface. Two synthetic routes, firstly electrochemical synthesis and then chemical oxidation, will be discussed in relation to the synthesis of polypyrrole.

### 1.5.1 Electrochemical Polymerisation of Polypyrrole

Electrochemical polymerisation of polymers such as polypyrrole, polythiophene, polyfuran, etc. have greatly dominated the field of conducting and semiconducting polymers where advancements in polymerisation techniques have led to the development of a field interfacing polymer science and electrochemistry.

The electrochemical polymerisation of pyrrole is usually performed in an electrolyte/molecular solvent system. The processing parameters, in particular the size and nature of the dopant counterions from the solvent/electrolyte system, and the nature of the solvent itself can have a marked impact on the properties of the resultant polymer film [37]. The oxidation / reduction process may involve either anion or cation (Fig. 1.6) exchange or a mixture of both.

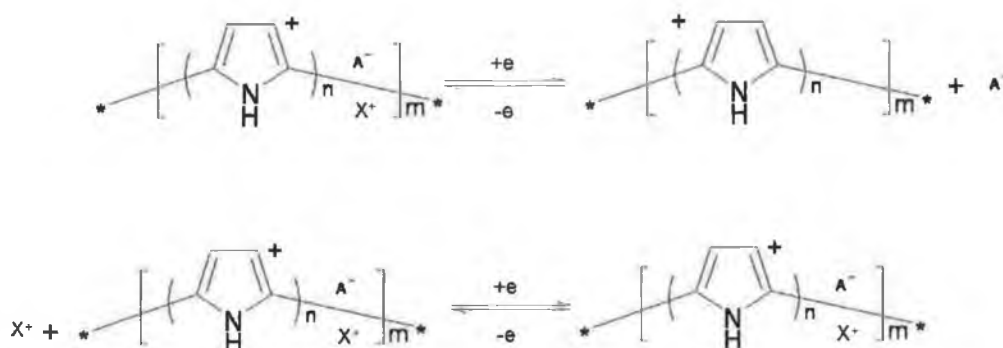


**Fig. 1.6 Redox processes for polypyrrole showing (top) anion and (bottom) cation exchange.**

Here  $n$  = number of charge centres per 3 - 4 monomer units, while  $m$  represents the polymer chain length, which determines molecular weight,  $A^-$  represents the counterion which is included to maintain charge neutrality along the polymeric backbone. This representation greatly simplifies the complexity of the electropolymerisation process, since polypyrrole, and CEPs in general, tend to be dynamic and interactive materials.

When the electroactive polymers are oxidised in an appropriate electrolytic medium, positive charges are generated along the backbone and solvated anions ( $A^-$ ) enter the polymer from the solution to maintain charge balance, see top of Fig. 1.6. It has been

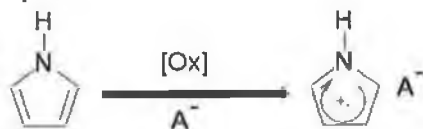
shown that the size and nature of the dopant counterion incorporated during synthesis can have a dramatic effect on the ion movement occurring during redox processes. If, for instance, the size of the dopant anion is such that it cannot be expelled during reduction, then cation ( $X^+$ ) exchange must occur to maintain charge neutrality as shown in the bottom schematic in Fig. 1.6.

The electrochemical synthesis of polypyrrole is better described when broken up into the following steps [37] (depicted in Fig. 1.7):

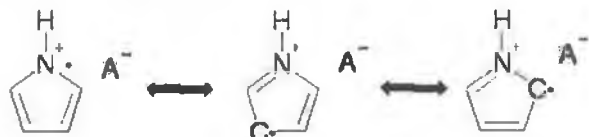
1. A neutral pyrrole monomer when oxidised yields a cation radical species. This cation radical resonates around the aromatic ring of the pyrrole unit. The appearance of  $A^-$  represents a dopant anion, incorporated to maintain charge neutrality along the polymer.
2. This cationic radical combines with another pyrrole monomer thus producing a dication of bipyrrrole.
3. The chain of polypyrrole propagates in this manner until two radical species couple. The resulting polymer then undergoes deprotonation.

Polymerisation is believed to proceed via this radical-radical coupling mechanism, whereby the natural repulsion of the radicals is assumed to be negated by the presence of other species such as solvent, counterions and also the monomer. When the polymer chain exceeds a critical length, the solubility is exceeded and the polymer precipitates onto the electrode surface. The electrochemical conditions, such as potential used, applied current density and temperature, the electrochemical cell design, the electrode material, the solvent, counterions and monomer all influence the nature of electropolymerisation and the characteristics of the resulting polymer [37].

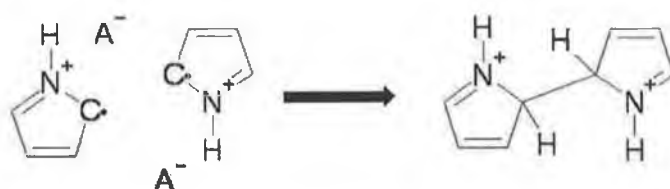
**Step 1. Monomer Oxidation**



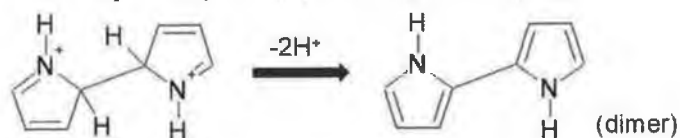
**Resonance forms**



**Step 2. Radical-radical coupling**



**Step 3. Deprotonation / Re-Aromatization**



**Step 4. Chain Propagation**

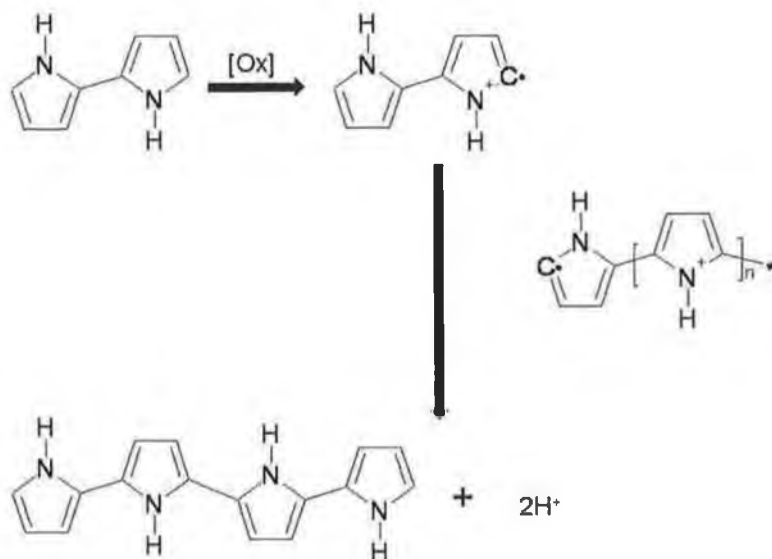


Fig. 1.7 Step-wise electrochemical synthesis of polypyrrole.

Electrochemical polymerization (ECP) is normally carried out in a single compartment electrochemical cell by adopting a standard three electrode configuration. This configuration typically consists of an electrochemical bath containing a monomer and a supporting electrolyte dissolved in an appropriate solvent.

A standard three electrode systems consists of a working electrode, a counter electrode and a reference electrode dipped in a single dual compartment cell. The working electrode acts as a substrate for deposition of the polymer. It is necessary that the electrode should not oxidise concurrently with the aromatic monomer [41]. For this reason, inert electrodes such as Pt, Au, SnO<sub>2</sub> substrates, ITO and stainless steel substrates have been used. A counter electrode, a metallic foil of Pt, Au or Ni is sometimes used. Reference electrodes such as the saturated calomel electrode (SCE), Ag/AgCl can be used.

Compounds that have relatively low anodic oxidation potentials are susceptible to electrophilic substitution reactions and can produce conducting polymers by ECP [41]. Thus, the simplest means of inducing the polymerisation is to apply a sufficiently positive constant potential. The potential will influence the rate of oxidation and hence that of polymerisation. Limits to the potential used do exist; too low and oxidation of the monomer may not incur deposition, too high and the polymer will become over-oxidised, resulting in a less conductive and more porous polymer product [42, 43] with lesser ability to store charge and lesser mechanical properties. ECP can also be carried out under constant current conditions (galvanostatically) or by dynamically cycling the voltage (by cyclic voltammetry). Potentiostatic conditions are recommended to grow thin films while galvanostatic conditions are recommended to grow thick films [44].

Since the electrochemical polymerisation reaction proceeds via radical cation intermediates, the nucleophilic character of the solvent and the electrolyte can impose certain restrictions on their choice [41]. The more nucleophilic the solution, the higher the possibility that the solvent will interact with these free radical intermediates and inhibit polymerisation [9]. Aprotic solvents, such as acetonitrile, benzonitrile can support the  $\pi$ -system of the polymer resulting in a more stable and conductive product [5]. The choice of supporting electrolyte depends on the solubility, degree of

dissociation and nucleophilicity criteria. Quaternary ammonium salts of the type  $R_4NX$  ( where  $R$  = alkyl or aryl radical and  $X = Cl^-, Br^-, I^-, PF_6^-$  etc.) are commonly used as supporting electrolytes in ECP of conducting polymers since they are soluble in aprotic solvents and are highly dissociated in them.

Once synthesised, charge can be reversibly added to or removed from the conducting polymer by cycling the material through its oxidised and reduced states. As the switch from oxidised to reduced state occurs, there is a coupled decrease in the conductivity. The switch involves mass and charge transport in the polymeric film. Monitoring of the redox peaks, according to the reduction and oxidation of the polymer as shown by the schemes in Fig. 1.6, can be used to characterise the PPy films during preparation [45, 46]. Both of these transport mechanisms have profound effects on the polymer. The mass transport of ions into and out of the polymer, cause the material to swell or shrink in a controlled manner. This may be used to develop actuators and separation membranes. The charge transport related to this movement of ions also has an effect on the polymer, resulting in a charged or non-charged material. Thus, the resistance, capacitance and flux of the material are affected. The surface tension of the material is also influenced by this movement of charge into and out of the material. Thus it is possible that a conducting polymer may be actively used to control fluid movement.

### **1.5.2 Chemical oxidative polymerisation of polypyrrole**

The experimental variables available in chemical polymerisation are greatly reduced compared with electrochemical oxidation. However, chemical polymerisation remains a process of interest because of its ease for scale-up and the tendency to form powders and colloidal dispersions. Chemical polymerisation of polypyrrole is easier than that of polyaniline in that it can be carried out in a neutral (non-acid) aqueous solution.

The mechanism for chemical polymerisation is similar to that described for electropolymerisation. However due to differing experimental conditions, the resulting polymers tend to have different characteristics. The conductivity of the resulting conducting polymer is dependent on the reaction conditions such as the oxidant and solvent used, the temperature, and the dopant counterion. For one-electron oxidants

such as  $\text{FeCl}_3$ , an  $\frac{[\text{oxidant}]}{[\text{pyrrole}]}$  molar ratio of approx. 2.3 is usually required. Two electrons are used for the oxidation of each pyrrole monomer unit, while the remaining 0.3 electrons is used for the oxidative doping of the neutral polypyrrole chain into a conducting form. In order to maintain charge neutrality along this polymeric chain, dopant counterions,  $\text{A}^-$ , are incorporated approximately one on every third pyrrole unit.

Though difficult to control the polymerisation once initiated, it is possible to dictate the conductivity of resulting polymers through the employment of specific binary systems (mixtures of two different oxidants), reaction temperatures and solvents [15].

Chemical polymerisation occurs in the bulk of the solution. The resulting polymers are insoluble and therefore precipitate out of solution. Spontaneous deposition onto various substrates can occur, if the substrate is present in the polymerising solution. Generally, in chemical deposition, the substrate is immersed or impregnated with a solution or vapour saturated with the monomer and then is exposed to an appropriate oxidant [47, 48]. This technique also occurs in the opposite direction, that is, the substrate can be immersed with the oxidant solution and then exposed to the monomer solution or vapour [49]. It is desirable to shift towards substrate deposition rather than bulk polymerisation, though the latter cannot be eradicated completely. Careful selection of parameters such as monomer concentration, oxidant-to-monomer ration, reaction temperature and appropriate treatment of the substrate surface, assist in the shifting of polymerisation from the bulk solution to the desired substrate [50], be it glass, plastic, metal, micro- and nano-porous, fibres or fabrics [51]. In situ vapour-phase deposition can also be used by passing pyrrole vapour over materials soaked in oxidant [52]. The surface resistance of these polymer-coated materials decreases with greater polymer deposition.

## 1.6 DOPING OF CONDUCTING POLYMERS

As mentioned previously, dramatic changes in the electronic state of polyacetylene could be achieved by doping the films to trace amounts of halogens. Doping of other CEPs results in a similar change in the conductivity of the polymer. Doping, the term, is analogous to that used in semiconductor systems. However, it differs in that it does not refer to the replacement of atoms in the material's framework. Instead, doping refers to the oxidation or reduction of the  $\pi$ -electronic system. Reagents such as iodine,  $\text{AsF}_3$  and bromine were shown to incur these increases in conductivity [53]. The result was an increase of conductivity of the polymer film from a range of  $10^{-8} - 10^{-5} (\text{S cm}^{-1})$  to a range of  $10^3 - 10^5 \text{ S cm}^{-1}$ . In comparison, Nylon<sup>TM</sup> has a conductivity of  $10^{-14} \text{ S cm}^{-1}$  and copper  $10^6 \text{ S cm}^{-1}$ . Fig. 1.8 shows the relative conductivities of common insulators, metals and conducting polymers.

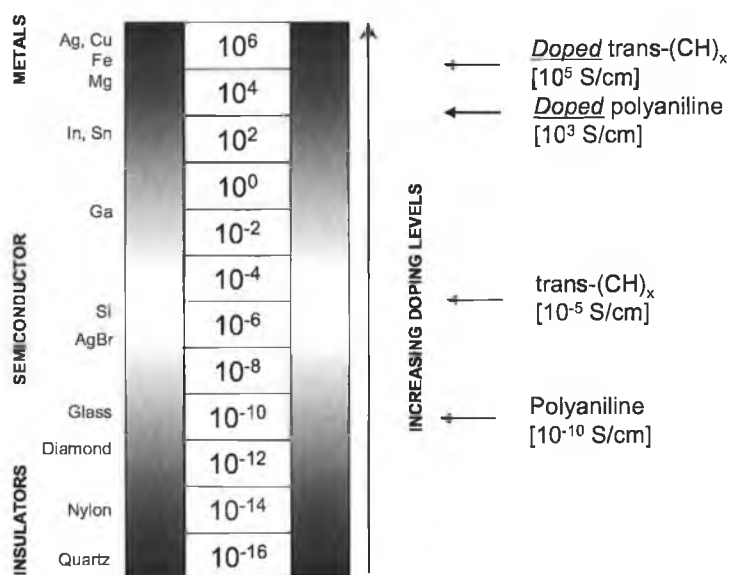


**Fig. 1.8 Electrical conductivity of conducting polymers in relation to common insulators and conductors.**



Doping can be achieved via the following methods:

1. Chemical
2. Electrochemical
3. Photochemical
4. Interfacial

It is enabled by the open morphology [54] and the weak interchain binding of the conducting polymer matrix which allows the diffusion of the dopant ion between the polymer chains. The strong intra-chain bonding maintains the integrity of the polymer during the diffusion process ensuring reversibility of the doping process. When doped with either electron accepting (A) or donating species (D), the number of charge carriers through the polymer chain increases, resulting in enhanced charge transfer [55]. The polymer chain acts as a poly(cation) in the presence of an  $A^-$  species and as a poly(anion) in the presence of a  $D^+$  species.

Doped conjugated polymers are good conductors for two reasons:

1. Doping introduces carriers into the electronic structure. Each repeat unit is a potential redox site and as such can be doped *n-type* (reduced) or *p-type* (oxidised) to a high density of charge carriers.
2. The attraction of an electron in one repeat unit to the nuclei in the neighbouring units leads to carrier delocalisation and charge mobility along the polymer chain, which extends into three dimension through interchain electron transfer.

Thus, doping is the forced introduction of charge into a conjugated polymeric structure. It can be facilitated via a number of methods, each leading to a wide range of interesting and important phenomena. The conductivity of conducting polymers is known to decline with time in ambient environments. This “ageing” process can be accelerated by rising temperatures and high humidity conditions mainly due to the loss of the dopants [7, 15], thus judicious choice of dopants is of utmost importance.

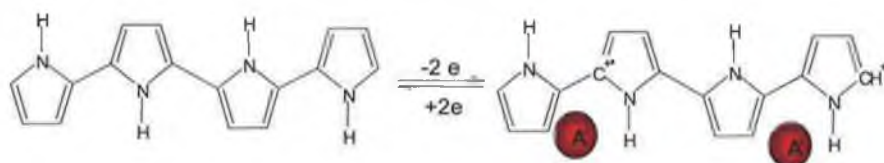


**Fig. 1.9** The forced introduction of charge into a conjugated polymeric structure, doping, here through electrochemical oxidation.

## 1.7 PROCESSIBILITY OF CONDUCTING POLYMERS

PANi, PPy and PT show greater environmental stability than polyacetylene but are also inherently limited in terms of their processing capabilities. Strong, inter- and intra-chain electron transfer reactions render PANi, PPy, and PT insoluble and infusible. This limits their processibility. In order to include conducting polymers in the design of novel sensor systems they must be either combined with processible materials or deposited onto various substrates making novel composite materials.

Deposition of conducting polymers methods can occur by dissolving the parent conducting polymer in a solvent and casting a film onto the desired substrate, allowing the solvent to evaporate, leaving a film of the conducting polymer. However, this method is limited because of the difficulties due to the insolubilities of the conducting polymers. A number of methods have been followed to address this problem. These include:

1. Side-chain functionalisation
2. Counter-ion induced processing
3. Colloidal dispersions

Functionalising groups on the conducting polymer can improve solubility. For example, by introducing an alkyl chain into the 3-position of a pyrrole monomer (see Fig. 1.10a), the resulting polymer is more soluble in organic solvents. Similarly, sulfonation of PANi (Fig. 1.10b) enhanced the solubility of this polymer in water. The side chains decrease interchain coupling and increase the entropy, thus enabling these derivatives to be processed from solution. However, it has been found that the conductivities of these chemically modified polymers were less than that of the unadulterated conducting polymer because of the distortion of the molecular structure of the conducting polymer [10, 56].

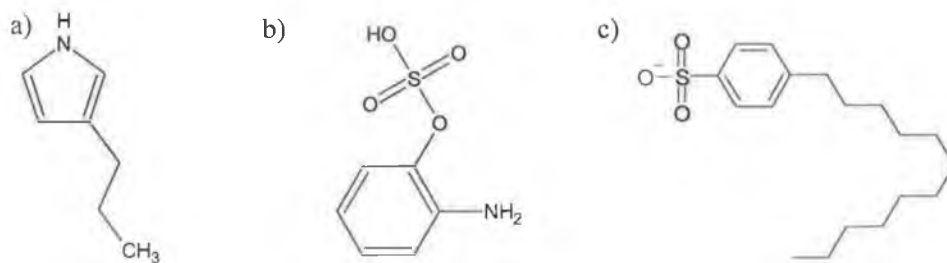


**Fig. 1.10** Molecular structure of a) substituted pyrrole monomers; b) sulphonated aniline monomer; c) dodecylbenzenesulfonate.

CEPs may also be rendered soluble by using bi-functional counterions such as dodecylbenzenesulfonate (Fig. 1.10c) during processing [56]. The charge on the  $\text{SO}_3^-$  head group forms an ionic bond with the positive proton on the CEP chain while the hydrocarbon tail is dissolvable in organic solvents. Soluble PANi may be processed by this method enabling it to be incorporated into polymer bends.

Template-guided synthesis of CEPs has been reported by S.C. Yang [56, 57]. The molecular template, a polyacid such as polystyrene sulphonic acid, binds the monomer to form molecular complexes which are dispersed in water as colloidal particles. Upon polymerisation, the monomers form the relevant polymer but remain attached to the template to form the template-CEP complex. By the careful choice of the template molecule and the polymerisation conditions, stable sub-micron size colloidal particles may be formed during polymerisation. Bjorklund and Liedberg [58] also observed colloidal formations when pyrrole was oxidised by  $\text{FeCl}_3$  in the presence of aqueous methylcellulose ( $M_n$  100,00), resulting in a PPy.methylcellulose sol being formed. Colloidal polypyrroles prepared in aqueous solutions are generally spherical, while the particle size is dependent on the synthetic conditions. The electrical conductivities of PPy colloids are generally of lesser magnitude than those forms by other means.

As referred to previously chemical deposition may occur in the bulk of the solution. Spontaneous deposition may be encouraged by placing the desired substrate in the polymerisation reaction environment [50]. The conducting polymer then polymerises and simultaneously deposits onto the substrate generating a novel composite material. This method of deposition has been utilised in the development of conducting textiles,

whereby the conducting polymer (PPy, due to its environmental stability) adheres to the textile substrate generating a composite material that retains the inherent properties of the textile (e.g. texture, hand, structure) but is also electro-conductive due to the presence of the PPy layer on the material.

## 1.8 NON CONDUCTING POLYMERIC MATERIALS

### 1.8.1 Polyurethane Foam

The polyurethane (PU) foam used in this experiment was soft, sponge like material that could be reversibly compressed. A picture of PU samples received is shown in Fig. 1.11. The PU samples were received from Foam Engineering Ltd, (a foam producing company in High Wycombe, England) in pre-cut sample sheet form. They were referred to as samples PU001-PU003 in Chapter 2. These PU samples varied in terms of density and hardness. Because it was our intention to use the developed sensors repeated in applications of high load (20-30 kg), the hardest PU (PU003) was selected as the base substrate for prototype development. All samples were washed in soapy water, titrated with Milli-Q water and oven dried before use. Samples were cut to size from the sheets.

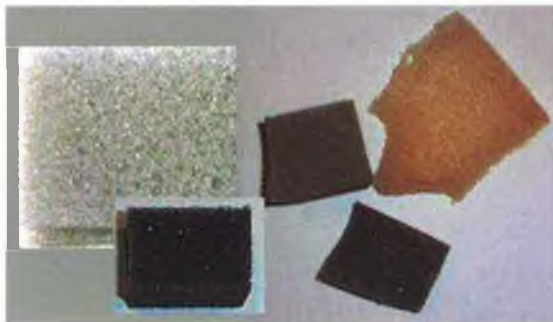


**Fig. 1.11** Selection of uncoated polyurethane foam from IRETEX, Kayfoam and Foam Engineering Ltd (18/125).

Polyurethane is a heterogeneous polymer. Generally its morphology is composed of short alternating block of hard and soft segments. The soft segment has a low glass transition temperature ( $T_g$ ) polyether, polyester or polyalkanediol, whereas the hard segment has a high  $T_g$  aromatic diisocyanate, linked with a low molecular weight chain extender [59].

The glass transition temperature is a phase change that is observed in amorphous polymers, characteristic of the polymer. Below a polymer's  $T_g$ , the polymer is brittle

and fragile, and will shatter if placed under any force, a similar phenomenon observed with glass. Above the polymer's  $T_g$  however, the chains of the polymer move more freely and the result is that the polymer is more elastic or rubber in nature and is able to resist a limited force placed upon it without permanently disrupting the polymer.

Polyurethanes are formed when isocyanate ( $\text{-N=C=O}$ ) reacts with a hydroxyl compound ( $\text{R-OH}$ ) according to the schematic shown in Fig. 4.3.2.

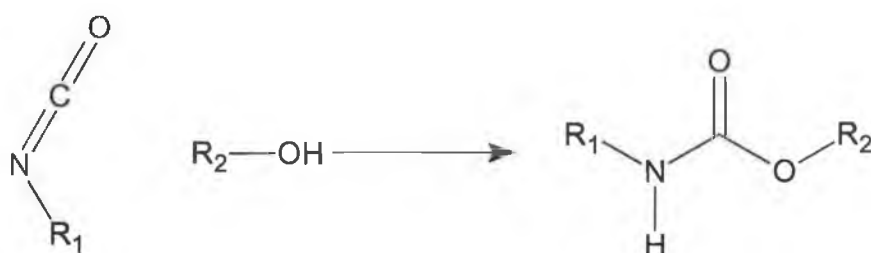


**Fig. 1.12** Reaction pathway for the polymerisation of polyurethane.

They contain a urethane linkage  $\text{R}_1\text{HN-C(=O)OR}_2$ , see Fig. 1.12. When a diisocyanate reacts with a diol, a linear polyurethane is obtained, whereas when the diisocyanate reacts with a polyol, a cross-linked polymer is formed. The urethane group does not usually contribute to the functionality of the polymer rather it incorporates functional groups within its matrix. Therefore, the properties of the polyurethane can be tailored by incorporation of the relevant functional group.

The diol can be replaced with a diamine, producing a polyurea. This polymer has alternating stiff domains separated by soft rubbery urea sections which characterise the polymer's elastomeric capabilities. Though this polymer was synthesised from diamine groups, this polymer is still referred to as polyurethane.

Polyurethanes can exist in various forms from rigid thermoset polymer to flexible soft elastomers to additives found in paint. They are very crystalline structures and are often used as copolymers with soft rubbery polymers. Another variant of the polyurethane polymer is foam structure.

Polyurethane foams can be classified as rigid or flexible foams. Rigid foams are closed cell structures that are highly cross-linked. They have good resistance to organic solvents and inorganic substances. Rigid foams are used mainly in the area of thermal insulation and in the area of aeronautical manufacture. Flexible foams are open cell structures and are resistant to detergents and solvents and are inert to oxidation. These types of foams are used in upholstery, clothing and packaging.

Polyurethane flexible foams are characterised by their density and also their hardness. The density of the foam is measured as the weight per volume of the foam ( $\text{kg/m}^3$ ). This term differs from the firmness or “hardness” of the foam. The latter value refers to the indentation force deflection (IFD) capability of the foam. The IFD is calculated by determining the force required to compress a 50 square inch circular indenter foot into a 4 inch thick sample (15 square inch or larger) to a stated percentage of the sample's initial height. Common IFD values are generated at 25% & 65% of the initial height [60]. The values for hardness are G which refer to N/kg. The surface of polyurethane is hydrophilic due to the presence of NH and C=O bonds in the polymer backbone and so provides a suitable site for polypyrrole deposition.

### 1.8.2 Polyethylene Foam

Polythelyene (PE) is another solid foam, compressible, but structurally harder than polyurethane. PE foam samples were received from Foam Engineering Ltd., High Wycombe, England, in sheet form. They were washed with soapy water and rinsed with water and oven dried before use. A picture of the foam together with the chemical structure of PE are shown in Fig. 1.13.

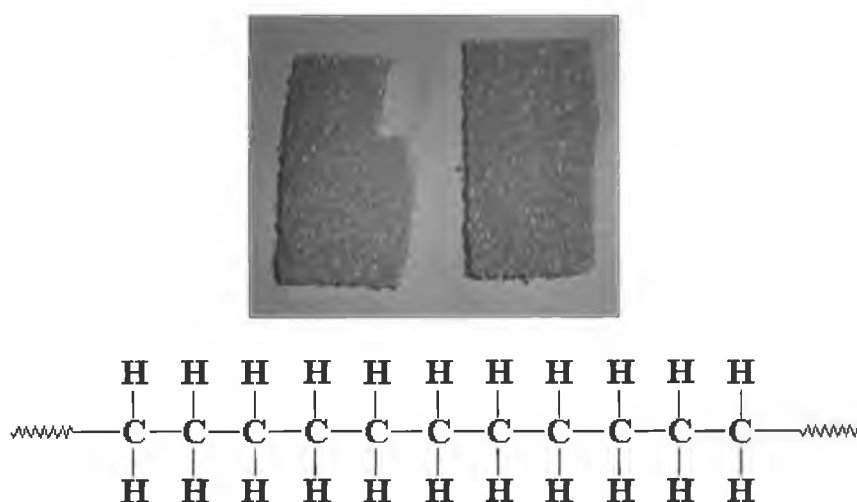


**Fig. 1.13**      **Photograph of PE foam and molecular structure.**

As can be seen in Fig. 1.13, polyethylene is, structurally, a very simple polymer. It only contains two elements; carbon and hydrogen and is non-polar in nature. It is quite versatile, found in numerous items, such as shopping bags, children's toys and bullet-proof vests. Crosslinking is possible by replacing hydrogens with other polyethylene chains. Linear polyethylene (or high density polyethylene *HDPE*) is much stronger than branched polyethylene (low density polyethylene *LDPE*), though the latter is much cheaper and so more cost-friendly for manufacturing. Ultra-high molecular weight polyethylene can also be fabricated, particularly in a fibrous fashion. These fibres are so strong that they can replace Kevlar in bullet-proof vests.



### 1.8.3 Other Solid Foams

#### *Specialised solid foams: Aveleo™*

Aveleo is a specialised polyolefin foam, produced by Aveleo™ especially for insoles, both for sporting and orthopaedic shoes. Thus, this substrate would be particularly suitable for applications such as prototype insole development. Aveleo is a closed cell polyethylene based foam shown in Fig. 1.14. It is cross-linked, is semi-rigid and self supporting and has a low specific weight. It is also free of CFCs, HCFCs plasticizers or heavy metal compounds. It is designed to be comfortable to wear, inert with a long-shelf life, non-colour staining, shock absorptive and aesthetically pleasing.

#### *Viscoelastic Foam: Kaymed Visco™*

Viscoelastic foam was originally developed by NASA for astronauts' seats to help reduce the pressure of G-forces and of spending a long time sitting in the same position. This open-cell foam is temperature sensitive, that is, when cold it is firm. However, if it is heated, e.g. by body-heat, it becomes soft and compresses easily. Thus, if someone were to sit or lie on it, the foam would compress, redirecting the pressure away from the points of contact throughout the entire foam matrix. If the source of pressure were then removed, the foam returns to its original shape. However, it does so very slowly, leaving an impression on the foam face. For this reason visco-elastic foam is sometimes referred to as “memory” foam [61, 62].



**Fig. 1.14** Left: Photograph of Aveleolen® received from IRETEx, right: Slow relaxation characteristic of visco-elastic foam [62].

*Fabric-based material: Polartec®*

The Polartec® material is a spacer material, spongy and compressible like the foam. It is designed so that it can stretch in four directions, including compression of the fabric.

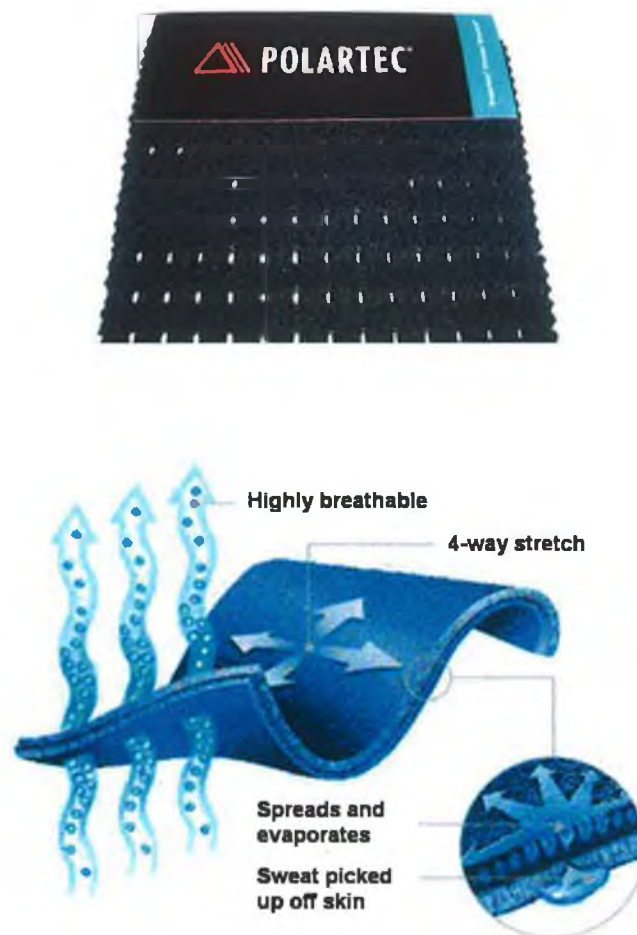


**Fig. 1.15** Detailed structure of Polartec® power stretch® [63].

## 1.9 COMPOSITE MATERIALS

Recently, tremendous advances have occurred in the development of various polymeric materials, seeing them supplant conventional materials such as metals and alloys in various applications, such as the automobile industry, the aerospace industry, the manufacture of household goods or light engineering machinery to name but a few. This replacement of materials brings about cost-effectiveness, reduction in size and weight, novel designs and new concepts in material science.

If polymers can be made conductive such as CEPs then the range of tools for communication to and control of the polymer's functions can be greatest expanded to include:

- *Electrochemical methods*; cyclic voltammetry (CV) or amperometric analysis can yield information such as the charge efficiency of a film during oxidation and reduction of the film. Peak separation is dependent on the polymer composition and preparation conditions.
- *Dynamic contact angle measurements*; this technique allows polymer-solvent interactions to be measured [64] providing information on the surface tension and the wettability of a polymer surface as a function of its redox state [65].
- *Resistometry*; this techniques involves the measurement of resistance changes of conducting polymers [66] to monitor effects of polymer thickness and cationic species of the supporting electrolyte.
- *UV-vis and Raman spectroscopy*; light absorption causes electronic transitions between the valence and conduction bands and the specific peaks in the spectrum are indicative of the nature of the charge carriers and the number of charge carriers present.
- *In-situ mechanical testing*; qualitative mechanical information enables the determination of parameters such as inherent stiffness, toughness & maximum stress resulting in permanent sample deformation [67, 68].

Other techniques which can be used for analysing CEP based sensors include quartz crystal microgravimetry and scanning probe microscopy.

CEPs, however, have limited physical and chemical properties, thus other techniques must be employed to make polymers conductive. That of composite-formation has been commercially exploited. This technique involves polymeric materials, such as those listed in section 1.8, being mixed with conductive fillers such as carbon black, acetylene black, carbon film, metal powders or CEPs. By combining conductive and non-conductive polymeric components, novel composite materials can be generated. These materials merge together the benefits of both constituent parts. There are a number of drawbacks with these materials:

1. their conductivity is highly dependent on processing conditions
2. an insulating surface layer often forms
3. articles may become brittle due to heavy loading of filler.

Smart textiles, however, are an example of novel conductive composite generated by such a merger.

#### **1.9.1 Smart Textiles**

The textile industry is focused on providing materials, yarns, clothing etc for consumer world at large. Recently a new field of research has emerged which has combined the benefits of the textile industry with the world of electronics and technology yielding products and devices referred to as electronic (e-) or smart textiles [69]. Smart textiles do not refer to materials such as breathing (air conditioning), fire-resistance, ultra-strong fabrics etc., but rather smart textiles are “wearable” materials and are able to perform local monitoring and computation and may also be coupled with wireless communication capabilities. The technology can incorporate a fibre, yarn or other textiles and enables or enhances its interaction with the environment or user. Thus, the characteristics associated with comfort and wearability (properties of standard, non-electronic garments are retained whilst integration of the technology is achieved. Many textile-based sensors are actually sensing materials used to coat a textile [70] or conductive/sensing materials formed into fibers and woven or knitted into a textile structure [71, 72].

### 1.10 APPLICATIONS FOR POLYMER COMPOSITE SYSTEMS

The potential applications of conducting polymers alone have been discussed in numerous reviews [12, 13, 69, 73-75]. There has been a rapid increase in the number of publications since the early 1980's, shown graphically in Fig. 1.16, reflecting the realisation that conducting polymers are a versatile product with numerous applications.

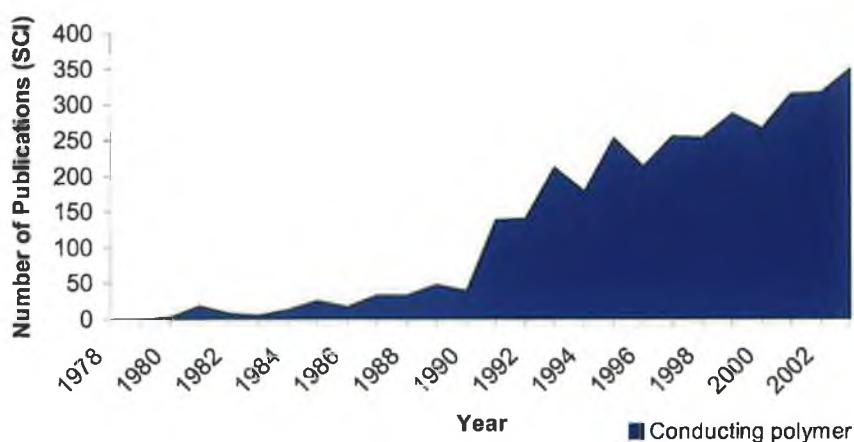


Fig. 1.16 Number of scientific papers published and patents issued in the area of conducting polymers for the past 25 years (source: own results from searching on Web of Science Citation Index).

In brief these applications lie in a number of technologies including:

- *Electrostatic discharge*; where the conducting polymeric film provides anti-static protection for electronic components.
- *Battery technology*; where the anode, cathode and electrolyte are of polymeric origin and are n- or p-doped to establish a cell potential between the electrodes.
- *Supercapacitor technology*; where the doped polymeric film utilise the redox properties of the polymer to store charge within.
- *Photovoltaics*; where the absorption of solar energy by a photosensitive conducting polymeric film results in the generation of an e.m.f in the associated circuitry.

- *Electrochromics*; where conducting polymers undergo a distinct colour change when the surrounding environment is changed, albeit by the application of an external potential, elevated temperatures or the presence of organic solvents [76].
- *Electroluminescence devices*; where electrons are injected from the cathode (aluminium, calcium or indium) and holes are injected from the anode (ITO) into the conducting polymer sandwiched between the electrodes. When the holes and electrons are injected into the polymer, they form positively and negatively charged polarons that can migrate under an applied field and radiatively recombine when they meet yielding electroluminescence [77].
- *Actuators*; where a volume change occurs when the polymer is oxidised and reduced due to ion movement in and out of the polymer.
- *Separation devices*; where the volume change incurs by oxidation and reduction of the conducting polymer is used to control the pore size of the separation membrane[78]. Selectivity to certain ions is based on size and charge.
- *Microfluidic controller*; by switching the reduction-oxidation (redox) state of a conducting polymer, the surface tension or wettability at the surface of the polymer thin film is controlled.
- *Corrosion protection*; conducting polymers in paints can provide sacrificial protection for metals in corrosive environments [79, 80].

However, if CEPs are combined with non-conducting polymer materials further applications, especially in the sensor technology, open up for these novel composite materials. These include: wearable physical and wearable chemical sensors. The conductive component possible due to the presence of the CEPs

### 1.10.1 Sensors

Computerization impacts on every aspect of modern life and society, but as we know, computers are inherently configured to process digitized data. This data must be collected, stored if required, and transferred to a computer from which useful content can be extracted, processed and interpreted. Sources for this data are generally textual, graphical, audio or sensor based. Sensors are interesting sources of data as they convert changes in the real world to detectable signals for the digital world through the following steps:

1. the ability to generate a selective response to a particular target species.
2. the ability to couple a transduction mechanism that will reliably relay the information detected by the sensor.
3. the ability to transfer the information in a reliably but energy inexpensive manner between point of detection and logging system.

Examples of the specific responses required occur during events such as enzyme-substrate reactions [81-85], calixarene host-guest [86, 87] or antibody-antigen [88, 89] interactions. Though these interactions occur on the nano- and sub-nanoscale scale, the use of sensors enables us to access this information. Thus a gateway between the molecular world and the digital world is realised.

### 1.11 WEARABLE SENSORS

The simultaneous miniaturisation of electronic components along with the increase of their complexity and ability has assisted with the advances in sensor research; the greatest benefit being the reduction of power consumption of these components. Also miniaturisation makes these sensors portable, enabling their use as on-body sensors or wearable systems. If we are to gather data from wearable sensors, then the computation devices and communication modules should also be wearable, lest we end up with a situation depicted in Fig. 1.17. Wearable systems can be broadly defined as mobile electronic devices that can be unobtrusively embedded in the users' outfit as part of the clothing or as an accessory.



**Fig. 1.17      The wearable PC?**

These systems differ from conventional mobile systems, in that they are operational and accessible with minimum disturbance to user activity. Wearable systems range from micro sensors that may integrate into clothing [90], to watches [91], rings [92], walking canes [93] or belt-worn PCs with a head mounted display [94].

When designing sensing systems, thought must be given to the users' of the system, both their requirements but also their sensory, physical and mental capabilities. Thus, the use of wearable sensors, which propose to integrate seamlessly into the user's personal space, should be of enormous benefit by limiting issues such as device accommodation and manipulation. However, a possible shortcoming of wearable sensors is the limited range of parameters that may be measured due to the reduced contact area between the body area, for example, the wrist or finger, and the device. One solution to this limitation could be the integration of sensors into a wearable platform that has a large area of contact with the body.

#### *Integration of sensors into wearable garments*

Integration can potentially occur on three different levels:

1. solutions adapted to clothes (e.g. mobile phone in the pocket),
2. electronics or micro-systems integrated in clothes or textiles with connectable modules and
3. functions integrated into textiles via direct insertion into the textile fibres (e.g. woven displays).



Unfortunately micro-electronic devices do not readily integrate into textiles and in most cases are stitched onto the fabric or hidden in the textile structure. Previous approaches to wearable monitoring of body functions and movements have been made using conventional components such as microcontrollers, LEDs, accelerometers, gyroscopes, strain gauges [95], piezoelectric materials [96, 97], fibre-optics [98], optoelectronic components [92] and pressure sensors [99, 100], incorporated into the user's clothing via a wristband, ring (Fig. 1.19) or strap of some form. Fig. 1.18 & Fig. 1.19 show further examples of integration strategies adopted by research groups and industries to incorporate micro-electronic devices into garments and wearable devices. These include the use of affixing components into place and making connections to them by sewing or embroidering conductive tracking with metallic yarns (Fig. 1.18), or by using metallic snap-fasteners to make the connections as shown in Fig. 1.18 & Fig. 1.19.

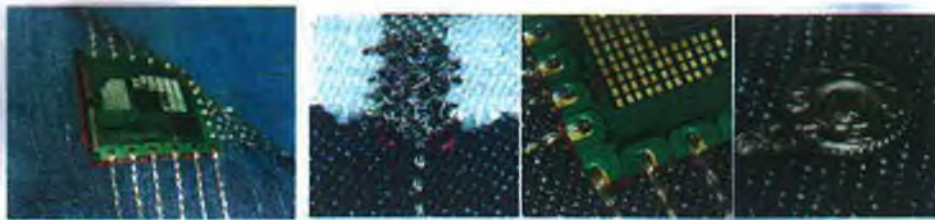


**Fig. 1.18** Left, flex sewed on textile (Fraunhofer IZM Berlin) [101], middle and right, embroidered interconnections for textile keypads, flexible electronic modules and snaps [102].



**Fig. 1.19** Left, embroidered circuit for mobile phone module, middle, display module attached with snaps [102], right, Conceptual diagram of a "heart monitoring" ring sensor [103, 104].

While this approach of using micro-electronics can offer precise monitoring of determined parameters, it requires the user to compromise their physical comfort in order to accommodate the device and will result in lower compliance with the device.

In certain applications this is an important issue. Clearly, it would be better if the device were to “disappear” into the user’s environment. This can be achieved in particular, through the use of textile-integration and textile-based sensors. It is the vision of many research and industrial institutes to integrate computers and sensors into clothing so that they are not just portable but truly wearable [105, 106]. Textile-based sensors avoid the problem of device discomfort by retaining the characteristics of the textile, i.e. comfort and wearability, while performing as a sensor and providing information to the user. Many academic and industrial projects exist at present, to investigate the potential of textile-based sensors for health monitoring purposes. Two examples include the SmartShirt™ developed by Sensatex [107] and the WEALTHY project [108], a pan-European based academic project (Fig. 1.20).

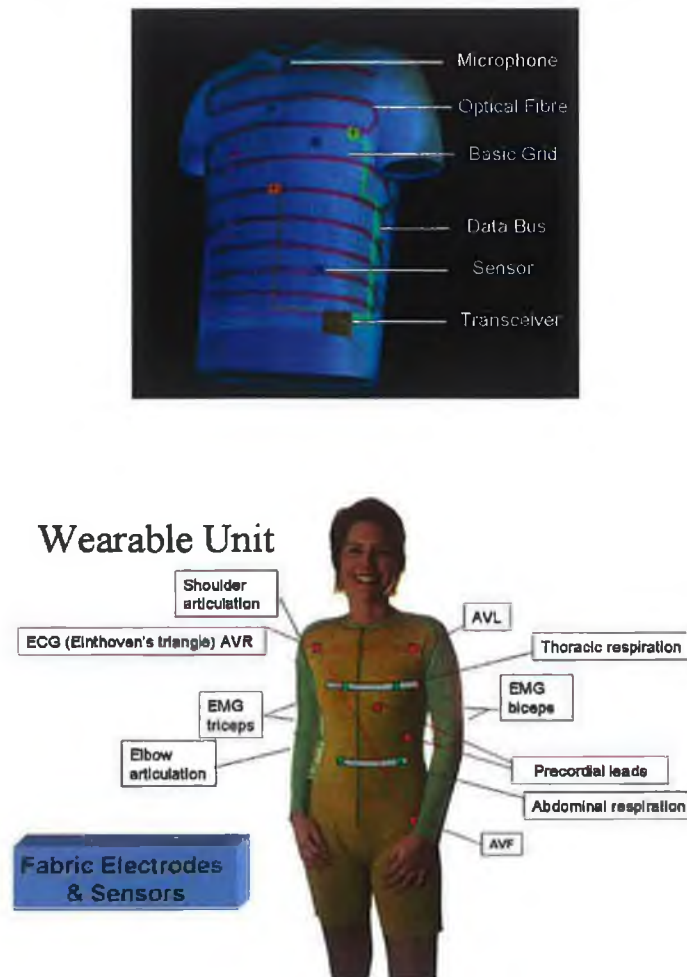


**Fig. 1.20** Examples of textile integrated and textile based sensors: (top) Sensatex’s ® SmartShirt, (bottom) Wealthy ® wearable ensemble [109].

In the context of wearable systems, monitoring can be categorized as either:

1. “Inward Looking”, i.e., to measure state and activity of the user, including movement, activity, and vital signs such as ECG, body temperature, cardiac frequency, respiration, blood oxygen saturation ( $SpO_2$ ), or as
2. “Outward Looking”, i.e., to measure parameters in the surrounding environment, for example in emergency/disaster situations, or in extreme environments as may arise during military actions and space experiments, and in certain sports, such as mountain climbing.

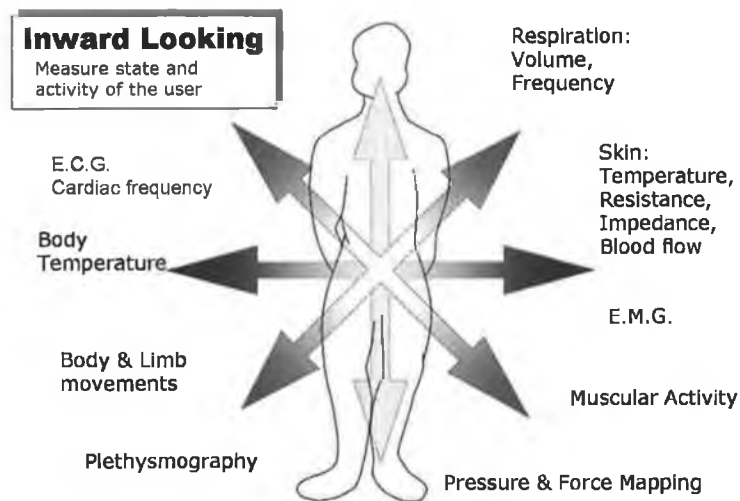


**Fig. 1.21** Inward Looking, schematic of the various internal parameters which could be monitored for a user's benefit.

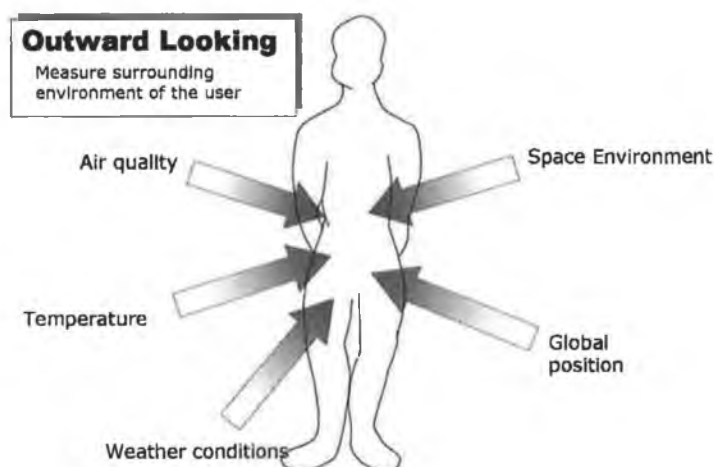


**Fig. 1.22** Outward Looking, schematic of the various external parameters that could be monitored for a user's benefit.

The PPy-coated PU foams presented in this thesis maybe utilized in either category, as pressure sensors, to monitor plantar pressure underfoot during walking or as a chemo-sensor that can be integrated in the wearer's clothing to monitor the chemical environment of the user. In all cases, however, it is desirable that the availability of information regarding the physical condition of the wearer, or his/her environment, should not compromise the comfort of the wearer.

#### **1.11.1 Impact of wearable sensors**

Traditional bio-monitoring technologies are rarely designed for continuous, on-body use; at present many of the medical devices used for sensing and bio-monitoring operate periodically, are invasive, or require clinical infrastructure for operation. This is often dictated by the level of precision and quality of signal required for medical analysis, as this can directly influence the clinical outcome of patient. However, this type of clinical monitoring only provides a brief window on the physiology of the patient. There are major limitations to this type of monitoring which include the failure to sample rare events of diagnostic, prognostic and therapeutic importance, failure to measure normal, or background, physiological responses as occur during activity, rest or sleep that reflect the progression of a condition. Continuous monitoring and recording of relevant physiological signals therefore offer a crucial improvement to these limits imposed by traditional monitoring schemes [110-112].

Thus, a niche for wearable sensors is highlighted. Continuous monitoring with wearable sensors is possible because the comfort element of the sensors prolongs user-compatibility and wireless capture of the data means that the wearer is free to pursue their daily activities without need to be confined to a laboratory or clinical setting. The sensors will need to provide reliable results under a wide range of working conditions, be robust against external physical, electrical and electromagnetic disturbances, and should not be easily broken, even when instructions for use are violated as it may be possible that the operators will be non-specialised. At present wearable sensors have been implemented in non-critical monitoring of patients [110] and people over long periods and has great implications for several disciplines such as rehabilitation [113, 114], sports medicine and ergonomics. In principle these devices have enormous

potential [115, 116] and are in many cases generating a paradigm shift from cure to prevention and from hospital-based healthcare to point-of-need diagnosis [117].

## 1.12 COMMUNICATION

Communication between sensors and retrieval of information is another important consideration in wearable technology. Communication networks are at the heart of modern society. The digitisation of communications and the availability of relatively inexpensive but powerful mobile computing technologies have established a global communication network capable of linking billions of people, places and objects. This pervasive technology means that people in research and industry now have multiple daily interactions with this digital technology. The means of connection to this communication network is of fundamental importance if a truly wearable sensor is to succeed. A wired system, though robust, often incurs high maintenance and will limit the freedom of the wearer, therefore hampering the retrieval of a true reflection of the wearer's activity. A wireless system would, therefore, be of more benefit but the integration of such a system brings with it its own added difficulties.

A wireless sensor network by definition [118] must include all of the following:

- Bi-directional communication with at least two nodes
- A sensor
- Networking software
- Network must be part of a LAN (local area network) and/or is connected to a gateway for Wide Area communications
- Single hops between nodes or nodes and gateway must be, on average, less than 1 mile (1500 m)

Wireless sensor networks enable dense sensing of an area, be it on the body or the surrounding space of the subject, see Fig. 1.23. Each node is a discrete sensor system, that contains a sensing, transduction and communication platform and so can monitor any number of pre-determined parameters, be they external or internal as described previously. By positioning these nodes on the body, information from all these points can be gathered simultaneously at the communication hub, generating a detailed overview of the status of the user. This hub may be a PDA device or a mobile phone,

which can enable the user to access the responses of each or all of the sensors. The information from this discrete “Body Sensor (or Area) Network” (BSN/BAN) may be transferred to an internet-enabled platform.

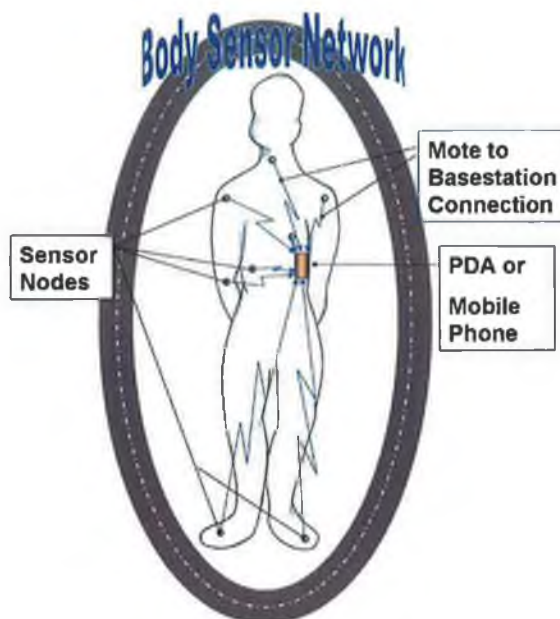


**Fig. 1.23** Schematic of Body Sensor Network (BSN), showing discrete sensor nodes positioned on the body, communicating with the central information centre.

In effect, the BSN becomes a mobile sensor node within a wider-based community sensor network (Fig. 1.24), enabling the monitoring and control of parameters, and situations at the Internet level. The storage of BSN data in an internet-level platform enable authorised users to access information regarding the status of the BSN user(s) or the environment in which the BSN user(s) is located. The communication is bidirectional. This enables relevant alerts to be sent to the BSN user depending on their condition and/or location. The use of such communicating networks has been shown to enhance the quality of life of its users [119, 120], where continuous monitoring was carried out without compromising the daily routine of the users. Many patients could benefit from continuous monitoring as part of a diagnostic procedure, optimal maintenance of chronic conditions or during supervised recovery from an acute event or surgical procedure, e.g. stroke rehabilitation, physical rehabilitation after hip or knee surgeries, myocardial infarction rehabilitation and traumatic brain injury rehabilitation. The assessment of the effectiveness of rehabilitation procedures has been limited to the

laboratory setting; relatively little is known about rehabilitation in real-life situations. Estimates can only be drawn from questionnaires, measures of heart rate, video assessment etc. Miniature wireless, wearable technology offers a tremendous opportunity to address this issue.

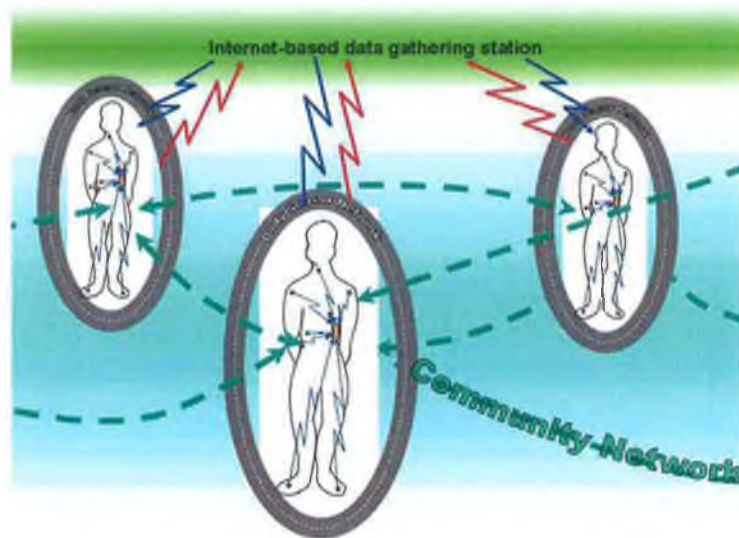


**Fig. 1.24** Schematic of BSNs functioning as sensor nodes within a wider-base community network by communicating with one another and an internet-based platform.

Factors which have limited the acceptance of continuous monitoring include:

- unwelding wires between the sensors and the monitoring system
- lack of system integration of individual sensors
- interference on a wireless communication channel shared by multiple devices
- non-existent support for massive data collection and knowledge discovery[121].



### 1.13 MARKET POTENTIAL

Research within the area of smart textiles and wireless communications have grown increasingly over recent years. In Fig. 1.25, the segments of interest where smart textiles and wearable devices are currently being investigated are listed, together with an indication of their “commercial attractiveness” in the following pie chart.

The attractiveness scores (range 1-10, where 1 = least attractive, 10 = most attractive) were determined using the following criteria:

- The extent of the final product’s demand / technology uptake on a global basis
- Indicative growth prospects
- Competitive pressure at the textile producer level and the proportion of the end-products’ value credited to the textile producer
- Barriers to entry, which determine long-term profit protection.

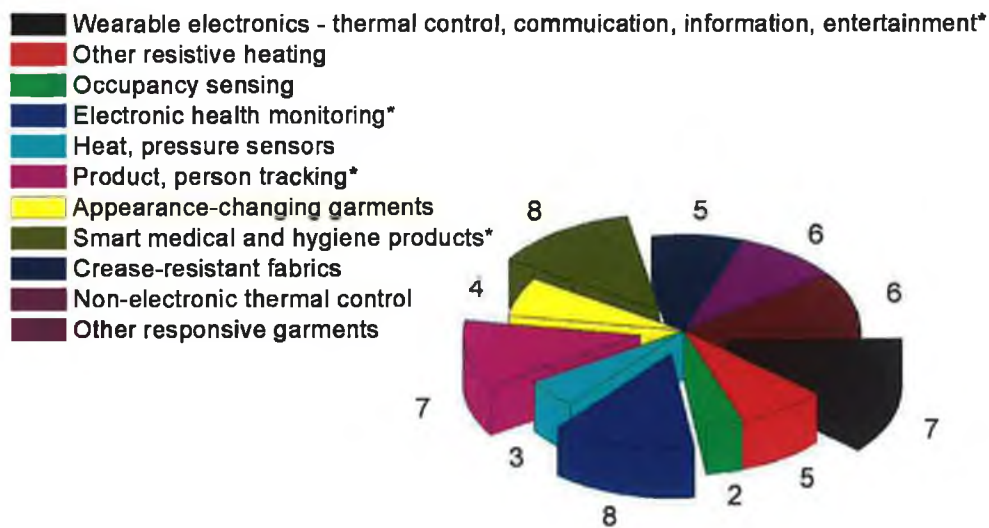


**Fig. 1.25** A pie chart showing the areas of research and technology where wearable systems have the most commercial potential. Those of greatest attractiveness are indicated with an asterisk.

While some segments face significant technological roadblocks or continue to experience the problem of relating the incremental cost of technologies to the value of



the derived benefit to the end-user, some smart textile products have been successfully introduced across a variety of applications. These tend to be socially-driven and include the medical healthcare [117, 122], automotive and protective clothing fields. Although the extent of technology integration is still rather low, the situation is improving, as novel textile technologies are being developed, e.g. flexible electronic components.

Several wireless sensor network markets were launched in 2005, and according to the report by ON world, [118], the increasing commercial adoption and customer deployment is accelerating. It is believed that this technology will have a profound impact on many markets and become ubiquitous within the next decade. Indeed, even in their “most conservative forecast” ON world predict that 127 million wireless sensors network nodes will be deployed worldwide by 2010 for an end user market worth \$8.3 billion.

In order to leverage BSN for use as a remote monitoring tool, several issues and considerations must be taken into account during the designs and development of the supporting platforms. These issues reflect both commercial and social needs, the more important ones being reliability, scalability, ease of use, energy constraints, security, and extra-BSN network restrictions [123]. These factors are part of the reason why it is challenging to agree on standards for wireless protocols, e.g. Zigbee, which have hitherto made the commercial sector cautious in adopting this technology.

## 1.14 CONCLUSION

Today's world of continuous bombardment of information has forced us to adopt new ways and methods to collect, process and distribute this information. Computers have become ubiquitous in the workplace and in home environments, collecting and processing this information as required, however all too often the level of human-machine interaction required to deal with this information load distracts the person from completing their work task. Mobile computing solutions aimed at reducing this level of interaction are still too complex, too obtrusive and too demanding on the user to be seamlessly integrated into complex work-processes and their usability in industrial scenarios and acceptance by workers is still limited. Approaches are being adopted [124] where software and hardware systems are being created in which users can be mobile but at the same time be fully integrated into the surrounding smart IT infrastructure.

The development of smart systems, where sensors and communication structures are all integrated, will have a huge impact on all society, especially the healthcare service, in electronic health monitoring and wearable electronics. These systems, for example will provide physicians with data for the timely detection and management of health risks, diagnosing early illnesses or injury, recommending treatment that would prevent further deterioration and enable confident professional decisions to be made based on objective information all in a reasonably short time. In addition it will be possible for the wearer to perform normal daily activities in a more "natural" environment without any discomfort.

If these smart systems could incorporate the use of the textile technology then there is an additional benefit that the realisation of customised sensor interfaces that can be specialised according to the final target and specific applications can be achieved in a cost effective manner.

The primary objective for research in this area is to combine functionality (i.e. ability to sense a useful parameter) with ease of integration into clothing, and comfort for the wearer. This combination, as has been showed with previous examples, to be

successful by coating textiles and fabrics with conducting polymers, especially polypyrrole, to develop sensor that detect biomedical actions. While these sensors are able to detect movement through the stretch of the material they are not as sensitive at detecting vertical pressures. Thus, it is our intention to coat polypyrrole onto compressible polymeric and textile-based substrates, such as open-cell foam structures, that are soft so that they can also be incorporated into wearable garments. This would increase the range of movements that would be detectable by polypyrrole-coated material sensors.

Another aspect of wearable sensor to consider is whether comfortable factor compromises the quality of signal detectable from the device. The issue is to determine whether the wearability of the sensor renders the signal unusable or whether there is a potential use for such a device? It has been our intention to show that it possible to make sensors that are comfortable to wear and that these sensors can indeed generate good quality output signals that can be transmitted and analysed to build-up an informative picture for the user in a number of different applications.

## 1.15 REFERENCES

1. Houghton, M., *The American Heritage Dictionary of the English Language*. 4th Edition ed. 2000: Houghton Mifflin Company.
2. DuPont.com: Annual Review, <http://www1.dupont.com/NASApp/dupontglobal/corp/index.jsp?page=/content/US/en/US/overview/glance/review/index.html>, Last Accessed: 18 November 2004, (2004)
3. Baekland, L., *Method of Making Insoluble Products of Phenol & Formaldehyde*, in *United States Patent and Trademark Office*. 1909: U.S.A.
4. Plastics History, <http://www.ftns.wau.nl/agridata/apme/plastics.htm>, Last Accessed: 18 November 2004, (2004)
5. Greene, R.L., Street, G.B., and Suter, L.J., *Superconductivity in Polysulfur Nitride (Sn)X*. *Physical Review Letters*, 1975. **34**(10): p. 577-579.
6. The Nobel Prize in Chemistry, 2000: Conductive Polymers, [http://www.kva.se/KVA\\_Root/files/newspics/DOC\\_200381417268\\_29385176325\\_chemadv00.pdf](http://www.kva.se/KVA_Root/files/newspics/DOC_200381417268_29385176325_chemadv00.pdf), Last Accessed: 25 Sept 2004, (2004)
7. Ansari, R. and Wallace, G.G., *Effect of thermal treatment on the electrochemical properties of conducting polypyrrole polymers*. *Polymer*, 1994. **35**(11): p. 2372-2377.
8. Chiang, C.K., Fincher, C.R., Park, Y.W., Heeger, A.J., Shirakawa, H., Louis, E.J., Gau, S.C., and Macdiarmid, A.G., *Electrical-Conductivity in Doped Polyacetylene*. *Physical Review Letters*, 1977. **39**(17): p. 1098-1101.
9. Dong, S. and Ding, J., *Study on polypyrrole film by electrochemical polymerization in aqueous solution*. *Synthetic Metals*, 1987. **20**(1): p. 119-124.
10. Sharma, A.L., Annapoorni, S., and Malhotra, B.D., *Synthesis and characterization of polynitrosoaniline*. *Polymer*, 2001. **42**(19): p. 8307-8310.
11. Song, Y.X., Wang, H.L., Zheng, Y.S., and Xu, C.X., *Preparation of high conducting polyaniline films and study on their electromagnetic shielding properties*. *Acta Polymerica Sinica*, 2002(1): p. 92-95.
12. MacDiarmid, A.G., *Polyaniline and polypyrrole: Where are we headed?* *Synthetic Metals*, 1997. **84**(1-3): p. 27-34.
13. Gurunathan, K., Murugan, A.V., Marimuthu, R., Mulik, U.P., and Amalnerkar, D.P., *Electrochemically synthesised conducting polymeric materials for applications towards technology in electronics, optoelectronics and energy storage devices*. *Materials Chemistry and Physics*, 1999. **61**(3): p. 173-191.
14. Hatfield, J.V., Neaves, P., Hicks, P.J., Persaud, K., and Travers, P., *Towards an integrated electronic nose using conducting polymer sensors*. *Sensors and Actuators B: Chemical*, 1994. **18**(1-3): p. 221-228.

15. He, F.F., Omoto, M., Yamamoto, T., and Kise, H., *Preparation of Polypyrrole Polyurethane Composite Foam by Vapor-Phase Oxidative Polymerization*. Journal of Applied Polymer Science, 1995. **55**(2): p. 283-287.
16. Joyner, K.H., Copeland, P.R., and MacFarlane, I.P., *An evaluation of a radiofrequency protective suit and electrically conductive fabrics*. Electromagnetic Compatibility, IEEE Transactions on, 1989. **31**(2): p. 129-137.
17. Ranby, B., *Conjugated Polymers and Related Materials: The Interconnection of Chemical and Electronic Structures*, Salaneck, W.R., Lundstrom, I., and Ranby, B., Editors. 1993, Oxford University Press: Oxford. p. Chapter 3.
18. Vuorio, M., Murtomaki, L., Hirvonen, J., and Kontturi, K., *Ion-exchange fibers and drugs: a novel device for the screening of iontophoretic systems*. Journal of Controlled Release, 2004. **97**(3): p. 485-492.
19. Santarosa, V.E., Peretti, F., Caldart, V., Zoppas, J., and Zeni, M., *Study of ion-selective membranes from electrodialysis removal of industrial effluent metals II: Zn and Ni*. Desalination, 2002. **149**(1-3): p. 389-391.
20. Van der Stegen, J.H.G., Veen, A.J.v.d., Weerdenburg, H., Hogendoorn, J.A., and Versteeg, G.F., *Application of the Maxwell-Stefan theory to the transport in ion-selective membranes used in the chloralkali electrolysis process*. Chemical Engineering Science, 1999. **54**(13-14): p. 2501-2511.
21. Chai, X.-S., Samp, J., and Hou, Q.X., *Novel mechanism for the Nafion membrane transfer of anthraquinones*. Journal of Membrane Science, 2006. **271**(1-2): p. 215-220.
22. Jain, S.L. and Sain, B., *Perfluorinated resinsulphonic acid (Nafion-H(R)) catalyzed highly efficient oxidations of organic compounds with hydrogen peroxide*. Applied Catalysis A: General. **In Press, Corrected Proof**.
23. Harmer, M.A. and Sun, Q., *Solid acid catalysis using ion-exchange resins*. Applied Catalysis A: General, 2001. **221**(1-2): p. 45-62.
24. Wang, H. and Xu, B.-Q., *Catalytic performance of Nafion/SiO<sub>2</sub> nanocomposites for the synthesis of [alpha]-tocopherol*. Applied Catalysis A: General, 2004. **275**(1-2): p. 247-255.
25. Seen, A.J., *Nafion: an excellent support for metal-complex catalysts*. Journal of Molecular Catalysis A: Chemical, 2001. **177**(1): p. 105-112.
26. Cheng, X., Yi, B., Han, M., Zhang, J., Qiao, Y., and Yu, J., *Investigation of platinum utilization and morphology in catalyst layer of polymer electrolyte fuel cells*. Journal of Power Sources, 1999. **79**(1): p. 75-81.
27. Fritsch, D., Randjelovic, I., and Keil, F., *Application of a forced-flow catalytic membrane reactor for the dimerisation of isobutene*. Catalysis Today, 2004. **98**(1-2): p. 295-308.
28. Hall, N., *Twenty-five years of conducting polymers*. Chem Commun (Camb), 2003(1): p. 1-4.
29. Heeger, *Handbook of Conducting Polymers*. 2 ed, ed. Skotheim, T.A. Vol. 2. 1986, New York: Marcel Dekker Inc. 688.

30. Heeger, A.J., *Semiconducting and Metallic Polymers: The Fourth Generation of Polymeric Materials*. Angewandte Chemie International Edition, 2001. **40**(14): p. 2591-2611.
31. Shirakawa, H., Louis, E.J., Macdiarmid, A.G., Chiang, C.K., and Heeger, A.J., *Synthesis of Electrically Conducting Organic Polymers - Halogen Derivatives of Polyacetylene, (CH)<sub>x</sub>*. Journal of the Chemical Society-Chemical Communications, 1977(16): p. 578-580.
32. Paul J. Nigrey, A.G.M.a.A.J.H., *Electrochemistry of polyacetylene, (CH)<sub>x</sub>: electrochemical doping of (CH)<sub>x</sub> films to the metallic state*. Journal of the Chemical Society, Chemical Communications, 1979. **14**: p. 594-595.
33. Zotti, G., *Electrochemical Synthesis of Polyheterocycles and their Applications*, in *Handbook of Organic Conductive Molecules and Polymers: Vol 2. Conductive Polymers: Synthesis and Electrical Properties*, Nalwa, H.S., Editor. 1997, John Wiley & Sons Ltd. p. 137-162.
34. Huckel, E.Z., Physik, 1931. **70**: p. 204-286.
35. Pople, J.A. and Walmsley, S.H., *Bond Alternation Defects in Long Polyene Molecules*. Molecular Physics, 1962. **5**(1): p. 15-20.
36. Su, W.P., Schrieffer, J.R., and Heeger, A.J., *Solitons in Polyacetylene*. Physical Review Letters, 1979. **42**(25): p. 1698-1701.
37. Wallace, G.G., Spinks, G.M., Kane-Maguire, L.A.P., and Teasdale, P.R., *Conductive Electroactive Polymers*. 2nd ed. Intelligent Materials System. 2003: CRC Press.
38. Ge, H. and Wallace, G.G., *Electrochemically Controlled Liquid Chromatography on Conducting Polymer Stationary Phases*. Journal of Liquid Chromatography, 1990. **13**: p. 3245-3261.
39. Bredas, J.L. and Street, G.B., *Polarons, Bipolarons, and Solitons in Conducting Polymers*. Accounts of Chemical Research, 1985. **18**(10): p. 309-315.
40. Various, *Handbook of Conducting Polymers*. 2 ed, ed. Skotheim, T.A. Vol. 2. 1986, New York: Marcel Dekker Inc. 688.
41. Diaz, A.F. and Kanazawa, K.K., *Extended Linear Chain Compounds*, ed. Miller, J.S. Vol. 3. 1982, New York: Plenum Press. 417.
42. Lewis, T.W., Wallace, G.G., Kim, C.Y., and Kim, D.Y., *Studies of the overoxidation of polypyrrole*. Synthetic Metals, 1997. **84**(1-3): p. 403-404.
43. Lewis, T.W., Spinks, G.M., Wallace, G.G., Mazzoldi, A., and De Rossi, D., *Investigation of the applied potential limits for polypyrrole when employed as the active components of a two-electrode device*. Synthetic Metals, 2001. **122**(2): p. 379-385.
44. Diaz, A.F. and Bargon, J.F., in *Handbook of Conducting Polymers*, Skotheim, T.A., Elsenbaumer, R.L., and Reynolds, J.R., Editors. 1986, Marcel Dekker, Inc.: New York. p. 81.

45. Skaarup, S., Bay, L., Vidanapathirana, K., Thybo, S., Tofte, P., and West, K., *Simultaneous anion and cation mobility in polypyrrole*. Solid State Ionics, 2003. **159**(1-2): p. 143-147.
46. Skaarup, S., West, K., Gunaratne, L., Vidanapathirana, K.P., and Careem, M.A., *Determination of ionic carriers in polypyrrole*. Solid State Ionics, 2000. **136**: p. 577-582.
47. Tang, M., Wen, T.-Y., Du, T.-B., and Chen, Y.-P., *Synthesis of electrically conductive polypyrrole-polystyrene composites using supercritical carbon dioxide: I. Effects of the blending conditions*. European Polymer Journal, 2003. **39**(1): p. 143-149.
48. Tang, M., Wen, T.-Y., Du, T.-B., and Chen, Y.-P., *Synthesis of electrically conductive polypyrrole-polystyrene composites using supercritical carbon dioxide: II. Effects of the doping conditions*. European Polymer Journal, 2003. **39**(1): p. 151-156.
49. Shenoy, S.L., Kaya, I., Erkey, C., and Weiss, R.A., *Synthesis of conductive elastomeric foams by an in situ polymerization of pyrrole using supercritical carbon dioxide and ethanol cosolvents*. Synthetic Metals, 2001. **123**(3): p. 509-514.
50. Malinauskas, A., *Chemical deposition of conducting polymers*. Polymer, 2001. **42**(9): p. 3957-3972.
51. Gregory, R.V., Kimbrell, W.C., and Kuhn, H.H., *Conductive Textiles*. Synthetic Metals, 1989. **28**(1-2): p. C823-C835.
52. Tan, S.N. and Ge, H.L., *Polymer*, 1996. **37**: p. 965.
53. MacDiarmid, A.G., Akhtar, M., Chiang, C.K., Cohen, M.J., Kleppinger, J., Heeger, A.J., Louis, E.J., Milliken, J., Moran, M.J., Peebles, D.L., and Shirakawa, H., *Electrically Conducting Covalent Polymers - Halogen Derivatives of (Sn)X and (Ch)X*. Journal of the Electrochemical Society, 1977. **124**(8): p. C304-C304.
54. Ito, T., Shirakawa, H., and Ikeda, S., *Simultaneous Polymerization and Formation of Polyacetylene Film on Surface of Concentrated Soluble Ziegler-Type Catalyst Solution*. Journal of Polymer Science Part a-Polymer Chemistry, 1974. **12**(1): p. 11-20.
55. Chiang, C.K., Park, Y.W., Heeger, A.J., Shirakawa, H., Louis, E.J., and MacDiarmid, A.G., *Conducting Polymers - Halogen Doped Polyacetylene*. Journal of Chemical Physics, 1978. **69**(11): p. 5098-5104.
56. Sato, M., Tanaka, S., and Kacriyama, K., *Journal of Chemical Society of Chemical Communications*, 1985: p. 713.
57. Sun, L., Yang, S.C., and Liu, J.M., *Molecular Complex of Polyaniline and Polyelectrolyte*. Polymer (Preprints), 1992. **33**: p. 379.
58. Bjorklund, R.B. and Liedberg, B., *Electrically Conducting Composites of Colloidal Polypyrrole and Methylcellulose*. Journal of the Chemical Society-Chemical Communications, 1986(16): p. 1293-1295.
59. Mahesh, G.N., Banu, P., and Radhakrishnan, G., *Investigations on polyurethane ionomers. II. 3,4-dihydroxycinnamic acid-based anionomers*. Journal of Applied Polymer Science, 1997. **65**(11): p. 2105-2109.

60. Test Method ASTM D3574, <http://www.pfa.org/glossary.html>, Last Accessed: 17 FEB 06, (2006)
61. Viscoelastic foam, <http://www.absolutecomfortonsale.com/sensus-memory-foam-3inch.htm>, Last Accessed: 16 FEB 06, (2006)
62. Visco Foam - Space Age Protection against Tossing and Turning, [http://www.magnadreampad.com/m\\_visco\\_foam.htm](http://www.magnadreampad.com/m_visco_foam.htm), Last Accessed: 16 FEB 06, (2006)
63. Polartec Power Stretch, <http://www.houdinisportswear.com/produkter/material/stretchinsulation.html>, Last Accessed: 16 FEB 06, (2006)
64. Bartlett, P.N., Grossel, M.C., and Barrios, E.M., *Electrochemistry and contact angle measurements on polymer films of omega-(3-pyrrolyl)-alkanoic acids in aqueous solution*. Journal of Electroanalytical Chemistry, 2000. **487**(2): p. 142-148.
65. Feng, L., Li, S.H., Li, Y.S., Li, H.J., Zhang, L.J., Zhai, J., Song, Y.L., Liu, B.Q., Jiang, L., and Zhu, D.B., *Super-hydrophobic surfaces: From natural to artificial*. Advanced Materials, 2002. **14**(24): p. 1857-1860.
66. Talaie, A. and Wallace, G.G., *Resistometry: A new characterization technique for conducting polymers*. Solid State Ionics, 1994. **70-71**(Part 1): p. 692-696.
67. Ding, J., Liu, L., Spinks, G.M., Zhou, D.Z., Wallace, G.G., and Gillespie, J., *High performance conducting polymer actuators utilising a tubular geometry and helical wire interconnects*. Synthetic Metals, 2003. **138**(3): p. 391-398.
68. Spinks, G.M., Wallace, G.G., Ding, J., Zhou, D., Xi, B., and Gillespie, J., *Ionic liquids and polypyrrole helix tubes: bringing the electronic Braille screen closer to reality*. Smart Structures and Materials 2003: Electroactive Polymer Actuators and Devices (EAPAD). 2003. **5051**: p. 372-380.
69. Marculescu, D., Marculescu, R., and Khosla, P.K. *Challenges and opportunities in electronic textiles modeling and optimization*. in *Design Automation Conference, 2002. Proceedings. 39th*. 2002.
70. De Rossi, D., Carpi, F., Mazzoldi, A., Paradiso, R., Scilingo, E.P., and Tognetti, A., *Electroactive Fabrics and Wearable Biomonitoring Devices*. AUTEX Research Journal, 2003. **3**(4).
71. Hertleer, C., Grabowska, M., Van Langenhove, L., Catrysse, M., Hermans, B., Puers, R., Kalmar, A., Van Egmond, H., and Mattys, D. *Towards a Smart Shirt*. in *Proceedings of Wearable Electronic and Smart Textiles*. 2004. Leeds, UK.
72. Farrington, J., Moore, A., Tilbury, N., Church, J., and Biemond, P. *Wearable Sensor Badge & Sensor Jacket for Context Awareness*. in *International Symposium of Wearable Computing*. 1999.
73. Honeybourne, C.L., *Solid Thin-Films of Extended Pi-Systems - Deposition, Characterization and Application*. Journal of Physics and Chemistry of Solids, 1987. **48**(2): p. 109-141.



74. Kaner, R.B. and Macdiarmid, A.G., *Plastics That Conduct Electricity*. Scientific American, 1988. **258**(2): p. 106.
75. Kanatzidis, M.G., *Conductive Polymers*. Chemical & Engineering News, 1990. **68**(49): p. 36.
76. Kane-Maguire, L.A.P., Pomputtkul, Y., Strounina, E.V., Moulton, S.E., Innis, P.C., and Wallace, G.G. *Conformational Changes in poly(2-methoxyaniline-5-sulfonic acid) induced by solvent and temperature*. in *International Conference of Synthetic Metals*. 2004. Wollongong, Australia: University of Wollongong.
77. Parker, I.D., *Journal of Applied Physics*, 1994. **75**: p. 1656.
78. Lee, H.S. and Hong, J., *Chemical synthesis and characterization of polypyrrole coated on porous membranes and its electrochemical stability*. *Synthetic Metals*, 2000. **113**(1-2): p. 115-119.
79. Gelling, V.J., Wiest, M.M., Tallman, D.E., Bierwagen, G.P., and Wallace, G.G., *Electroactive-conducting polymers for corrosion control: 4. Studies of poly(3-octyl pyrrole) and poly(3-octadecyl pyrrole) on aluminum 2024-T3 alloy*. *Progress in Organic Coatings*, 2001. **43**(1-3): p. 149-157.
80. Yang, S.C., Racicot, R.J., Clark, R.L., Liu, H., Brown, R., and Alias, M.N., *Electroactive polymer coatings for corrosion control*, in *USA*. 1995, The Board of Governors for Higher Education, State of Rhode Island and (Providence, RI): USA.
81. McQuade, D.T., Pullen, A.E., and Swager, T.M., *Conjugated polymer-based chemical sensors*. *Chemical Reviews*, 2000. **100**(7): p. 2537-2574.
82. Killard, A.J., Zhang, S., Zhao, H., John, R., Iwuoha, E.I., and Smyth, M.R., *Development of an electrochemical flow injection immunoassay (FIIA) for the real-time monitoring of biospecific interactions*. *Analytica Chimica Acta*, 1999. **400**(1-3): p. 109-119.
83. Hammerle, M., Schuhmann, W., and Schmidt, H.-L., *Amperometric polypyrrole enzyme electrodes: effect of permeability and enzyme location*. *Sensors and Actuators B: Chemical*, 1992. **6**(1-3): p. 106-112.
84. Schuhmann, W., *Amperometric substrate determination in flow-injection systems with polypyrrole--enzyme electrodes*. *Sensors and Actuators B: Chemical*, 1991. **4**(1-2): p. 41-49.
85. Schmidt, F.J., Aalders, A.L., Schoonen, A.J.M., and Doorenbos, H., *Calibration of a Wearable Glucose Sensor*. *International Journal of Artificial Organs*, 1992. **15**(1): p. 55-61.
86. Diamond, D., *Calixarene-Based Sensing Agents*. *Journal of Inclusion Phenomena and Molecular Recognition in Chemistry*, 1994. **19**(1-4): p. 149-166.
87. Schazmann, B., McMahon, G., Nolan, K., and Diamond, D., *Identification and recovery of an asymmetric calix[4]arene tetranitrile derivative using liquid chromatography and mass spectrometry*. *Supramolecular Chemistry*, 2005. **17**(5): p. 393-399.

88. Gooding, J.J., Wasiowych, C., Barnett, D., Hibbert, D.B., Barisci, J.N., and Wallace, G.G., *Electrochemical modulation of antigen-antibody binding*. Biosensors and Bioelectronics, 2004. **20**(2): p. 260-268.
89. Killard, A.J., Deasy, B., O'Kennedy, R., and Smyth, M.R., *Antibodies: production, functions and applications in biosensors*. TrAC Trends in Analytical Chemistry, 1995. **14**(6): p. 257-266.
90. Burton Analog Clone MD Snowboarding Jacket, [http://www.minidisc.org/part\\_Burton\\_Analog\\_Clone\\_MD\\_Snowboarding\\_Jacket.html](http://www.minidisc.org/part_Burton_Analog_Clone_MD_Snowboarding_Jacket.html). Last Accessed: 02 FEB 06, (2006)
91. Atzmon, O., *Innovative Mobile-Health Solutions Promise to Improve Elderly Care and Save Costs*. MST News, 2005. **5**: p. 42-44.
92. Rhee, S., Yang, B.-H., and Asada, H. *The ring sensor: A new ambulatory wearable sensor for twenty-four hour patient monitoring*. in *20th Annual International Conference IEEE Engineering in Medicine and Biology Society*. 1998. Hong Kong.
93. Ritz, M. and Konig, L., *Laser Technique Improves Safety for the Blind*. MST News, 2005. **5**: p. 39-40.
94. Anon. in *International Symposium on Wearable Computing*. 2002. University of Washington.
95. Spinks, G.M., Wallace, G.G., Liu, L., and Zhou, D., *Conducting polymers electromechanical actuators and strain sensors*. Macromolecular Symposia, 2003. **192**: p. 161-169.
96. Ishida, R., Yonezawa, Y., Maki, H., Ogawa, H., Ninomiya, I., Sada, K., Hamada, S., Hahn, A.W., and Caldwell, W.M., *A wearable, mobile phone-based respiration monitoring system for sleep apnea syndrome detection*. Biomed Sci Instrum, 2005. **41**: p. 289-293.
97. Paradiso, R., Loriga, G., and Taccini, N., *A wearable health care system based on knitted integrated sensors*. IEEE Trans Inf Technol Biomed, 2005. **9**(3): p. 337-44.
98. Davies, M.L., Hamilton, C.J., Murphy, S.M., and Tighe, B.J., *Polymer membranes in clinical sensor applications: I. An overview of membrane function*. Biomaterials, 1992. **13**(14): p. 971-978.
99. Someya, T., Sekitani, T., Iba, S., Kato, Y., Kawaguchi, H., and Sakurai, T., *A large-area, flexible pressure sensor matrix with organic field-effect transistors for artificial skin applications*. PNAS, 2004. **101**(27): p. 9966-9970.
100. Locher, I., Kirstein, T., and Troster, G., *From Smart Textiles to Wearable Systems*. MST News, 2005. **2**: p. 12-13.
101. Strese, H., John, L.G., and Kaminorz, Y., *Technologies for Smart Textiles*. MST News, 2005. **2**: p. 6-7.
102. Kallmayer, C., Linz, T., Aschenbrenner, R., and Reichl, H., *System Integration Technologies for Smart Textiles*. MST News, 2005. **2**: p. 42-43.

103. Rhee, S., Yang, B.H., and Asada, H.H., *Artifact-resistant power-efficient design of finger-ring plethysmographic sensors*. Ieee Transactions on Biomedical Engineering, 2001. **48**(7): p. 795-805.
104. Yang, B.H. and Rhee, S., *Development of the ring sensor for healthcare automation*. Robotics and Autonomous Systems, 2000. **30**(3): p. 273-281.
105. Marculescu, D., Marculescu, R., Zamora, N.H., Stanley-Marbell, P., Khosla, P.K., Park, S., Jayaraman, S., Jung, S., Lauterbach, C., Weber, W., Kirstein, T., Cottet, D., Grzyb, J., Troster, G., Jones, M., Martin, T., and Nakad, Z., *Electronic textiles: A platform for pervasive computing*. Proceedings of the Ieee, 2003. **91**(12): p. 1995-2018.
106. Cottet, D., Grzyb, J., Kirstein, T., and Troster, G., *Electrical characterization of textile transmission lines*. Ieee Transactions on Advanced Packaging, 2003. **26**(2): p. 182-190.
107. SmartShirt, <http://www.sensatex.com/>, Last Accessed: 10 AUG 06, (2006)
108. Wealthy - Wearable Health Care System, <http://www.wealthy-ist.com/>, Last Accessed: 10 AUG 06, (2006)
109. WEALTHY, <http://www.wealthy-ist.com>, Last Accessed: 03 FEB 06, (2006)
110. Bonato, P., *Wearable sensors/systems and their impact on biomedical engineering*. IEEE Eng Med Biol Mag, 2003. **22**(3): p. 18-20.
111. Binkley, P.F., *Predicting the Potential of Wearable Technology*. Ieee Engineering in Medicine and Biology Magazine, 2003. **22**(3): p. 23-24.
112. Engin, M., Demirel, A., Engin, E.Z., and Fedakar, M., *Recent developments and trends in biomedical sensors*. Measurement, 2005. **37**(2): p. 173-188.
113. Huch, M. and Strese, H., *Ambient Assisted Living - Preparing an Article 169 Measure*. MST News, 2005. **5**: p. 8-10.
114. Asada, H.H., Shaltis, P., Reisner, A., Rhee, A., and R.C., H., *Mobile monitoring with wearable photoplethysmographic biosensors*. Ieee Engineering in Medicine and Biology Magazine, 2003. **22**(3): p. 28-40.
115. Dittmar, A., Delhomme, G., and Roussel, P., *Biomedical Micro-sensor and Micro-systems*. REE, 1997. **8**: p. 13-22.
116. Sommer, T.J., *Ambient Assisted Living Initiative for the Ageing Population: Rationale, Opportunities, Challenges and Impact: the MST Case*. MST News, 2005. **5**: p. 6-8.
117. Lymberis, A. and Olsson, S., *Intelligent biomedical clothing for personal health and disease management: State of the art and future vision*. Telemedicine Journal and E-Health, 2003. **9**(4): p. 379-386.
118. On World, *Wireless Sensor Networks - Growing Markets, Accelerating Demand*, 2005,
119. Kwon, H.S. and et al, *Establishment of blood glucose monitoring system using the Internet*. Diabetes Care, 2004. **27**: p. 478-483.

120. Park, S. and Jayaraman, S., *Enhancing the Quality of Life Through Wearable Technology*. Ieee Engineering in Medicine and Biology Magazine, 2003. 22(3): p. 41-48.
121. Jovanov, E., Milenkovic, A., Otto, C., and de Groen, P.C., *A wireless body area network of intelligent motion sensors for computer assisted physical rehabilitation*. J Neuroengineering Rehabil, 2005. 2(1): p. 6.
122. Troster, G., Kirstein, T., and Lukowicz, P., *Motion Aware Clothing for the Personal Health Assistant*. Studies in Health Technology and Informatics, 2005. 117: p. 63-71.
123. Van Halteren, A., Bults, R., Wac, K., Dokovsky, N., Koprnikov, G., Widya, I., Konstantas, D., and Jones, V., *Wireless Body Area Networks for Healthcare: the MobiHealth Project*, in *Wearable eHealth Systems for Personalised Health Management*, Lymberis, A. and De Rossi, D., Editors. 2004, IOS Press: Amsterdam. p. 181-193.
124. An Integrated Project in the Sixth Framework Programme,  
<http://www.wearitatwork.com/>. Last Accessed: 30 NOV 05, (2005)

## **Chapter 2 MATERIALS & METHODS**

## 2.1 INTRODUCTION

### 2.1.1 Preparation of PPy-coated materials via chemical deposition

As mentioned previously, in Chapter 1, polypyrrole (PPy) can be synthesised chemically into powders and fibres. It is possible to deposit PPy onto a number of substrates, be they hard (PMMA channels) or soft (Lycra, Nylon). The ability to deposit PPy onto soft materials is beneficial because the resulting composite material retains the soft tactile properties of the fabric, while becoming conductive due to the presence of PPy, thus it can be easily integrated into clothing as required. The degree of conductivity (and conversely resistivity) of the composite material has been shown previously to be affected by parameters such as concentration of conducting polymer [1] doping, polymeric defects and amount of conjugation along the chain. When it is connected into a simple voltage divider circuit, electrons will pass through the material. This output signal at  $V_{out}$  is proportional to the resistance of the foam,  $R_{foam}$ , which in turn is dependent on the status and surrounding environment of the material.

It has been shown that strain gauges could be constructed from polypyrrole both in pure film form and coated fabric form (PPy-Lycra) [2, 3]. Our aim is to develop a similar sensor based on a PPy-composite which will be soft and compressible so that it can be easily integrated into clothing without compromising the comfort of the wearer. Applications for this such as pressure event detection due to biomimetic actions can then be realised. For this reason an open-cell solid foam was targeted as the substrate of choice for PPy deposition. The greatest change of dimensions for this type of material occurs when it is exposed to vertical forces such as compressions to which it responded reversibly. The porosity and large surface area of this type of material are also beneficial in the application of gaseous analyte detection. In this chapter, a number of substrates and preparation techniques were examined for the purpose of developing a prototype material.

### 2.1.2 Characterisation techniques

#### *Electrical behaviour*

Current will always prefer to flow through the least resistive pathway, thus the more conductive pathway present in the material, the more current will pass through it. In 1826 a German physicist, Georg Simon Ohm discovered that current flowing through a material was directly proportional to the electrical force that produced it. This relationship is known as Ohm's law, (Equation 2.1) where  $V$  represents the voltage, in volts, or electromotive force which produces the current,  $i$ , (in Ampere), and  $R$  represents the electrical resistance in Ohms.

$$V = iR$$

Equation 2.1

Therefore, at constant voltage the amount of current flowing through a material is inversely proportional to the resistance of the material. PPy is electroactive. By depositing PPy onto a substrate the whole material is rendered electroactive. Thus, when the PPy-PU foam is connected into a circuit and held under constant voltage, current will flow through the material. This yields a resistance value for the material. Because the electrical conductivity of the material is facilitated by the PPy, the resistance of the material should be dependent on the amount of PPy deposited onto it. Retrieval of information from the sensing device employed these assumptions in order to characterise the behaviour of the substrate after deposition of PPy.

### *Surface Topology*

The surface area of a material is important in many aspects of chemistry, in particular in many important industrial processes such as:

1. Heterogeneous catalysis
2. Semi-conductor thin film (micro-electronics)
3. Corrosion (thin film coatings)
4. Electrochemical processes (adsorption).

Chemical reactions that occur at the surface of solids may differ sharply from reactions in the bulk, due in part to the presence of additional reaction pathways of much lower activation energy at the surface, hence facilitating the reaction to proceed. Many catalysts, such as microporous aluminosilicates and zeolites, are materials of high surface area facilitating many reactions to proceed more efficiently.

A material with a large surface area is indicative of a porous material, the higher the surface area the larger the pores. Finely detailed surface structures also increase the surface area of a material, a mechanism utilised in biomedical systems such as the kidney or the lungs (Fig. 2.1). Indeed, a technique often used to increase the surface area of a material is to roughen its surface, thus inducing these fine structures on its surface and increasing its surface area.

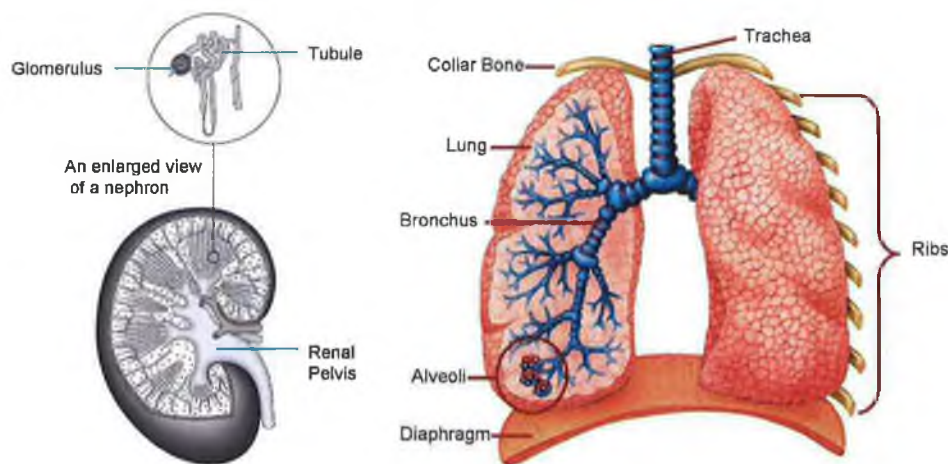


**Fig. 2.1** Schematic of kidney and lungs systems with a close-up of the fine detailed structure of the Glomerulus and the alveoli respectively, to increase the surface area within the organ [11, 12].



Examination of the surface of the coated and uncoated materials was performed in order to enable characterisation. This was carried out by examining each sample with a scanning electron microscope.

While an optical microscope (Greek: micron = small and scopos = aim) is an instrument commonly used for viewing objects that are too small to be seen by the naked or unaided eye [13], it was found to be unsuitable for surface topology examination due to the limit of resolution (0.2 micrometres ) caused by the inherent diffraction of light. If, instead of light rays, beams of electrons, which have much smaller wavelength than visible light are used then images of greater resolution can be achieved. Then, rather than relying on refraction, lenses for electron microscopes rely on a magnetic fields that are approximately parallel to the direction that electrons travel. Variants of electron microscopes include:

- Scanning electron microscope (SEM): electrons bombard the surface of the specimen and are gathered to generate an image of the topology of the specimen.
- Transmission electron microscope (TEM): electrons pass through the specimen and generate images of the specimen's crystallographic structure.

In an SEM (shown graphically in Fig. 2.2) the electrons are emitted thermionically from a tungsten or lanthanum hexaboride ( $\text{LaB}_6$ ) cathode (Fig. 2.2(1)) and are accelerated towards an anode (Fig. 2.2(2)). The electron beam, which typically has an energy ranging from a few hundred eV to 50 keV, is focused by one or two condenser lenses into a beam with a very fine focal spot sized 1 nm to 5 nm. The beam passes through pairs of scanning coils in the objective lens (Fig. 2.2(3 & 4)), which deflect the beam in a raster fashion over a rectangular area of the sample surface. As the primary electrons strike the surface of the specimen ((Fig. 2.2(5)) they are inelastically scattered by atoms in the sample.

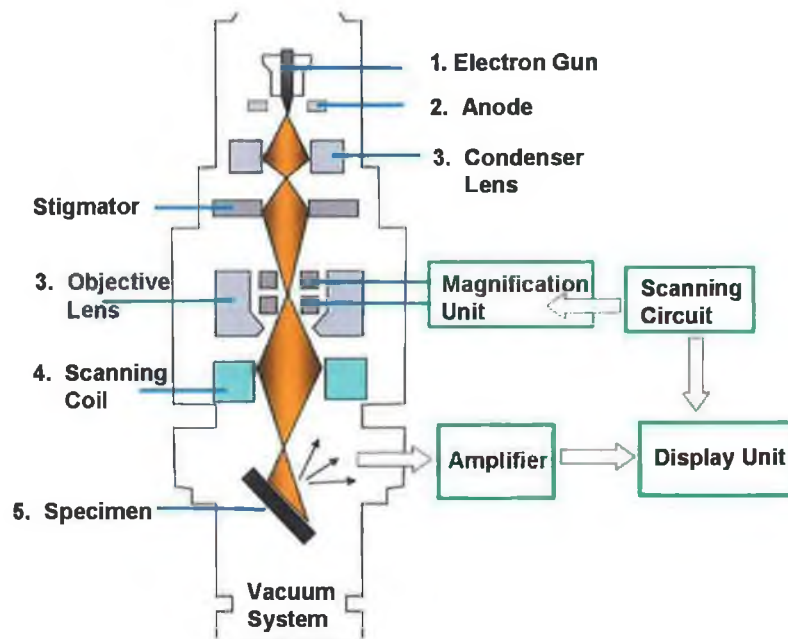


**Fig. 2.2 Schematic drawing of the electron optics of a SEM.**

Through these scattering events (shown in Fig. 2.3) the primary electron beam effectively spreads and fills a teardrop-shaped volume, known as the interaction volume, extending about less than 100 nm to 5  $\mu\text{m}$  depths into the surface. Interactions in this region lead to the subsequent emission of secondary electrons which are then detected to produce an image. X-rays, which are also produced by the interaction of electrons with the sample, may also be detected in an SEM equipped for energy dispersive X-ray (EDX) spectroscopy or wavelength dispersive X-ray spectroscopy.

The most common imaging mode monitors low energy ( $<50\text{ eV}$ ) secondary electrons. Due to their low energy, these electrons originate within a few nanometers from the surface. The electrons are detected by a scintillator-photomultiplier device and the resulting signal is rendered into a two-dimensional intensity distribution that can be viewed and saved as a digital image. This process relies on a raster-scanned primary beam. The brightness of the signal depends on the number of secondary electrons reaching the detector. If the beam enters the sample perpendicular to the surface, then the activated region is uniform about the axis of the beam and a certain number of electrons "escape" from within the sample. As the angle of incidence increases, the

"escape" distance of one side of the beam will decrease, and more secondary electrons will be emitted. Thus, steep surfaces and edges tend to be brighter than flat surfaces, which results in images with a well-defined, three-dimensional appearance. Using this technique, resolutions less than 1 nm are possible.

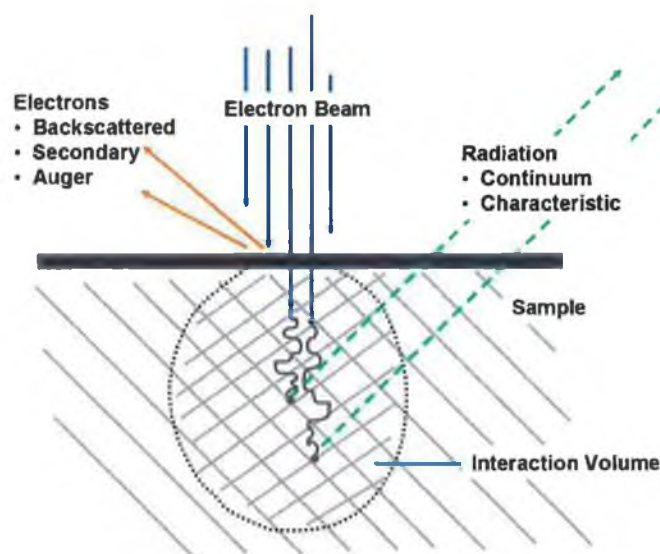


**Fig. 2.3 Schematic illustration of electron beam interaction with a solid with generation of secondary radiation as a result of fluorescence excitation by primary radiation.**

The spatial resolution of the SEM depends on the size of the electron spot which in turn depends on the magnetic electron-optical system which produces the scanning beam. The resolution is also limited by the size of the interaction volume, or the extent of material which interacts with the electron beam. The spot size and the interaction volume are both very large compared to the distances between atoms, so the resolution of the SEM is not high enough to image down to the atomic scale, as is possible in the transmission electron microscope (TEM). The SEM has compensating advantages, though, including the ability to image a comparatively large area of the specimen; the ability to image bulk materials (not just thin films or foils); and the variety of analytical modes available for measuring the composition and nature of the specimen. Depending on the instrument, the resolution can fall somewhere between less than 1 nm and 20 nm.

Thus, SEM images were taken of the coated and uncoated materials to observe what changes PPy deposition incurs on the substrate.

#### *Determination of Surface Area using the Randles-Sevcik's Equation*

Electrochemical techniques, as discussed previously in Chapter 1 have been employed to communicate with and characterize conducting polymer systems. Some of the techniques which have proven successful include chronoamperometry, chronopotentiometry, chronocoulometry, sweeping voltammetry, and impedance measurements. It is possible to obtain information such as charge capacity, doping concentration, and redox states by monitoring the polymer's electrochemical response to a particular procedure. These polymeric systems may be complex, as discussed previously again (Chapter 1) but still follow conventional Nernstian electrochemical rules. For example, the surface area of an electrode can be deduced by measuring the peak currents,  $i_p$ , from the voltammograms for an electrochemical system run at different scan rates. This relationship derived by Randles and Sevcik is described as follows [14]:

$$i_p = 0.4463 \left( \frac{F^3}{RT} \right)^{1/2} n^{3/2} A D_0^{1/2} C_O^* \nu^{1/2}$$

**Equation 2.2**

where,  $n$  is the number of electrons appearing in half-reaction for the redox couple,  $\nu$  is the rate at which the potential is swept (V / sec),  $F$  is Faraday's constant (96485 C / mol),  $A$  is the electrode area (cm<sup>2</sup>),  $R$  is the universal gas constant (8.314 J / mol K),  $T$  is the absolute temperature (K), and  $D$  is the analyte's diffusion coefficient (cm<sup>2</sup>/sec) and  $C_O$  is the initial concentration of the species to be oxidised.

If the temperature is assumed to be 25°C (298.15 K), the Randles-Sevcik equation can be written in a more concise form,

$$i_p = (2.69 \times 10^5) n^{3/2} A D_0^{1/2} C_O^* \nu^{1/2}$$

**Equation 2.3**

where the constant is understood to have units of  $C \text{ mol}^{-1} \text{V}^{-1/2}$

According to Equation 2.3, a linear relationship exists between the peak current, measured in Amperes, for a given electrochemical system and the square root of the scan rate used to drive the electrochemical reaction. This relationship is controlled by a number of other factors, the number of electrons involved in the electrochemical reaction,  $n$ , the area of the working electrode,  $A$ , the diffusion coefficient,  $D_0$ , and the concentration of the oxidised species,  $C_0$ . Thus, by plotting a graph of  $i_p$  vs.  $v^{1/2}$ , it would be possible to determine the area of the working electrode, given that all other factors are known.

PPy in its oxidised state is conducting and as such is electroactive. Thus, by using a piece of PPy-PU as a working electrode within an electrochemical setup, it may be possible to determine the area of said electrode using the Randles-Sevcik's equation.

#### *Determination of the piezoresistive behaviour of the PPy-coated PU foam*

It is our intention to coat the entire substrate (e.g. PU foam) with conducting PPy, therefore rendering the material electrically resistive. PU is a porous compressible material onto which the PPy was deposited. If the material were to be compressed, the foam structure would collapse leading to an increase in the number of contact points through the foam (Fig. 2.4). If the PU foam was coated throughout with PPy, this compression would imply that there was also an increase in the conductive pathways throughout the foam. Therefore, there would be more conductive pathways throughout the foam, making it less resistive. This bringing together of conduction pathways through the material is similar to the percolation effect observed in materials such as carbon black-loaded polymers. The resistance of the material therefore would expect to contain two regions, divided by a critical point, after which the resistance of the material changes dramatically due to the percolation effect. A similar response is observed when using PPy-PU foam whereby the mechanical stress induces the percolation effect on the measured resistance. Thus, the sensing device functions as a piezoresistive material, indicating changes in compressive forces as peaks of current or troughs of resistance. In the following sections, the mechanical and electrical properties of the PU and PPy-PU foam were investigated.

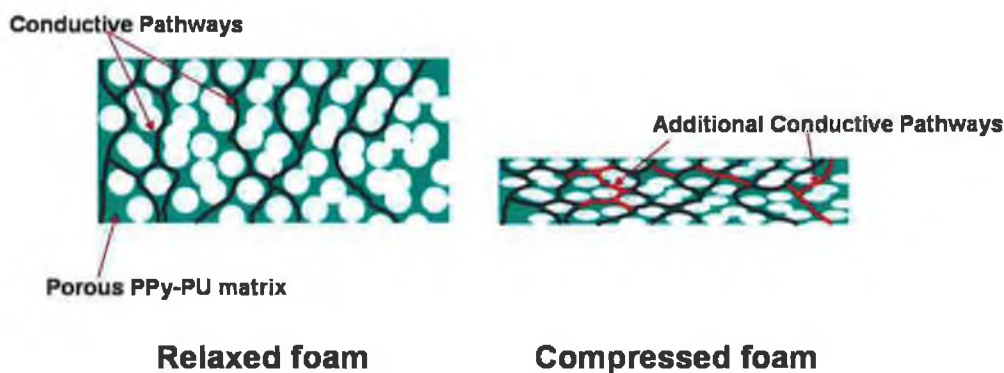


**Fig. 2.4** Schematic of PPy-PU foam relaxed and compressed, showing the presence of additional conductive pathways leading to a change in the measured resistance.

## 2.2 MATERIALS

A number of substrate materials were selected for deposition, to assess whether deposition was achievable. From these materials, a suitable substrate was selected for prototype development.

### 2.2.1 Substrates

Solid foam synthesis, as described in the following section on polyurethane (PU), requires much specialised equipment and so was not carried out in the laboratory. Instead samples of various solid foams were obtained from a number of commercial companies. Their details as available are listed in the following table, Table 2.1

**Table 2.1** Inherent Properties of acquired solid foam samples.

ID Number	Material	Source	Density (kg/m <sup>3</sup> )	Hardness <sup>1</sup> (G)
PU001	Polyurethane (PU)	Foam Engineering Ltd	18	125
PU002	PU	Foam Engineering Ltd.	29	170
PU003	PU	Foam Engineering Ltd.	21	250
PE001	Polyethylene (PE)	Foam Engineering Ltd.	18	-
PE002	PE <sup>2</sup>	Foam Engineering Ltd.	45	-
PU004	PU	Iretex	-	-
AV001	Aveleo	Iretex	-	-

<sup>1</sup> The values for hardness are quoted as G; G = N/kg

<sup>2</sup> PE refers to polyethylene foam

*Polyurethane Foam (PU)*

PU foam samples were received from Foam Engineering Ltd., High Wycombe, England, and IRETEX, Leixlip, Ireland in sheet form. They were washed with soapy water and rinsed with water and oven dried before use.

*Polyethylene Foam (PE)*

PE foam samples were received from Foam Engineering Ltd., High Wycombe, England, in sheet form. They were washed with soapy water and rinsed with water and oven dried before use.

*Specialised solid foams: Aveleo™*

A sample of Aveleo was received from IRETEX, Leixlip, Ireland. The sample was washed with soapy water, rinsed with Milli-Q water and dried prior to deposition of PPy.

*Viscoelastic Foam: Kaymed Visco™*

Samples of viscoelastic foam were received from Kayfoam Ltd., Dublin. They were washed with soapy water, rinsed with Milli-Q water and dried prior to deposition of PPy.

*Fabric-based material: Polartec®*

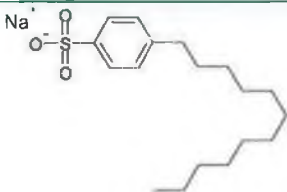
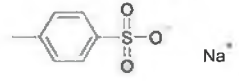
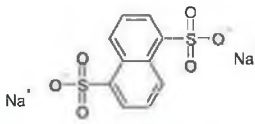
The sample of Polartec® was received from Polartec®. It was washed with soapy water, rinsed with Milli-Q water and dried prior to deposition of PPy.



### 2.2.2 Reagents

It has been shown that doping PPy with acids will improve the conductivity of the polymer [9, 10]. This is achieved by enhancing the long-term stability of the polymer's conductivity by localising charge within the polymeric structure. Three different sulphonic acid-salts, listed in Table 2.2, were selected to observe the changes the dopant anion has on the resulting material.

**Table 2.2** List of dopant anions used for polymerisation of PPy

NAME	ACRONYM	STRUCTURE	MOLECULAR WEIGHT (g/mol)
Dodecylbenzene sulfonic acid, sodium salt	DBSA		348.48
p-Toluene sulfonic acid, sodium salt	pTSA		194.18
1,5-Naphthalenedisulphonic acid, disodium salt	NDSA		332.25

All chemical were received from Sigma Aldrich, and used as received. All solutions were prepared using Milli-Q water. Pyrrole was received from Sigma-Aldrich. It was distilled and stored under nitrogen in a fridge at 4°C prior to use. All solutions were made up with Milli-Q water.

## 2.3 EXPERIMENTAL

### 2.3.1 Deposition Procedure

The following coating procedure was used for the coating of all the above-mentioned materials. The “smart” materials were prepared by the in situ chemical polymerisation of the monomer pyrrole, to retain the inherent properties present in the original substrate. The chemical polymerisation of pyrrole was a modified version of that used by Oh [15].

The following describes the quantities and procedure used for the deposition of polypyrrole onto a piece of polyurethane foam of dimensions  $10 \times 5 \times 2.5 \text{ cm}^3$ , using a 250 ml solution of pyrrole/NDSA and 250 ml solution of  $\text{FeCl}_3$ . Although the volumes of solutions changed depending on the dimensions of the material to be coated, the molar quantities of the solution remained constant and in a constant ratio with one another.

A 250 ml solution containing 0.04M pyrrole and 5.4mM of the dopant anion was prepared using Milli-Q water. The substrate sample was soaked in this solution in a 1 L black plastic basin for 1 hour, under constant stirring. 250 ml of 0.04M  $\text{FeCl}_3$  was added to the plastic basin and the foam sample was continuously stirred for a further 2 hours at room temperature and then allowed to stand overnight. The resulting PPy-coated sample was then removed from the container and rinsed with Milli-Q water to remove any loose bound PPy and blotted dry using tissue paper before being placed in an oven at  $40^\circ\text{C}$  overnight. The weight and the electrical resistance, see section 2.3.2, of the PPy coated foam were then recorded.

This coating procedure was repeated to produce a series of PPy-coated samples.

#### *Variation in washing procedure*

It was noticed that once dried, PPy-PU foam was seen to rub off the foam matrix. Upon this observation, the washing protocol was changed from that described in section 2.3.1.

#### **Materials**

The chemicals were used as described in section 2.3.1 as previously described. The PU substrate was sourced from F.E. Ltd, ET 21/250G (PU003) and was rinsed with Milli-Q water and dried prior to deposition.

#### **Procedure**

The experimental procedure, as described previously in section 2.3.1 was followed as stated, i.e. using a 250 ml solution of 0.04M pyrrole and 5.4mM of NDSA together with a 250 ml solution of 0.04M  $\text{FeCl}_3$  in order to deposit PPy.NDSA onto the PU foam. However, instead of a single washing, the coated foam was rinsed with Milli-Q water and oven-dried a total of three times between depositions. The electrical resistance of the PPy-PU foam was measured as described in section 3.3.2.

### **2.3.2 Electrical Resistance Measurements**

The electrical resistivity of the PPy-coated PU foam was measured using a constant current multimeter, HP 34410A (Hewlett Packard, Ireland) via a two-point-probe technique [16]. The data was collected by a PC using the HP bench software, version 1.1 or Agilent IntuiLink software, version 1.01, as supplied with the manufacturers. Data was collected at various sampling rates as dependent of the experiment. Data collected using the bench software was saved in .csv format (comma separated values) and exported to Microsoft Excel for further data manipulation and analysis. Data collected using the IntuiLink software was saved directly into Microsoft Excel, where again it was analysed. The multimeter was connected to the PC via a RS 232 connection. This enabled the recording and monitoring of the resistance behaviour of the material through a single channel.

Electrical connections to the PPy-PU foam were made via crocodile clips. Self-adhering copper shielding foil (# 512-187), used as received from Radionics Ireland, was also used in making connections to the PPy-PU foam substrate.

#### *Variation of electrical resistance with sensor size*

For the stationary experiment, a sample of PPy-PU foam ( $120 \times 30 \times 10 \text{ mm}^3$ ) was prepared as described in section 2.3.1 by repeatedly coating PU foam (PU003) from F.E. Ltd with PPy.NDSA until it was coated with a total of 4 layers of PPy.NDSA. Electrical contact to the PPy-PU foam was made by piercing the foam with two wires and connecting directly to the HP multimeter. The electrical resistance of the foam was measured for 20 minutes at a sampling rate of 2 Hz. After measurement, the PPy-PU foam sample was cut to reduce the length of the material by 5 mm. Electrical contact was again made and the resistance measured for 20 minutes. This measuring and preparation of the sample continued until the sample was of the dimensions,  $5 \times 30 \times 10 \text{ mm}^3$ , whereafter the sample was cut to  $2.5 \times 30 \times 10 \text{ mm}^3$ , then  $1 \times 30 \times 10 \text{ mm}^3$ .

#### **2.3.3 SEM examination**

Scanning electron microscopy (SEM) examination of substrate, PPy-coated and uncoated using a Hitachi S-3000N scanning electron microscope. PPy-coated samples were mounted onto studs using a conducting adhesive. These samples were not sputter-coated but examined using an electron beam of strength 20 keV. The cross-sectional area of a piece of PPy-PU foam was also examined by SEM. For this, a piece of PPy-PU foam was sliced using a scalpel and mounted onto a stud using a conducting adhesive. The PPy-PU foam sample was not sputter-coated but examined using an electron beam of strength 20 keV. Uncoated PU foam samples were sputter-coated with gold for one minute at 1kV prior to examination with the SEM.

### 2.3.4 Surface Area Determination using electrochemistry

#### *Materials*

Platinum (Pt) wire, of diameter 250 $\mu$ m was received from Engelhard. It was oxidised in a butane flame prior to electrochemical experimentation. Potassium ferricyanide ( $K_3FeCN_6$ ), and KCl were obtained from Sigma and were used as received. All solutions were prepared with Milli-Q water.

#### *PPy-PU electrode preparation*

The PPy-PU foam was prepared according to the procedure outlined in section 2.3.1. A sample of PPy-PU foam was examined using the electrochemical method described below prior to each PPy.NDSA deposition. The PPy-PU foams were cut to the approximate size of volume 0.1 cm<sup>3</sup>.

For the determination of the surface area of the PPy-PU foam, a working electrode was constructed by hooking the prepared piece of PPy-PU foam onto the end of a platinum wire and then directly connecting this wire to the potentiostat. A Pt counter electrode and Ag/AgCl (3M KCl) reference electrode, together with an electrolyte of 5 mM  $K_3FeCN_6$  in 0.5M KCl were used to complete the electrochemical cell.

All experiments were performed at room temperature (25°C). Data for all experiments was collected using the Gamry Potentiostat and analysed using Echem Analyst Software (version 4.2)

#### *Determination of Diffusion Coefficient for Ferricyanide ( $K_3FeCN_6$ )*

Determination of the diffusion coefficient was carried out using a 250mm diameter Pt working wire (surface area = 0.2356cm<sup>2</sup>), a coiled Pt counter electrode, a Ag/AgCl (3M KCl) reference electrode and an electrolyte of 5mM  $K_3FeCN_6$  in 0.5M KCl.

A series of cyclic voltammograms were run using the Pt working electrode at room temperature in the potential window from 0.6V to -0.2V. The scan rates were varied from 10 to 500mV/s.

#### *Determination of Electrode surface area for PPy-PU foam samples*

A series of electrochemical experiments were then carried out for each PPy-PU sample, whereby the PPy-PU foam formed the working electrode. The potential window of 0.6 to  $-0.2\text{V}$  was used and the scan rate was varied from 20 to 1000 mV/s.

### **2.3.5 Piezoresistive response of PPy-PU foam samples**

#### *Materials*

The foam samples used during this thesis were commercially sourced, and as such their mechanical details were not obtainable. Therefore, deliberate examination of their mechanical properties was required. For this purpose a number of selected for examination using an Instron<sup>TM</sup> tensile testing machine. This piece of equipment would enable a compression profile of the materials to be generated showing the mechanical behaviour of the material in such an environment.

The PPy-PU foam samples used during these experiments were prepared by repeatedly coating the substrate material (listed in Table 2.3) according to the procedure outlined in section 2.3.1 until the desired coating was achieved.

The electrical resistance of the PPy-PU foam samples was recorded using the multimeter as described previously in section 2.3.2.

The PPy-coated and uncoated foam samples that were used for the Instron<sup>TM</sup> examination are listed in Table 2.3. This table lists the samples examined using the tensile-testing machine, together with a brief description of their properties.

#### *Apparatus*

Three methods for determining the effect of loading pressure or force onto the PPy-PU foam samples were used. The schematics of the apparatus used are given in Fig. 2.5 - Fig. 2.9.

*In house-design*

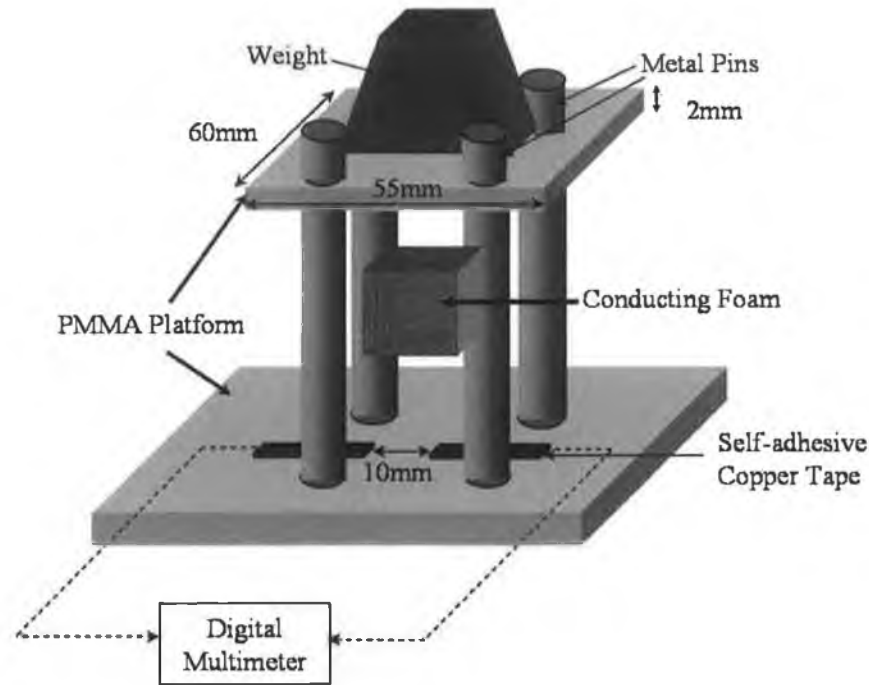


**Fig. 2.5 In-house design loading platforms used to examine the piezoresistive behaviour of the PPy-PU foam.**

The first setup, as illustrated in Fig. 2.5 was made up of two PMMA platforms. Four metal pins ( $l = 10 \text{ cm}$ ,  $d = 0.2 \text{ cm}$ ) were fixed to each corner of a bottom platform ( $10.0 \times 5.0 \times 0.6 \text{ cm}^3$ ) so that there was  $3.0 \text{ cm}$  separation between the pins. Four holes ( $d = 0.21 \text{ cm}$ ) were drilled into the upper platform ( $5.5 \times 6.0 \times 0.2 \text{ cm}^3$ ,  $6.203 \text{ g}$ ) so that it could thread through the four pins. The purpose was to give stability to the weight placed on the centre of the top platform and to maintain the platform in a horizontal position during compressions. The PPy-PU sample prepared, as in section 2.3.1, was placed in between the two platforms and secured to the bottom platform by using two pieces of self-adhesive copper tape, separated by a distance of  $1 \text{ cm}$ . When known weights were placed onto the upper platform, the foam was compressed and the change in resistance was measured by the HP multimeter as described in Chapter 2, section 2.3.2.

### *Clamp Setup*

The second setup, shown in Fig. 2.6 and Fig. 2.7, employed a clamp to sandwich the foam sample. Two clamps were used during testing. The first was a manual clamp, Fig. 2.6, which required manually tightening of the clamp jaws to compress the foam. Electrical connections to the foam were facilitated by Cu tape adhered to the opposing jaw of the clamps.

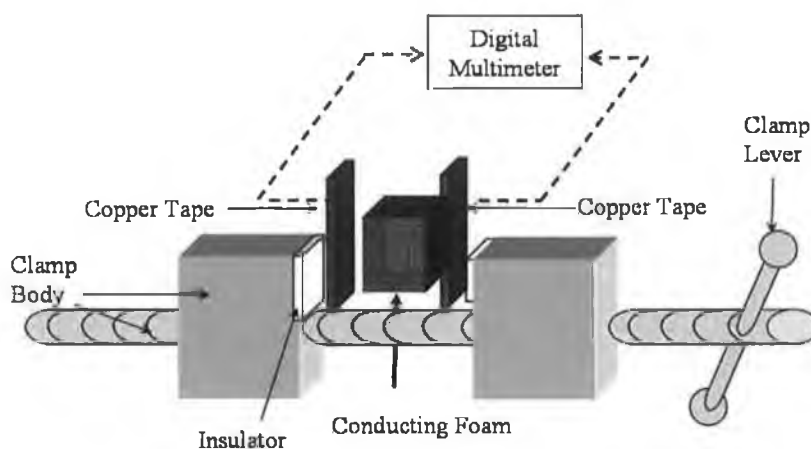


**Fig. 2.6 Manual clamp for compression studies of PPY-PU foam.**

The second clamp was modified from a Harvard PHD 2000 syringe driver pump, received from Harvard Apparatus, MA, USA, shown in Fig. 2.7. The syringe driver was controlled manually via the keypad interface on the console and later automatically by programming the movement of the piston via the com port to the back of the console. During operation the piece of PPY-PU foam was placed between jaws (between the piston and the opposite wall) of the syringe driver. The syringe driver was programmed to compress and relax the foam regularly and continuously at a frequency of 0.025 Hz over the period of 20 minutes. The electrical contact points to the foam by threading two wires into the foam at adjacent edges to the jaws of the syringe pump. The piston was programmed to move into the PPY-PU foam, fully compressing it to a maximum force of 890 N and out of the PPY-PU foam, allowing the foam to relax. The electrical resistance of the foam was continuously monitored using the constant current multimeter at a sample rate of 1 Hz as described in section 2.3.2. All experiments were run at room temperature and atmospheric pressure.





**Fig. 2.7 Harvard Apparatus, syringe driver, PHD 2000 for automatic compression of PPy-PU foam.**

### *Instron™ Testing*

The stress versus resistance profiles were obtained with an Instron™ machine (model 4202). This machine systematically loaded (compressed) and unloaded a pre-determined weight onto the foam sample. The samples were placed (one at a time) between the piston and the stage. The position and load on the piston was monitored as it was steadily lowered onto the sample compressing it. The data was collected using the Series IX software as supplied by Instron™, which measured the position and load acting on the crosshead at a rate of 10 data pt/sec. The rate of loading and unloading (speed of the crosshead position) was 2 mm/min throughout the experimentation. The dimensions of the piston head were 50.44 mm x 32.86 mm x 13.02 mm. Sample specimens were prepared by cutting out a section, dimensions 20 mm x 15 mm x 40 mm from the relevant foam sample.

The resistance of the coated samples was continuously monitoring during the loading and unloading cycles of the Instron™ machine to determine the effects of force on the resistance of the material. The resistance was measured by using a potential divider circuit, as illustrated in Fig. 2.8, whereby the foam represented the variable resistor. The voltage input,  $V_{in}$ , was set at 5V and the load resistor,  $R_L$ , was 50k $\Omega$ . The voltage output,  $V_{out}$ , was recorded continuously. Contacts to the coated foam samples were made by adhering copper tape to the piston-head and the sample stage and placing the coated foam samples between.

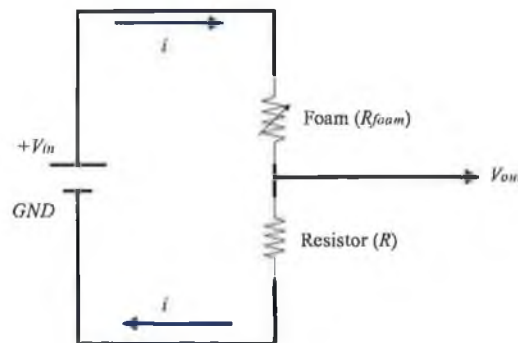


**Fig. 2.8 PPy-PU foam connected into resistor-in-series circuit.**

The measured output voltage,  $V_{out}$ , is dependent on the resistance of foam, thus any changes in the resistance of the foam will be reflected as a change in the output voltage. These two parameters are linked via the following equation, Equation 2.4, where the terminology is illustrated in Fig. 5.3.9

$$V_{out} = V_{in} \left( \frac{R}{R + R_{foam}} \right)$$

Equation 2.4

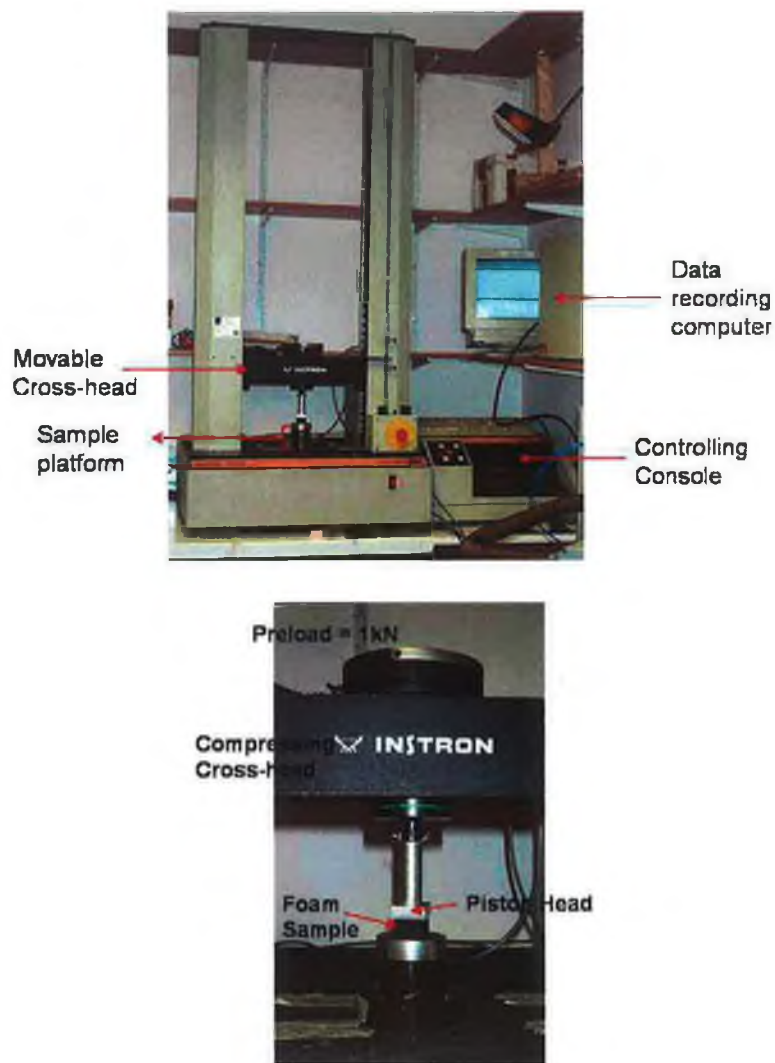


Fig. 2.9 Picture of Instron instrument used for compression testing of foam samples, with a zoom-in on the compression head and the foam sample.

Table 2.3 List of samples and their properties examined using the Instron™ machine

ID Number	Source	Material	Density (kg/m <sup>3</sup> )	Hardness Value	Coating with PPy.NDSA
7A	IRE-TEX	<i>Polyurethane Foam (PU)</i>	-	-	NO
13A	F.E. Ltd ET18/125G	<i>PU</i>	18	125	NO
14A	F.E. Ltd ET29/170G	<i>PU</i>	29	170	NO
15	F.E. Ltd ET21/250G	<i>PU</i>	21	250	YES
15A	F.E. Ltd ET21/250G	<i>PU</i>	21	250	NO
18	IRE-TEX	<i>PU</i>	-	-	YES x 2
20	IRE-TEX	<i>PU</i>	-	-	YES x 4
23	F.E. Ltd PEX 18 BLK	<i>Polyethylene Foam (PE)</i>	-	-	NO
24	F.E. Ltd PEX 45 BLK	<i>PE</i>	-	-	NO

## 2.4 RESULTS & DISCUSSION

### 2.4.1 The effect of the dopant anion on the electrical resistance of the coated PU foam.

The resistance results,  $n = 5$ , measured using the constant current multimeter for the coated PU foam samples (sample PU003) are listed in the following tables: Table 2.4 - Table 2.6.

**Table 2.4** Effects of polymer loading on conductivity of PU foam (PU003), where  $wt$  and  $\Omega$  are the weight and resistance of the foam sample. The subscript  $n$  denotes the weight and resistance of the foam material after the  $n$ th polypyrrole deposition layer. Note: Dopant anion = NDSA

No. of Coatings (n)	Total Weight deposited (g)	Ratio $wt_n / wt_1$	Resistance ( $k\Omega/cm$ )	Ratio $\Omega_1 / \Omega_n$
0	0.000	-	-	0.000
1	0.103	1.000	1.20	1.000
2	0.475	4.626	0.31	3.79
3	0.693	6.756	0.29	4.06
4	1.078	10.510	0.23	5.14

**Table 2.5** Effects of polymer loading on conductivity of PU foam (PU003), where  $wt$  and  $\Omega$  are the weight and resistance of the foam sample. The subscript  $n$  denotes the weight and resistance of the foam material after the  $n$ th polypyrrole deposition layer. Note: Dopant anion: pTSA

No. of Coatings (n)	Total Weight deposited (g)	Ratio $wt_n / wt_1$	Resistance ( $k\Omega/cm$ )	Ratio $\Omega_1 / \Omega_n$
0	0.000	-	-	0.000
1	0.037	1.000	146.546	1.000
2	0.240	6.550	14.243	10.29
3	0.468	12.747	7.501	19.61
4	0.614	16.738	12.932	11.36

**Table 2.6** Effects of polymer loading on conductivity of PU foam (PU003), where wt and  $\Omega$  are the weight and resistance of the foam sample. The subscript n denotes the weight and resistance of the foam material after the nth polypyrrole deposition layer. Note: Dopant anion: DBSA

No. of Coating: (n)	Total Weight deposited (g)	Ratio $wt_n / wt_1$	Resistance (k $\Omega$ /cm)	Ratio $\Omega_1 / \Omega_n$
0	0.000	0.000	-	0.000
1	0.017	1.000	3110.000	1.000
2	0.427	25.100	0.740	4202
3	0.397	23.371	1.500	2073
4	0.739	43.453	1.400	2222

Comparing the results shown in Table 2.4 – Table 2.6, the dopant anion which yielded the optimum resistance measurements was found to be NDSA. When using NDSA, the greatest amount of PPy was deposited and the lowest resistance measurements were obtained. These findings are illustrated in Fig. 2.10

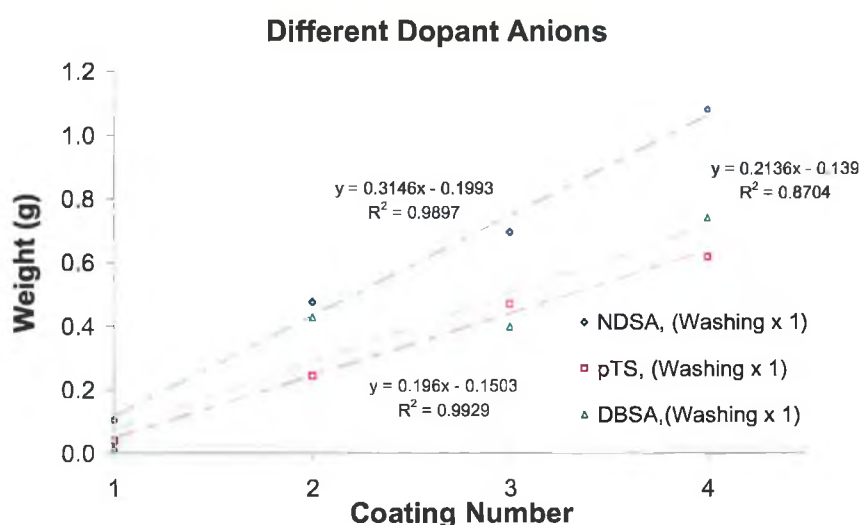


**Fig. 2.10** Weight change observed with successive coatings of PU foam with doped PPy.

Thus, NDSA was selected as the dopant anion of choice for subsequent PPy polymerisation and deposition. Suitable substrates were then analysed to determine compatibility with PPy.NDSA.

#### 2.4.2 The effect of loading PPy.NDSA onto different substrates

##### *Solid Foams: Polyurethane Foam*

When the PU foam sample was coated with PPy.NDSA, the tactile properties (i.e. softness and compressibility) of the foam were not obscured. However, the weight of the sample increased due to the presence of PPy.NDSA. Also the resistivity of the material changed with every coating of PPy.NDSA. These changes for the PU foam samples PU003 are listed in Table 2.4. The original details of each PU foam substrate sourced can be found in Table 2.1.

As can be seen in the following graph, Fig. 2.11, the effect the deposition of PPy.NDSA onto PU foam was shown to result in an increase to the overall weight of the foam. This coincided with a reduction in the electrical resistance of the foam as measured using the constant current multimeter as described in section 2.3.2, the results of which are shown in Fig. 2.12.

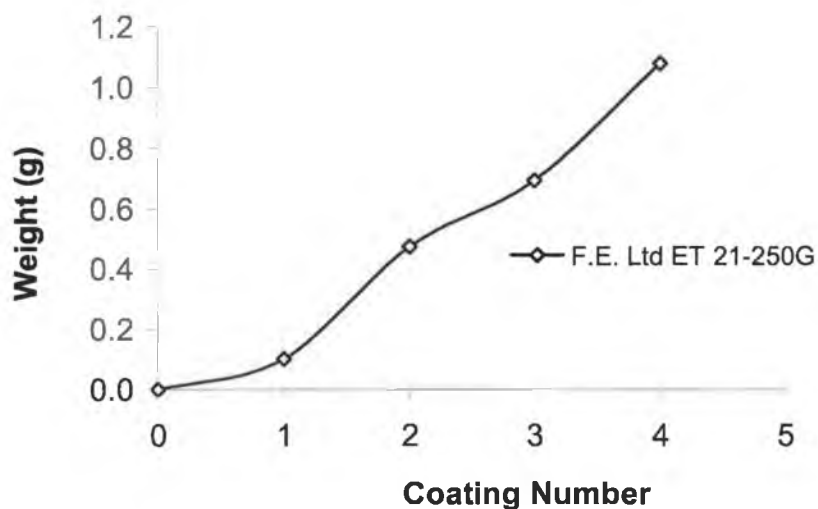


**Fig. 2.11** Coating of PU003 (F.E. Ltd PU-ET 21/250G) sample with PPy.NDSA and resulting changes in weight of the material.

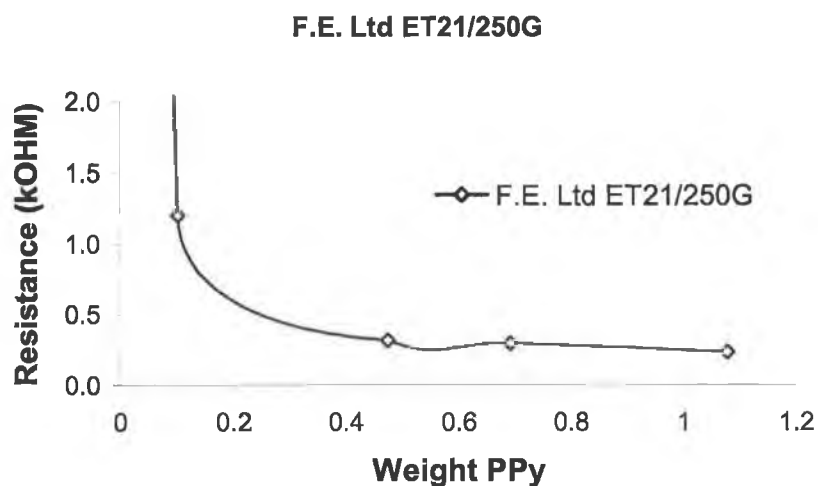


**Fig. 2.12** Plot of the gradual increase of PPy.NDSA deposited onto the PU003 (F.E. Ltd PU-ET 21/250G) sample and resulting changes in resistance of the material.

Coating the PU foam a total of four times was shown to saturate the substrate with doped PPy. The PPy-PU foam became brittle to touch and occasionally tore when compressed. Also doped PPy was noticed to flake off the surface of the PU substrate despite rigorous washings between deposition. It was noted, also, that the resistance of the PPy-PU foam did not change dramatically after the second coating, that the resistance change was approximately equal to the 90% change observed after the second coating. Thus, the 3<sup>rd</sup> and 4<sup>th</sup> coatings lead to over-deposition of PPy onto the PU foam structure.

#### **The effect of varying the washing protocol**

The effects of increasing the number of washes between PPy depositions, in terms of the weight of polymer deposited and the resistance of the material are shown in following graphs, Fig. 2.13 & Fig. 2.14.



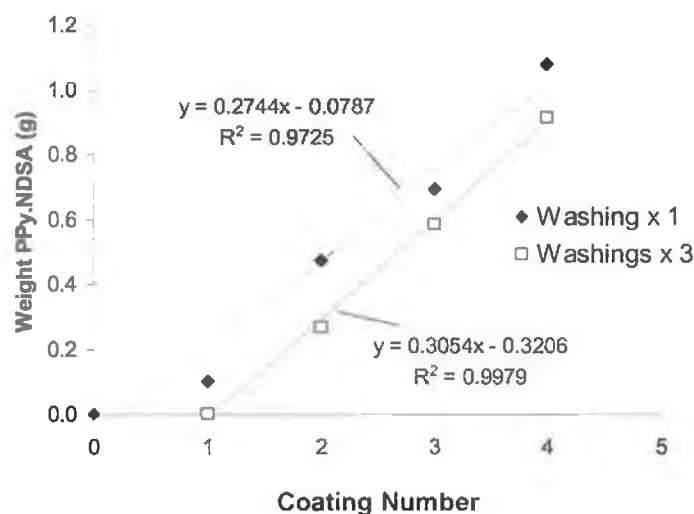


**Fig. 2.13** Effect of using two different washing protocols on the weight of PPy.NDSA deposited onto the PPy-PU foam.

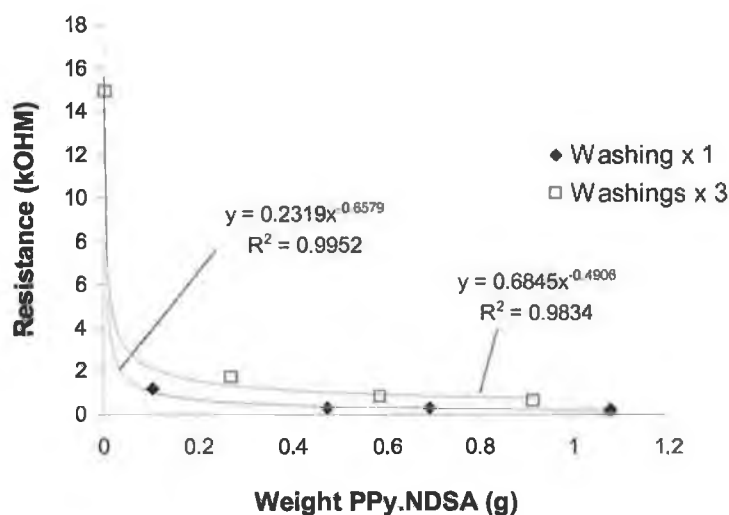


**Fig. 2.14** Effect of using different washing protocol on the resistance of the PPy-PU foam.

It can be readily seen, in Fig. 2.13, that the increased number of washes resulted in smaller amounts of PPy being deposited onto the PU foam compared to the samples washed once. This more gradual deposition of PPy.NDSA resulted in a more gradual change to the resistance of the foam, see Fig. 2.14. The final resistance for PPy-PU foam washed three times between each deposition was 0.62 kΩ/cm compared to 0.23

k $\Omega$ /cm for that washed once between each deposition. This value is still very much useful for the development of sensors.

The purpose of this study was to evaluate whether the PPy.NDSA coating would be robust enough to withstand washings as would be expected with wearable sensors. These triple washings (washing x 3) were performed without detergent between depositions. The results show that the single washing, (washing x 1) though sufficient may not have been rigorous enough to remove the loose PPy.NDSA bound to the PU foam. It can be seen that the electrical resistance of the PPy-PU foam coated using this new washing protocol is still very good (<1k $\Omega$ /cm) and would be of use for the future development of sensor prototypes.

#### *Polyethylene Foam*

PPy, when oxidised, becomes hydrophilic in nature. Polyethylene (PE), however, has a hydrophobic surface and so did not accommodate the deposition of PPy onto its surface. Instead the PPy flaked off the surface of the PE. Therefore, this material was not suitable as a substrate for conducting polymer-coated sensors and was not used during subsequent sensor fabrication. In contrast the NH and C=O bonds found in PU offered hydrophilic sites for PPy deposition.

#### *Specialised Foams: Avelo*

Unsuccessful deposition

PPy did not adhere to this solid non-polar foam.

#### *Viscoelastic Foam: Kaymed Visco™*

Unsuccessful deposition.

This foam lost its visco-elastic properties when deposition was attempted.

*Fabric-based material: Polartec®*

The Polartec® was shown initially to accommodate the deposition of PPy onto its surface. However as can be seen from Table 4.5.2, the resistance of the PPy-Polartec® material increased after the second coating with PPy.NDSA until it became non-conducting.

**Table 2.7** Effects of polymer loading on resistance of Polartec® fabric, where wt and  $\Omega$  are the weight and resistance of the foam sample. The subscript n denotes the weight and resistance of the foam material after the nth polypyrrole deposition layer. Note: Dopant anion = NDSA

No. of Coatings (n)	Total Weight deposited (mg)	Ratio $wt_n / wt_1^*$	Resistance (k $\Omega$ /cm)	Ratio $\Omega_1 / \Omega_n$
0	0.00	-	-	-
1	5.10	1.00	7.78	1.00
2	9.70	1.90	40.33	0.19
3	7.70	1.51	>1000	-

This indicated that the deposition of PPy. NDSA onto the Polartec® material did not form a continuous layer, conducive to conductivity. Thus, the Polartec® material is not suitable for the deposition of conductive PPy.NDSA.

### 2.4.3 Variation of electrical resistance per PPy-PU foam sample.

The resistance of the PPy-coated PU foam was measured at a number of points around the foam piece, to determine whether variations in resistance occurred in this piece. The resistance measurements are shown in Fig. 2.15. Each point represents the average resistance measurement of three repeats, while the error bars represent the standard deviation of these replicate measurements.

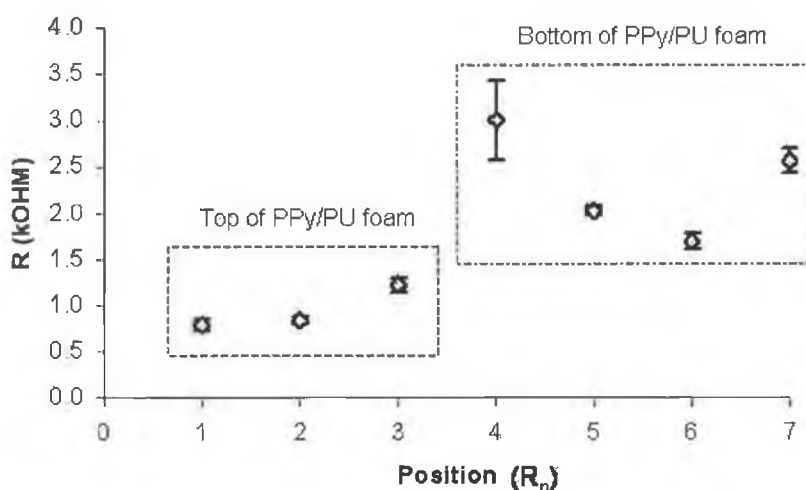


**Fig. 2.15** Resistance of PPy/PU foam measured at 7 discrete points, using a two point-probe method.

As can be seen in Fig. 2.15, there are variations in the measured resistance moving from position to position on the foam, so much so that the measurements can be grouped into two sections, those for the top of the PPy-PU foam and those for the bottom of the PPy-PU foam. The difference in the measured resistance between these groups is thought to stem from the deposition setup, whereby the foam substrate floated in the deposition solution, thus leading to the variation in deposition environment around the foam. Techniques, such as the use of a grid over the foam substrate, were implemented to deter this floating action, however variations in the electrical resistance measurements were present. The standard deviations, shown as error bars in Fig. 2.15, show that the repeated measurements are good. The resistance reading at  $R_4$  is much

larger than the others – this was due to tearing of the foam, which occurred during these measurements. This disruption of the PU platform, on which the PPy.NDSA was coated, resulted in an increase in the resistance of the materials. Thus, a problem using direct clipping to the foam has been identified, that is that the material is susceptible to tearing due to the force of the clip.

Therefore, in order to overcome this tearing, Cu tape was used as a contact. This resulted in a thin layer of PPy-PU foam being removed with each replacement of Cu tape. The average resistance ( $n=5$ ) of each layer is shown in Fig. 2.16. The error bars represent the standard deviation of each measurement ( $n=5$ ).

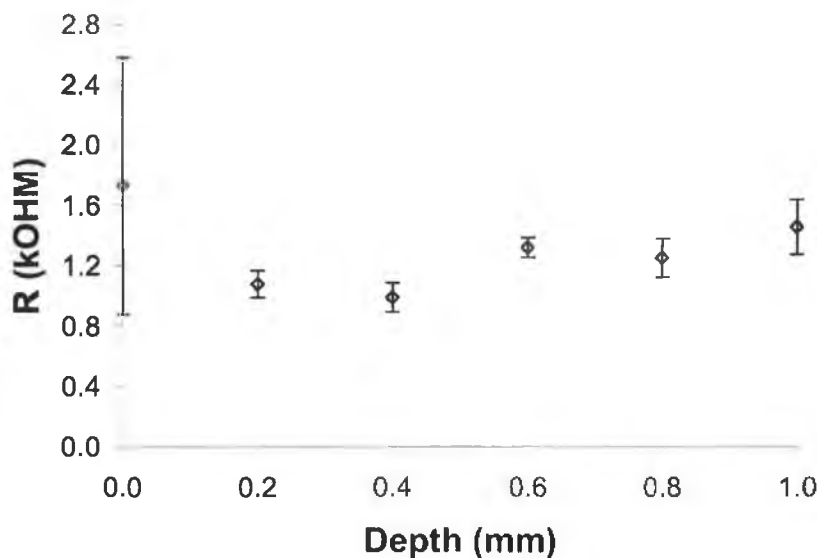


**Fig. 2.16** Resistance of PPy/PU foam using Cu strips as contacts to the foam. Each Cu tape was removed after measurement stripping a thin layer of the foam, thus exposing different layers for resistance measurements.

From Fig. 2.16, it can be seen that there is slight variation in the resistance measured as the depth into the foam is increased. However, as its deepest point (1mm) the resistance of the PPy-PU foam is still less than 20% of the measured surface resistance.

#### 2.4.4 The effect of varying the dimensions of the sensor.

The following graph, Fig. 2.17 shows the measured resistance of the PPy-PU foam which was incrementally reduced in length, according to section 0 to determine its effect on the measured resistance. Each data point represents the average resistance ( $n = 2400$ ) of the PPy-PU for each given length.

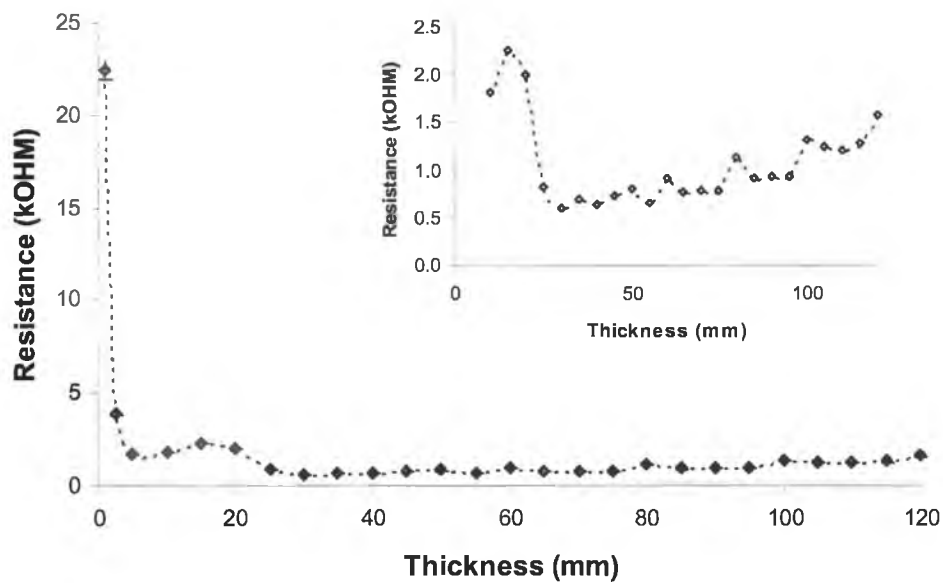


Fig. 2.17 Effect of reducing length of PPy-PU foam on the measured resistance.

It can be seen that as the size of the foam decreased, from 120 to 25 mm, the resistance of the PPy-PU foam did not change significantly, perhaps decreasing very slightly. This would indicate that a sensor of length 25 mm would have a similar baseline resistance reading to one of length 120 mm. However, there is a limit to the smallness of the foam sensor as can be seen by the peak in resistance observed for PPy-PU foam less than 20 mm. This is because at these dimensions, the PPy-PU foam sensor is a thin sheet of foam of little depth. Therefore, the conductive pathways through the 3D-structure of the foam are reduced to those of 2D-structure. This lack of conductive pathways leads to the observed increase in resistance.

#### 2.4.5 SEM examination of PPy-coated and uncoated PU foam samples

Scanning electron microscopy (SEM) analysis of the PU and PPy-coated PU foam was carried out on a number of samples and the resulting images are shown in the following pages. The progression of coating PU foam (Fig. 2.18) gradually with polypyrrole doped with NDSA are shown in Fig. 2.21 & Fig. 2.22 for the first coating, Fig. 2.21 - Fig. 2.25 for the second, Fig. 2.26 - Fig. 2.28 for the third and Fig. 2.29 - Fig. 2.33 for PU foam coated with four layers of polypyrrole.

The porous structure of the PU foam, is confirmed by SEM analysis (Fig. 2.18). In addition to the porous structure resulting from the irregular distribution of pores throughout the material, the SEM analysis of the surface of the PU foam showed the smoothness of its surface. As can be seen in Fig. 2.18 and Fig. 2.19, the surface of the PU foam was smooth with very little structural detail observed at these magnifications.

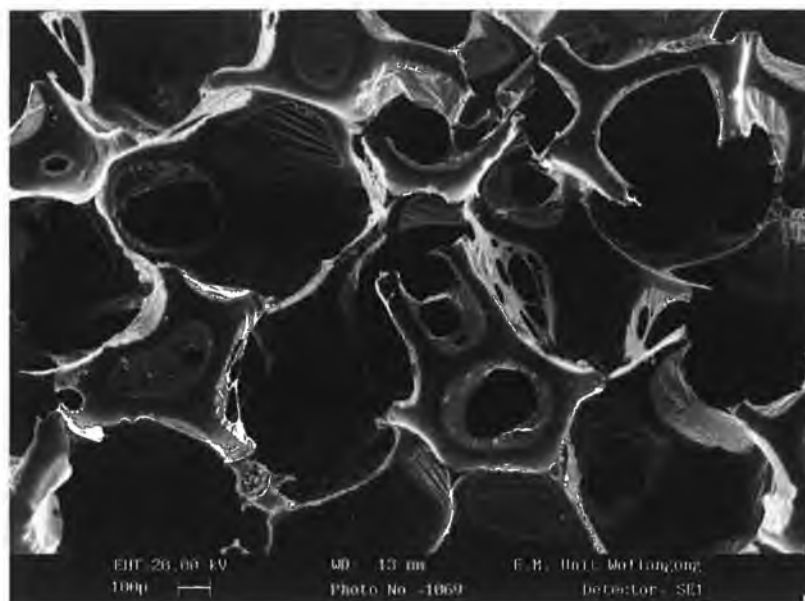


**Fig. 2.18** SEM of PU foam sputter-coated with AU for one minute prior to SEM analysis, at 20 kV (x 100).

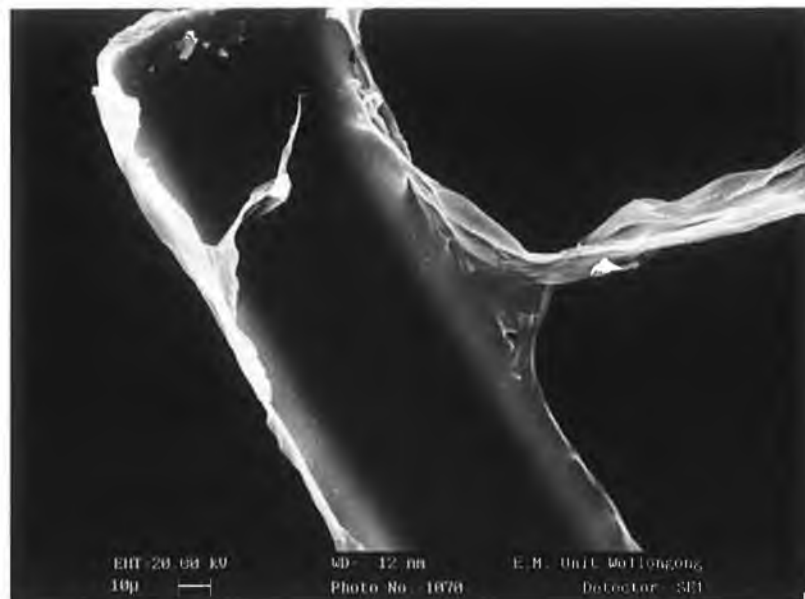


**Fig. 2.19** SEM of PU foam sputter coated with Au for one minute prior to SEM analysis, at 20 kV, x 1000.

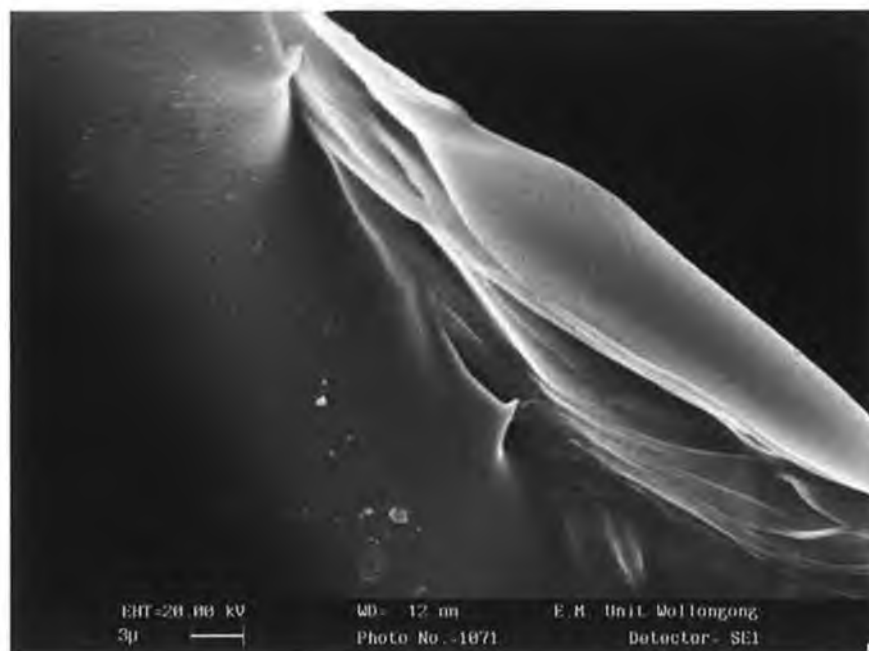


**Fig. 2.20** SEM of PU foam sputter coated with Au for one minute prior to SEM analysis, at 20 kV x 5000.



When the PU foam was coated with PPy.NDSA, deposition of PPy.NDSA occurred. This was confirmed both by the observed increase in weight of the material (Fig. 2.11) and decrease in the electrical resistance of the material (Fig. 2.12.) The effect of depositing PPy onto the surface of the PU foam is shown in the following images Fig. 2.21 - Fig. 2.33.

Fig. 2.21 - Fig. 2.22 show SEM images of PU foam coated once with PPy.NDSA. From these images the initial deposition of PPy onto the PU surface could be observed as nodular growth of PPy onto the smooth PU surface. The porous structure of the PU foam was retained, with PPy growth occurring on the edges of the PU pores. However, smooth sections of PU are also observed which indicate that this layer of PPy.NDSA was not thick enough to cover the entire PU structure. Since it is the PPy which infers the electrical pathways through the material, this partial PPy covering is responsible for the high resistance of the material.

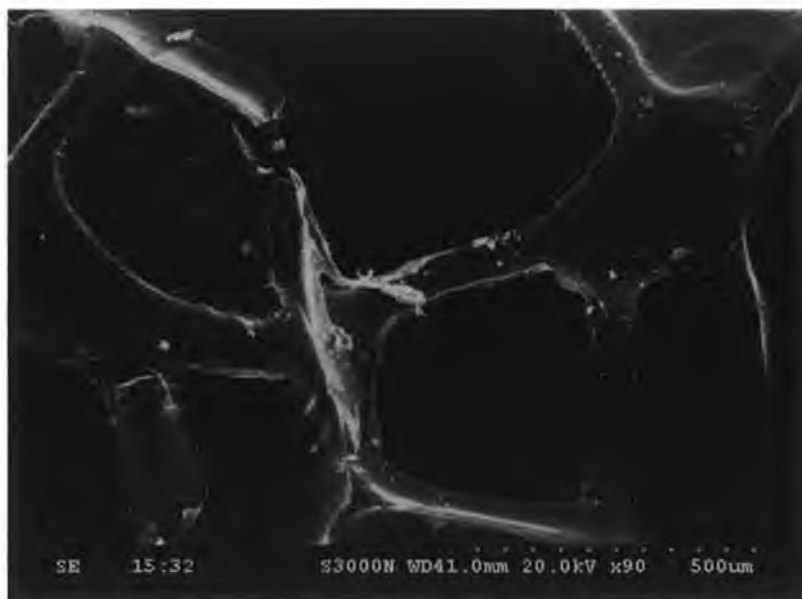


**Fig. 2.21** SEM of PU foam coated once with PPy.NDSA, at 20 keV, x 90.

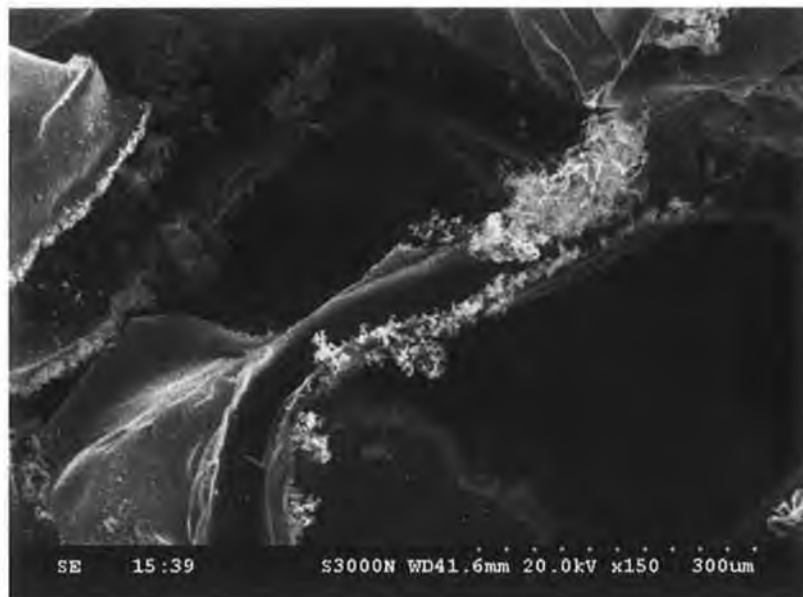


**Fig. 2.22** SEM of PU foam coated once with PPy.NDSA, at 20 keV, x 150.

Fig. 2.23 - Fig. 2.25 show SEM images of PU foam coated twice with PPy.NDSA. The nodular formation of PPy is again observed, however the population of PPy nodules on the surface of the PU foam is more abundant, indicating more PPy present in these samples. The greater the amount of PPy present in the samples, the more conductive the samples. The detailed structures of PPy can be observed to have formed completely around the PU pores (Fig. 2.23 & Fig. 2.24), indicating a more continuous layer of PPy on the surface of the PU. This complete layer would dramatically reduce the resistance of the material, confirming the observations for the electrical characteristics of the material. The presence of the PPy nodules at the pore edges would contribute to the active surface area of the overall material, in a similar manner as the presence of glomeruli increase the surface area within the kidney (Fig. 2.1).

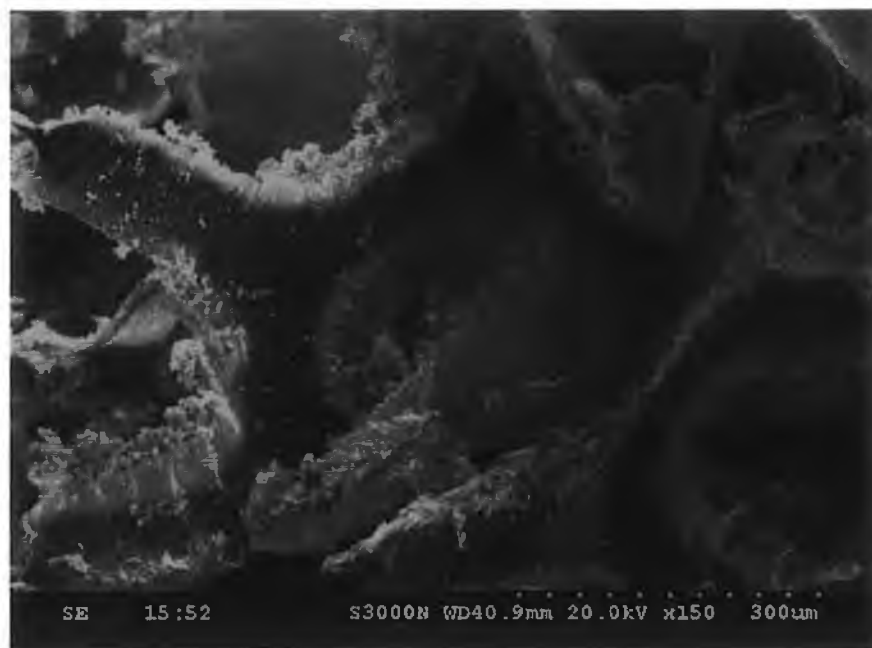


**Fig. 2.23** SEM of PU foam coated twice with PPy.NDSA, at 20 keV, 150.

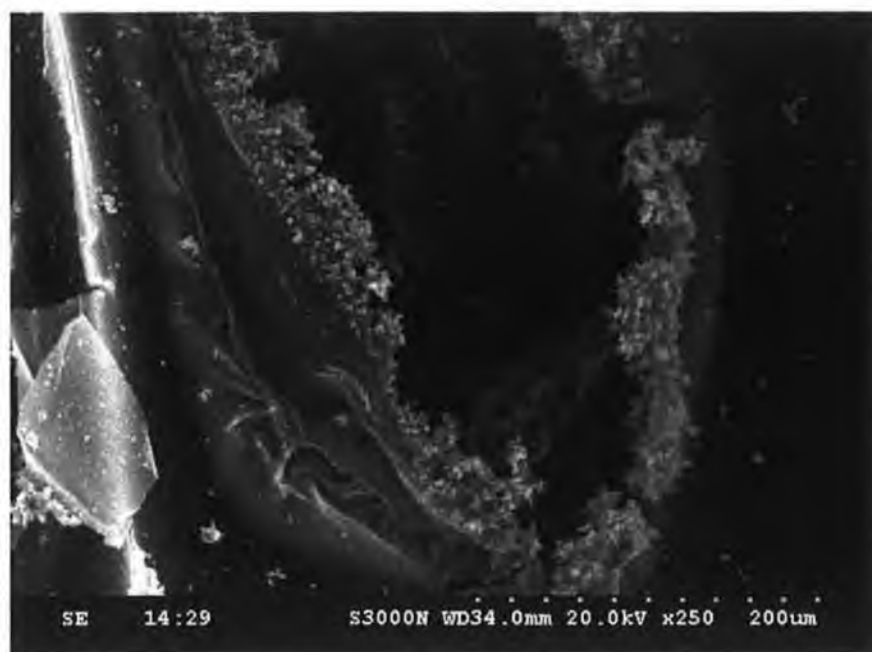


**Fig. 2.24** SEM of PU foam coated twice with PPy.NDSA, at 20 keV, x 250.



In addition to growth at the pore edge, PPy formation was observed along the smooth parts of the PU foam, as can be seen in Fig. 2.24. The continued growth of PPy in this nodular fashion as shown in Fig. 2.25, resulted in dense clusters being formed, which eventually grow to form a complete covering, as indicated to the left of the image in Fig. 2.25.

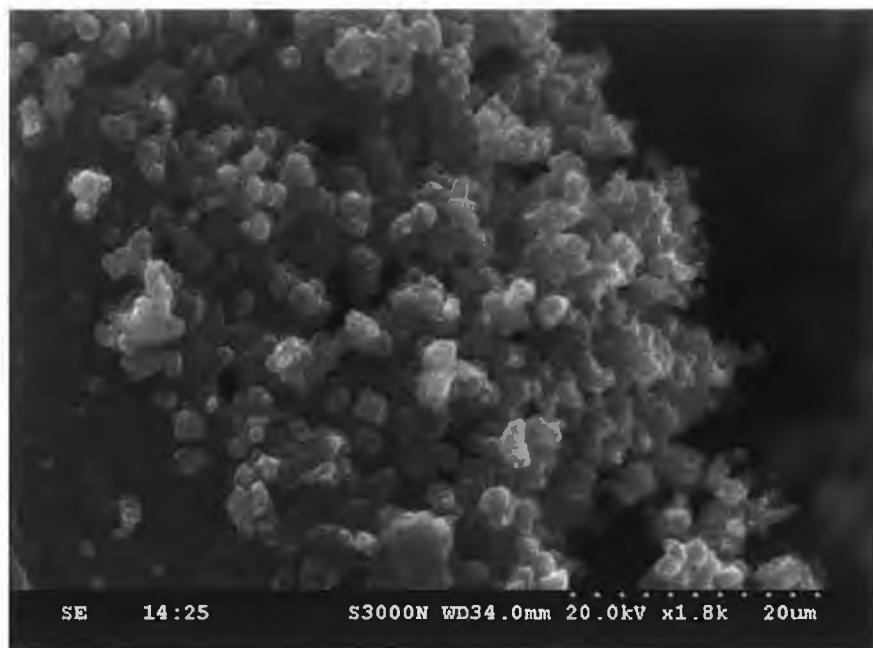


**Fig. 2.25** SEM of PU foam coated twice with PPy.NDSA, at 20 keV, x 1800.

Fig. 2.26- Fig. 2.28 show SEM images of PU foam coated three times with PPy.NDSA. Again, the nodular formation of PPy is observed in all images. The growth of PPy can be seen to cover the smooth and edge section of the PU foam, observed in Fig. 2.26. The gradual growth of PPy around the pore edge (Fig. 2.27) can be seen to gradually decrease the size of the pore. However, the detailed structure of the PPy nodules leads to an increase in the active surface area. In certain sections of these PU foam samples coated three times with PPy, the growth of PPy was extended to form films of PPy which fill the pores of the PU foam (Fig. 2.28).

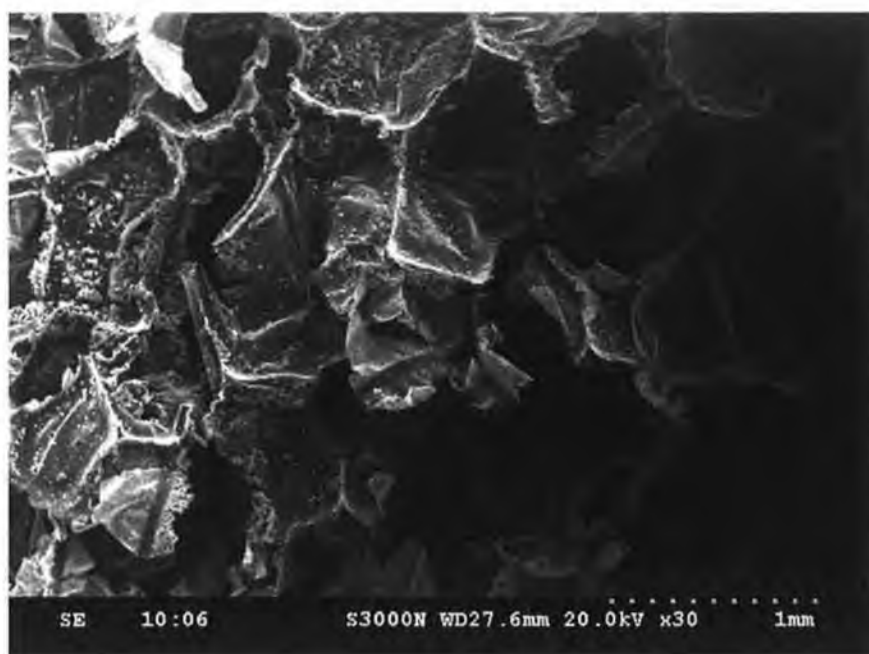
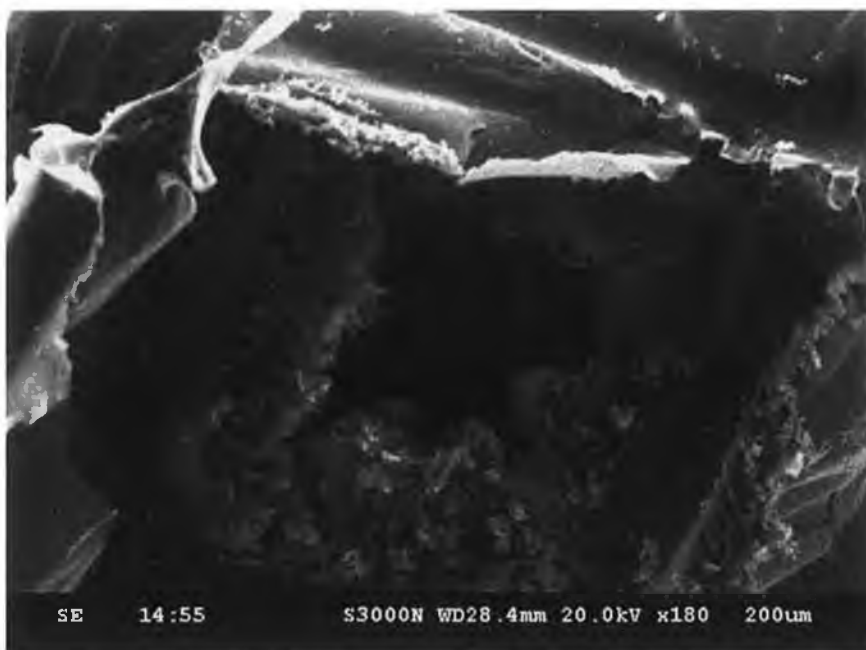
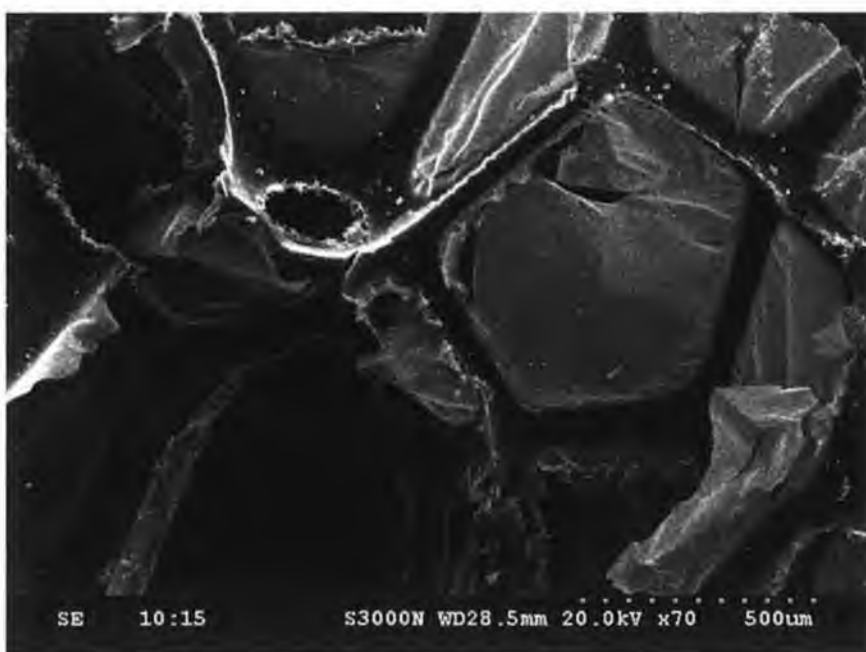


Fig. 2.26 SEM of PU foam coated three times with PPy.NDSA, at 20 keV, x 30.

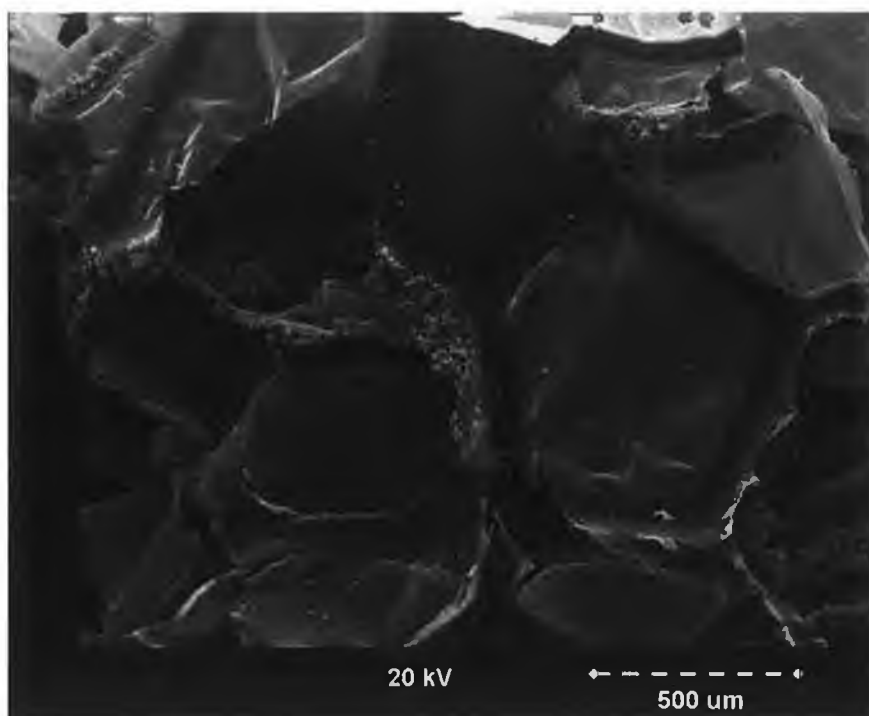


**Fig. 2.27** SEM of PU foam coated three times with PPy.NDSA, at 20 keV, x 180.



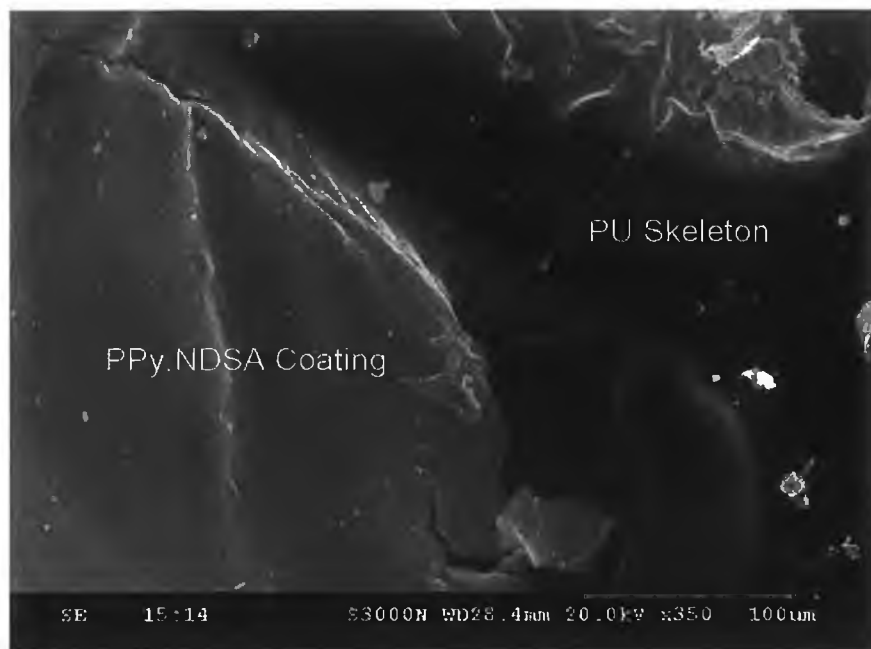
**Fig. 2.28** SEM of PU foam coated three times with PPy.NDSA, at 20 keV, x 70.

Fig. 2.29 – Fig. 2.33 show SEM images of PU foam coated four times with PPy.NDSA. The effect the fourth coating of PPy.NDSA is seen to be the filling of the PU pores with the conducting polymer, as observed in Fig. 2.29. In this SEM, the skeleton of PU is observed, similar to that observed in previous SEMs but the majority of the pores for this material were filled with PPy.NDSA. The granular surface of PPy was observed on the sections which covered these pores (Fig. 2.30) and showed the growth of PPy nodules of 1-4  $\mu\text{m}$  diameter at the edge and smooth surfaces.



**Fig. 2.29** SEM of PU foam coated four times with PPy.NDSA, at 20 keV, x 70.





**Fig. 2.30** SEM of PU foam coated four times with PPy.NDSA, at 20 kV, x 350.

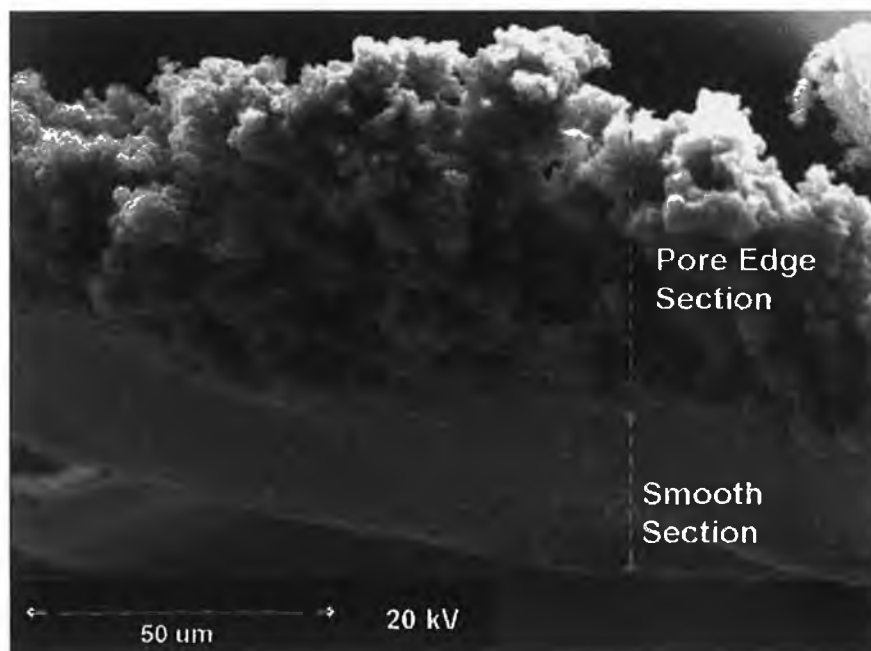


**Fig. 2.31** SEM of PU foam coated four times with PPy.NDSA, at 20 kV, x 900.

This growth of PPy at these two regions is shown in greater detail in Fig. 2.31. This clustered growth is denser than what was observed in samples with lesser coatings. Thus, the continued growth of PPy resulted in more dense clusters forming. This gradual covering of the fine nodular detail lead to the formation of smoother films of PPy, which bridged the pores of the PU foam as seen in Fig. 2.32.

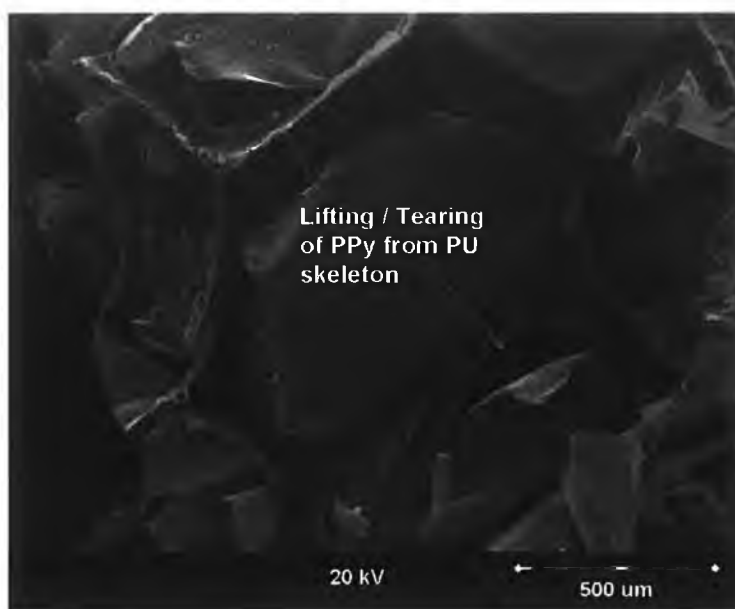


**Fig. 2.32** SEM of PU foam coated four times with PPy, at 20 kV, x 70.

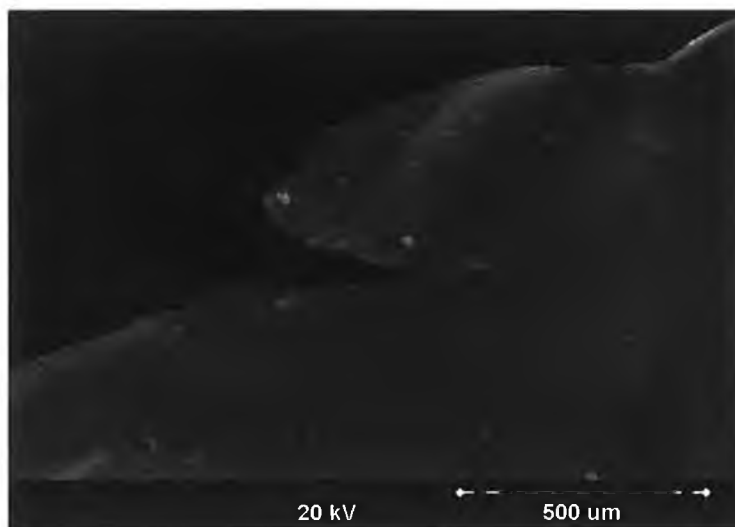


**Fig. 2.33** SEM of PPy layer after four depositions onto PU foam, showing tearing of the PPy layer, x 800.

Another effect of coating the PU foam four times with PPy.NDSA was that tearing of the PPy layer was observed to occur within the pores of the PU foam. Thus, the PPy layer was being subjected to physical pressures beyond its capacity. Tearing of the PPy layer within the pores would constitute disruptions to the conductive pathways through the material. Any additional deposition of PPy onto the PU foam would lead to an increase concentration of PPy within the pores, which would be susceptible to tearing. Thus, the addition of PPy, as facilitated by this fourth coating, could not contribute to the improvement of the conductivity of the material, resulting in the plateau of resistivity of the material observed in Fig. 2.12. Thus, it was decided that four coatings of PPy onto the PU foam was the maximum loading to be used. These SEM images confirmed also that the PPy had percolated throughout the entire PU matrix and bonded to all available surfaces.

## 2.4.6 Surface Area Determination using Electrochemistry

### *Determination of Diffusion Coefficient for Ferricyanide ( $K_3FeCN_6$ )*

The following voltammograms were obtained using the Pt working electrode, when the potential was scanned from 0.6 to  $-0.2V$ .

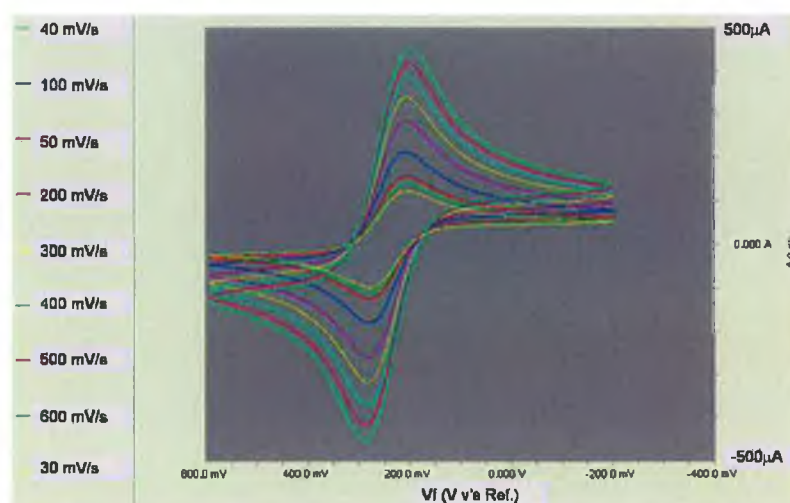


**Fig. 2.34** Number of voltammograms for Pt working electrode in 5 mM  $K_3FeCN_6$  in 0.5M KCl solution vs. Ag/AgCl ref electrode for scan rate from 30 mV-600 mV.

These voltammograms depict the regular peaks indicating faradaic currents for oxidation and reduction of the ferricyanide. Using the associated software, such as that displayed in Fig. 2.35, the peak currents,  $i_p$ , were determined for the 12<sup>th</sup> scan at each scan rate. These results are tabulated in Table 2.8.

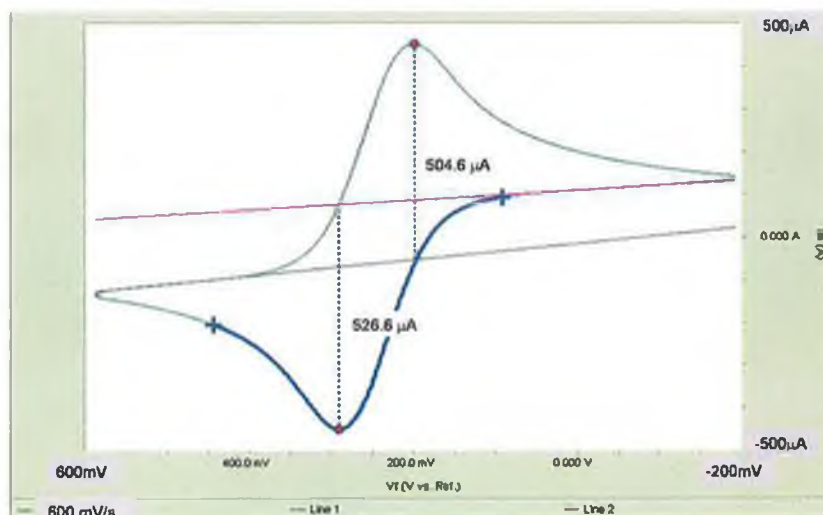


Fig. 2.35 Cyclic Voltammograms for Pt working electrode in 5 mM  $K_3FeCN_6$  in 0.5M KCl solution vs. Ag/AgCl ref electrode at scan rate of (top) 200 mV/s and (bottom) 600 mV/s.

Table 2.8 Peak Currents for each scan rate

Scan Rate $v$ (V/s)	$i_p$ ( $\mu A$ )
0.1	227.8
0.2	309.4
0.3	372.5
0.4	424.4
0.5	467.1
0.6	504.6
0.05	163.4
0.04	148.4
0.03	132.0

By plotting the peak current intensity,  $\mu A$ , vs. the square root of the scan rate,  $(V/s)^{1/2}$ , see Fig. 2.36, it was possible to calculate the diffusion coefficient of the  $K_3FeCN_6$ .

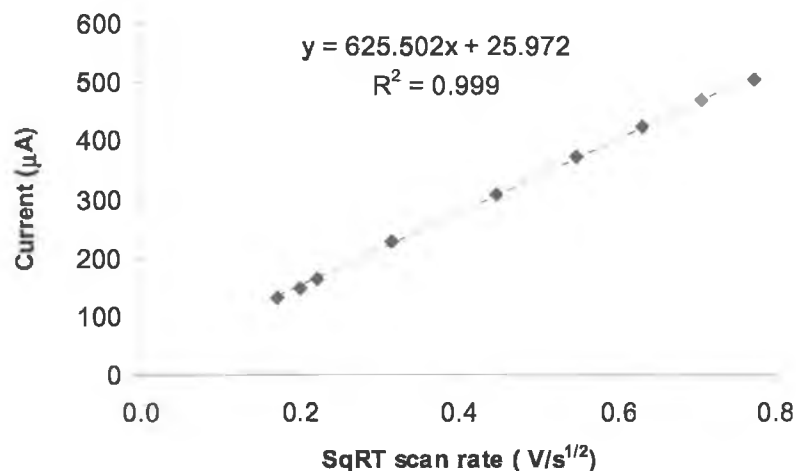
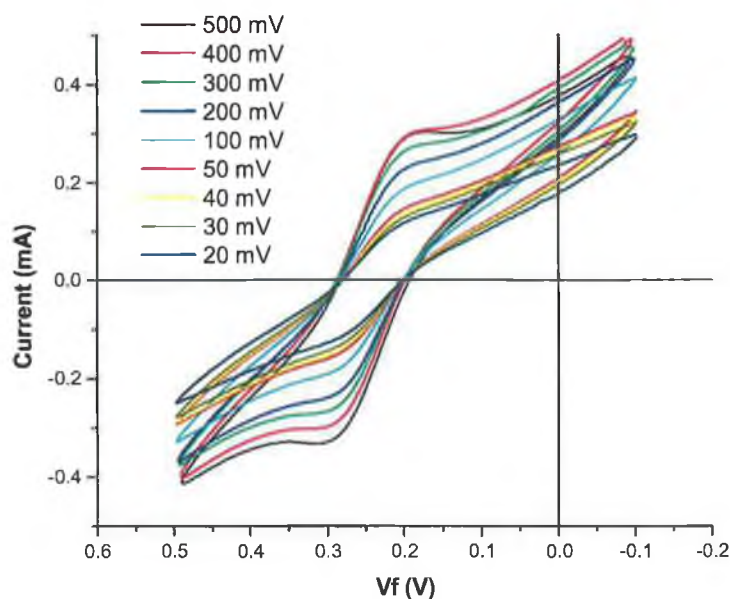


Fig. 2.36 Plot of current vs square root of scan rate for Pt working electrode in 5 mM  $K_3FeCN_6$  in 0.5M KCl solution vs. Ag/AgCl.

For this electrochemical system ( $K_3FeCN_6$ ),  $n=1$ . Therefore, the diffusion coefficient is calculated to be  $3.91 \times 10^{-8} \text{ cm}^2/\text{sec}$  at room temperature ( $22^\circ\text{C}$ ). This coefficient was less than that reported for  $Fe(CN)_6^{3-}$ , given as  $7.6 \times 10^{-6} \text{ cm}^2/\text{sec}$  [17] though discrepancies can occur due to different experimental conditions.

#### *Determination of Electrode surface area for PPy-PU foam samples*

A series of electrochemical experiments were carried out for each PPy-PU sample, whereby the PPy-PU formed the working electrode. The PPy layer on the PU foam is electroactive and thus, by connecting the PPy-PU foam to the potentiostat, the surface area of the electrode should be greatly increased.



**Fig. 2.37** Voltammogram for PPy.NDSA (1) PU foam connected as working electrode, in 5 mM  $K_3FeCN_6$  in 0.5M KCl solution vs. Ag/AgCl.

Fig. 2.37 shows the voltammograms obtained for the working electrode constructed using a piece of PU foam coated once using PPy.NDSA and attached to a Pt wire. Anodic and cathodic peaks due to the respective oxidation and reduction of ferricyanide can be seen to occur at 0.2 and 0.3V. It can be seen that the voltammograms is eschewed from that obtained using just the Pt wire, Fig. 2.35. This is because in this second plot, the electrochemical activity of PPy.NDSA must also be considered. PPy.NDSA is electroactive but not perfectly so and as such conductivity gets lost through the polymeric matrix and capacitive currents must also be considered. This leads to the eschewed voltammograms depicted in Fig. 2.37. Similar voltammograms were obtained for the foam working electrodes and can be seen in Appendix A.

The following graph, Fig. 2.38, plots the relationship of the peak currents to square root of the scan rate. As can be seen a linear relationship exists for each foam working electrode.

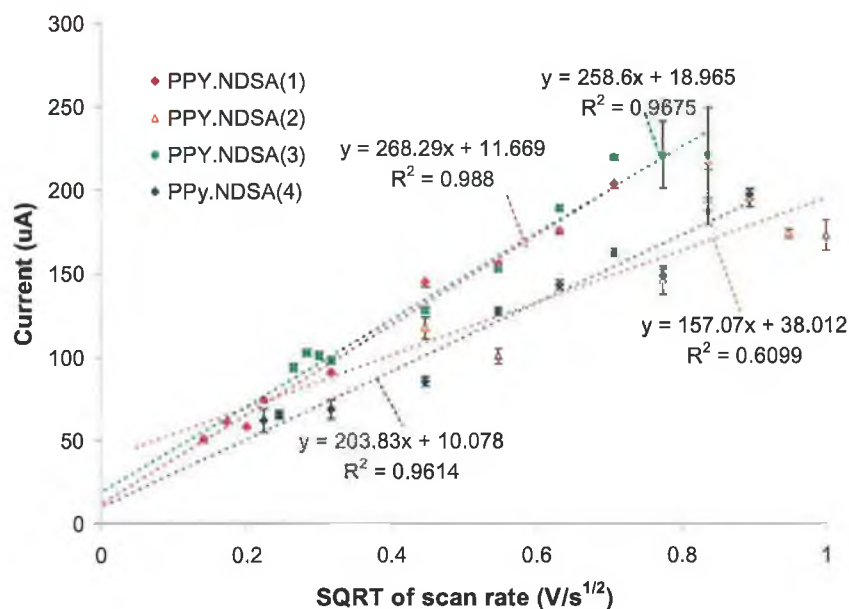


**Fig. 2.38** Current vs. square root of scan rates (20-500mV/s) for PU foam coated with different amounts of PPy.NDSA(n), where (n) represents the number of coating of PPy.NDSA deposited onto the PU foam.

Therefore, by using the diffusion coefficient for ferricyanide, calculated in section 2.4.6, the electroactive surface area of each PPy-PU working electrode could be calculated. These values are listed in Table 2.9.

**Table 2.9** List of calculated surface areas for PPy-PU foam working electrode.

PPy.NDSA (n)	Surface Area (cm <sup>2</sup> )	Volume (cm <sup>3</sup> )	Surface Area: Volume (cm <sup>2</sup> /cm <sup>3</sup> )
1	1.01	0.098	10.35
2	0.59	0.052	11.46
3	0.97	0.072	13.48
4	0.77	0.106	7.26

From the values listed in Table 2.9, it can be seen that the active surface area of the PPy-PU foam, acting as the working electrode, increased with successive coatings of



PPy. This phenomenon was expected because this method of determining the surface area of the foam required that the foam be conductive. After the first coating, it was previously observed, using SEMs (Fig. 2.21 & Fig. 2.22) that a complete coating of the foam was not achieved. Thus, the PPy layer did not reflect the surface area of the foam. After the second coating all of the PU foam appeared using SEMs (Fig. 2.23 - Fig. 2.25) to be coated in a continuous layer of PPy, thus the surface area of the material was much greater. The third coating of PPy, increased the population of nodular PPy growth on the PU foam which itself would increase the surface area of the foam, thus leading to a further increase in the measured surface area. After the fourth coating of PPy, these nodular growths were "filled-in", thus the fine detail was obscured, leading to the observed slight decrease in surface area. These observations corroborate the SEM observations and electrical behaviour of the PPy-coated PU foam samples.

### 2.4.7 Piezoresistive behaviour of PPy-PU foam

#### *Placing individual weights onto the foam*

Using the first setup as described in section 0, individual weights were placed onto the upper platform, causing the PPy-PU foam to compress. The resistance of the foam was measured using the multimeter as described previously and the results of this study are shown in Fig. 2.39. Here the PPy-PU foam was gradually compressed ( $n=2$ ) by placing weights on top of a platform, causing the foam to collapse. The error bars represent the standard deviation associated with each reading.

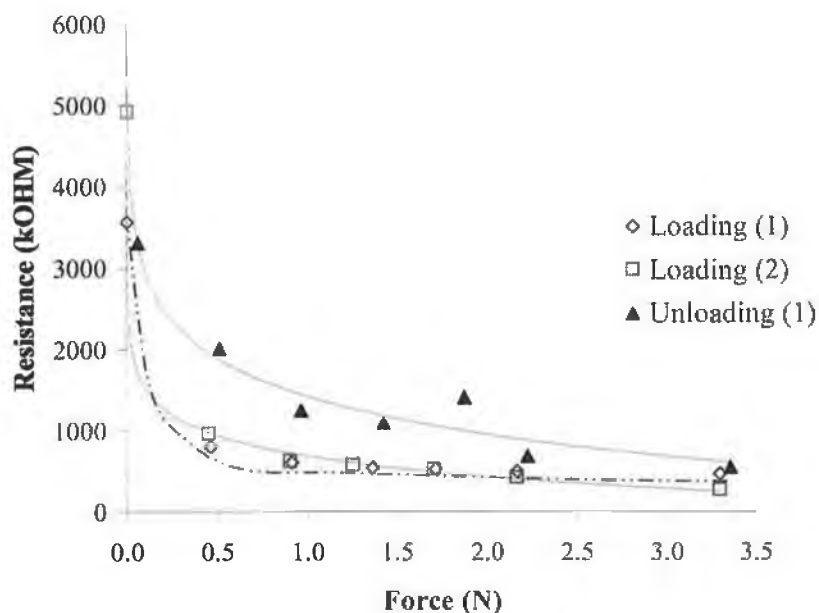


**Fig. 2.39** Plot illustrating the effect of placing weights on top of PPy-PU foam on the measured resistance of the material.

### Sensor Responses

The resistivity (and conversely the conductivity,  $\sigma$ ) of CEPs depend on the density of the charge carrier, i.e. polarons, present in individual polymer chains and the efficiency of charge movement between chains. Hence, the conductivity of a continuous conducting polymer film is described by MacDiarmid [18] as:

$$\sigma_{bulk} = f(\sigma_{intra}); f(\sigma_{inter}); f(\sigma_{domain})$$

Equation 2.5

where  $\sigma_{bulk}$  is the bulk conductivity of a conducting polymer, which is a cumulative result of the intra-molecular ( $\sigma_{intra}$ ), inter-molecular ( $\sigma_{inter}$ ), and the inter-domain ( $\sigma_{domain}$ ) conductivities of the polymer film structure.

One would expect the conductivity of the PPy-PU foam to also obey Equation 2.5. Given that the PU foam contains a large number of empty holes, when a pressure is exerted to compress the foam, it reduces the foam's overall volume, thus increasing the contacting area of the surface that is covered with PPy film. This in turn enhances the apparent density of the polaron and also shortens the conducting path length (increases magnitude of  $\sigma_{inter}$  and  $\sigma_{domain}$ ) to result in an increase in bulk conductivity. This effect was verified by using this first setup where the measured resistance recorded decreased as the compressing weight was increased see Fig. 2.39.

The overall relationship between the weight applied to the foam, i.e. the stress, and the resulting resistance is best described as a power relationship ( $y = 1250.6x - 0.1671$ ,  $R^2 = 0.96$ ). However, above 90g a linear relationship was found to exist. The sensitivity of the foam in this linear region was  $-171.34 \text{ k}\Omega/\text{N}$ ,  $n=2$ . The full dynamic range of response was not investigated because only limited weights could be fitted onto the small platform. The data indicates that the resistance  $R$  of the foam is proportional to the force,  $F$ , applied onto it. Therefore, a simple relationship can be established where:

$$\frac{1}{R} = kF + C$$

Equation 2.6

where  $k$  is a proportionality constant and  $C$  is a constant term.

*Further investigation of the piezoresistive nature of PPy-PU foam*

Using the setup as described in section 0, the PPy-PU foam was manually compressed in a quasi-static manner using a clamp. For these studies the strain was calculated as the percentage change in length of the foam compared to the original dimensions of the material. The following graph, Fig. 2.40 was obtained.

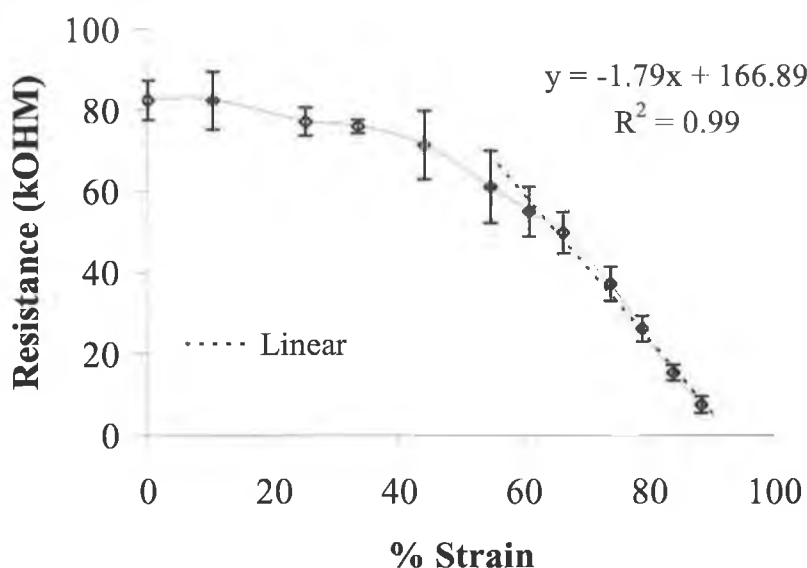


**Fig. 2.40** The resistance changes vs. the % strain for a single PPy-PU foam sample (n=3). The compressions were facilitated by using the manual clamp.

With this setup, greater strains could be placed on the foam and its behaviour monitored. Fig. 2.40 shows the relationship between the resistance of the PPy-PU foam and the % strain placed upon the foam. The limit of compression occurs at approximately 90%. This value was equivalent to 1.9 mm compared to the original length of 1.7 cm.

As with Fig. 2.39, two distinct regions of behaviour were observed in Fig. 2.40. In the first, the slope of the line decreases gradually until a specific point, approximately equal to 60% of the foam's original length. After this point, the slope of the line decreases much more steeply, in a linear fashion. This observation can be explained as follows: initially when the PPy-PU foam was compressed the interstitial spaces within the foam

decreases gradually with very slow increases in the contacting area between PPy coated surfaces (i.e. air was being squeezed out). When the compression finally reached a critical point (ca. 60% of the original length) where a massive increase in the contact area was achieved and a sharp drop in resistance was observed. Further compression resulted in more intimate contact between PPy chains and a linear change ( $R^2 = 0.99$  between 50- 90% length change) in resistance was observed.

The average sensitivity ( $n=3$ ) of the PPy-PU foam in this region was  $-1.79 \text{ k}\Omega/\%$  strain. Thus, a linear relationship existed between the measured resistance of the foam and the % strain experienced by the foam. Due to limits in both systems it was not possible to simultaneously determine both the stress and the strain and also the resistance of the foam during compressions. Thus, the Instron™ testing was carried out.

#### *Response time*

Before investigating the repeatability of the system, it was necessary to determine if hysteresis occurred in the system. In order to do this, the first setup was used. Three different weights were placed onto the foam corresponding to the values of 9.1 N, 13.7 N and 27.5 N. Each weight was placed atop of the PPy-coated PU foam and the output response was recorded. As can be seen in Fig. 2.41, this output signal was proportional to the magnitude of weight placed upon the sensor. Also observed was that the rate of change for each weight was similar, thus the foam sensor required longer times to reach equilibrium for the greater weights compared to the smaller weights. However, the times to reach steady state were different and were found to depend on the weight used in such a manner that bigger applied weight resulted in shorter time to reach equilibrium. When the lightest weight of ca. 9.1 N was applied an interesting response feature was observed where the weight seemed to have sunk down slowly with the foam structure adjusting to accommodate the weight. It resulted in a response time of ca. 11 sec. When the weight applied was increased to 13.7 N a response time of ca. 15 sec was obtained. The slow weight accommodation feature was barely visible suggested that a force or weight that exceeded the internal energy of the foam would yield a quick response. This hypothesis was proved by further increasing the weight to 27.5 N, which resulted in a response and it reached a plateau in ca. 17 sec. These response times are quite slow ( $> 5 \text{ sec}$ ) because the entire foam structure is not being compressed by the

force of the weight placed on top of it. Therefore, time is required to allow the vibrations caused by the partial compression of the structure to come to equilibrium. If these responses are compared to the results obtained when the entire foam was compressed, see Fig. 2.44, it can be seen that the response times was reduced to ca. 5 sec. Thus in order to reduce the response time of the sensor, the dimensions of the sensor should be reduced so that the area of the force matches the area of the sensor. Further investigations into the dynamic nature of these materials may require through the use of a dynamic mechanical testing machine.

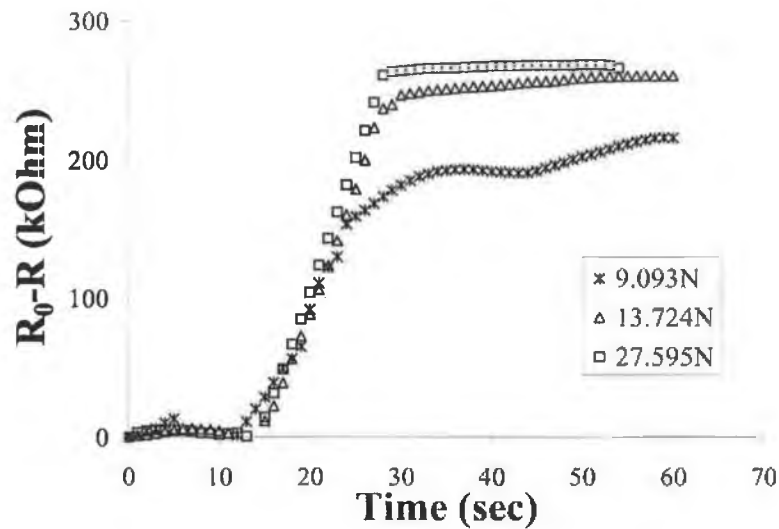


**Fig. 2.41** Normalised ( $R_0-R$ ) trace of PPy coated PU foam as pressure sensor when exposed to different forces.

### *Loading and Unloading Profiles*

Data recorded during testing of the PPy-PU foam using the first setup, using the individual weights, showed that a distinct difference exists for the resistance profile during loading of the polymer and unloading, as shown previously in Fig. 2.39.

Because the plots for the loading and unloading traces do not overlap, this behaviour suggests that energy is lost during compression of the foam. The main reason for this is that when the foam has been subjected to intense compression, it results in hysteresis in the PU substrate, i.e. loss of internal energy, and it would take a long time (hours) to get back to normal baseline. Instron™ testing of the bare PU foam confirmed this hysteresis. Fig. 2.42 shows the stress-strain results from the Instron™, for the PU foam sample (PU004) obtained from Iretex. Note the values for % strain are negative to indicate that the strain is compressive in nature.

The data was normalised by subtracting the position of the crosshead at any given time, ( $L_f$ ), from the initial position of the crosshead ( $L_i$ ). This was equal to the change in the length of the foam sample. Dividing this term by the initial length of the foam sample gives the strain (engineering strain,  $\epsilon_E$ ) incurred on the foam at every stage. The stress applied to the foam can be calculated by dividing the force applied over the foam area. Using the definition of engineering stress ( $\sigma_E$ ), the area is assumed to be constant. Thus, by plotting the  $\sigma_E$  vs. the  $\epsilon_E$ , the slope of the graph as the material is compressed up to a change of 20% should be equal to the Young's modulus of the material ( $E$ ).

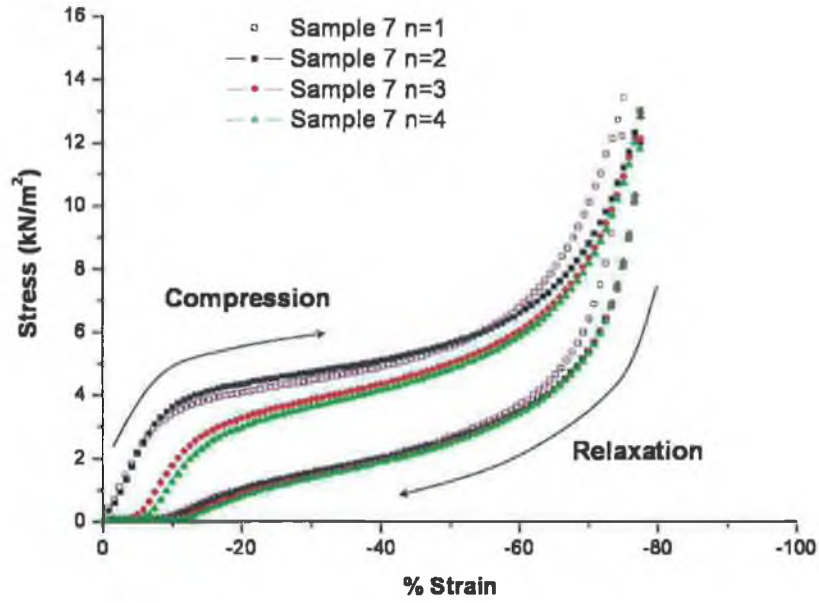


Fig. 2.42 Loading and unloading profile of Iretex foam. The arrows indicate the profile during compression and again during relaxation.

As the foam is gradually compressed, the force ( $F$ ) moves over the distance ( $\delta L$ ), resulting in a certain amount of work ( $W$ ) being done. This is calculated as:

$$W = F * \delta L$$

Equation 2.7

However, during these experiments that force varies in magnitude, therefore in order to determine the work done under these conditions, we must look at the load-displacement graph, i.e. the stress-strain graph. According to the equations for stress and strain,  $F = \sigma_{ave} \times L$  and  $\delta L = \epsilon L$ . Thus for unit volume, work is calculated as:

$$W = \frac{\sigma_{ave} * \epsilon_f}{2}$$

Equation 2.8

In this case the work done by the load is equal to the area under the curve. As the load is applied, strains are produced and their presence increases the energy within the foam. Energy is defined as the capacity of a body to do work. The energy, as calculated in Equation 2.8, is a measure of the elastic strain energy per unit volume absorbed by the



foam as a result of its deformation under the load. From the principle of conservation of energy, this energy ( $U$ ) is equal to the work done ( $W$ ) by the load, assuming that no other energy transfer, such as heat occurs.

Thus,

$$U = W = \sum_L P(x)dx$$

**Equation 2.9**

This energy is sometimes referred to as internal load, so as to distinguish it from the work done by the load. The unit of strain energy is Joule. The area under a complete stress-strain diagram gives a measure of a material's ability to absorb energy and is referred to as toughness. The larger the area under the curve, the tougher the material. A high modulus of toughness is important when a material is subject to impact loads, as would occur during plantar pressure monitoring. The difference between the curve for compression and that for relaxation for PU foam, is representative of the amount of internal energy consumed by the system during each compression. Similarly, with the other PE foam a difference between the compression and relaxation profile was observed, see Fig. 2.43.

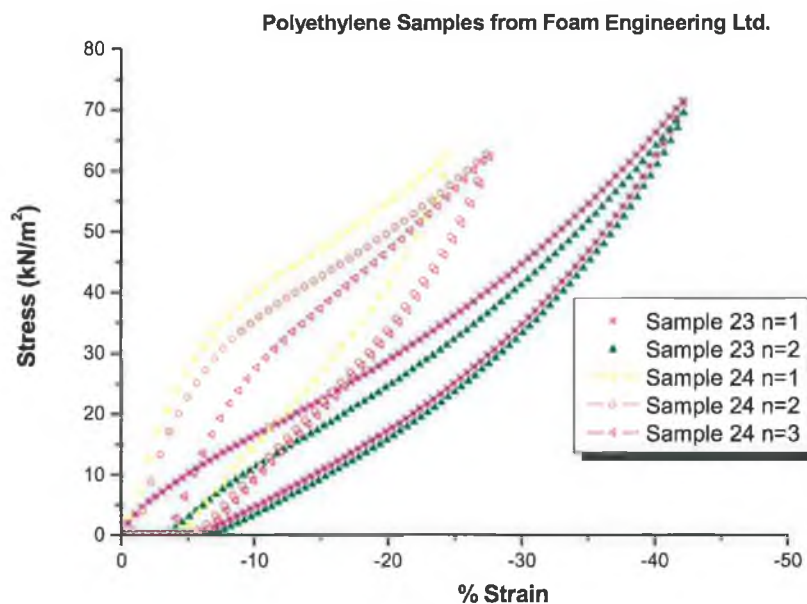


**Fig. 2.43** Stress-strain profile of polyethylene samples, PEX 18 BLK and PEX 45 BLK, both from F.E. Ltd.

Values for the internal energy of each of the foam samples were calculated using Equation 2.9, which are listed in Table 2.10. The values for the internal energy were normalised by dividing the calculated internal energy by the volume of the individual sample.

From this table it can be seen that the uncoated PE foam was almost 3½ times tougher than the uncoated PU foam. Also the coating of PPy onto the PU was seen to alter the overall strain energy density for the material. By coating PU foam twice with PPy.NDSA, the toughness of the resulting material increased by 3.6%, but after subsequent coatings decreased by 42.0% compared to the uncoated PU foam. Thus despite the coatings of PPy.NDSA the resulting material was soft and so still applicable for wearable applications.

**Table 2.10**      **List of internal energy for materials.**

<b>ID</b> <b>Number</b>	<b>Source</b>	<b>Material</b>	<b>Strain Energy</b> <b>Density</b> <b>(mJ/m<sup>3</sup>)</b>	<b>Coating with</b> <b>PPy.NDSA</b>
7A	IRE-TEX	<i>Polyurethane</i> <i>(PU)</i>	8374	NO
13A	F.E. Ltd ET18/125G	<i>PU</i>	791	NO
14A	F.E. Ltd ET29/170G	<i>PU</i>	874	NO
15	F.E. Ltd ET21/250G	<i>PU</i>	9321	YES x 4
15A	F.E. Ltd ET21/250G	<i>PU</i>	4201	NO
18	IRE-TEX	<i>PU</i>	8679	YES x 2
20	IRE-TEX	<i>PU</i>	12608	YES x 4
23	F.E. Ltd PEX 18 BLK	<i>Polyethylene</i> <i>Foam (PE)</i>	12446	NO
24	F.E. Ltd PEX 45 BLK	<i>PE</i>	12347	NO

### *Description of Stress-Strain Profile*

Each loading profile (Fig. 2.42) indicated three regions of behaviour for the PU foam, a linear portion ( $\lambda_L$ ), a stress-plateau ( $\lambda$ ) and a hardening portion ( $\lambda_H$ ) [19-21]. The interesting feature is the relatively long stress plateau for the foams.

The first region is linear. Compression in this region leads to the collapse of the porous holes within the foam structure.

Then the slope of the graph changed. At this stage all the air has been pushed out of the foam and so the material acted as a solid rather than a porous structure. Within this plateau range the stress is constant. The slope of the stress-strain curve for all PU samples, both coated and non-coated were similar, indicating that the PPy-coating has little effect on the PU matrix. After a certain amount of compression, the slope of the stress-strain curve changed indicating a change to the mechanical properties of the foam. In this region, the hardening region, the specimen is believed to buckle outwards in one region leading to the constant stress value. With continued loading, the growth of cold compressed regions increases at the expense of the non-compressed regions until the sample is uniformly compressed. When a material is forced into this region, either by compression or extension, hysteresis will occur, as the material will never be able to recover to 100% of its original shape and size. This region resembles the “cold-drawing stage” observed during stretching of a material.

Because the region where the foam can resist buckling has been surpassed, the compression was terminated shortly after entering this third region. Unloading of the foam was then initiated. Extended exposure to forces in this region can lead to permanent disruption of the foam structure.

The unloading profile again showed three different unloading characteristics. These regions are less distinct and the second unloading stress plateau was again relatively long and linear. The speed with which the crosshead was moving was faster than the rate of recovery of the foam. This was indicated by the sharp drop in force with respect to the position of the crosshead, in that the foam does not recover to 100%. This behaviour continued until the crosshead reached its initial position. The stress was seen

### *Repeatability of compressions using in-house setup*

Using the first setup, described in section 0, a fixed weight (235 grams or  $2.31 \text{ N/cm}^2$ ) was repeatedly placed onto and then taken off the platform, repeatedly compressing a piece of conducting foam while continuously monitoring the resistance of the PPy-PU foam. The data has been smoothed, using a 5-point moving average smoothing algorithm and normalised by dividing the resistance ( $R$ ) by the baseline resistance (for this PPy-PU foam sample  $R_0 = 9.5 \text{ M}\Omega$ ) of the sensor. The foam responded rapidly with a drop in resistance when the weight was placed on the upper platform and reached a pseudo-equilibrium within seconds and recovered in approximately 5 sec after the load was removed. It can be seen from the trace that the baseline resistance is much noisier than the resistance compressed sample. It was because the foam, being a light-weight sponge like material, is sensitive to external vibration; when the foam was compressed it changes into a denser material and this vibration effect is less significant.

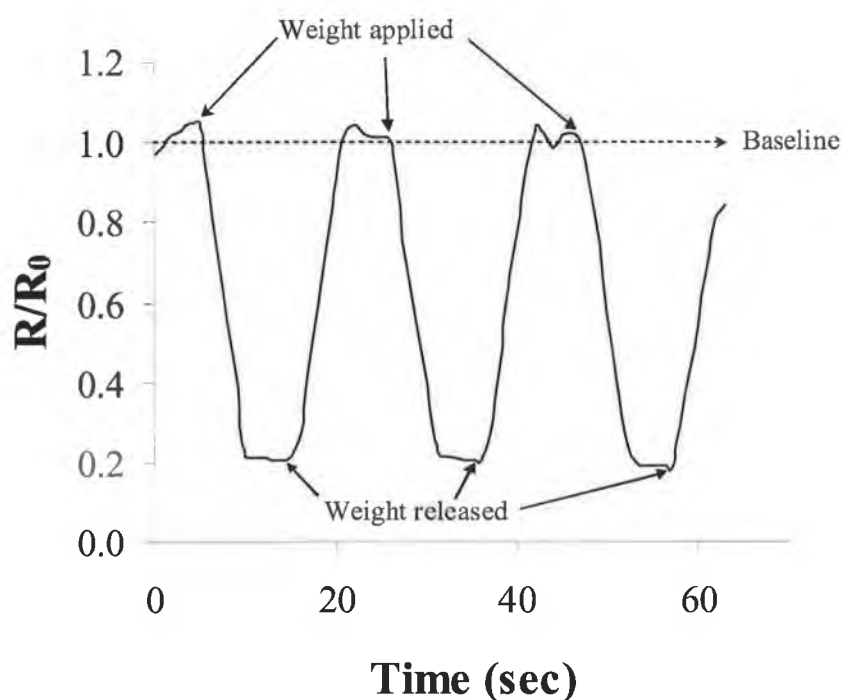


**Fig. 2.44** Normalised ( $R/R_0$ ) trace of PPy coated PU foam when repeatedly exposed to a force of  $2.31 \text{ N/cm}^2$ .

#### *Repeatability of compressions using Harvard pump setup*

The use of the Harvard syringe driver enabled the automatic compression and relaxation of the PU foam to be monitored. The following graph shows the response of the PPy-PU foam when it was repeatedly compressed to 50% of its original width and allowed to relax over the period of 1 hour. The following graph, Fig. 2.45 shows the resistance readings taken during 10 minutes of this study.

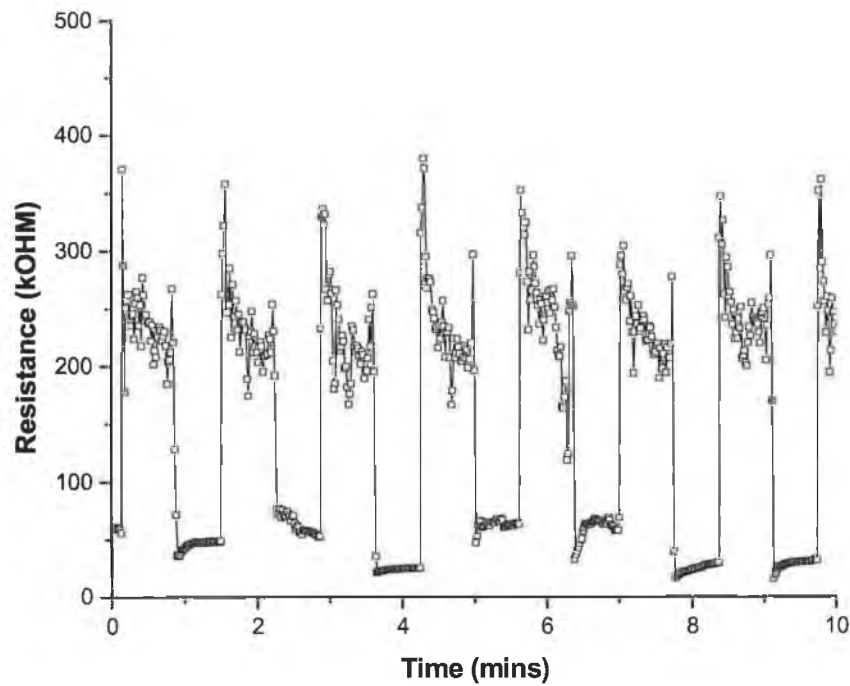


**Fig. 2.45** The continuous resistance readings for PPy-PU foam while being repetitively compressed and uncompressed.

This graph shows the real-time logging of resistance of foam during repeated compression and relaxation cycles. The rate of compression and relaxation was 0.1 cm/sec. Also  $l_{final} = 50\% l_{original}$ .

These results show that PU foam is a complex material, characteristic of a system with hysteresis. Though, this effect is present, it is repeatable and so this material can be used as the basis for a strain gauge material.

## 2.5 CONCLUSION

Polyurethane (PU) foam was selected as the substrate of choice for all subsequent sensor fabrications. Foam Engineering Ltd. was selected as the source for PU foam for the prototype wearable sensors.

The electrical resistance of the foam can be measured using a constant current multimeter. Electrical contacts to the PPy-PU foam could be made via direct clipping using crocodile clips or through the use of self-adhering Cu tape. PPy was shown, via SEM examination, to penetrate throughout the foam, which indicated that the source of the conductivity was not isolated to surface conducting pathways.

Polypyrrole (PPy) is an electroactive conducting polymer. When it was deposited onto a substrate it rendered the complete substrate electroactive also, without compromising the inherent mechanical characteristics of the substrate. This electroactive capacity of the PPy-PU foam was utilized in determining the surface area of the material. Using the Randles-Sevcik's Equation it was possible to relate the surface area of the electrode to the peak current,  $i_p$ , measured, using cyclic voltammetry, at various scan rates. According to this method, the surface area was determined to be one order of magnitude greater than the volume of the sample. The effect of coating PPy onto the PU foam was seen to increase the active surface area of the material, with the maximum surface area obtained after three coatings. It was seen using SEMs that the surface of the PU foam was coated with a continuous layer of PPy after two coatings, but that the third coating increased the population of PPy clusters on the surface, thus contributing to the surface area of the material. After the fourth coating, these clusters were covered over making the PPy layer denser with the loss of detail due to the presence of the nodules. Thus, the maximum surface area was achieved after three coatings. This method provided a means to estimate the surface area of the PPy-coated PU foam. Such information like this is useful to obtain especially if the material is to be applied as chemosensor, where the sensitivity of the sensor will depend on the active surface area of the material.

In this chapter a number of parameters for developing the wearable prototype were identified. Firstly, the base material was selected. This material, a solid polyurethane

foam, proved to be a suitable substrate for the deposition of conductive PPy. Secondly the dopant anion, 1,5-naphthalene disulphonic acid, disodium salt was selected as the dopant anion of choice for synthesis of conductive PPy. Next, the ruggedness of the PPy.NDSA coating on the PU foam was investigated by increasing the number of substrate washes between depositions. The results found that the final overall electrical resistance of the material was less than that for single washings but that it remained below  $1\text{ k}\Omega/\text{cm}$  and so was still very useful in the development of sensor prototypes.

The piezoresistive behaviour of the PPy-PU foam was examined within this chapter. It was shown that the electrical resistance of the PPy-PU foam is dependent on the force placed on the foam. This relationship, linear in the range of 0.88-3.43 N, which would imply that this novel material may be used as a strain gauge, within the area of wearable sensors, due to its soft compressible nature, which has not been masked despite the PPy-coating. Studies where this material has been implemented into wearable chemo- and physical- applications occur in forthcoming chapters.

Coating the polyurethane foam with polypyrrole was shown to affect the energy absorbing capability of the basic mechanical properties of the foam, producing a material that was stiffer than the base material. However, this change in mechanical properties did not alter the stress-plateau of the material, ensuring the material remained soft and compressible. It was noted that the change in resistance observed, during compressions, was due to the collapse of the porous structure of the foam matrix, which increased the contact points throughout the coated foam. In turn, this lead to more conductive pathways through the foam, resulting in the lower resistance values observed when the foam was compressed.

## **2.6 FURTHER STUDIES**

A number of further studies may be carried out on the characterisation of the PPy-PU foam structures. Firstly in order to confirm the coating of PPy onto the PU substrate, it may be necessary to perform EDX analysis of the coated and uncoated samples. For these studies it would be necessary to tag the PPy with a substituent groups containing an atom of differing mass to nitrogen and carbon as both these atoms are present in both PPy and PU which make analysis impossible to decipher. Secondly



dynamical mechanical analysis of the PPy-PU foam may be necessary to perform to determine the elastic modulus, yield strength, shear strength, and stress relaxation while performing various mechanical testing procedures, such as stress-strain, fatigue, and creep on these materials.

## 2.7 REFERENCES

1. Stussi, E., Stella, R., and De Rossi, D., *Chemoresistive conducting polymer-based odour sensors: influence of thickness changes on their sensing properties*. Sensors and Actuators B: Chemical, 1997. **43**(1-3): p. 180.
2. Steele, J., Wallace, G.G., and Munro, B. *Intelligent Knee Sleeve: A valid and reliable device to combat ACL injuries*. in *Journal of Science and Medicine in Sport*. 2002. Australia.
3. Steele, J., Wallace, G.G., Munro, B., Bowles, K.-A., Spinks, G.M., Campbell, T., Innis, P., and Megill, W. *Bouncing breasts, Noisy Knees and Intelligent Polymers: Where are we now?* in *International Workshop on Advanced Materials for Sensors and Actuators-Role of Nanotechnology*. 2002.
4. Mahesh, G.N., Banu, P., and Radhakrishnan, G., *Investigations on polyurethane ionomers. II. 3,4-dihydroxycinnamic acid-based anionomers*. Journal of Applied Polymer Science, 1997. **65**(11): p. 2105-2109.
5. Test Method ASTM D3574, <http://www.pfa.org/glossary.html>, Last Accessed: 17 FEB 06, (2006)
6. Viscoelastic foam, <http://www.absolutecomfortonsale.com/sensus-memory-foam-3inch.htm>, Last Accessed: 16 FEB 06, (2006)
7. Visco Foam - Space Age Protection against Tossing and Turning, [http://www.magnadreampad.com/m\\_visco\\_foam.htm](http://www.magnadreampad.com/m_visco_foam.htm), Last Accessed: 16 FEB 06, (2006)
8. Polartec Power Stretch, <http://www.houdinisportswear.com/produkter/material/stretchinsulation.html>, Last Accessed: 16 FEB 06, (2006)
9. Li, Y. and He, G., *Effect of preparation conditions on the two doping structures of polypyrrole*. Synthetic Metals Special Issue Chlamydiae, 1998. **94**(1): p. 127-129.
10. Li, Y. and Fan, Y., *Doping competition of anions during the electropolymerization of pyrrole in aqueous solutions*. Synthetic Metals, 1996. **79**(3): p. 225-227.
11. Glomerulonephritis, [http://www.kidneyfoundation.ab.ca/Be\\_Informed/about/commoncauses\\_glomerulonephritis.htm](http://www.kidneyfoundation.ab.ca/Be_Informed/about/commoncauses_glomerulonephritis.htm), Last Accessed: 24 MAY 2006, (2006)
12. Oxford University Press, *Oxford Illustrated Science Encyclopedia*. 2003, Oxford Press.
13. Microscope, <http://en.wikipedia.org/wiki/Microscope>, Last Accessed: 25 MAY 06, (2006)
14. Bard, A.J. and Faulkner, L.R., *Electrochemical Methods Fundamentals and Applications*. 2nd ed. 2001, Hoboken: John Wiley & Sons Inc.

15. Oh, K.W., Park, H.J., and Kim, S.H., *Electrical property and stability of electrochemically synthesized polypyrrole films*. Journal of Applied Polymer Science, 2004. **91**(6): p. 3659-3666.
16. Wu, J., Zhou, D., Too, C.O., and Wallace, G.G., *Conducting polymer coated lycra*. Synthetic Metals, 2005. **155**(3): p. 698-701.
17. Surface area, <http://chem.ch.huji.ac.il/~eugenik/surfacearea.htm>. Last Accessed: 07 MAR 06, (2006)
18. MacDiarmid, A.G., *Polyaniline and polypyrrole: Where are we headed?* Synthetic Metals, 1997. **84**(1-3): p. 27-34.
19. Gibson, L.J., *Cellular solids*. Mrs Bulletin, 2003. **28**(4): p. 270-271.
20. Wang, Y., Gioia, G., and Cuitino, A.M., *The deformation habits of compressed open-cell solid foams*. Journal of Engineering Materials and Technology-Transactions of the Asme, 2000. **122**(4): p. 376-378.
21. Gioia, G., Wang, Y., and Cuitino, A.M., *The energetics of heterogeneous deformation in open-cell solid foams*. Proceedings of the Royal Society of London Series a-Mathematical Physical and Engineering Sciences, 2001. **457**(2009): p. 1079-1096.

## **Chapter 3    APPLICATION OF PPY-COATED PU FOAM: CHEMO-SENSING**

### 3.1 INTRODUCTION

In principle, CEPs (conductive or conjugated electroactive polymers) can be incorporated into sensors to detect a wide variety of chemical targets. For example, in unadulterated form they can detect de-doping agents such as ammonia and basic moieties. However, it is also possible to increase the range of target analytes by incorporating different additives. These include synthetic receptors and functional groups, ligands, crown ethers, chiral structures, protein ligands, nucleotides and DNA [123].

The response of conducting polymers to a chemical stimulus can be identified by changes in its optical properties (e.g. colour) or electrical characteristics such as current flow, capacitance or resistance. The third of these is examined more closely in this chapter. The conductivity of polypyrrole is known to be dependent on the conjugation length of the polypyrrole chain, the longer the conjugation chain, the higher the conductivity of the polypyrrole [37, 38, 223]. Anything that can interfere with the charge transport along this conjugated path will have an effect on the charge mobility along the polypyrrole [224]. This interference is observed as a change in the resistivity of the polypyrrole. In general, chemically derived changes in resistivity or conductivity of a conducting polymer are usually due to the presence of electron accepting ( $A^-$ ) or donating ( $D^+$ ) analytes, as described in Chapter 1. The ability of the chemical stimulus to interact with the PPy will influence the magnitude of change to the resistivity of the material. If, for instance, the PPy is coated onto a highly porous material such as the open-celled PU foam introduced in Chapter 2, then the concentration of PPy exposed to the chemical stimulus will be greater than if a simple film of PPy was utilised. The porosity of this PU substrate also lends itself to the flow-through of the chemical stimulus, beneficial for example in gas-sensing applications where purging of the material can easily be facilitated by the porous nature of the PU substrate. Also the fact that the entire PPy-PU foam substrate is compressible and soft, then textile integration also remains a possibility. Thus the application of the PPy-PU in the development of a wearable gas chemosensor is possible. The prototype presented in this chapter combines the benefits of the PU foam (high surface area-to-volume ratio) with that of the PPy (high selectivity to ammonia vapours over other volatile gases) to develop a

sensor that can be used for real-time analysis of a gas flow. The results presented in this chapter are from initial experimental trials performed with the PPy-PU foam sensor.

## 3.2 EXPERIMENTAL

### 3.2.1 Chemical Selectivity

#### *Sample Preparation*

A piece of PU foam was coated as described in Chapter 2 from which a circular sample piece, of diameter 15 mm x 10 mm depth was cut.

The PPy-coated PU was fitted into a flow cell as shown in Fig. 3.1. Two Cu contacts were fitted to the inside of the polypropylene flow cell so that when the PPy-coated PU foam was inserted, contact was made to the foam. External wires were soldered to the copper contacts and fed to the multimeter. The resistance of the PPy-PU foam was measured using this constant current multimeter (34401A HP multimeter) and the data was collected by PC, as described in Chapter 2, section 2.3.2.

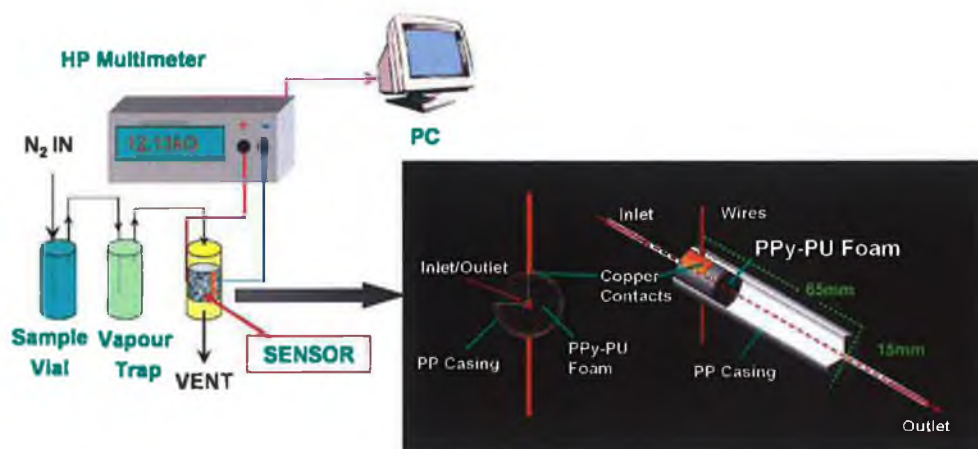


Fig. 3.1 Schematic of flow cell, wherein the PPy-PU foam was placed and connected to the multimeter for continuously monitoring, with an inset of the PPy-coated PU foam sensor.

The sensor flow cell (Fig. 3.1) was fitted with tubing (internal diameter = 0.0812", Cole Parmer, US) for gaseous analysis. Nitrogen gas was used as the carrier gas at a flow rate of 0.2 ml / sec  $\pm$  3%. Target vapours were produced by bubbling nitrogen through the volatile liquid (volume  $\sim$  30 ml), thus giving a continuous flow of saturated gas.

The vapour concentration was dependent on the vapour pressure of the liquid, values listed in Table 3.1. A vapour trap was positioned before the sensor cell to prevent any condensate passing through the sensor cell.

### *Chemicals*

**Table 3.1** Vapour pressure values for target organic vapours.

<b>Target Vapour</b>	<b>Vapour Pressure (kPa at 294K)</b>
Water	2.49
Toluene	3.47
Acetone	25.56
Ammonia	882.41
Propanol	78985.73

The change in resistance observed by the sensor was controlled by the contents of the headspace of the organic vapour. The analytes tested were water, toluene, acetone, ammonia and propanol. All headspace analysis experiments were carried out at room temperature ( $21\text{ }^{\circ}\text{C} \pm 4\text{ }^{\circ}\text{C}$ ) and at atmospheric pressure.

### 3.2.2 Stability Studies

The stability of both polymeric components, PPy and PU, is a concern when developing a prototype. Previous stability studies of PU have shown that it is a stable material in ambient conditions and that decomposition is induced only in environments of extreme salinity humidity and heat [227, 228]. PPy, on the other hand can oxidise in the presence of air, resulting in the loss of conjugation and hence a loss of conductivity. However, this phenomenon is slow and gradual until temperatures of ca. 230 °C have been reached. At this point bulk oxidation and decomposition occurs [215, 229]. The increase in the electrical resistance of PPy when exposed to ambient conditions has been documented as a result of the slow oxidation of PPy by atmospheric oxygen [42, 46, 49, 229-232]. In an effort to monitor this deterioration of the conductivity of the polypyrrole a stability study was initiated.

#### *Humidity Sensitivity*

Two humidity tests were performed to assess the any effects humidity would have on the performance of the PPy-PU gas sensors.

#### **Humidity test #1**

The first, employed the use of a series of saturated salt solutions, listed in Table 3.2. These salts solutions were prepared in order to provide environments of controlled humidity. The PPy-PU foam sensor was attached to the vial and allowed to equilibrate for 2 minutes for each resistance reading.

**Table 3.2**      **Relative Humidity Values for Saturated Salts solutions [233].**

<b>Salt</b>	<b>% Relative Humidity</b>
Lithium chloride	11
Magnesium chloride	33
Magnesium Nitrate	54
Sodium chloride	75
Potassium chloride	85
Potassium sulphate	97



#### **Humidity test #2:**

The second humidity test employed the use of a potassium sulphate saturated solution. Three PPy-PU foam samples were enclosed within a desiccator, wherein the saturated solution was introduced. The PPy-PU foam samples were kept within this closed environment for a number of months, during which time their resistance was periodically recorded using the HP multimeter as described in Chapter 2, section 2.3.2.

Nine PPy-PU foam samples to be prepared as per Chapter 2, three for each specific environment. Electrical contacts was made to each PPy-PU foam sample using Pt wire threaded through the foam and twisted at each end to secure. The electrical resistance of each of these PPy-PU foam samples was measured using a constant current multimeter (HP) as described in Chapter 2, section 2.3.2.

#### *Environment Preparation*

Three different environments were identified for monitoring;

1. ambient (lab air);
2. dry (sealed at room temperature);
3. wet (sealed at 90% RH).

The dry conditions were prepared by sealing the PPy-PU foam sample into a petri-dish which contained molecular sieves, thus providing a dry atmosphere. The wet conditions were prepared by storing the PPy-PU foam samples in a desiccators, within which a saturated salt solution of potassium sulphate was introduced to provide an atmosphere of 97% relative humidity.

#### *Protecting the sensors against the effects of humidity*

A protective coating was prepared for the PPy-PU foam samples. The first consisted of a polyisobutylene (PIB) coating made from a 3.75% solution of PIB in a 3:2 solution of hexane: toluene. This coating was deposited on previously coated PPy-PU foam samples using a Pasteur pipette. Electrical connections, made prior to the PIB coating, were made via Pt wire. The samples were allowed to dry overnight in the fume-hood at room temperature before been placed into their particular environment, i.e. ambient, dry or wet. Resistance measurements were made as described before in Chapter 2, section 2.3.2.

A second coating was also assessed. This one, a printed circuit lacquer (PCB for short), was an aerosol spray, commercially available from Radionics, RS 569-290. The aerosol is described as an anti-corrosive lacquer for protecting circuit boards from external moisture. Its contents were listed as follows: Acetone (30-60%), Isobutane (5-10%), Butane (10-30%), Propane (10-30%), Xylene (10-30%). Electrical connections, made prior to the PCB coating, were made via Pt wire. The samples were sprayed a total of three times and allowed to dry overnight in the fume-hood at room temperature before being placed into their particular environment, i.e. ambient, dry or wet. Resistance measurements were made as described before in Chapter 2, section 2.3.2.

#### *Temperature Sensitivity*

The effect of temperature on the performance of the PPy-PU foam was assessed using a Memmert oven at temperatures of 40, 50 & 60 °C. The sample vial, containing the PPy-PU foam, as used for the chemical analysis, with wires attached, was placed into the oven and the resistance continuously measured while the temperature was changed from ambient to 60 °C.

### 3.3 RESULTS & DISCUSSION

#### 3.3.1 Sensitivity

The resistivity is related to resistance through the following equation:

$$R = \frac{\rho L}{A}$$

Equation 3.1

Where  $R$  = resistance in Ohms,  $L$  = length in metres,  $A$  = area in metres squared. Thus  $\rho$  = resistivity in Ohm metres. All measurements recorded the resistance of the material and will be quoted in Ohms.

Due to the experimental setup, the length and area of the sensor can be assumed to remain constant throughout the experiment. Therefore, the changes in resistivity incurred were directly proportional to changes in the overall resistance of the PPy-PU foam as were measured by the multimeter. The changes in resistance are caused by changes to the PPy-layer coated onto the PU foam. In order to compare the response of the sensor to each vapour the relative change in resistance was calculated as:

$$\frac{R_t - R_0}{R_0} \times 100$$

Equation 3.2

where  $R_t$  is the resistance at time  $t$ , and  $R_0$  is the baseline resistance prior to sample introduction.

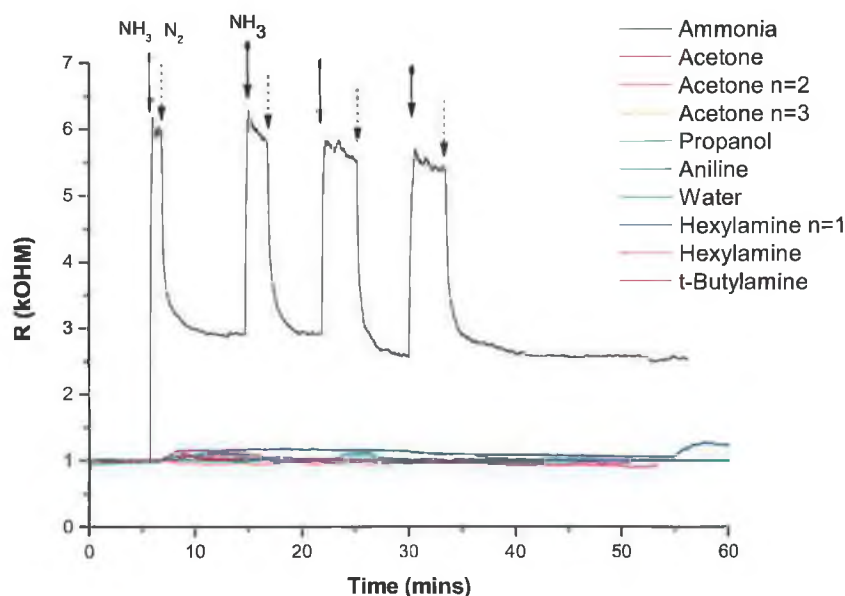


**Fig. 3.2 Real-time resistivity response of PPy-PU foam to different gas phase analytes using a constant current multimeter (HP 34401A).**

From Fig. 3.2, it can be seen that the greatest change in resistance was obtained when the sensor was exposed to ammonia-saturated nitrogen gas plug, with an increase in resistance of the sensor from 1 to ca. 6 k $\Omega$ . This initial rapid response reduced to 2.5 k $\Omega$  when a flow of nitrogen was purged through the system. This shift in the baseline is evident of hysteresis within the system. The resistance response of the sensor again increased with subsequent exposures to ammonia-saturated nitrogen gas in a reproducible manner. The percentage resistance change for the subsequent exposures to ammonia-saturated gas were approximately the same differing by a maximum of 10% showing the repeatability of the sensor for ammonia detection.

These changes in resistance were brought about by the de-doping of the PPy layer within the PPy-coated PU foam. When the ammonia interacted with PPy, the lone pair of electrons on the imine nitrogen donate their charge to the PPy backbone, negating the need for the dopant. However, the dopant (here NDSA) was of such a large size that it was relatively immobile, as compared to other dopant anions such as Cl<sup>-</sup>. The NDSA anion, therefore, was trapped within the PPy structure of the system without contributing the charge-flow process. However, conformational changes must occurred

in order to accommodate the charge changes on the polypyrrole backbone, which are difficult to reverse. This resulted in a shift in the baseline resistance as seen in Fig. 3.2 & Fig. 3.3. A similar phenomenon was described by Gutafsson and Lundstrom [225] whereby the irreversible and reversible changes in conductivity of polypyrrole caused by ammonia gas were investigated. Therefore, this would suggest that the sensor requires pre-treatment before it can be used as a sensor for repeated analysis.

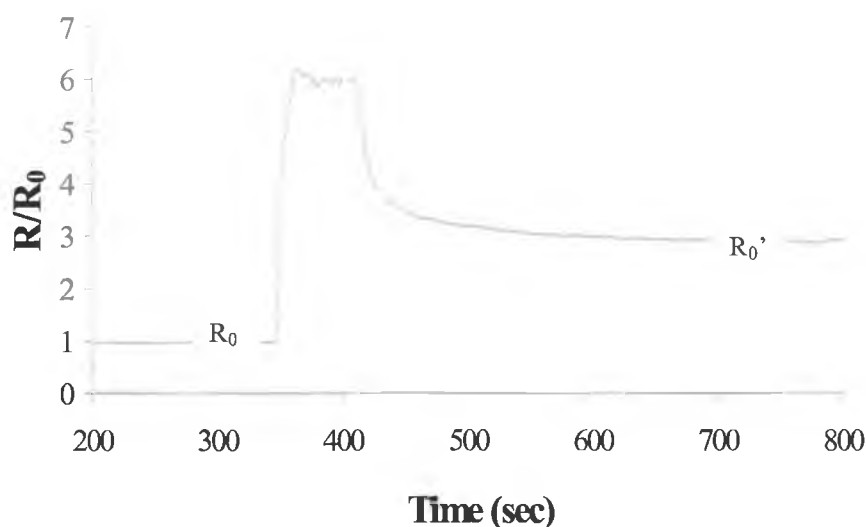
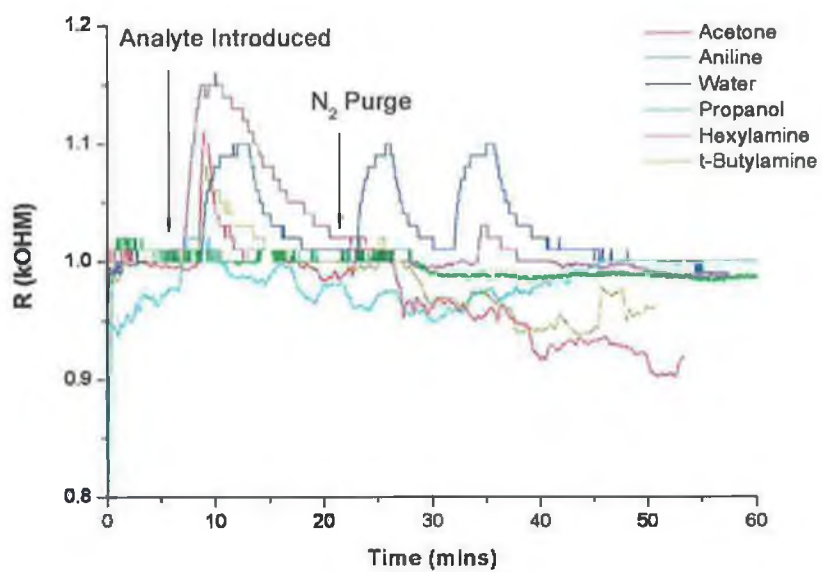


Fig. 3.3 Initial response to ammonia-saturated-nitrogen gas.

The responses of the PPy-PU foam to the other vapour analytes was not as large as that observed for ammonia. However, in Fig. 3.4 it can be seen that the sensor responded repetitively to exposures of water and to hexylamine. Both these analytes, again, have de-doping capabilities facilitating these observed changes. The effect of the alkyl group is to raise the energy of the lone pair of electrons on the N and so hexylamine is better able to interfere with the conjugation chain of PPy, therefore inducing the observed change to the resistance of the sensor. However, the size of hexylamine (101.19 g/mol) and t-butylamine (73.14 g/mol) inhibit their diffusion through the matrix, resulting in the slow recovery of the sensor and the slow response of the sensor to subsequent exposures. Ammonia and water, on the other hand, are small molecules (17.03 and

18.00 g/mol respectively) and so can more easily diffuse through the matrix to affect the conjugation of the PPy chain.



**Fig. 3.4** Real-time resistance responses of the PPy-PU foam sensor when exposed to acetone, aniline, water, propanol, hexylamine and t-butylamine.

### 3.3.2 Response Time

The response time of the sensor to ammonia, that is the time taken from the offset to signal stabilisation was determined to be approximately 1 minute, comparable with commercially available ammonia detectors [226]. The recovery time, however, was longer at approximately 4 minutes. This recovery time maybe improved with increasing flow rates of the purging nitrogen gas. The response times for the other organic vapours, listed in Table 3.3, though very low were difficult to calculate for definite, as the change in resistance observed was extremely low.

**Table 3.3** Response of sensor to organic vapours.

<b>Organic vapour</b>	<b>Average Change Resistance</b>	<b>% in Resistance</b>	<b>Relative Response (<math>R/R_w</math>)<sup>3</sup></b>	<b>Response Time (mins)</b>	<b>Recovery Time (mins)</b>
Acetone	$0.82 \pm 0.60$		0.09	$0.89 \pm 0.12$	$1.85 \pm 0.80$
Propanol	$2.09 \pm 1.45$		0.22	$1.46 \pm 0.19$	$1.77 \pm 0.66$
Water	$9.45 \pm 0.91$		1.00	$2.54 \pm 0.33$	$7.90 \pm 2.70$
Ammonia	$99.57 \pm 9.34$		10.54	$0.82 \pm 0.15$	$3.54 \pm 0.82$

The sensitivity of the sensor, is indicated in Fig. 3.2 by the amplitude of the resistance response. It can be readily seen that the PPy-PU sensor is much more sensitive (10 times as sensitive when compared to the response to water) to ammonia vapour than any other vapour.

<sup>3</sup> The relative responses listed in Table 3.3 were listed in comparison with the response of the sensor to water ( $R_w$ ). These were normalised by dividing the response to the analyte ( $R_v$ ) by the response to water ( $R_w$ ) as per the following equation:

$$\frac{R_v - R_{0v}}{R_w - R_{0w}}$$

**Equation 3.**

$R_{0v}$  is the baseline resistance prior to vapour exposure and  $R_{0w}$  is the baseline resistance prior to exposure to water.

The high sensitivity of this sensor to ammonia was due to the direct interactions of the ammonia vapour with the PPy layer. The lone pair in the ammonia directly attacks the positive charge on the PPy chain, shortening the conjugation length of the polymer and so increasing the resistance of the PPy. The other vapours cause the PU matrix to swell (or contract) through solvation. Thus, these responses were diffusion controlled. In an effort to improve the response times of these sensors the bulk to surface area ratio of the sensor should be made smaller, thus maximising the amount of sensor in contact with the gaseous analyte. As can be seen in Table 3.3, the response times of this type of sensor are relatively fast, thus the foam sensor is a good design as it has a low bulk to surface area ratio as determined in Chapter 4. The recovery to baseline is always slower for diffusion limited responses as it depends on the concentration difference to drive the process. Faster responses and recoveries maybe achieved using higher concentration of gaseous analytes.

However, this type of interaction is not selective and it is difficult to unequivocally attribute the change in resistance of the PPy-coated PU foam to any one type of vapour. Thus, instead of one sensor sensitive and selective to the target vapour, an array or series of sensors with differing substrates would need to be constructed. Then, the relative response of all the sensors could be used to identify the vapour. However, the substrate has been limited to polyurethane, thus further investigations into arrays is limited.



### 3.3.3 Humidity Sensitivity

#### *Short term Humidity Study*

It was previously noted in Fig. 3.4 that the PPy-PU sensor responded repeatedly when exposed to water vapour. Thus, further humidity studies were warranted.

During the first humidity study, the PPy-PU sensor was exposed to the sealed headspace of a saturated salt solution. The changes in the measured resistance from this study can be seen in Fig. 3.5.

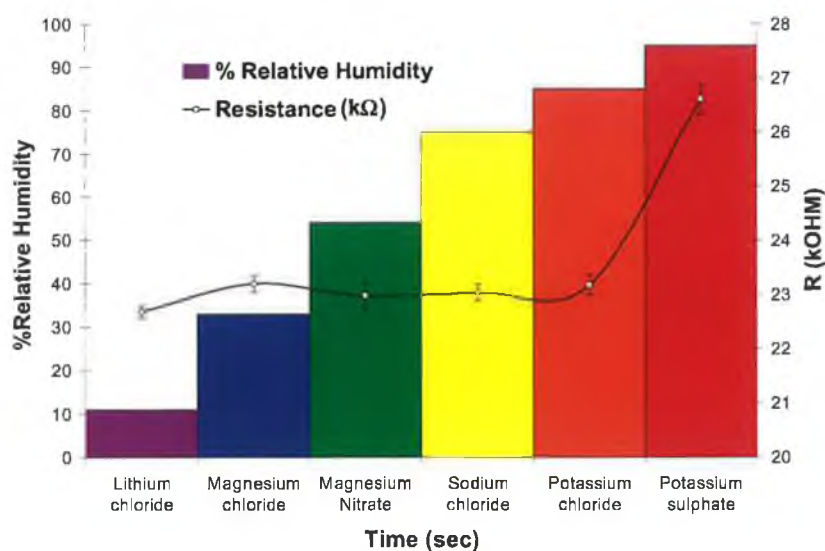


**Fig. 3.5** Resistance response of PPy- PU sensor when exposed to sealed saturated salt environments, yielding headspaces of differing relative humidity levels.

It can be seen that there is no dramatic change in the resistance until the relative humidity reaches approximately 85%. After this point there is an increase in the resistance of the sensor. This is because after this point water is able to interfere with the charge transport along the polypyrrole chains by hydration of the dopant anion[234], leading to an increase in the resistance observed.

### Long Term Humidity Study

The following graphs, Fig. 3.6 - Fig. 3.8, show the effect the environment has on the resistance of the PPy-coated PU foam. It can be readily seen in Fig. 3.6 that the effect that ambient conditions have on the PPy-PU sensor is to increase its electrical resistance gradually over time. Since the length and area of the PPy-PU samples are kept constant throughout the experiment, the measured resistance of each sample is proportional to the resistivity of each sample, according to Equation 3.1. The amplitude of resistivity, as mentioned previously, is due to the nature of the PPy coating on the PU substrate. Therefore, according to Fig. 3.6, the PPy layer coated onto the PU substrate changed over the 6 weeks of the experiment. Similar results for coated fabrics have been reported by Wu, [215], showing the gradual oxidation of PPy in air. This change in measured resistivity is thought to be due to shortening of the PPy conjugation length, the length of polymeric chain over which the  $\pi$ -electrons are delocalised. The longer this  $\pi$ -system is, the greater the conductivity of the polymer. If a moiety interacts with the PPy of the  $\pi$ -system, then the conjugation is disrupted and the length of conjugation shortened which leads to a decrease in conductivity throughout the sample (or conversely an increase in the resistivity throughout the sample). It can be seen that after 50 days, the resistance of the sample began to stabilise.

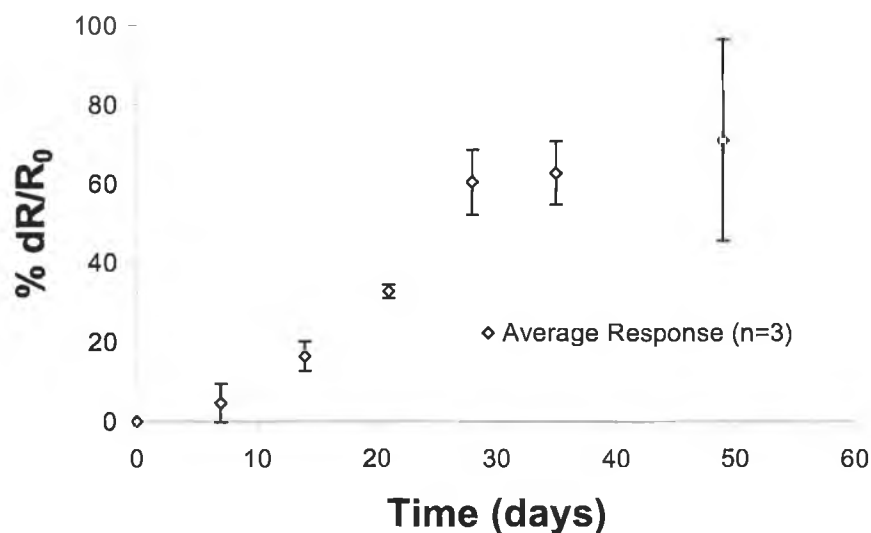


**Fig. 3.6 Resistance profile of PPy-PU foam samples kept at ambient conditions. The average trendline is for three PPy-PU samples.**

In contrast, the resistance of the samples stored in dry conditions (in the presence of molecular sieves) decreased over the 6 weeks. These changes are depicted in Fig. 3.7. These changes in resistance are of much smaller magnitude (20%) compared to the change observed in the ambient sample (75%). By removing the moisture in the air it can be seen that the resistance of the sample was stabilised very slowly after about 30 days.

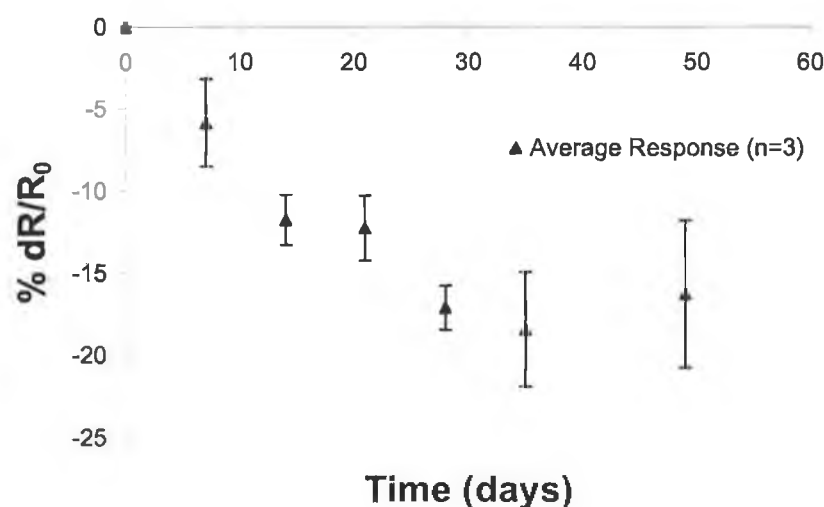


**Fig. 3.7** Resistance profile of PPy-PU foam samples kept at dry conditions. The average trendline is for three PPy-PU samples.

The third controlled environment investigated the effects humidity and moisture had on the resistance of the PPy-PU foam samples. The results of this investigation can be found in Fig. 3.8. It can be seen that the resistance increases over the course of the 6 weeks. This increase in resistance, however, is not as large as the increase observed in the “ambient” samples (~ 40 % change for wet sample v’s 75 % change for ambient samples). This maybe due to the enclosed wet environment thus limiting the supply of oxygen to the coated materials.

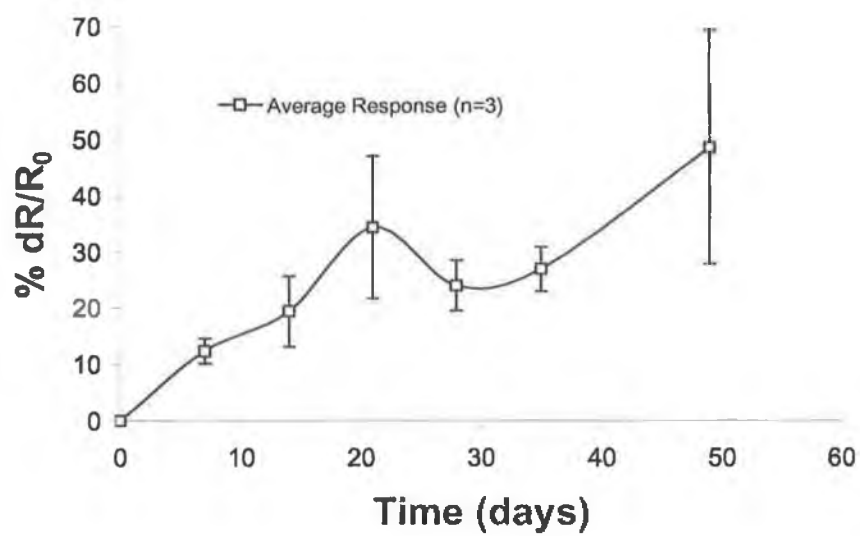


**Fig. 3.8 Resistance profile of PPy-PU foam samples kept at wet conditions (97% RH). The average trendline is for three PPy-PU samples.**

### 3.3.4 Temperature Sensitivity

Previous TGA analysis of PPy-coated fabrics has shown that PPy.NDSA is stable up to ca. 260°C [215, 235]. After these temperatures thermal decomposition of the PPy and counterion occurs with sample weight loss. However, the intended use of these sensors is for on-body monitoring, thus their maximum operation temperature should not exceed 40°C (313K).

However, the response of the sensor was monitored to determine whether changes to its resistance could be incurred by temperature changes. In Fig. 3.1, these temperature effects can be observed. It can be seen that between 295K and 335K, the resistance of the materials is raised slightly in relation to the temperature.

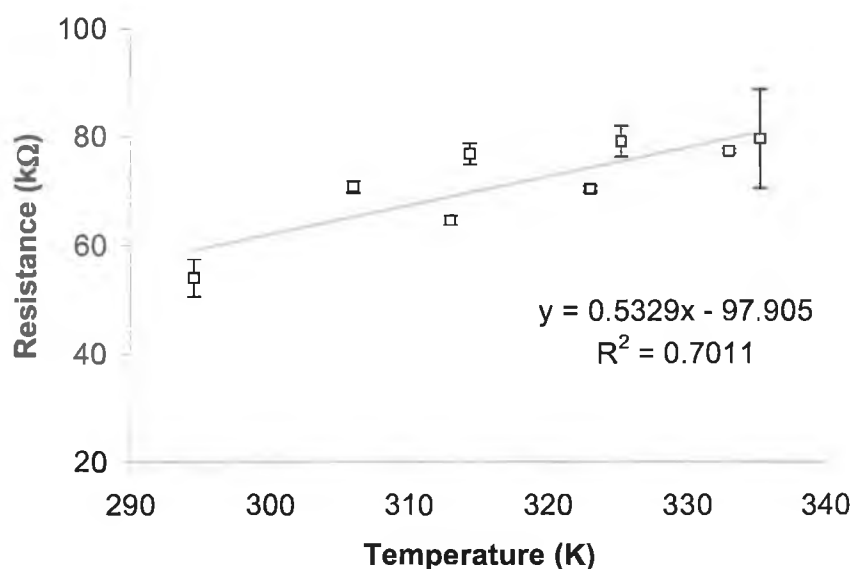


Fig. 3.1 Effect of temperature on resistance of PPy-PU sensor.

Because of the gradual increase in resistance to temperature, this change is not thought to be due to the degradation, but rather to the swelling of the polyurethane foam, which will increase the gap spacing with the foam matrix. The softening point for polyurethane elastomers occurs ca. 340 K [236], thus swelling of the PU matrix prior to the softening may occur. This would lead to the gradual decrease in the number of bridging conductive pathways and hence an increase in the resistance of the sensor.

### 3.3.5 Protecting the sensors against the effects of humidity

These changes in resistance observed in the graphs Fig. 3.6-Fig. 3.8 indicate a drifting effect in the response of the sensor. In order to combat this effect, a protective coating for the PPy-PU foam samples was proposed. The two protective coatings selected were a PIB coating and PCB laquer.

PIB, polyisobutylene, is a non-polar hydrophobic polymer and so is water repellent. PCB referred to a commercially available printed circuit board lacquer which is used in the electronics industry to protect electronic equipment against moisture effects. Thus, it was proposed that these polymeric compositions would be able to provide a certain degree of protection to the PPy-PU from hydrophilic moieties such as ammonia and water vapour or moisture, thus minimising the drift of the sensor. The following graphs show the resistance changes observed for the sensors for each environment over the number of weeks.

#### *Ambient Conditions*

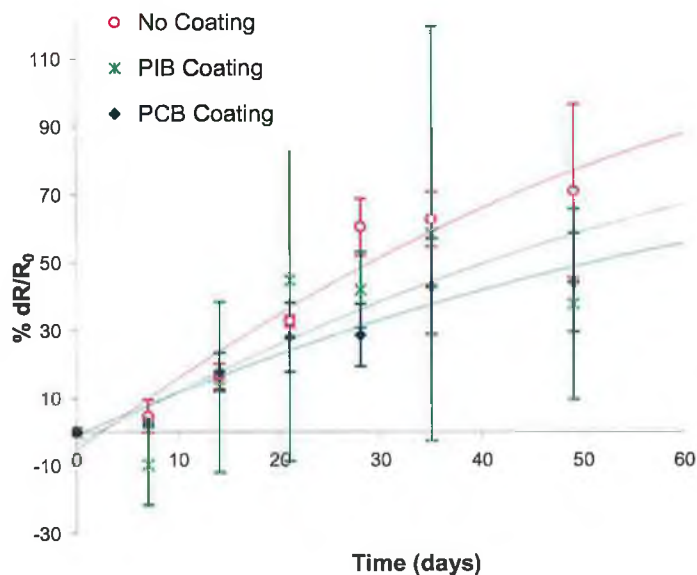
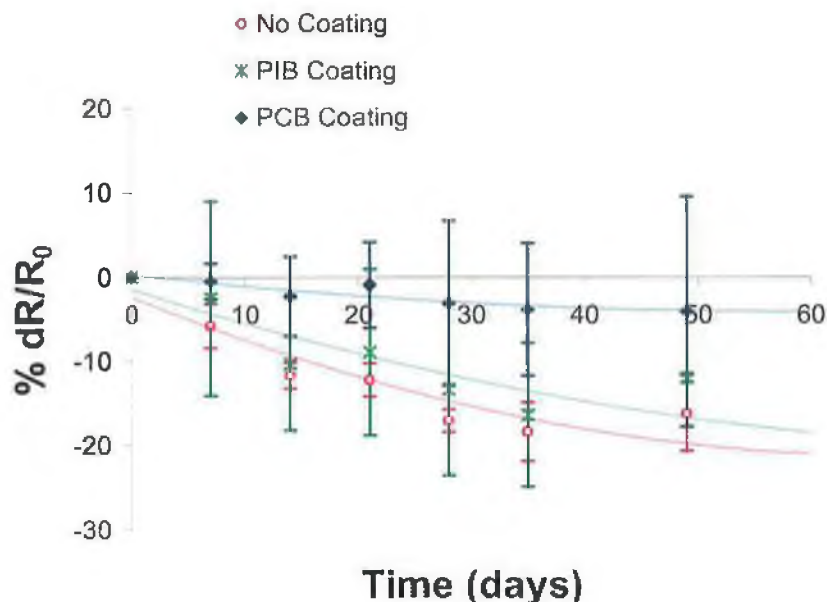


Fig. 3.9 Resistance profile of PIB-, PCB- coated and uncoated PPy-PU foam samples kept at ambient conditions. The trendline represents the polymeric fit for the data.

In Fig. 3.9, the percentage resistivity behaviour of all samples are shown. Each data point represents the average for three distinct sensors prepared as described in the experimental section. As can be seen, the resistivity of all the sensors increases over the 60 day period of the experiment, the non-coated samples increasing the most. At first, both the uncoated and PCB coated PPy-PU foam samples increased their resistivity by ca 5% over the first 5 days. This would indicate the exposure of the PPy layer to oxidative attack. However, after day 35, the resistivity of the PCB samples began to level-off and stabilise. In comparison the samples coated with PIB showed a slower on-set of increased resistivity. PIB is a non-polar membrane and as such should repel aqueous and polar moieties. Thus, the samples coated with PIB, though showed a later on-set of increased resistivity, the final resistivity of these samples after day 35 exceeded that for the PCB-coated samples. This would indicate that though initially resilient to environmental conditions the PIB layer is not robust enough to protect the PPy layer from oxidative attack. This may also indicated that other non-polar vapours may be present in the ambient conditions of the experiment which contributed to the degradation of the PIB layer.

The use of these two membranes have shown that the measured resistivity can be lowered by use of an external membrane or coating on top of the PPy-PU foam structure. The use of a non-polar membrane assisted in delaying the effect of exposure to air and oxidative attack. However it was shown not to be robust enough to protect the PPy-PU foam sensor over the 60 period. The PCB lacquer on the other hand, though perhaps too thin to prevent any oxidative attack, could assist with stabilising the resistivity of the PPy layer on the foam samples. Thus in order to maintain the initial resistance of the PPy-PU foam sensor, the air and oxygen would need to be scavenged to prevent the oxidative aging of the samples.

### Dry Conditions



**Fig. 3.10** Resistance profile of PIB coated PPy-PU foam samples kept under dry conditions. The trendline represents a polymeric fit for the data.

Again in dry conditions the previously observed decrease in resistance (Fig. 3.7) occurred again. Both the uncoated and the PIB-coated samples decreased by ca 20% of their original resistivity reading, whereas the sample coated with PCB lacquer decreased by approximately 4%. Under these conditions, the molecular sieves absorb all moisture from their surrounding environment. Thus, these observed decreases in resistance are thought to be due to the further removal of water and oxidative moieties from the PPy-PU foam structure. The lesser decrease observed for the samples coated with PC lacquer would indicate that the PCB lacquer did not allow this to occur. Thus the resistivity measurements for these sensors remained constant over the 60 day period



### *Wet conditions*

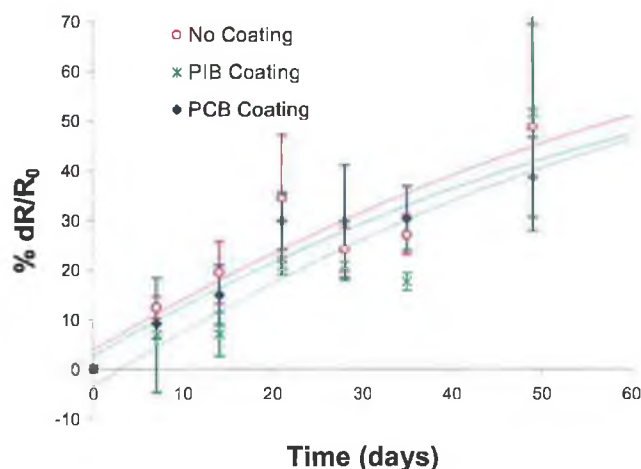


**Fig. 3.11** Resistance profile of PIB-, PCB- coated and uncoated PPy-PU foam samples kept at wet conditions (97% RH). The trendline is fitted for a polymeric fit to the data.

The effects of coating the PPy-PU foam sensors with and without a protective layer can be seen in Fig. 3.11. The percentage increase of resistivity are again the greatest for the uncoated samples, showing an approximate 50% rise in resistivity over the 60-day period. PIB, initially delayed this rise in resistivity, as would be expected from a hydrophobic protective layer. Thus, this again demonstrated that the PIB coating was able to delay the on-set of aging, but failed after approximately 35 days. The samples coated with PCB lacquer showed an initial increase in resistivity, but this levelled off after 20 days.

During the experiment, it was noted that the mechanical properties of the PIB PPy-PU foam samples were very different from the PPy-PU samples, primarily in the fact that the PIB coated samples felt “sticky” compared to the non-PIB samples. This “stickiness” also affected the compressibility of the PPy-PU foam samples. Thus, for the development of a pressure sensitive sensor, PIB was not suitable. However, if this material were to be used as a chemical sensor, utilising the sensors low bulk to surface area ratio and whereby little or no mechanical stress would be placed on the PU structure, then a coating similar to PIB or PCB lacquer would need to be considered as an integral part to maintain the baseline resistivity of the sensor. However, further optimisation of the composition of this protective coating would be required.

### 3.4 CONCLUSION

To conclude, the PPy-coated PU foam described in Chapter 2 was applied successfully as a chemosensor. It was shown that PPy-coated PU foam responded selectively (up to 10 times) to ammonia over other volatile organic vapours. The response of the sensor has been repeatable ( $RSD < 10\%$ ) and rapid (response time = 0.82 minutes). Initial hysteresis effects were a problem for this PPy-PU gas-sensor. This was due to the irreversible interactions of ammonia with the PPy layer on the foam sensor. However, after initial conditions of the sensor, a repeatable response could be generated by the sensor when exposed to ammonia. The response of the sensor to other volatile organic vapours resulted in unselective and small responses. These responses were diffusion controlled and so were slower than the response towards ammonia. Because of the large surface area of the sensor, it was possible that vapours could get trapped within the polymeric substrate. Due to possible solvation of the polyurethane, swelling of the sensor could occur and cause distortions in the resistance of the PPy-coated PU foam.

It could be seen that temperature and humidity do affect the measured resistance of the PPy-PU foam. In an effort to improve the stability and performance of the sensing material in such conditions the final product would require a protective encapsulating layer. This protective layer would be required to form a barrier against any moisture entering or exiting the material. The structure of this protective layer would need to be developed so that it would not compromise the physical, mechanical or tactile properties of the foam, as doing so would negate the use of use a material for wearable applications. Also if connections were made to the PPy-coated PU foam prior to external coating, the encapsulation would aid the binding of the final sensor.

In addition to being soft and wearable, the advantage of this type of chemical gas sensor lies in its high surface area-to-volume ratio enabling it to potentially detect low concentrations of volatile organic vapours, in particular ammonia gas, rapidly. However, the full potential of the PPy- PU sensor as a chemical sensor was not entirely investigated but these initial studies compared well with similar findings by Wang et al. [237].

### 3.5 REFERENCES

1. McQuade, D.T., Pullen, A.E., and Swager, T.M., *Conjugated polymer-based chemical sensors*. Chemical Reviews, 2000. **100**(7): p. 2537-2574.
2. Wallace, G.G., Spinks, G.M., Kane-Maguire, L.A.P., and Teasdale, P.R., *Conductive Electroactive Polymers*. 2nd ed. Intelligent Materials System. 2003: CRC Press.
3. Various, *Handbook of Conducting Polymers*. 2 ed, ed. Skotheim, T.A. Vol. 2. 1986, New York: Marcel Dekker Inc. 688.
4. Turcu, R., Neamtu, C., and Brie, M., *Effects of Thermal Annealing on the Electrical-Conductivity of Polypyrrole Films*. Synthetic Metals, 1993. **53**(3): p. 325-332.
5. Jiang, X.Q., Harima, Y., Zhu, L.H., Kunugi, Y., Yamashita, K., Sakamoto, M., and Sato, M., *Mobilities of charge carriers hopping between pi-conjugated polymer chains*. Journal of Materials Chemistry, 2001. **11**(12): p. 3043-3048.
6. Gustafsson, G. and Lundstrom, I., *The Effect of Ammonia on the Physical-Properties of Polypyrrole*. Synthetic Metals, 1987. **21**(2): p. 203-208.
7. Ammonia Gas Sensors,  
<http://www.armstrongmonitoring.com/product/catalog.php?cat=1&subcat=4>, Last Accessed: 07 JUN 06, (2006)
8. Rutkowska, M., Krasowska, K., Heimowska, A., Steinka, I., and Janik, H., *Degradation of polyurethanes in sea water*. Polymer Degradation and Stability, 2002. **76**(2): p. 233-239.
9. Yang, X.F., Tallman, D.E., Croll, S.G., and Bierwagen, G.P., *Morphological changes in polyurethane coatings on exposure to water*. Polymer Degradation and Stability, 2002. **77**(3): p. 391-396.
10. Thieblemont, J.C., Brun, A., Marty, J., Planche, M.F., and Calo, P., *Thermal analysis of polypyrrole oxidation in air*. Polymer, 1995. **36**(8): p. 1605-1610.
11. Wu, J., Zhou, D., Too, C.O., and Wallace, G.G., *Conducting polymer coated lycra*. Synthetic Metals, 2005. **155**(3): p. 698-701.
12. Mazzoldi, A., De Rossi, D., Lorussi, F., Scilingo, E.P., and Paradiso, R., *Smart Textiles for Wearable Motion Capture Systems*. AUTEX Research Journal, 2002. **2**(4): p. 199-2003.
13. Malinauskas, A., *Electrocatalysis at conducting polymers*. Synthetic Metals, 1999. **107**(2): p. 75-83.

14. Lewis, T.W., Wallace, G.G., Kim, C.Y., and Kim, D.Y., *Studies of the overoxidation of polypyrrole*. Synthetic Metals, 1997. **84**(1-3): p. 403-404.
15. Rudge, A., Raistrick, I., Gottesfeld, S., and Ferraris, J.P., *A Study of the Electrochemical Properties of Conducting Polymers for Application in Electrochemical Capacitors*. Electrochimica Acta, 1994. **39**(2): p. 273-287.
16. Kim, D.Y., Lee, J.Y., Moon, D.K., and Kim, C.Y., *Stability of reduced polypyrrole*. Synthetic Metals, 1995. **69**(1-3): p. 471-474.
17. Skaarup, S., West, K., Gunaratne, L., Vidanapathirana, K.P., and Careem, M.A., *Determination of ionic carriers in polypyrrole*. Solid State Ionics, 2000. **136**: p. 577-582.
18. Lide, D.R., *Handbook Chemistry and Physics*. 85th Edition (Hardcover) ed. 2004, Florida: CRC Press.
19. Okuzaki, H., Kondo, T., and Kunugi, T., *Characteristics of water in polypyrrole films*. Polymer, 1999. **40**(4): p. 995.
20. Cataldo, F. and Omastova, M., *On the ozone degradation of polypyrrole*. Polymer Degradation and Stability, 2003. **82**(3): p. 487-495.
21. Polymers Database, *Polyurethane elastomer*. 2004, CRC.
22. Wang, Y., Sotzing, G.A., and Weiss, R.A., *Conductive Polymer Foams as Sensors for Volatile Amines*. Chem. Mater., 2003. **15**(2): p. 375-377.

## **Chapter 4   APPLICATION OF PPY-COATED PU FOAM: PLANTAR PRESSURE SENSING**

## **4.1 INTRODUCTION**

In Chapter 1, wearable sensors were highlighted as having enormous potential [1, 2] in the research area of bioengineering, impacting on several connected disciplines such as rehabilitation, sports medicine and ergonomics. Hitherto, the PPy-PU foam has been shown to successfully detect incidents of forces placed upon it found in chapter 5. The generation of these forces can occur in different ways, but three different situations have been highlighted for investigation, all of which relate to bioengineering and body monitoring applications:

1. Plantar Pressure in a shoe
2. Breathing
3. Limb Movement

## **4.2 WHY MONITOR PLANTAR PRESSURE?**

Plantar pressure is the force experienced underfoot during ambulatory activities, such as walking or running. It is important to monitor plantar pressure as it can indicate incorrect posture, injury or on-set of a disease or condition. A number of examples where the monitoring of plantar pressure is important are discussed in the following sections.

#### 4.2.1 Diabetes

Diabetes mellitus is a chronic disorder in which the body's ability to use sugars is reduced. This can cause raised levels of glucose in the blood and its excretion in the urine. These changes are the result of a deficiency of the pancreatic hormone, insulin. There are two main types of diabetes: type 1 or insulin-dependent diabetes mellitus (IDDM), and type 2 or non-insulin-dependent diabetes mellitus (NIDDM).[3]

Most people with diabetes have no initial trouble with their feet, but progressive damage to the blood vessels and nerves can cause severe problems. Damage to the blood vessels can cause poor circulation in the large blood vessels in the legs (Ischaemia) and the small blood vessels in the skin (Peripheral vascular disease)

Damage to the nerves can cause a loss of sensation in the feet, therefore pain sensation can be lost so that the feet may not be protected against damage. Consequently, foot problems are the most common cause of hospital admissions for people with diabetes [4]. In developing countries, such as India, these admissions may account for up to 40% of the available healthcare resources. Diabetes currently affects more than 194 million people worldwide and is expected to reach 333 million by 2025, the majority of these cases occurring in developing countries [5]. At present, Ireland has the lowest diabetes incidence at 3.4% according to the World Health Organisation [6]. However, this figure is regarded by the Diabetes Federation of Ireland to be an underestimate. They believe that as many as 50% of patients do not realise that they are suffering with this disease and develop at least one serious complication by time of diagnosis. It is estimated that the number of cases of diabetes across Europe will increase by 21% in the next 20 years. Thus a strategy to deal with this chronic disorder must be implemented.

For people with diabetes the issue of limb survival is paramount. It has been shown that people with diabetes exerted up to 20-30 kg/cm<sup>2</sup> of plantar pressure during ambulatory movements [7]. This is at least two orders of magnitude greater than the average force that is applied to the metatarsals during normal gait [8]. The repetitive action of pounding the skin with such abnormally high pressures such as would be experienced by diabetic patients can lead to ulceration of the skin. Images of the extent of these

ulcers are shown in Fig. 4.1. If infected, these ulcers can lead to gangrene, which finalise with limb amputation. It is believed that reductions of between 45% and 85% amputations can be achieved through the adoption and implementation of guidelines which include regular foot inspections, improvement in education in self-care for people with diabetes and appropriate footwear [9]. However, another associated implication of diabetes is reduced visual capacity, thus making the task of foot inspections more difficult. Therefore, it would be beneficial to design a wearable sensing system to monitor plantar pressure for the user.



**Fig. 4.1 Photographs of diabetic feet, highlighting the debilitating nature of ulcers to this group of people.**



#### 4.2.2 Obesity

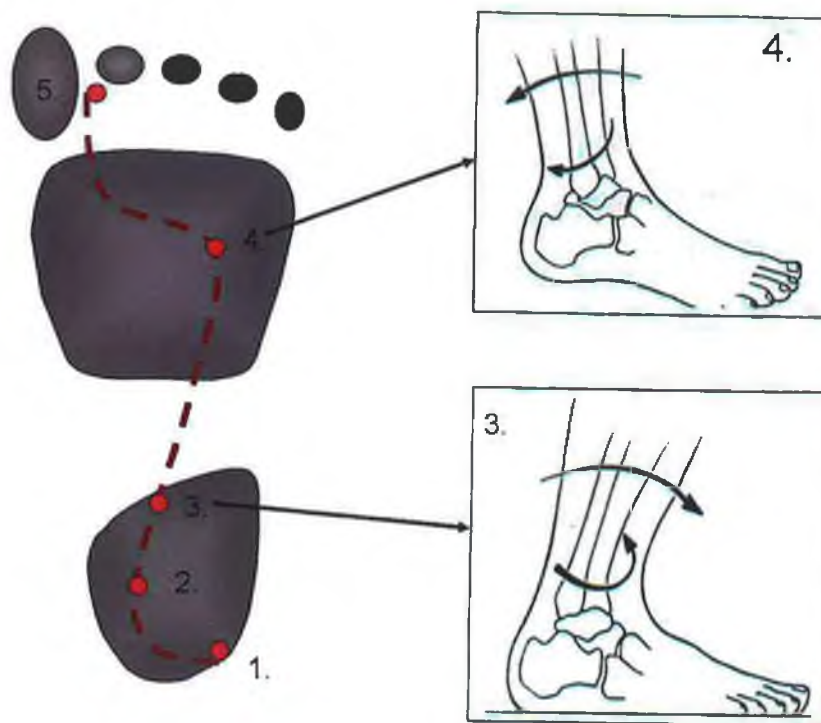
In 1997, the WHO predicted that obesity would become an “escalating epidemic” which if left unaddressed would affect millions of people worldwide [10]. In response a number of national taskforces were established to tackle this problem. However levels of obesity across all the age-groups have continued to rise significantly in much of Western Europe, since 1997 and so efforts have been intensified to tackle the issue. The measures adopted include changing habits of diet and exercise. Ideally the daily calorie intake for an adult male/female is 2,500/2,000 calories. This number can be controlled by limiting food intake, changing quality and type of food intake and increasing levels of exercise. Simple exercise such as walking is able to significantly reduce the total calorie intake. It has been reported that by performing on average 10,000 steps per day can significantly reduce the occurrence of obesity in women [11]. Simple pedometers, such as the one shown in Fig. 4.2 are now commonly available informing the wearer as to how many steps they have taken. These pedometers contain a lever arm with a pendulum attached to a spring. With each step the pendulum swings past a magnetic field and one event is electronically recorded and displayed on the digital read-out. Devices such as these are simple to use and are light-weight (the one shown weighing less than 20g). However, though simple, these devices (€7 - €25) are deliberate “add-ons” and require the user to carry them with them at all times to accurately record their levels of exercise. A better solution would be to integrate the measuring device into the close environment of the user, removing the need for user intervention.



Fig. 4.2 Photograph of a commercially available (Brunton Digital Pedometer PED1204) pedometer.

### 4.2.3 Walking

The task of walking, though an inherent means of movement for most people, is a complex process of limb rotations, flexions and balance. The process consists of two phases of leg movement; the swing phase and the stance phase. The swing phase, as the name would suggest, refers to the swinging motion of the leg, above the ground, in the direction of movement. The stance phase is a little more complex. It is described using the sequence of numbered points listed below. Each numbered point refers to the number position shown in Fig. 4.3. The dotted line through the centre of the footprint represents the estimated path of the centre of mass (CoM) during walking.



**Fig. 4.3** Illustration of centre of mass (CoM) progression during walking, with highlights of foot action as positions 3 & 4. Position 3 is a schematic of foot pronation and position 4 is a schematic of heel rise, with the associated rotation of the leg at each point. Each point is explained in the following text.

1. **Heel Strike:** contact is made with the outside of the heel & bending of the ankle towards ground (plantar flexion) occurs.
2. **Loading Response:** balancing of weight onto straight leg.
3. **Movement of CoM** (Centre of Mass) inwards (medially) causing the foot to pronate (swivel inwards), allowing the tibia to rotate inwards as shown in Fig. 4.3.
4. **Movement of CoM** to forefoot and slightly outwards (laterally), allowing the tibia to rotate outwards. Heel rises from ground as shown in Fig. 4.3.
5. **Toe Off:** CoM moves over big toe to push off with bending of the ankle. Simultaneously the opposite heel comes into contact with the ground at this point.

#### 4.2.4 Traditional methods of monitoring pressure underfoot

The conventional method of measuring pressure exerted underfoot during ambulatory activities, such as walking, is by using force-plates. These devices rely on advanced integrated electronic components, examples of which are shown in Fig. 4.4 [12, 13] to map out and digitally display and log the pressure exerted on them. Such technology [14-16] has been incorporated into mats, as shown in Fig. 4.5. These devices are currently commercially available (price-tag is 1000 of euros) but due to the precision of the electronics required, the overall cost of the equipment is substantial and as a result such these devices are scarce and if available are only such in a clinical or academic setting.



**Fig. 4.4** Photo of Si-Chip on ceramic pressure sensor module, containing facilities for signal conditioning [13].



**Fig. 4.5 Photo of footscan® Analogue plate [17].**

An output from a commercially available force-plate mat, footscan®, can be seen in Fig. 4.6. This device can record up to 500 frames of data per second, using small sensors 5 mm x 7 mm in size. This gives the footscan® a resolution of 2.86 sensors per cm<sup>2</sup>. These types of systems can be used to monitor the pressure and force distribution in both static and dynamic modes, the latter allowing the biomechanics of the foot to be analysed. For example, the footscan® system was able to determine the centre of mass (CoM) of the person, illustrated by the red line along the centre of the footprint in the top two images in Fig. 4.6. These images were composite profiles of the pressure and force distribution for both feet of the subject. The amount of pressure exerted at each point was displayed using a colour-coded scale; where red indicated the greatest amount of pressure, while yellow to blue indicated areas of lesser pressure. The progress of the person's footprint could be further analysed by extracting a series of still images from the dynamic recording. These images, shown in Fig. 4.6 in the second and third row, may be of benefit to physicians and physiotherapists wishing to isolate and identify incidences of pressure hot-spots during walking. This output shows the range of information available from such commercially available systems.

Studies have been carried out in academia, whereby the dynamic gait of a subject population was monitored using force-plates in conjunction with multi-camera settings. These studies yielded statistics necessary to generate biomechanical models for normal walking [18-20]. Similar studies have been carried out to model the biomechanics and motor control of gait in diseased patients, such as those suffering with Parkinson's disease [21-25]. By developing these biomechanical models, the progression of the disease can be monitored and correction to the patient administered.

These force-plate systems are indispensable in developing these biomechanical models, due to their sensitivity, reliability and reproducibility of force readings. However, due to their lack of mobility, it is not always possible to examine the patients' regular gait behaviour using the equipment as used during these studies. Thus, exact determination of a person's gait profile during daily activities cannot be obtained. Incorporation of such technology into insoles has recently occurred [14] which begins to tackle this problem. However, the issue of cost is still a major drawback.

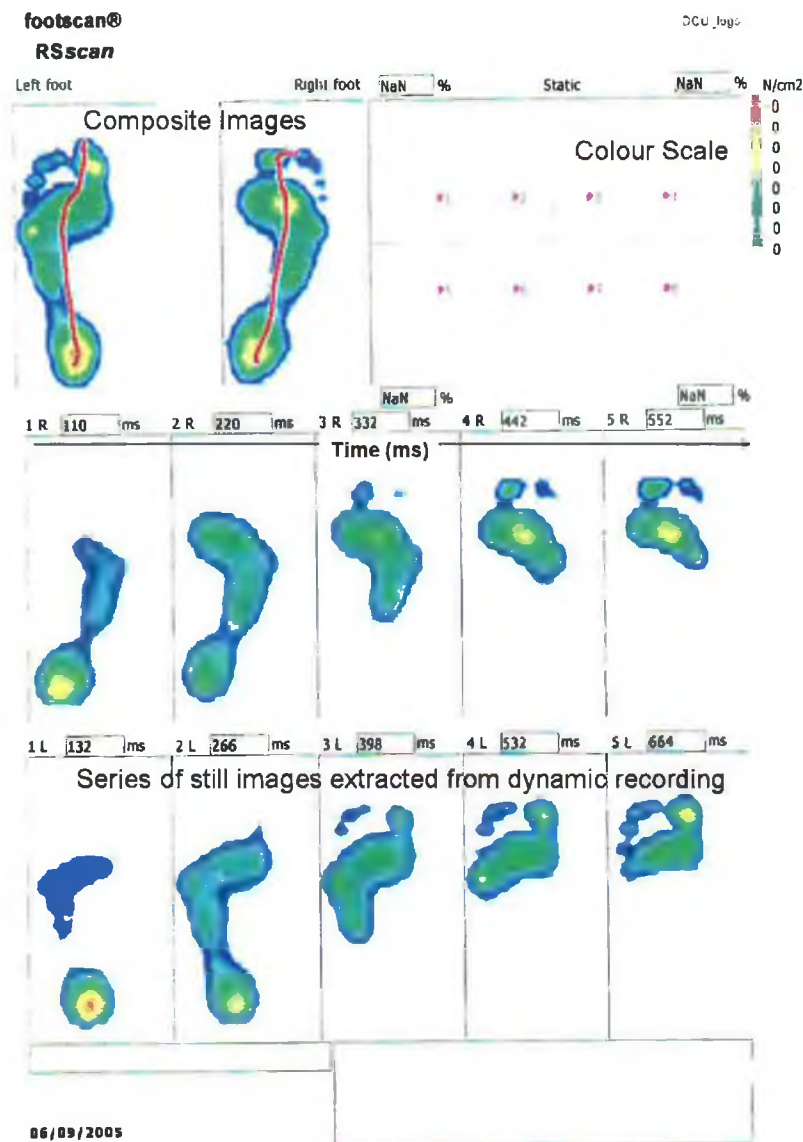


Fig. 4.6 Pressure profile of one subject's footprints using the footscan®, DCU, Top Row: Left foot composite image, Right Foot composite; Middle Row: Pressure Profile Time sequence (Right Foot 120 ms intervals); Bottom Row: Pressure Profile Time sequence (Left Foot 130 ms intervals).

### *Designing a Smarter Shoe*

Shoes have for too long been sensible. However, there are developments currently afoot where shoes are becoming smart [26-29], smart, in the sense that they can sense their environment, and alter their physical properties to adapt to any changes within that environment. This concept will have huge implications for many especially athletes whose needs, such as cushioning and arch support, may change during exercising, depending on the terrain they are encountering. A commercially available example of a smart shoe is the “1”, developed by the German sporting-goods maker, Adidas. A Hall-sensor is located in the heel, Fig. 4.7-1., which can take up to 1,000 readings per second regarding the changes in the magnetic field strength in the heel. These changes are proportional to the pressure exerted on the heel during each heel strike, which in turn is proportional to the terrain over which the athlete is moving. This information is collected by a data logger and processed using an on-board micro-processor, located at the mid-section of the foot, Fig. 4.7-2. The microprocessor controls the length of the cable, Fig. 4.7-3, thus, controlling the rigidity of the heel. These changes enable the shoes, priced at \$250 per pair, to alter their physical properties, depending on whether they are being used on soft or hard ground, making the user more comfortable and less prone to injury during exercise. A user interface (Fig. 4.7-4) enables the wearer to manually set the range of compression desired.

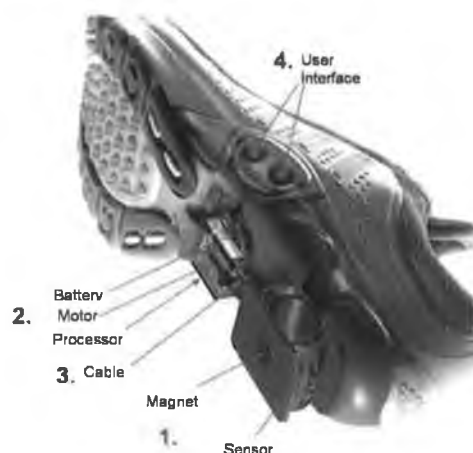


Fig. 4.7 Schematic of Adidas' “1” smart shoe [28].

#### 4.2.5 Insole Prototype

The Adidas “1” smart shoe shows the commercial interest that is available for developing wearables that will be able to sense and adapt to changes in their environment. The marketing strategy is to empower the wearer to control their environment through their shoes. However, though these shoes are wearable and mobile they do little to inform the wearer of the spatially distributed pressure as was obtainable from the force-plates. Thus, there is a niche for developing a pressure-sensitive foot-device that would be comfortable, cost effective, mobile, and be able to gather spatially distributed information. Such a wearable device, an insole, could be developed using the PPy-coated PU foam. This device would be able to inform the wearer of how many steps they performed during the day, how much pressure they have applied and where this pressure occurred across the profile of the foot during each step. The advantage of this material is that it is soft and flexible and can be used to form an integral part of the insole. With each footstep, pressure on the foam would cause compression, which would be registered as a decrease in resistance across the foam. This signal could be then recorded and displayed or logged for data analysis.

Hitherto, monitoring of a single PPy-PU foam sensor had been performed to great success. However the information gathered by a single sensor is limited, as only one channel of information is obtained and therefore spatially distributed information across the insole is not accessible. For biomechanical studies, the area to be assessed is often quite large, thus necessitating multiple sensors to work together to generate an informative picture of what is taking place. The incorporation of wireless technology with spatially distributed pressure sensors would be beneficial and ultimately enhance the wearer’s knowledge of their activity during the day and enable correction, if necessary, to maintain a healthy lifestyle.



### 4.3 INCORPORATION OF WIRELESS TECHNOLOGY

As mentioned previously, the aim of this project is to develop a fully integrated polymeric sensing system to continuously monitoring the movements of the wearer. If successful, this type of information technology will be beneficial in telemedicine systems, enabling the early detection of abnormal conditions and prevention of serious consequences [32]. What are required now are medical devices and monitoring systems, which the user-friendly, enabling the patient themselves to use them. However, they must still refrain from intruding on the patient's daily activities. Personal medical monitoring systems, such as Holter monitors, have been successfully used to continuously collect ECG data for off-line processing. However, systems with multiple sensors for physical rehabilitation often feature unwieldy wires between electrodes and the monitoring system. These wires limit the patient's activity and level of comfort, therefore negatively influencing the measured results.



**Fig. 4.8 Holter monitor, a portable device for monitoring cardiac activity (ECG data) [33].**

Initial plantar pressure sensing prototypes developed with PPy-PU foam sensors relied upon hard-wiring to either a multimeter or a potentiostat to gather information. While these sensing systems have been comfortable to wear, the movements of the wearer have been limited by the presence of the wires requiring the wearer to remain within close proximity of the data recorder. Thus, information obtained could not reflect the “normal activities” of the wearer. It was desirable, then, that the communication element of the sensing device would also be wearable and mobile, therefore impacting less on the physical and social comfort of the wearer.



Wireless communication refers to the transfer of this information between two points without the need for direct hard-wiring. With reference to the integrated polymeric sensing device this would mean that the signal could be transmitted from the sensor location to a logging and display location, the basestation, without the need for direct wiring between the two points. This would greatly increase the mobility of the sensor, which would be beneficial in the development of a wearable sensing device.

#### 4.4 EXPERIMENTAL

The PPy-PU foam was prepared by repeatedly coating PU foam (PU003, source F.E. Ltd) with PPy.NDSA according to the procedure outlined in Chapter 2. Samples of approximately  $2 \times 1 \times 1 \text{ cm}^3$  were cut from this material and positioned into each insole prototype.

##### 4.4.1 Prototype #1: Hard-wired collection of data

5 PPy-coated PU foam samples were cut to dimensions of  $2 \times 1 \times 1 \text{ cm}^3$  and positioned into a left insole at the following distinct locations:

- Around the heel (3)
- Right-hand side forefoot (1)
- Left-hand side forefoot (1)

A photo of the proposed insole prototype is shown in Fig. 4.9.

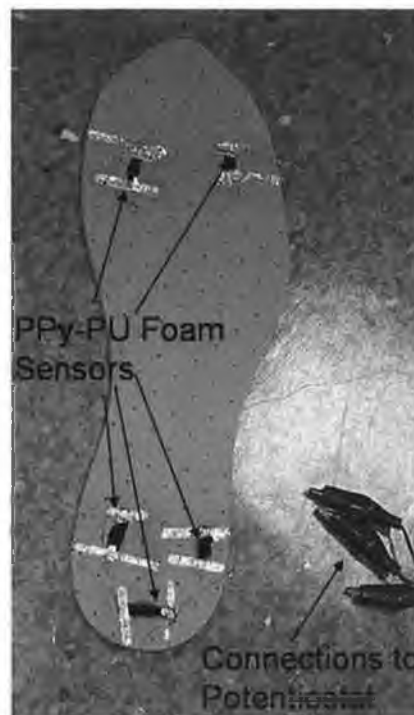
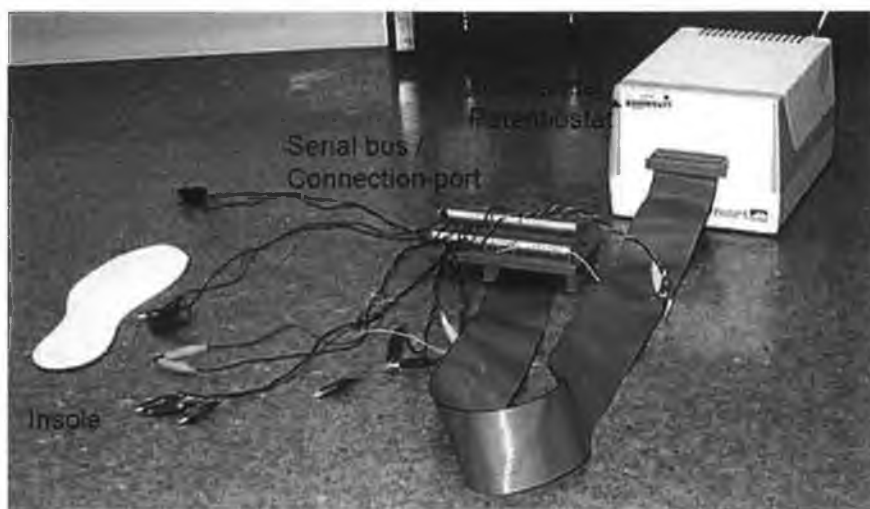


Fig. 4.9 Photo of the proposed insole prototype showing the locations of each PPy-PU foam sensor.

### *Instrumentation*

A 16-channel potentiostat, the ELMS potentiostat 16 version 1.00, was sourced from Whistonbrook Technologies, England. Each channel consisted of a unique working, and counter electrode. All reference electrodes were common. It was used in 2-electrode configuration whereby all the counter electrodes were connected to their respective reference electrodes. Data was collected with the ELMS software provided by the manufacturers (version 1.00), and recorded directly into Microsoft Excel for further manipulation and analysis.

Contact to each of the foam sensors was achieved by threading a thin wire to either side of the foam sensor. These wires were connected to the multi-channel potentiostat using crocodile clips as shown in Fig. 4.10. The data was recorded at a rate of 2 Hz for the trial.



**Fig. 4.10**      **Photo of insole connected to the 16-channel potentiostat.**

Each subject was instructed to place their left foot on the insole, as shown in Fig. 4.11. The subject was instructed to move their weight repeatedly from their toes (forward) to their heels (backwards).

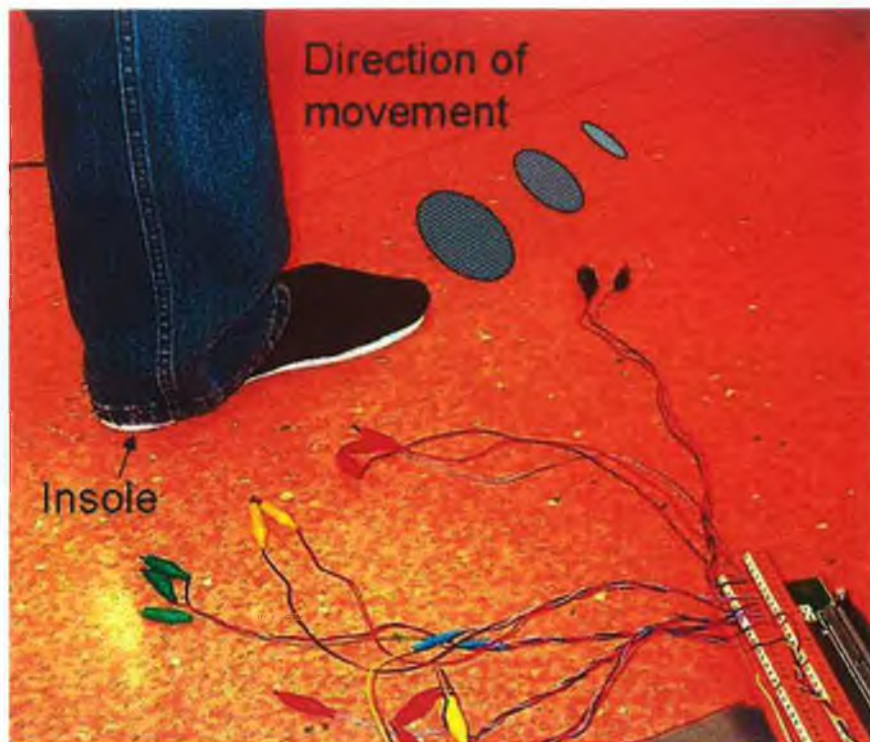


**Fig. 4.11** Photo of insole connected to the 16-channel potentiostat. Experiments were carried out without shoes and required the subject to stand onto the insole as shown here.

#### 4.4.2 Prototype #2: Wireless collection of data

##### *Instrumentation*

The wireless test-bed used during experimentation, was constructed by using wireless-enabled 868Hz Mica Motes. These MicaMotes are 3<sup>rd</sup> generation mote modules developed by Crossbow Technologies for low-power, wireless, sensor networks. A sensor board was built for the foam sensor which used a variable resistor to set up a voltage divider, as shown in Fig. 4.12. The voltage output from this potential divider was then fed into the analogue to digital converter (ADC channel) of the Mote hardware, yielding a value (an ADC value) relative to the voltage of the battery source, in this case 3V. The range for the ADC values was 0-1023. The ADC values were recorded for each trial and relayed to the base station for observation and processing. A small lightweight Mica2Dot (MPR500), see Fig. 4.14, was used as the wearable sensor mote and a MICA2 series (MPR400) mote, see Fig. 4.14 functioned as the base-station. The MICA2 module was connected directly to a laptop through the RS232 port and was within a 10 m radius (within the same room) of the transmitting mote at all times. Both motes used the low power microcontroller, ATmega 128L and the Chipcon CC1000 FSK-modulated radio transceiver. Data from the foam sensor was recorded at a sampling rate of 20 Hz and transmitted from the Mica2Dot at a rate of 2Hz.

TinyOS [34] was used on the motes and an Oscopie Programme, developed by Intel, was used to display and record the data.

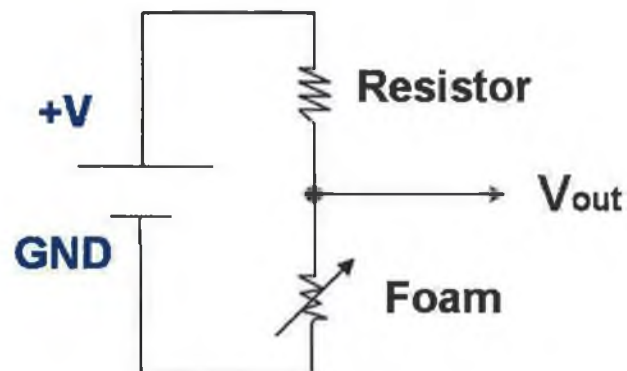


Fig. 4.12 Electronic circuit diagram of potential divider on Mote sensor board, including resistor and foam sensor as a variable resistor.

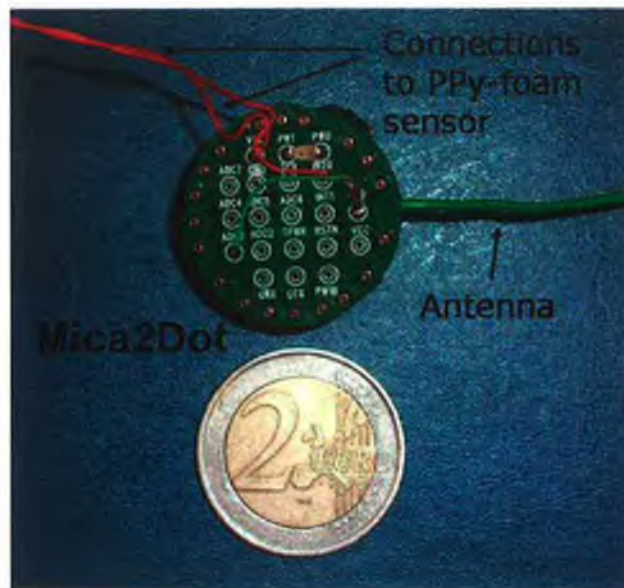
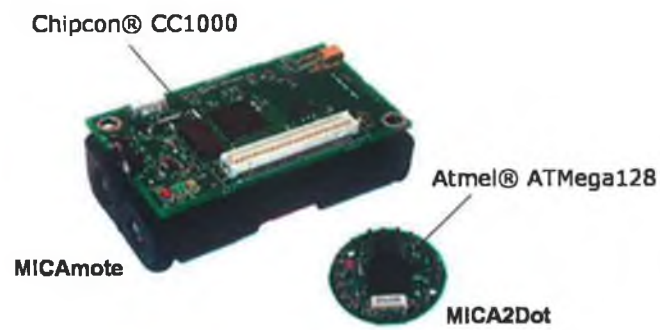


Fig. 4.13 Picture of Mica2Dot (MPR500) and Mica2Mote (MPR400) [35].

### Data Analysis

Analysis of the data from the foam sensor was performed using OriginPro Software v7.5 (Silverdale Scientific, UK). It was possible to plot the received ADC values in real-time to observed the response of the sensors during movement. However, in order to monitor the changing resistance of the foam sensors ( $R_{foam}$ ), conversion of the ADC values was required. This was performed using Microsoft Excel, using the equations, 8.2 - 8.4:

$$\frac{ADCValue}{1024} \times 3V = V_{out}$$

Equation 4.1

Equation 4.1 converted the ADC values into voltage values. These voltage values referred to the voltage out ( $V_{out}$ ) as indicated in Fig. 4.12. The  $V_{out}$  values are related to the resistance of the foam sensor, as in a potential divider system of two resistors,  $R$  and  $R_{foam}$ , using the following equation:

$$V_{out} = \frac{R_{foam}}{R + R_{foam}} \times V_{in}$$

Equation 4.2

$V_{in}$  referred to the input voltage of the system, which in this case would come from the coin celled battery, which was 3V. Thus, by rearranging Equation 4.2, the resistance of the foam could be calculated using

Equation 4.3, where  $V_{out}$  was calculated from Equation 4.1:

$$R_{foam} = \frac{V_{out}R}{V_{in} - V_{out}}$$

Equation 4.3

### *Prototype Setup*

The subject was given two insoles with integrated PPy-PU foam sensors located at the heel and under the first metatarsal head (forefoot) for both feet. The subject was instructed to position these insoles into her own shoe as per a regular cushioned insole. The connections to the wireless transmitter module, the mote, were made by attaching wiring to the shoe to connect the mote and the foam sensors shown in Fig. 4.14. The mote was secured to the shoe. Data was collected by the base-station at a rate of 20 Hz. Fig. 4.15 shows a photo of a runner with the insole and transmitter module attached.



**Fig. 4.14** Picture of Mica2Dot (MPR500) connected to the PPy-PU foam.

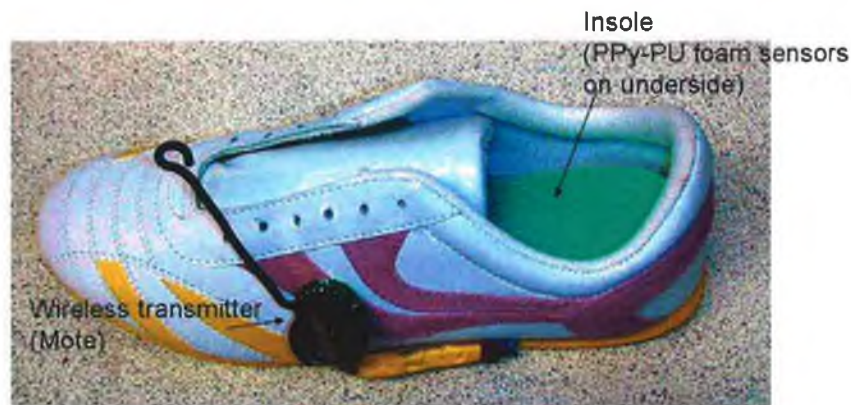


**Fig. 4.15** Photo of runner with pressure sensitive insole (PPy-PU foam sensors not visible) with associated data transmitter, Mote.

Two motes were used during testing, one per shoe. Due to hardware limitations at the time of testing, one mote had one active channel for data gathering, whereas the second mote had two active channels to record the information from both PPy-PU foam sensors.



### *Exercise Protocol*

The subject was instructed to walk or shuffle (move without lifting her feet off the ground) a distance of 4.5 meters repeatedly for one minute. The information from the PPy-PU foam sensors was collected by the mote and transmitted at a rate of 20 Hz to the basestation for display and storage purposes.

## 4.5 RESULTS & DISCUSSION

### 4.5.1 The hard-wired gathering of data from multiple PPy-PU foam sensors.

The following graphs show the pressure profiles obtained when a subject walked across the pressure-sensitive insole. The data from three of the five channels (two at the heel and one at the fore-foot position) provided information regarding the distribution of pressure of the wearer on the insole. The data from these three channels were normalised by the following equation (Equation 4.4):

$$\frac{R - R_0}{R_{\max} - R_0} \times 100$$

Equation 4.4

As can be seen in Fig. 4.16, this insole, into which the PPy-PU foam sensors were integrated could identify events of pressure occurring at each of the sensors' locations.

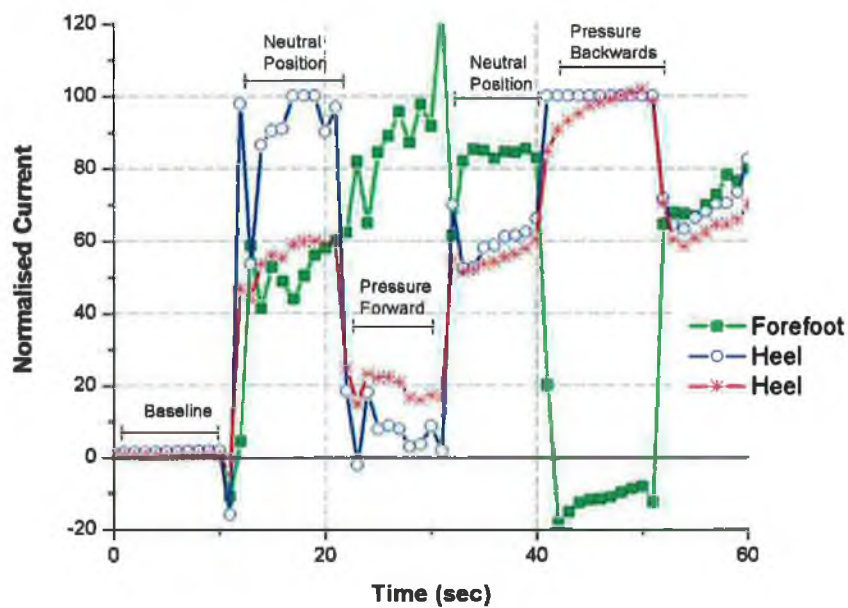
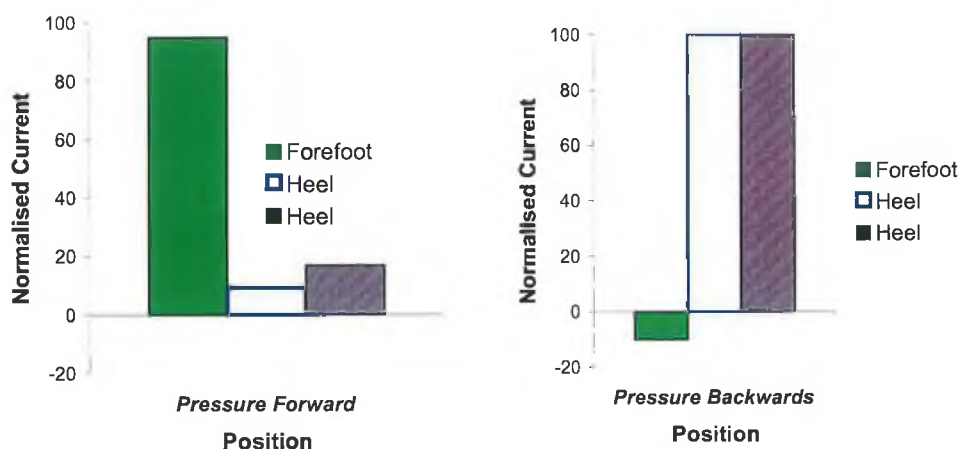


Fig. 4.16 Normalised current values for three PPy-PU sensors positioned at the forefoot and the heel.

When the subject assumed a neutral position, that is the subject stood squarely on the floor balancing their weight evenly across both feet, pressure was exerted onto each of the three sensors. When the subject balanced their weight onto their toes (pressure forward), more pressure was exerted on the forefoot sensor and less onto the heel sensors, confirming the correct position was performed. This yielded a patterned response shown in Fig. 4.17 (left).



**Fig. 4.17** Normalised responses from three PPy-PU foam sensors for the subject in pressure forward position (left) and with pressure backwards (right).

Conversely, when the subject balanced their weight onto their heels (pressure backwards) the amount of pressure exerted onto the heels increased, whereas the pressure on the fore-foot sensors decreased, again correlating correctly with the position required, shown in Fig. 4.17 (right). Thus, by using three PPy-PU foam sensors simultaneously, the spatial distribution of pressure across the insole could be determined for two different stance postures.

While it was possible to distinguish between these two events (pressure forwards compared to pressure backwards), the combined responses of the sensors to the neutral position was more difficult to determine, as highlighted in Fig. 4.18. These inconsistencies maybe due to unbalance of the subject, where their exact position may not return to the exact same position. In order to be able to have better decision making capabilities, more channels of information would need to be integrated into the insole prototype.

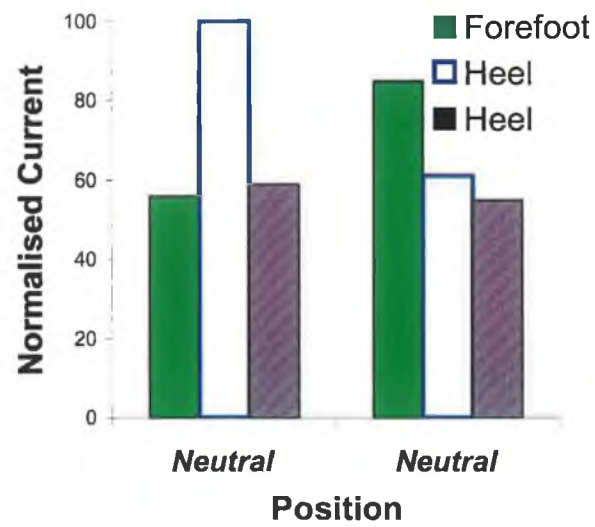


**Fig. 4.18** Normalised responses from PPy-PU sensors to neutral position.

Quantitative information would require further optimisation and calibration of the response of the PPy-PU foam sensors, e.g. to reduce or characterise the mechanical hysteresis of the materials [30] which would enable the application of algorithms to automatically identify the posture of the subject.

#### 4.5.2 The wireless gathering of data from multiple PPy-PU foam sensors

The data from both motes were recorded simultaneously in real-time, as shown in Fig. 4.19. The Mica2Dot mote recorded the voltage difference across the load resistor, gathering 10 readings per 0.5 seconds as a number of analogue to digital converter (ADC) units and transmitted to the logging basestation. Thus the response recorded by the basestation was equal to the number of ADC units transmitted by the Mica2Motes.

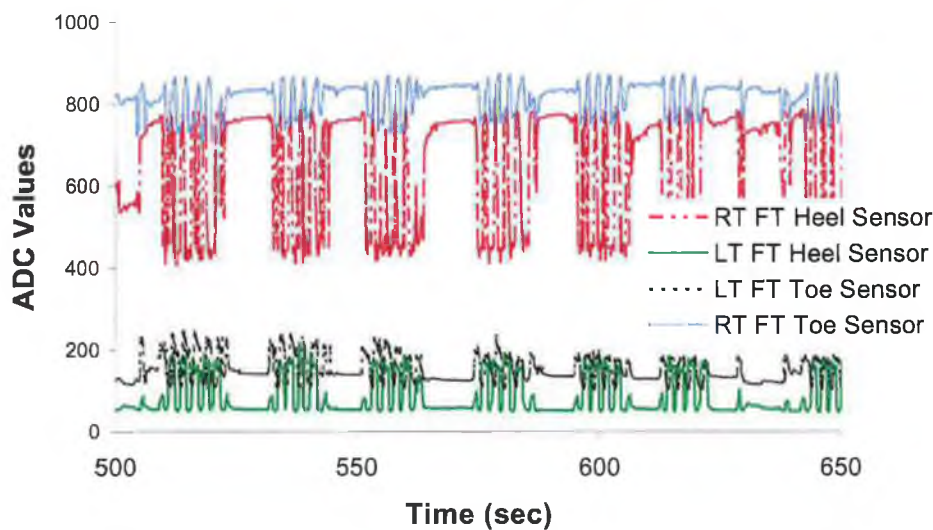


**Fig. 4.19** Real data plot from four PPy-PU foam sensors as recorded by the MICA2 at a rate of 20 Hz.

In order to determine parameters such as phase change and count the number of steps performed, the data was decoupled and analysed separately before comparison between sensors were performed. It was through these comparisons, (two sensors on one foot or one sensor on each foot) that parameters such as phase shift and cadence could be determined.

### *Comparison of two sensors on one foot*

#### **Walking**

As mentioned previously, walking is comprised of a number of movements of the body. By positioning a PPy-PU foam sensor beneath the heel and the large metatarsal, see Fig. 4.20, the pressure bearing events of the heel strike and the toe push off should be detectable.



**Fig. 4.20** Schematic of PPy-PU foam sensors located on the right foot.

During walking, a time lapse naturally occurs between the heel strike and the toe push-off, indicating the rolling action of the foot during walking. Thus, if positioned correctly, a time delay should occur between the peak pressure for the heel sensor and the peak pressure for the toe sensor. The data from these two sensors were gathered in real-time and normalised using Equation 4.4 to maximise the responses from each sensor. The resulting graph, the normalised responses from two PPy-PU sensors in a single insole, is shown in Fig. 4.21. In this graph, it can be seen that a footstep began with an increase of pressure on the heel sensor, e.g. after 144 seconds. This pressure event corresponded to the heel strike of the subject. After 144.2 seconds, the values from this sensor decreased indicating that the pressure moved away from the heel, as would occur during the rolling action of the foot during walking. As the pressure decreased at the heel location to a minimum, the values recorded by the toe sensor increased, indicating greater pressure at this location. The maximum pressure recorded by the toe sensor, as would be experienced during toe push-off, occurred in this incidence at 144.8 seconds. Thus, pressure was transferred from the heel to the toe in 0.6 seconds. This time delay is important as it corresponded to the phase shift for this subject's right foot. It is also important to note the overlap of maximum pressure for the

toe sensor and minimum pressure for the heel sensor, e.g. at 144.8 seconds. This would indicate that at the time maximum toe pressure (toe push-off) there was a minimum amount of pressure was place on the heel as would occur during heel-lift. These two responses together, thus, can be used to describe the stance phase of walking. At 145 seconds, it can be seen that the readings for both sensors are at a minimum, indicating minimum pressure at both of these locations. This is because at this point the foot was off the ground as would occur during the swing stage of walking. The weight of the subject at this time was placed on the other foot, while the leg was swung forward in the direction of movement, until the next heel strike at 145.45 seconds. The average phase shift for this subject was 0.56 seconds (%RSD = 7.04%, n=9). Thus, the outline of a foot-step could be identified using these two PPy-PU foam sensors. The time for stance phase of the right foot was measured to be 1.22 seconds (%RSD = 6.50%, n=9) indicating that the right foot makes contact with the ground 49 times per minute.

The patterned response from the two sensors is unique for a foot-step and is different from the response obtained for a turning action of the subject, e.g. at 148.9 seconds. At this point, high pressure is recorded simultaneously by the heel and the toe sensors. This corresponded to the dual-stance period as the subject reached a stationary stance momentarily, while turning.

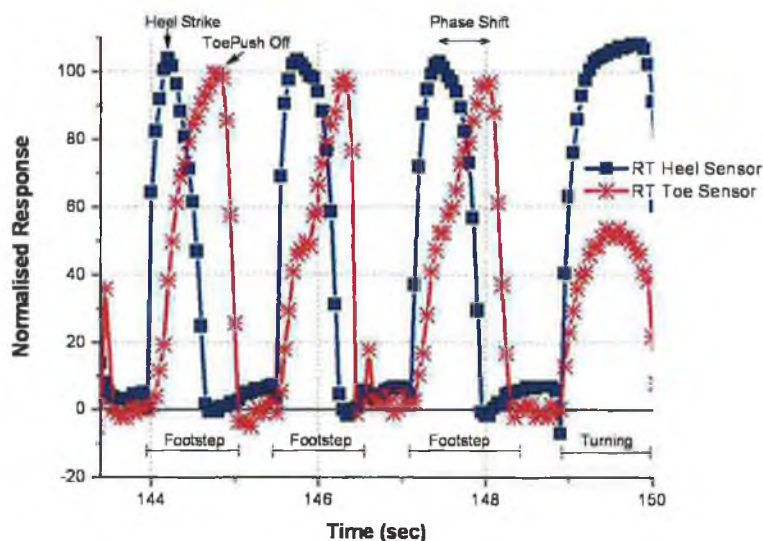
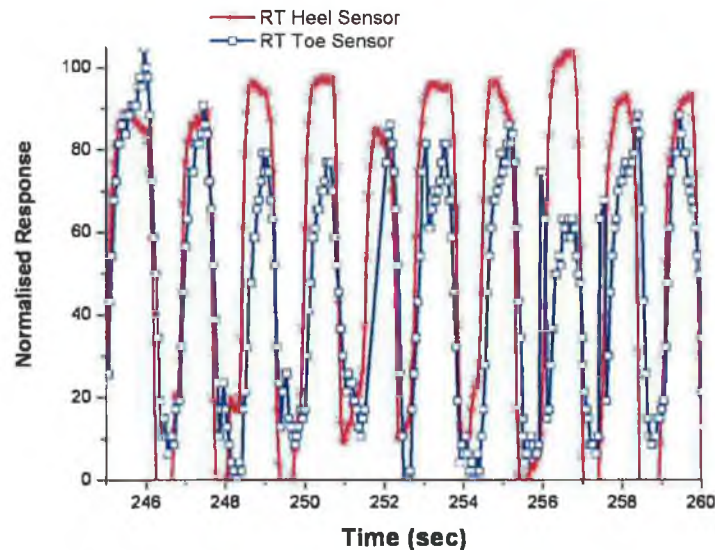


Fig. 4.21 Normalised response for two PPy-PU foam sensors located at the heel (RT Heel Sensor) and the large metatarsal head (RT Toe Sensor).



### Shuffling

Shuffling is a form of sliding movement whereby both feet are in constant contact with the ground and there is minimal leg-lift. As a result, there is very little or no rolling action of the foot during walking. Shuffling is not an optimal method of moving, however people develop this gait profile as a result of neurological conditions such as Parkinson's disease. In Fig. 4.22, the data recorded for the heel (red) and forefoot (blue) sensor are graphed. The peaks shown in this graph represent pressure events for both locations. It can be seen that they occur almost simultaneously (0.2 seconds %RSD = 47.05, n=12) indicating that pressure was being applied at these two locations at the same time. The absence of a phase shift signifies the absence of the rolling action of the foot, which occurs during normal walking motion.



**Fig. 4.22** Response of two PPy-PU foam sensors located at the heel and the large metatarsal head.

Clearly it is possible to distinguish actions such as walking (Fig. 4.21) from shuffling (Fig. 4.22). It is more difficult to distinguish shuffling from e.g. turning, however augmentation of the information, e.g. location or GPS positioning, enables this to be achieved. The responses of these two sensors show the fast response time of the sensors and their ability to detect pressure events. The responses are reproducible. The result of this is that additional information, such as type of movement and phase shift can be gathered as well as the number of steps performed.



*Comparison of three sensors, two on one foot and one on the other foot*

**Walking**

As mentioned previously, there is a time difference between the heel strike of the foot and the toe push off, which are indicative of the rolling action of the foot. This information was gathered using two sensors positioned to the front and back of the foot. However, additional information such as cadence (step frequency), stride length and step time could be obtained when both feet are monitored comparatively. For this comparison, data was recorded by three PPy-PU foam sensors located at the heel and toe of the right foot and the toe of the left foot. These locations are displayed in Fig. 4.23. The colours for each location correspond to the colours of the data-traces obtained using these sensors in the following graphs, Fig. 4.24 - Fig. 4.25.



**Fig. 4.23** Schematic of PPy-PU foam sensor locations for both feet. The sensor on the left forefoot (black) and left heel (green) could be compared with the sensor on the right forefoot (blue) and the right heel (red).

A section of the data recorded by the four foam sensors is shown in Fig. 4.24 and Fig. 4.25. Again, the initiation of pressure at the heel and transfer to the front of the foot can be observed by following the red trace and then the blue trace between 513.4 and 515 seconds. After 515 seconds there is no plantar pressure acting on the right foot sensors as the right foot is lifted off the ground during the swing phase. At this point the weight of the subject is on the left foot as indicated by the peak pressures for the left heel and toe sensors between 514.65 and 516.3 seconds. The pressure, then, drops off the left foot as the weight of the subject is transferred back to the right foot. This repetitive transference of pressure is observed between 510 and 520 seconds. It can be seen that the toe push-off occurred immediately before the heel strike of the opposite foot, showing the transference of pressure from one foot back to the other.

The step time was determined to be the time difference between the peak pressures for the heel strike for the right foot. For this experiment this time was calculated to be 2.36 seconds (%RSD = 11.58, n=7) or a cadence of 25.45 steps per minute. If the distance to be covered is known and the number of steps taken to cover the length, then further parameters maybe calculated. In this case the distance was 6 m and it took 8 steps to cover this distance. This would equate to a stride length of 0.75 m, and a walking speed of 1.15 km/hour.

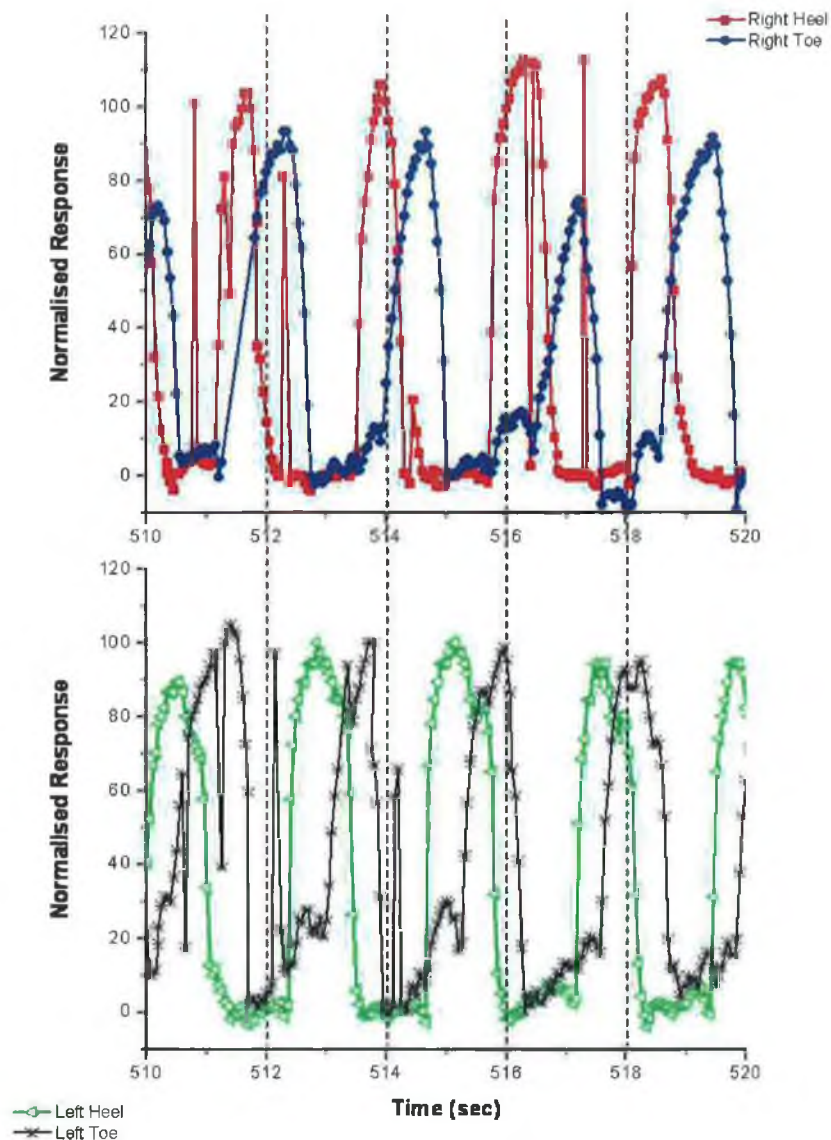


**Fig. 4.24** Normalised response all four PPy-PU foam sensors located at the heel and forefoot (large metatarsal head) for both feet.

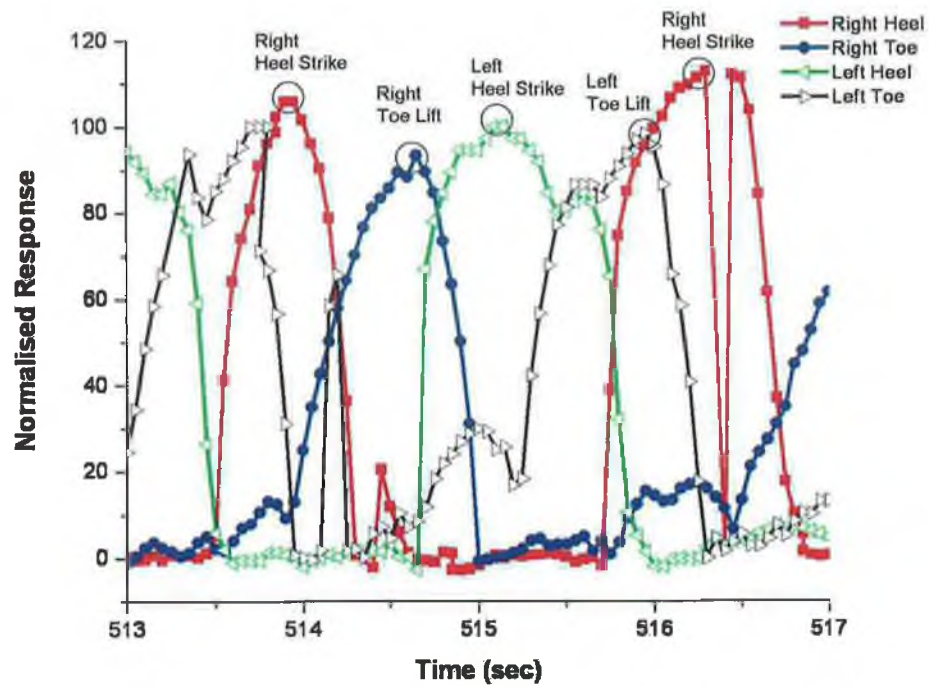


Fig. 4.25 Normalised response from four PPy-PU foam sensors as in Fig. 4.24.

### **Shuffling**

Again, the profile for shuffling, shown in Fig. 4.26, is very different from that for walking (Fig. 4.24). Fig. 4.26 showed that the frequency of peaks pressures or foot steps was much greater for shuffling than was observed during walking. Also observed was the concurrence of peak pressures for heel and toe sensors, shown also in Fig. 4.27, for both feet. This indicated the absence of the foot rolling during the movement. This would imply that the weight was distributed evenly on the ground between the heel and toe, that is that the foot landed flat on the ground and was lifted in a similar fashion. As mentioned previously, the purpose of the foot rolling action is to facilitate leg and hip rotation which are characteristic of walking enabling the subject to move comfortably. Absence of these actions may indicate injury possibly at the foot or at the associated locations of the leg or hip. The step time was calculated to be 1.31 seconds (%RSD = 11.56,  $n = 10$ ), which is equivalent to approximately 46 steps per minute, which is greater than that calculated for walking. The number of steps performed to cover the set distance of 6 m was 18 steps. Therefore, the stride length and speed of the subject while shuffling was 0.333 m and 0.90 km/hour respectively, which is much slower than the speed calculated for walking at 1.15 km/hour. The increased number of steps and the slower overall speed of movement are characteristic of shuffling, where the lack of leg-swing and leg-lift necessitate the need to perform more steps to reach their destination.

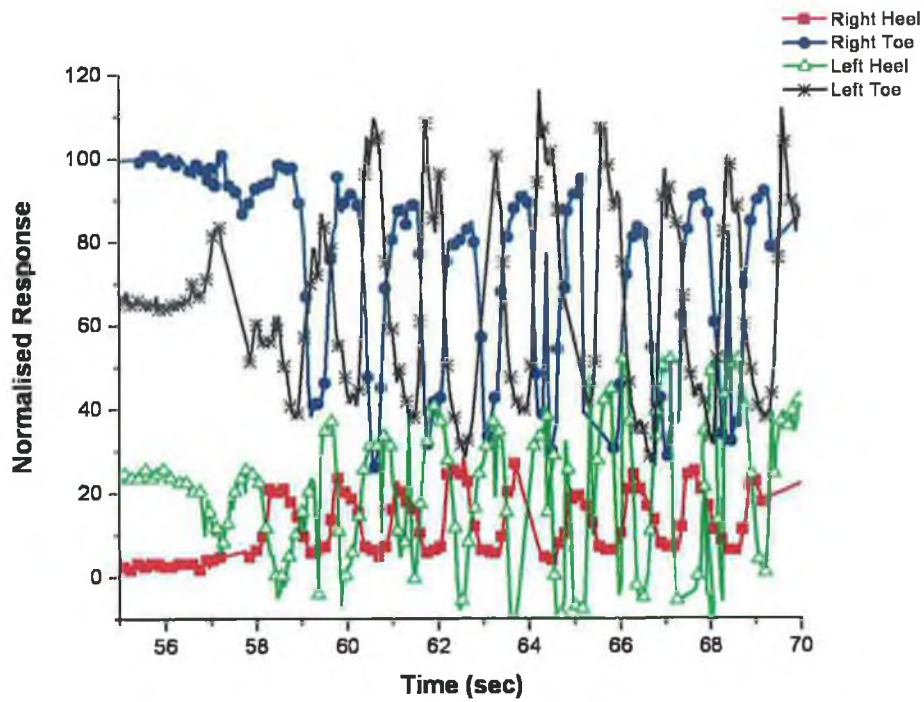


Fig. 4.26 Normalised response from three PPy-PU foam sensors for shuffling action.

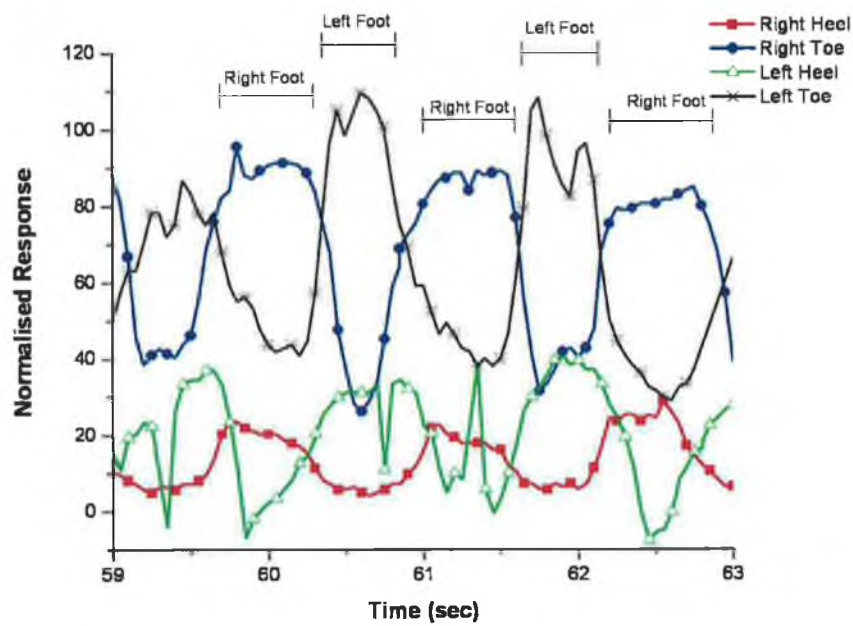


Fig. 4.27 Normalised response, as in Fig. 4.26, for shuffling action.

### 4.5.3 Issues with the wireless system

The use of wireless transmitters and base-station enhanced the mobility of the subject to perform the desired exercise protocol. However, the use of such equipment raises questions regarding power consumption and longevity of the prototype. In order to address these questions, two aspects must be examined in regard to both wearability and optimum performance of electronic components.

These are:

1. The performance of the power source
2. The power consumption of sensing device.

The performance of the power source in any given application, is inherently dependent on the output voltage of the power source and the capacity of charge it can deliver to the sensing device to enable operation. In terms of wearability, the smaller the size of the power source, the better its integration compatibility. Thus, a button battery such as lithium coin batteries (Fig. 4.28) would be desirable. However, these types of power sources, which have a current capacity of 220 mAh, are designed for applications which require low quiescent currents ( $>1$  mA) with short pulses of up to a few hundred  $\mu$ A on demand, e.g. as power sources for calculators, and watches. However, during operation of the Mica2Dot motes, currents greater than this threshold are required for sampling and transmission of data [35, 36]. Thus, the power sources are not being used under its optimum operation conditions. If these conditions are prolonged then the current capacity of the power source is significantly curtailed. If the power source is limited by its wearability (size), then the power consumption of the sensing device must be arranged to maximise the use of this power source.



**Fig. 4.28** Photo of three Li-Mn batteries commercially available [37].

The power consumption of the sensing device is primarily dependent on three aspects, the power consumption for the ATM128L microchip, which includes the ADC channels, the power consumption for the radio transmitter, and the power consumption for the sensor board, in this case the potential divider.

According to Cross-bow, [35], the operating current for the ATM128L microchip in active mode was 6 mA and for the radio transmitter, operating at 868MHz at a minimum power output of -20 dBm was 8.6 mA. Thus, before the inclusion of the sensor board the current required for operation of the Mica2Dot mote was 14.6 mA, which is above the optimum 1 mA for the Li-Mn battery. It is possible to conserve power by reducing the sampling and transmission rates, however in the area of biomechanical monitoring, sampling rates must be at least 18 Hz to record human activity [38]. Therefore, a compromise must be reached, between the resolution of data recorded and transmitted, and the overall current consumption of the sensing device.

The current consumption by the potential divider was calculated by rearranging Ohm's

law:

$$i = \frac{V_{in}}{(R_{resistor} + R_{foam})}$$

**Equation 4.5**

The resistance of the resistors used in the potential dividers were 330k $\Omega$  and the range of resistance of the foam was 40-300k $\Omega$ . This is equivalent to a current consumption of 5-8  $\mu$ A. This value is negligible compared to the current consumption for the microchip and radio transceiver. Thus, the total current consumption of the sensing device is 14.6 mA. For a 220 mAh capacitive battery this equates to 15 hours of continuous usage. This figure, however is only an estimation of the maximum longevity of the sensing device, and it assumed optimum operating conditions for the battery. In reality for exercise programs of approximately 30 minutes, the batteries are useful for approximately 9 hours, provided that the devices are disconnected when not in use. Thus, the wireless protocol is useful in the short-term monitoring of biomechanical activity.



However, problems of balancing current consumption, sampling and transmission rates with the wearability of the power source do exist, but will require further investigations in terms of hardware and software management.

#### 4.6 CONCLUSION

To conclude, five PPy-PU foam sensors were integrated into a single insole in order to obtain a pressure profile that would occur underfoot during ambulatory activities. Data was successfully obtained from three of these sensors. These results showed different profiles or patterned responses for different stance postures for the left foot. Thus, this prototype demonstrates the principle of integrating multiple soft pressure sensitive sensors into a wearable device for the gathering of spatially distributed information. This gathering of information from multiple sensor locations enables a pressure-profile for the entire area to be generated. Clearly these results demonstrate the feasibility of being used to monitor deteriorating gait for rehabilitation purposes in chronic progressive diseases or as a training technologies for athletes. The tracking of pressure events at certain locations on the foot can, for example, provide an impartial means for determining whether the two feet (opposite heel and toe) of the athlete were on the ground at the same time, an obligation in fast walking [31]. At present this is judged by external adjudicators who must watch the feet of the athletes without interfering with the progress of the athlete. This method is prone to personal interpretation so an impartial means such as the one provided by the pressure sensitive insole would prove invaluable to competitors and umpires alike.

The first prototype, however, was limited by virtue of the measuring protocol used in this experiment. Hard wiring limited the range of mobility of the prototype, preventing the wearer from performing routine daily activities. Thus, a different measuring protocol, such as the incorporation of wireless technology was required in further prototypes, such as prototype #2.

The use of the three PPy-PU foam sensors, integrated into an insole design of prototype #2, could be used to identify the gait of a subject, be it walking or shuffling. Parameters such as cadence and phase shift between heel and toe pressure could be determined from the sensor profiles recorded. The use of wireless transmitters and base-station



enhanced the mobility of the subject to perform the desired exercise protocol. The forces exerted by the foot against the ground are of major interest within the area of biomechanics and the availability of a wearable, wireless platform allows this assessment in a realistic setting. The sensing technique is a low-cost approach to wearable computing. While problems relating to the compatibility of the power source to the power requirements of the sensing device do exist, the main benefit of this approach is that it takes physiological measurements out of the clinical setting and into a more realistic lifestyle of the wearer.

#### 4.7 REFERENCES

1. Dittmar, A., Delhomme, G., and Roussel, P., *Biomedical Micro-sensor and Micro-systems*. REE, 1997. **8**: p. 13-22.
2. Sommer, T.J., *Ambient Assisted Living Initiative for the Ageing Population: Rationale, Opportunities, Challenges and Impact: the MST Case*. MST News, 2005. **5**: p. 6-8.
3. What is Diabetes? <http://www.diabetesireland.ie>. Last Accessed: 10 MAY 2006, (2006)
4. Pierson, A., *Put Feet First Prevent Amputations*. Irish Nurse, 2005. **7**(5): p. 33.
5. International Diabetes Federation, *Diabetes Atlas*. second edition ed. 2003.
6. Diabetes Prevalence, [http://www.who.int/ncd\\_surveillance/infobase/web/InfoBasePolicyMaker/report/s/reportViewer.aspx?UN\\_Code=372&rptCode=BCP&dm=2](http://www.who.int/ncd_surveillance/infobase/web/InfoBasePolicyMaker/report/s/reportViewer.aspx?UN_Code=372&rptCode=BCP&dm=2), Last Accessed: 10 MAY 2006, (2006)
7. Ralphs, G., Lunsford, T.R., and Greenfield, J., *Measurement of Plantar Pressure Using Fuji Prescale Film - Preliminary Study*. Journal of Prosthetics and Orthotics, 1990. **2**(2): p. 130.
8. Lemmon, D.R., Jacobs, C.R., and Cavanagh, P.R. *Finite Element Modeling of the second ray of the foot with flexor muscle loading*. in *20th Annual Meeting of the American Society of Biomechanics*. 1996. Atlanta, Georgia, USA: American Society of Biomechanics.
9. International Diabetes Federation, *Diabetes and Foot Care - Time to Act*. 2005.
10. Various, *Obesity: preventing and managing the global epidemic. Report of a WHO consultation*. World Health Organ Tech Rep Ser, 2000. **894**: p. i-xii, 1-253.
11. Number of daily steps impact obesity factors in women, <http://www.acsm.org/publications/newsreleases2004/steps050504.htm>, Last Accessed: 28 FEB 06, (2006)
12. Silicon Pressure Sensors, <http://www.cismst.de>, Last Accessed: 25 April, 2006, (2006)
13. Silicon Pressure Sensor Modules, <http://www.cismst.de>, Last Accessed: 25 April, 2006, (2006)

14. Quality in pressure distribution measurement, <http://www.novel.de/generalinfo/aboutnovel.htm>, Last Accessed: 28 FEB 06, (2006)
15. FotoScan, <http://www.precision3d.co.uk/>, Last Accessed: 28 FEB 06, (2006)
16. Foot Scanners, [http://www.ucs.si/foot\\_scanners.asp](http://www.ucs.si/foot_scanners.asp), Last Accessed: 28 FEB 06, (2006)
17. footscan Plates, <http://www.rsscscan.co.uk/>, Last Accessed: 12 MAY 2006, (2006)
18. Huang, G.T. and Herr, H.M., *Toward a Three-Dimensional Forward Model of Human Walking*, Cambridge
19. Palmer, M.L., O'Riley, P., and Herr, H.M., *Characterisation of the Human Foot/Ankle System During Normal Walking Gait*, Cambridge
20. Shelburne, K.B., Pandy, M.G., Anderson, F.C., and Torry, M.R., *Pattern of anterior cruciate ligament force in normal walking*. Journal of Biomechanics, 2004. **37**: p. 797-805.
21. Morris, M.E., Huxham, F., McGinley, J., Dodd, K., and Iansek, R., *The biomechanics and motor control gait in Parkinson disease*. Clinical Biomechanics, 2001. **16**(6): p. 459-470.
22. Kimmeskamp, S., *Heel to toe motion characteristics in Parkinson patients during free walking*. Clinical Biomechanics, 2001. **16**(9): p. 806-812.
23. Nieuwboer, A., Dom, R., De Weerd, W., Desloovere, K., Fieuws, S., and Broens-Karucsik, E., *Abnormalities of the spatiotemporal characteristics of gait at the onset of freezing in Parkinson's disease*. Mov Disord, 2001. **16**(6): p. 1066-1075.
24. Sofuwa, O., Nieuwboer, A., Desloovere, K., Willems, A.-M., Chavret, F., and Jonkers, I., *Quantitative Gait Analysis in Parkinson's Disease: Comparison With a Healthy Control Group*. Archives of Physical Medicine and Rehabilitation, 2005. **86**(5): p. 1007-1013.
25. Melnick, M.E., Radtka, S., and Piper, M., *Gait Analysis and Parkinson's Disease*. The Interdisciplinary Journal of Rehabilitation, 2002.
26. Marriott, M., *Designing a Smarter Shoes*, in *New York Times*. 2004: New York.
27. Adidas 1, <http://www.popsci.com/popsci/print/0,21553,768198,00.html>, Last Accessed: 02 March 2005, (2005)
28. the adidas 1, <http://www.adidas.com/us/ProductsModules/adidas1/adidas1.html>, Last Accessed: 02 FEB 2005, (2005)

29. Paradiso, J.A., Hsiao, K., Benbasat, A.Y., and Teegarden, Z., *Design and implementation of expressive footwear*. Ibm Systems Journal, 2000. **39**(3-4): p. 511-529.
30. Dunne, L.E., Tynan, R., O'Hare, G.M.P., Brady, S., Diamond, D., and Smyth, B. *Coarse Sensing of Upper Arm Position Using Body-Garment Interactions*. in *International Forum on Applied Wearable Computing*. 2005. Zurich: Wear it at work.
31. bAhlstrom, D., *Flashes of Brilliance: The Cutting Edge of Irish Science*. 2006, Dublin: Royal Irish Academy. 176.
32. Park, S. and Jayaraman, S., *Enhancing the Quality of Life Through Wearable Technology*. Ieee Engineering in Medicine and Biology Magazine, 2003. **22**(3): p. 41-48.
33. Holter Monitor,  
[http://heartcenter.seattlechildrens.org/what\\_to\\_expect/holter\\_monitor.asp](http://heartcenter.seattlechildrens.org/what_to_expect/holter_monitor.asp), Last Accessed: 14 FEB 06, (2006)
34. Gay, D., Levis, P., von Behren, R., Welsh, M., Brewer, E., and Culler, D., *The nesC language: A holistic approach to networked embedded systems*. Acn Sigplan Notices, 2003. **38**(5): p. 1-11.
35. MPR MIB Series Users Manual,  
[http://www.xbow.com/Support/Support\\_pdf\\_files/MPR-MIB\\_Series\\_Users\\_Manual.pdf](http://www.xbow.com/Support/Support_pdf_files/MPR-MIB_Series_Users_Manual.pdf), Last Accessed: 31 JAN 06, (2006)
36. uPart, *Integrate uPart with light, movement, temperature measurement (uPart 014xilmt)*, 2005,
37. Varta Lithium Coin Cells, <http://www.peats.com/cgi-bin/shop/db.cgi?view=1&id=1794&type=6&sid=1379897x0>, Last Accessed: 17 May 2006, (2006)
38. Bouten, C.V., Koekkoek, K.T., Verduin, M., Kodde, R., and Janssen, J.D., *A triaxial accelerometer and portable data processing unit for the assessment of daily physical activity*. IEEE Trans Biomed Eng, 1997. **44**(3): p. 136-47.

## **Chapter 5   APPLICATION OF PPY-COATED PU FOAM: BIOMIMETIC SENSING**

## 5.1 INTRODUCTION

In the previous chapter, the compressible PPy-PU foam was used to develop a prototype for monitoring plantar pressure events and pressure distribution underfoot during walking. In the applications presented within this chapter, the compressibility of the PPy-PU foam was again used to characterise a body movement, however in this chapter the sensors will be utilised to record information regarding breathing rates and limb, in particular, torso movement.

Many ubiquitous and wearable computing applications rely on the availability of context information regarding the physical state of the wearer. Indeed the availability of such information has the potential to greatly reduce the cognitive load imposed on the user and can usefully inform the operation of an ambient system. Unfortunately, many of the existing sensing technologies used to obtain this kind of data require the user to sacrifice comfort or social normalcy. Very often, for example, the user must wear constrictive apparatuses to maintain consistent sensor positioning, adhesion of sensors to the skin, or endure the discomfort of bulky, solid, protruding sensor structures. However, information related to the wearer's context can often be acquired by monitoring the physical state of the wearer indirectly – including physiological signals, movements, and body state – by integrating the appropriate sensors into a garment and deducing body actions from garment reactions [1-3].

This chapter is focused on evaluating and understanding the potential of the PPy-PU foam sensors for gathering context information in a minimally obtrusive manner: instead of monitoring changes in limb position or body length or circumference measures, information was gathered from the pre-existing dynamic physical forces that operate between the wearer's body and a garment during body movements. In the studies presented herein, the soft, washable, pliable PPy-PU pressure sensor was used to monitor dynamic pressure data from a subject. Importantly, this sensor technology can be readily embedded into a "normal" garment, retaining the structural and tactile properties of a textile structure, while at the same time, gathering data from changes in the wearer's state, which arise out of everyday movements.

### 5.1.1 Wearable sensors

As mentioned previously, (Chapter 1) in recent years the number of applications for wearable technologies has grown considerably [4]. Often these applications focus on the sensing of the human body, monitoring one or sometimes multiple parameters to describe various body functions, either to the user themselves or perhaps to a specialist who has remote access to the devices' information bank. At present many of the medical devices used for sensing and monitoring of the human body are invasive (the best sample for diagnostic testing is often blood), uncomfortable to wear or require clinical infrastructure for operation. This is often dictated by the level of precision and quality of signal required for medical analysis, as this can directly influence the clinical outcome of patient.

While the use of wearable sensors for monitoring critical health indicators is a very active area of research, the area of non-critical continuous monitoring is the focus of rapidly increasing research interest. These situations may include, for example, continuous gait analysis, heart rate monitoring or continuous measuring of breathing rates. Essentially the key-advantage these wearable sensor technologies can offer the user is device convenience; i.e. the devices or sensors integrate into the personal space of the user and do not interfere with their daily activities. The form that the sensors adopt is application dependant, but at all times it must not sacrifice the users' physical or social comfort. Communication between sensors and retrieval of information is another important consideration in wearable technology. A wired system obviously incurs maintenance and will limit the freedom of the wearer, therefore hampering the retrieval of a true reflection of the wearer's activity. The primary objective for research in this area is to combine functionality (i.e. ability to sense a useful parameter) with ease of integration into clothing, and comfort for the wearer. However, often the use of a comfortable sensor compromises the quality of signal detectable from the device. The issue is to determine whether the wearability of the sensor renders the signal unusable or whether there is a potential use for such a device?

One of the most compelling needs for wearable technology is in the continuous monitoring of the human body, be that for medical monitoring or to inform the

operation of a context -aware computerized application. While technologies that have already been made wearable (such as music players or telephones) function nearly as well (or sometimes better) in a portable or carried, non-wearable design, almost all continuous body-sensing technologies must be worn to be effective. Sensing in the wearable environment is crucial for many applications, but often existing sensor technologies pose significant wearability problems when integrated into the user's personal space. However, because of their ubiquitous, constant-wear nature, body sensors must prioritize the effects of the technology on the user's physical and social comfort. Traditional sensing technologies applied to the wearable environment are rarely designed for continuous, on-body use: those that require skin contact are generally designed to be used in a hospital or doctor's office, and those that do not, e.g. using dry contact electrodes, are generally designed for use in stationary devices. The durability of existing sensors often relies on them being robust and sturdy, e.g. a stiff material that can withstand mechanical stress. However, this idea of durability is not suitable for the wearable environment where a solid stiff device would cause discomfort. Thus, it is necessary to develop durable "soft sensors" if they are to be successfully used in wearable applications.

The research presented in this chapter investigates the ability of the modified foam sensor to be used in a continuous body-monitoring application and discusses its potential for developing an on-body monitoring sensor system.

### **5.1.2 Sensing body movement and joint angle**

Sensing of large-scale body movements is useful in many applications: for sports, medicine, device interface, and context awareness, to name a few. As such, it is a heavily-researched area. Previous approaches to wearable monitoring of body movements have been made using traditional technologies, including accelerometers [5, 6], gyroscopes [6], strain gauges [7-9], piezoelectric materials [10-12], fiber-optics [13, 14], and pressure sensors [15, 16]. Of these, textile -integration has been achieved in the cases of piezoresistive elements, strain gauges, and pressure sensors. However, most prior research into joint movements has relied on sensors either strapped to the body [5, 17, 18] adhered to the skin, or integrated into a skin-tight garment [7]. This approach



can provide a precise measure of the movement of the body itself, but as previously mentioned it imposes on the user some degree of adaptation to accommodate the device. This adaptation can take the form of physical discomfort (using a bulky, constrictive, or adhesive device), inconvenience (wearing an extra layer of clothing, donning a body-mounted device), or social discomfort (wearing a visually abnormal adornment that creates bulky discontinuity or deviates from the user's aesthetic norm).

Textile-based sensors (smart textiles) offer a solution for discomfort by retaining the characteristics of the textile, i.e. comfort and wearability, while performing as a sensor and providing information to the user. The characteristics of a textile-based sensor are flexibility, surface area, washability, stretch and texture. However, they must also include the properties required for electronic devices including durability, low power consumption, and ease of connection into a circuit. Unfortunately not all traditional sensor materials are suitable for integration into textiles. For example metallic components, designed to function in rigid environments do not make for comfortable garments and will soon break in such a high-flex environment. So the problem remains as to how to connect fabrics into electronic circuits.

Textiles coated with conducting electroactive polymers offer a potential solution to this problem, by making the fabrics themselves electroactive, without compromising the qualities of the fabrics. Indeed PPy-coated textiles have been used in previous wearable sensing applications [19-21]. These applications generally employed knitted textiles, where the material's ability to sense stretch and strain was due to increased conductivity through the material. Thus the material itself is the sensor.

It has already been shown within this thesis, that textile-like structures, such as PPy-coated PU foams, are capable of sensing changes in planar or perpendicular pressure. Mechanical testing of the material showed that the effect of a weight or force being applied to the PPy-PU foam resulted in the compression and shortening the overall length of the foam which yielded a proportional decrease in the electrical resistance measured across the foam in a linear fashion. Results from tests carried out using the Instron<sup>TM</sup> tensile testing instrument, have showed that the stress-strain profile of the uncoated PU foam sample and that of the PPy-coated PU foams sample were similar showing regions of elastic and inelastic responses to force. Hysteresis effects were

observed during the tensile testing of the foam. These effects were observed for the coated and uncoated samples, thus these were believed to originate from the PU substrate. The effect of the PPy coating was to make the entire foam conducting without compromising the soft, compressible mechanical properties of the foam substrate.

In this chapter, the performance of the modified foam based sensors for on-body sensing is examined. The sensing element is integrated into generic, “normal” torso garments: a long-sleeved woman’s t-shirt, and a close fitting t-shirt. The sensors in these shirts obtain data about the wearer indirectly; instead of attempting to merge device and body through close contact and firm attachment, the sensors record the physical forces that act on the garment as the wearer moves. By modeling the reactions of the garment, the actions of the body can be deduced. One prior study has used this technique of garment- (vs. body-) modeling, [5], but from this study no evaluation was published of the garment’s ability to monitor movements. Similar work has also been conducted using a lower-body garment to detect movement patterns [10], but this work used piezoelectric films in place of CEP sensors.

### **5.1.3 Respiration Rates**

The respiration rate is the number of breaths a person takes per minute (BPM). This parameter can be monitored in a non-invasive manner, and can be linked to a number of physiological responses such as activity rate, stress, emotional activity or indeed medical conditions such as sleep apnoea [22]. Respiratory rates of 15-20 BPM are representative of resting breathing frequency in an adult population free from respiratory disease. Conventionally respiratory rates are measured using a pneumotachograph (Fig. 5.1), which is a clinical apparatus which is used to record the rate of airflow to and from the lung. The advantage of this type of sensor is that it can yield detailed information on volume and direction of breath, but it does require a head-mounted breathing tube to be worn. Other devices such as a plethysmograph can also be used to record breathing rates by measuring volume changes around the chest to determine lung capacity. However, though sophisticated, these devices require hard-wired interconnections to external equipment and cannot be used outside a specialized clinical environment.

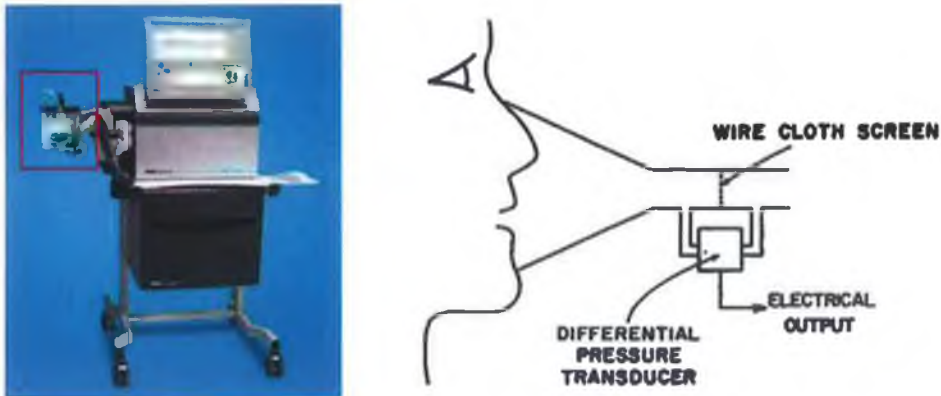


**Fig. 5.1** Photograph of a commercially available pneumotachograph from medi soft (left) and a schematic of how the device is used (right) [23].

Thus, a device which a user can comfortably wear while providing information about their breathing rates on a continuous basis would be useful.

## 5.2 BACKGROUND STUDY

Once it had been established that the PPy-PU foam sensor could respond repeatedly to compressive actions, a simple breathing harness was designed. In this prototype, the PPy-coated PU foam was incorporated into a harness to wrap around the thoracic cavity as in Fig. 5.2 .

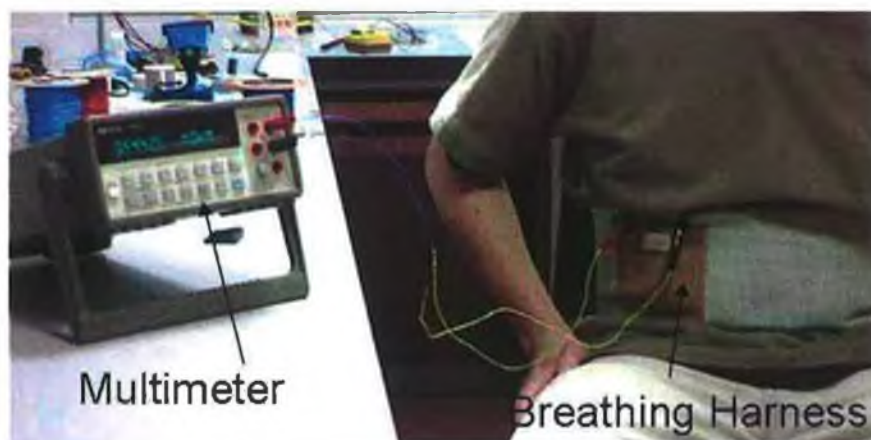


**Fig. 5.2** Photo of breathing harness and multimeter as monitoring device.

The expansion and contraction of the lungs during breathing causes the ribcage to move accordingly. This movement of the ribcage during breathing would then exert pressure on the conducting foam causing an increase in conductivity of the material. Fig. 5.3 shows a real time trace which illustrates the repeated movement of the ribcage of the subject during breathing. Initially a deep breathing pattern was observed from a standing posture that showed high amplitude and slow rate. When the subject changed to a sitting down posture and breathed normally a decrease in the amplitude of the signal with an increase in breathing rate was observed. When the subject resumed the deep breathing exercise the amplitude of the responses increased and the rate slowed down. This simple experiment illustrated that the breathing device was able to trace the rate and amplitude of breathing. Therefore, it has the potential, with optimised sensor design to be incorporated into wearable garment.

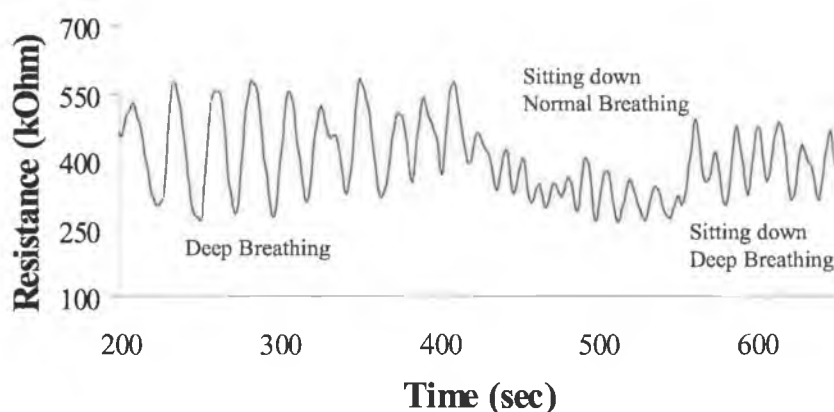


**Fig. 5.3 Real time trace of PPy coated PU foam as pressure sensor to monitor ribcage movement while breathing [24].**

However, limitations to the prototype design did exist, both in function and means of extracting information. Thus, further studies were carried out to assess the performance of a breathing monitoring using the PPy-PU foam sensor. What follows are the findings of these subsequent studies

### 5.3 EXPERIMENTAL

#### 5.3.1 Prototype #3: Hard-wired module for collection of data

##### *Torso Garment*

The test garment presented here as prototype #1 contained PPy-PU foam sensors in six locations: the top outer edge of each shoulder, the back of the neck, the superior protrusion of each scapula, and the right side rib cage under the bust (Fig. 5.4). The sensor positions were chosen to test the foam response to different physiological actions. These included breathing, shoulder movement, neck movement, and the effect of assuming a supine or a seated position on the amount of pressure exerted on the shoulder-blade.

The PPy-PU foam was prepared, as mentioned previously in Chapter 2, by repeatedly coating PU foam (PU003, source F.E. Ltd.) with PPy.NDSA. Samples of approximately 3 cm x 5 cm x 1.5 cm<sup>3</sup> were cut from this material and placed at a number of points in a custom designed garment designed by Lucy Dunne, UCD, see Fig. 5.4

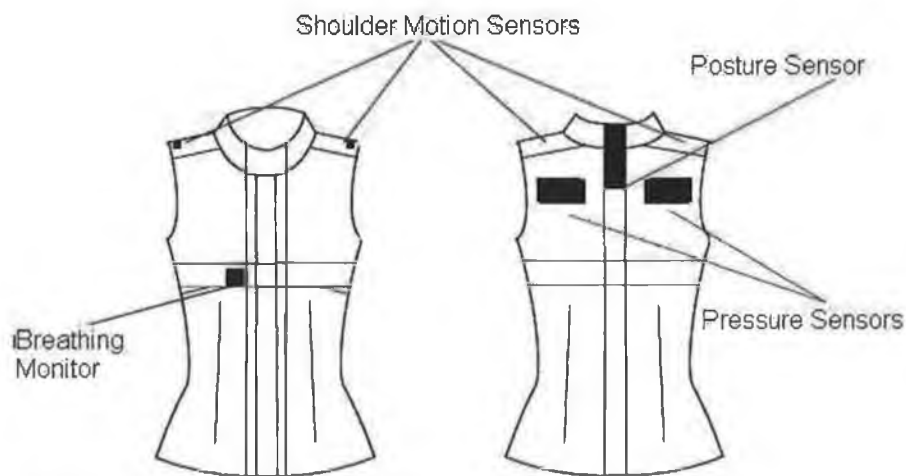


Fig. 5.4 Garment Structure and sensor layout.

The test garment was a sleeveless, collared shirt, closely fitted and non-extensile. The outer garment layer was a 100% polyester satin weave, and the inner layer was a 100% acrylic satin weave. The collar was 80% nylon, 20% elastine jersey knit. The structure of the garment was crucial to the quality of data obtained, as its textile composition, design, and fit moderated the amount of force present between the body and the sensors. In this study, the prototype garment was fitted to one test subject, to eliminate inter-subject anthropometric variation.

Sensors were sewn between the two garment layers, allowing them to be easily removed and interchanged. In each test, two wire leads were attached to the foam sensors and to a constant current digital multi-meter, as described earlier in Chapter 2, section 2.3.2. Data was collected at a rate of 3 points per second. The finished prototype garment is shown in Fig. 5.5.



**Fig. 5.5** Prototype pressure-sensitive torso garment.

### *Biomimetic Actions*

#### **Breathing**

The breathing sensor was attached on the subject's left-side rib cage, under the bust. The sensor measured  $2.75 \times 1.5 \times 0.5 \text{ cm}^3$ . Data was gathered with the subject standing, and the subject was instructed to breathe deeply for a period of approximately one minute.

#### **Shoulder Movement**

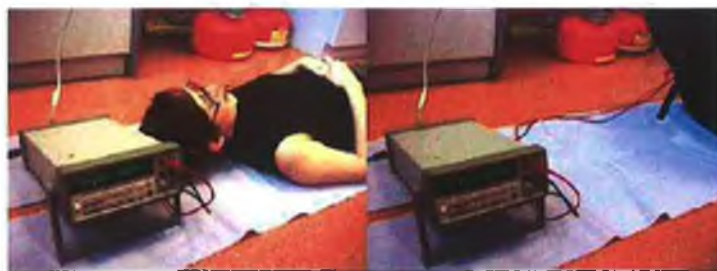
Two shoulder movement sensors were attached at the outer edge of the garment at the apex of each shoulder (above the subject's axilla). The sensors measured  $1.5 \times 2.0 \times 0.5 \text{ cm}^3$ . Data was gathered with the subject seated, and the subject was instructed to raise one shoulder repeatedly to its maximum height.

#### **Neck Movement**

The neck motion sensor was attached vertically along the subject's spine, at the back of the neck extending from 4 cm below the top of the collar (approximately 2<sup>nd</sup> vertebra) to 2.5 cm below the neckline of the garment (approximately 4<sup>th</sup> vertebra). The sensor measured  $1.5 \times 5.5 \times 0.5 \text{ cm}^3$ . Data was gathered with the subject seated, and the subject was instructed to perform four full neck extensions (backwards movement) and three full neck flexions (forward movement).

#### **Shoulder Blade Pressure**

Two pressure pads were attached, one over the superior edge of each scapula. The sensors measured  $8 \times 4 \times 0.5 \text{ cm}^3$ . Data was collected with the subject alternately supine and seated, on a hard surface.



**Supine Position      Seated Position**

**Fig. 5.6 Photo of subject wearing limb monitoring prototype, performing the supine and seated positions for should blade pressure analysis.**

The function of each sensor was to monitor pressure changes associated with body movement listed as above. For example, breathing can be monitored by placing a PPy-PU foam sensor near the thoracic cavity and observing the changes in resistance due to the pressure changes caused by the expansion and relaxation of the rib-cage or a shrugging movement can be monitored by examining changes in a sensor placed on top of the shoulder.

#### *Local Feedback Mechanism*

The change in compression of the foam can be monitored by using a simple potential divider circuit as shown in Fig. 5.7, where the change in resistance of the foam varied the amount of power going to the LED (light-emitting diode) lighting. When the PPy-PU foam was compressed the resistance across it dropped allowing more power to get to the LED which resulted in the LED being illuminated and not when the PPy-PU foam was relaxed. A photo of the finished prototype is shown in Fig. 5.8. This is a qualitative measure, very useful for simple local feedback to the wearer. Similar feedback mechanisms can include buzzers or actuators to provide sensory feedback regarding an event to the wearer.

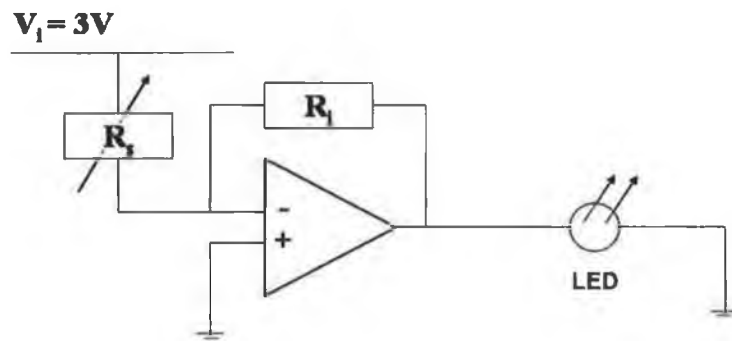


**Fig. 5.7** Electronic circuit for PPy-PU foam sensor with LED output.  $R_s$  represents a variable resistor, while  $R_f$  represents the PPy-PU foam sensor. Power for this circuit is provided by a 3V coin battery.





**Fig. 5.8** Photos of LED circuitry which was connected to the foam.

#### *Hard-wired logging of data*

In order to obtain a more quantitative study of the PPy-coated PU foam, the it was connected to a constant current multimeter, as described previously in Chapter 2, section 2.3.2. The data was collected using the associated software, HP version 1.1 at a rate of 3 Hz.

### **5.3.2 Prototype #4: Inclusion of the wireless module and validation of breathing monitoring device**

#### *Breathing Prototype Garment Development*

In previous chapters, the PPy-coated PU foam was shown to identify pressure events by a change in its measured resistance. This response has been used to develop a number of prototypes for bio-monitoring, where soft sensors are required. The breathing monitor was one such prototype. As could be seen in previous studies (Fig. 5.13), the repeated movement of the ribcage during breathing, could be traced using a PPy-PU foam sensor. The inhalation, whereby the lungs are filled, exerted pressure onto the PPy-PU foam. On exhalation, the lungs emptied and the PPy-PU foam sensor could relax. This resulted in an expected series of peaks and troughs for the PPy-PU foam sensor, corresponding to the cyclic movement of the ribcage during breathing. In comparison with, for example, the shoulder movements, whereby the movements can be unpredictable, breathing is relatively slow, it is periodic and it must happen.

Limitations of the previous breathing monitor were identified, the two most important being:

- the limit of mobility of the wearer due to the data gathering technique employed
- the validity of the data gathered from the monitoring system.

For these reasons the breathing monitor was upgraded to include a wireless transmission module to avoid situations such as those shown in Fig. 5.2 and Fig. 5.6, where the hard-wiring used to retrieve the signal from the PPy-PU foam sensors required the subject to remain within close proximity to the measuring device.

As mentioned previously many medical devices used to monitor physical functions are highly sophisticated, often requiring specialised training and clinical infrastructure. This is often dictated by the level of precision and quality of signal required for medical analysis, as this can directly influence the clinical outcome of patient. Thus, these clinical apparatuses are often the gold-standards for monitoring bodily functions. In order to validate the responses detected by the PPy-PU foam sensor, a simultaneous study was carried out using the prototype and a metabolic system to monitor the

breathing rates of a group of subjects. The results were then compared to observe whether any significant difference occurred between the two datasets.

#### *Stationary Breathing Programme*

A 20 minute breathing programme was performed with 10 randomly chosen subjects, aged  $23 \pm 3$  years. The programme was broken into 5 one-minute stages of different breathing patterns. To initiate the test subjects inhaled deeply and held their breath for 10 seconds before exhaling. Subjects then proceeded to breathe normally for 1 minute. They were then instructed to breath at a paced rate of 10 breaths per minute signalled by the Respiratory Rate (RR) value on the metabolic system's display for 1 minute. Stage three required the subjects to breathe deeply for 1 minute, while stage four required them to breathe at a rate corresponding to approximately 40 breaths per minute as indicated by RR for 1 minute. Finally for stage five, the subjects were instructed to take shallow inspirations with minimal displacement of the chest for 1 minute.

#### *Metabolic System Equipment*

For all tests, the subject was required to wear the prototype garment and a standard clinical metabolic monitor, a Vmax (229 Metabolic System, SensorMedics). All subjects were required to wear a nose clip, mouthpiece and supporting head brace (Fig. 5.9) in compliance with the Vmax for the standard measurements of breathing, which was recorded directly to PC. The sensor in the Vmax registered the starting time of each inhalation. This was used as a marker for each breath. These breaths were counted manually per stage.

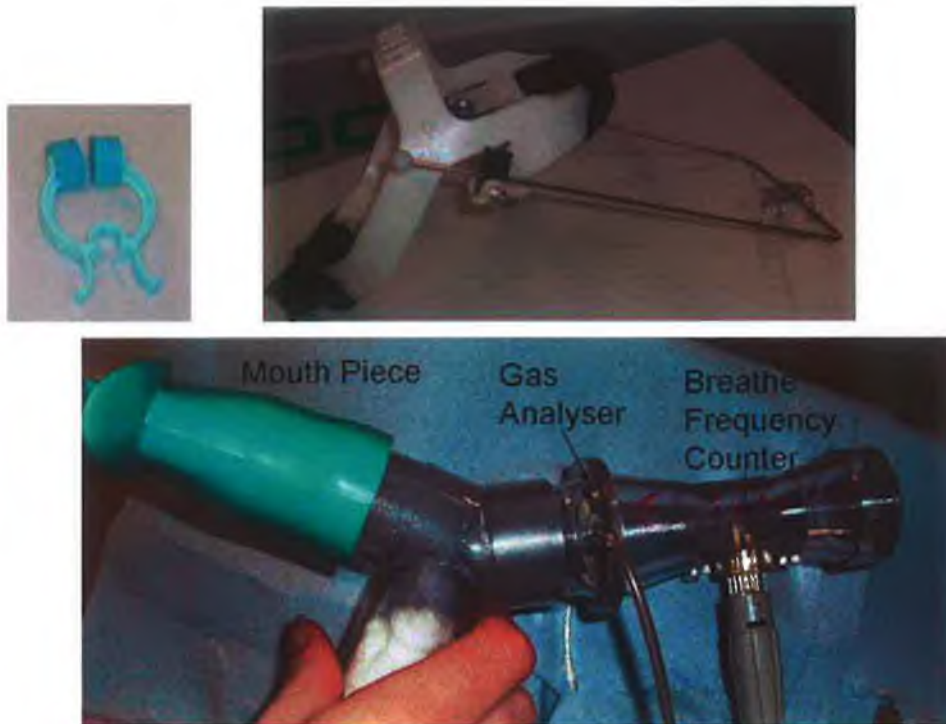
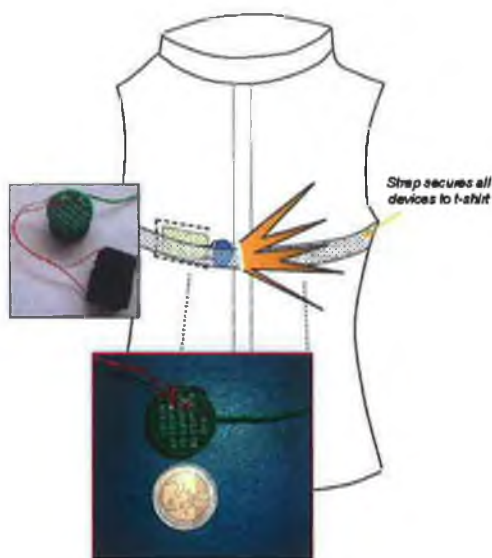


Fig. 5.9 Photo of nose clip, headgear support and mouth-piece for Vmax metabolic system.

#### *Wearable Breathing Prototype*

The prototype garment used in this study consisted of a Lycra-based t-shirt, into which the foam-based PPy sensor was integrated. The foam-based PPy sensor was sewn into a pocket on the t-shirt test garment and two wire leads were attached to the sensor. The voltage across the sensor was measured using a standard resistor bridge setup. The finished prototype is shown in Fig. 5.10. A non-extensile gross-grain ribbon strap was fastened around the rib cage of the subject, to secure a wireless mote and also maximise the response from the sensor. Retrieval of information from the foam sensors was facilitated by the use of a Crossbow Mica2Dot wireless mote platform through which the signal from the sensor were transmitted at a rate of 20 Hz to the base-station for logging and display purposes.

During respiration compression of the foam sensor resulted in an increase in conductivity through the sensor which was displayed as a peak, thus each peak was representative of a breath. Analysis of the data from the foam sensor was performed using OriginPro Software v7.5 (Silverdale Scientific, UK) to pick out and count the peaks recorded by the sensor. Comparison of the values was then performed to assess whether any statistical difference existed between the two data sets.



**Fig. 5.10** Sketch of Lycra-based t-shirt into which the PPy-PU foam was positioned. The Mica-mote was attached to the shirt.

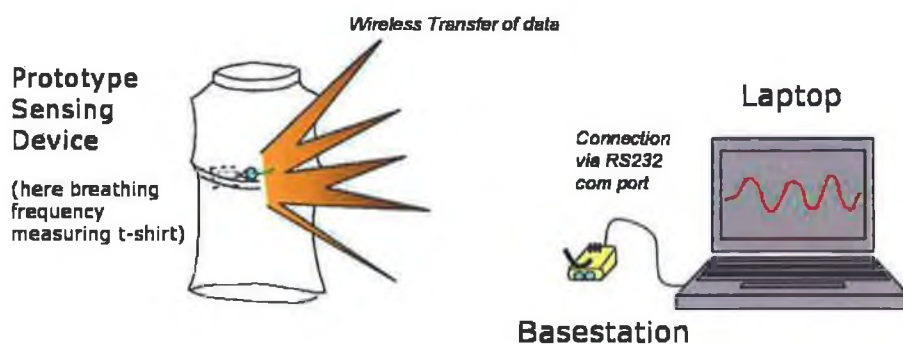


**Fig. 5.11** Cartoon depicting the transfer of information from the integrated sensing device, here a t-shirt which measures breathing frequency, to a basestation connected to a laptop for logging and display purposes.

### *Exercise programme*

An exercise programme was devised to establish what effects movement caused by exercise would have on the performance of the PPy-PU foam breathing monitor. The subject was required to wear the peripheral devices for the metabolic system and the prototype breathing monitor as for the stationary programme. The exercise programme required the subject to cycle continuously for 9 minutes; 3 minutes at intensity rates of 75, 150 & 225 Watts. These intensities were determined by the controls on the exercise bicycle used during the exercise trial.



**Fig. 5.12** Photo of subject wearing this prototype in addition to the apparatus required by the Vmax metabolic system.

## 5.4 RESULTS & DISCUSSION

### 5.4.1 Monitoring of different body movements using PPy-PU foam sensors: Prototype #3

All graphs obtained using this sensing system (Fig. 5.13 - Fig. 5.16) showed a clear change in the resistance corresponding to the pressure exerted onto the PPy-PU foam. The occurrence of these pressure events can then be correlated to the movements of the wearer to provide feedback or confirmation of their actions.

#### *Breathing*

The following graph, Fig. 5.13, shows the real-time resistance profile for the breathing sensor, located at the rib-cage.

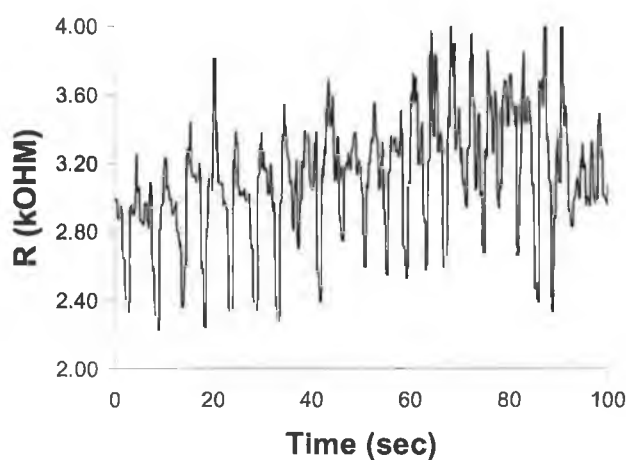


**Fig. 5.13** Resistance response of PPy-PU foam sensor to deep breathing.

As can be seen in this graph a series of maximum and minimum resistance values were recorded that appear in a repeated fashion over the course of the experiment. This cyclic response corresponded to the expected pattern for breathing since during breathing the inhalation and exhalation of air into and out of the lungs would cause pressure to be continuously exerted and then released from the PPy-PU foam. Thus,

when the subject inhaled the ribcage expanded allowing the lungs to inflate. This caused the PPy-PU foam to be compressed resulting in a drop in resistance (of approx. 20%). When the subject exhaled the lungs emptied releasing the pressure against the PPy-PU foam which resulted in the increase in measured resistance. This response was repeatable, where each trough is representative of a breath. Thus, the PPy-PU foam sensor could positively identify a series of pressure events which corresponded to breathing. However, what is also observed in this graph is drift and noise associated with the output signal. It is thought that the noise of the signal is due to the connections of the foam to the recording device, in this case, the multimeter. The porous nature of the PU foam makes difficult the task of securing robust connections to the foam. For example a wire, threaded through the PU substrate would result in a change in the response of the PPy-PU foam. Thus, the response of the PPy-PU foam sensors will have noise associated with them. However, the action of compressing and relaxing the PPy-PU foam resulted in a larger signal change from the sensor and thus could be distinguished from the noise artefacts.

#### *Shoulder Movement*

Fig. 5.14 shows the resistance changes recorded by the PPy-PU foam sensor located at the shoulder in response to shoulder raisings and lowerings. When the shoulder was raised, the PPy-PU foam was compressed and a drop (approx. 95%) in resistance was observed. When the shoulder was lowered the foam was decompressed and the resistance rose to approximately the original value. Thus, the pressure events recorded by the PPy-PU foam sensor correlated to the movement of the shoulder. Again, this response was repeatable.

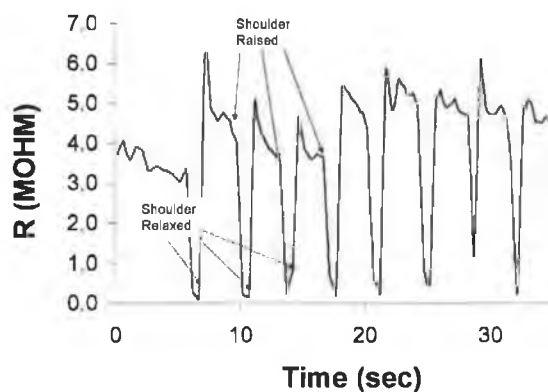


**Fig. 5.14** Resistance response to right shoulder raisings and lowerings.



### *Neck Movement*

The next graph (Fig. 5.15) showed the real time resistance profile of the sensor placed behind the neck to monitor any movement backwards, which would indicate strain on the neck. Forward movement, that is movement of the head away from the foam sensor, was also performed. Due to the design of the garment and the location of the sensor, the foam was continually under a certain amount of strain, thus this movement was also detected by the PPY-PU foam sensor. However, because the sensor was not in the direction of the pressure event, this response was less intensive and resulted in a smaller change in resistance recorded (shown to the right of Fig. 5.15). Thus, from this graph, it can be seen that the PPY-PU foam sensor located at the neck could positively identify pressure events correlating to movement of the neck. However, it is more difficult to distinguish between the types of movement this sensor is monitoring. This highlights the advantage of using multiple sensors in concert to build-up an information picture from the data gathered by these sensors.

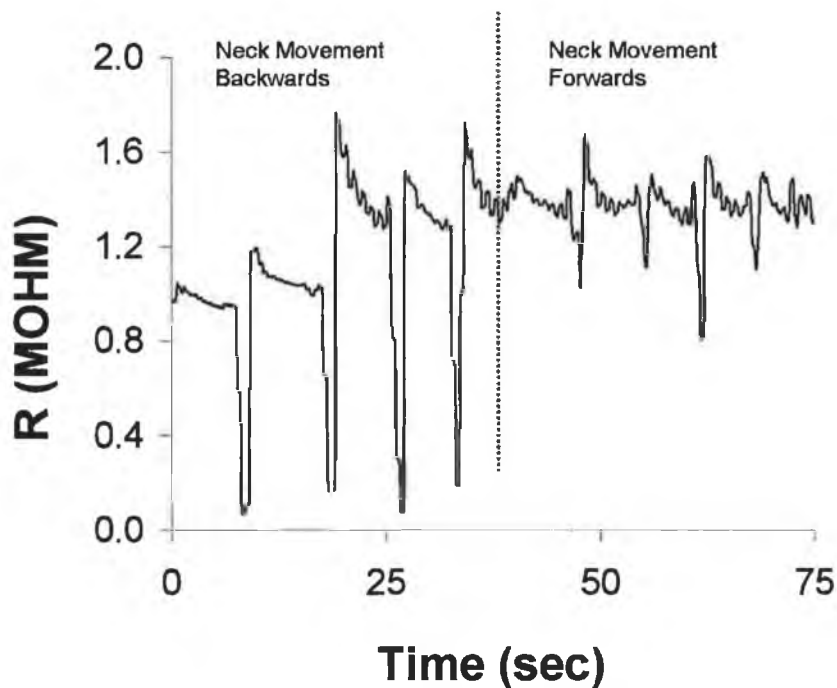


**Fig. 5.15** Resistance response to neck movement.

### *Shoulder Blade Pressure*

The following graph (Fig. 5.16) shows the real-time resistance profile of the sensor placed under the left shoulder blade. The wearer lay down in the supine position as would be normal for a patient confined to bed. Forward and sideward movements were performed to see if any changes would be observed. A steady low resistance baseline was initially observed. This corresponded to the wearer lying down, putting pressure on the shoulder blade area. This pressure monitoring is important in the area of bed-sore management, where extensive periods of high pressure result in skin ulcers as this can lead to other serious and sometimes fatal consequences. A forward and upward movement of the upper body decompressed the foam, which was indicated by the rise in the resistance observed. Rolling onto the left shoulder was indicated by a spike and a plateau of lower resistance. Rolling onto the right shoulder was indicated by a plateau of higher resistance. This was expected because the foam was decompressed but still under some strain from the garment, similar to the response by the neck sensor to forward movement of the neck in Fig. 5.15. Again, when the wearer lay down again a steady resistance reading is obtained.

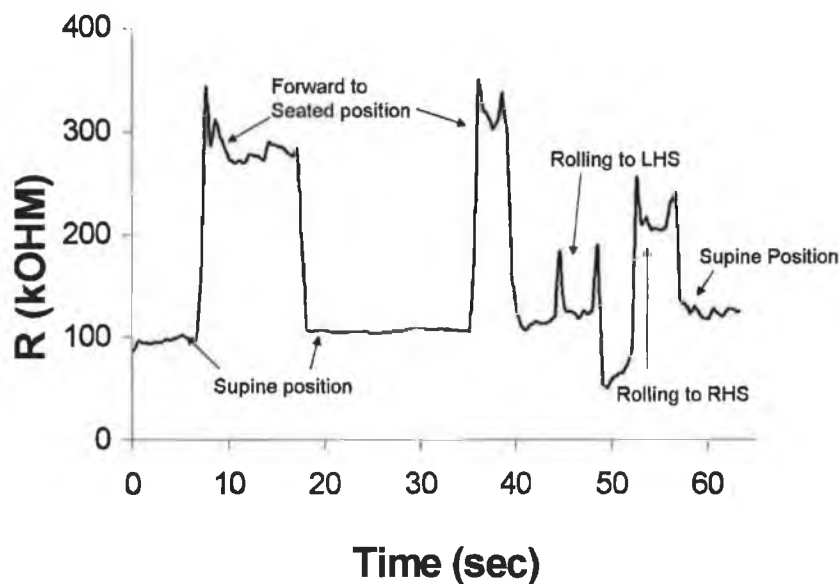


**Fig. 5.16** Resistance response to constant scapula pressure, under left shoulder blade only.

As demonstrated, pressure sensing in the wearable environment can provide useful descriptive information about the physical state of the user. Conducting electroactive polymers are attractive for sensing in a garment-integrated context because of their

ability to retain the tactile and mechanical properties of a textile-based structure. In every case during these trials, the sensors could positively identify pressure events in real-time which could be clearly correlated to the movements of the wearer. However, more investigation is necessary to determine the accuracy of the foam sensor responses, particularly the repeatability of response. In the garment integration, the foam sensors had little effect on the comfort or wearability of a standard garment.

Thus the sensors were successful in completing their tasks of monitoring pressure events associated with body movements and were also successful in their integration into the garment housing structure. However, a number of limitations were highlighted by these sensors. As mentioned previously in Chapter 2, the age of the sensor had a significant impact on the absolute resistance of the sensors. It has been shown previously that if PPy is left to open to atmosphere then there is a gradual increase in the electrical resistance due to oxidation of the polymeric backbone [25]. However, the coating itself did not delaminate from the foam substrate, even during hand-washing of the foam sensors. This indicated that if the oxidation were prevented, the sensor would be durable and washable over an indefinite period of time. Alternatively the sensors may be swapped for fresh sensors, negating the need to avoid oxidation of the PPy layer. In a garment-integrated context, washability of components is important to the preservation of normal user patterns of care and maintenance of clothing.

In the torso integration, the raw pilot test data indicated that foam sensors can provide detectable responses to all of the body signals investigated, although careful sensor placement is important to the quality of data gathered. For example, the results for the neck movements showed us that a single sensor could inform the wearer that a movement had occurred, but not what type of movement had occurred. This type of information could only be gathered if the number of sensors was to be increased and the diversity of the sensors broadened to include other technologies.

In this study, inter-subject anthropometric variation was controlled by limiting the number of subjects to one, and by custom-engineering the garment to fit that subject precisely. However, in a real-world scenario such control would not be possible, and sensor locations across a broad variety of body shapes and sizes would be hard to predict. Similar issues would arise with sizing, fit, and sensor locations on the foot.

Because of the increased number of sensors and precision of locations, this variable would become even more difficult to control, however were the number and locations of sensors increased still more to create a uniform grid of pressure sensors, the fit issue could be avoided.

As mentioned already, these sensors were susceptible to both drift and noise of the signal. Since the position and the relative resistance of the PPy-coated PU sensors are crucial to their sensitivity, calibration of the sensors would be required on a regular basis. This calibration would involve setting the baseline resistance and range of the measured resistance of the sensors as determined through a series of standard repeatable exercises by the subject. Once these parameters are set subject monitoring could be commenced.

There are many applications of wearable sensing for which this type of sensor is particularly well suited. For example, in the monitoring of high-pressure body areas for individuals with reduced tactile sensation (such as diabetics suffering from neuropathy) the foam sensor would allow pressure points to be monitored without introducing a solid sensor element into a pressurised area close to the skin that could create more irritation. Rigid sensors in such an area could easily create more irritation and exacerbate the problem, but a foam sensor not only would not create irritation, it could actually protect the body from irritants by providing an additional layer of cushioning on key pressure points.

Outside of medical applications, knowledge of the state of the body is essential in many wearable, mobile, and ubiquitous computing applications. It is common in wearable and ubiquitous computing applications for a system to make decisions based on its perception of the needs and wants of the user. A subtle, comfortable sensor that demands no attention or adaptation from the user can allow the application to function invisibly, reducing the cognitive load on the user.

#### 5.4.2 Monitoring of breathing rates using a wireless communication module: Prototype #4

##### *Monitoring different breathing styles*

The five breathing patterns used in this study were selected to represent the variety of breathing styles a person may perform during daily activities. Deep breathing and hyperventilation represented the extreme limits to breathing without causing undue discomfort to the subjects.

Fig. 5.17 - Fig. 5.22 show the normalised response as detected by the PPy-PU foam sensors for the five breathing styles; normal breathing, deep breathing, paced breathing at 10 breaths per minute, hyperventilation, shallow breathing and holding the breath for approx 30 seconds. The symbols show the response of the sensor as read by the mote 10 times per 0.5 second, while the black line represents the average point (n=10). The data was transmitted by the mote to the base station at a 20 Hz.

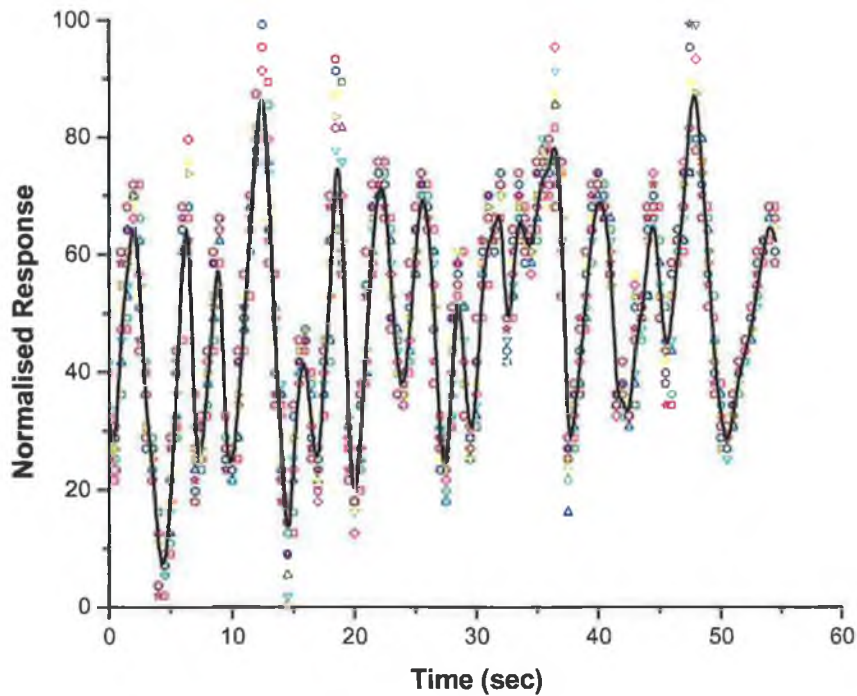
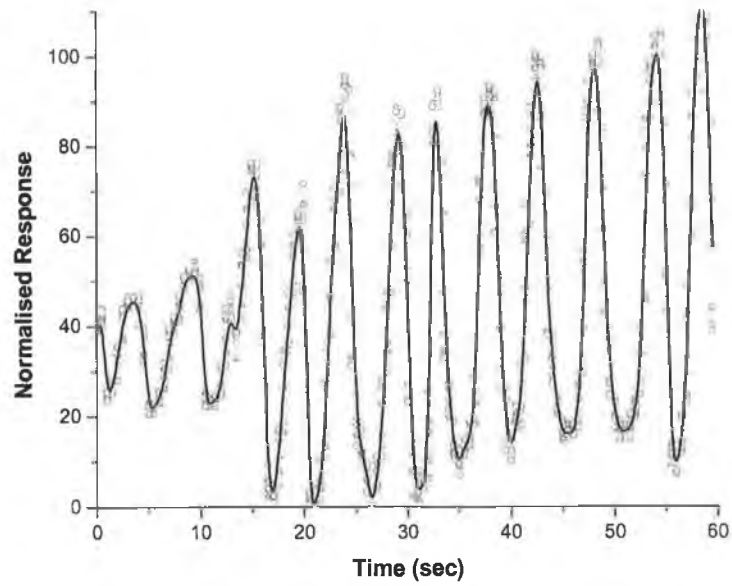
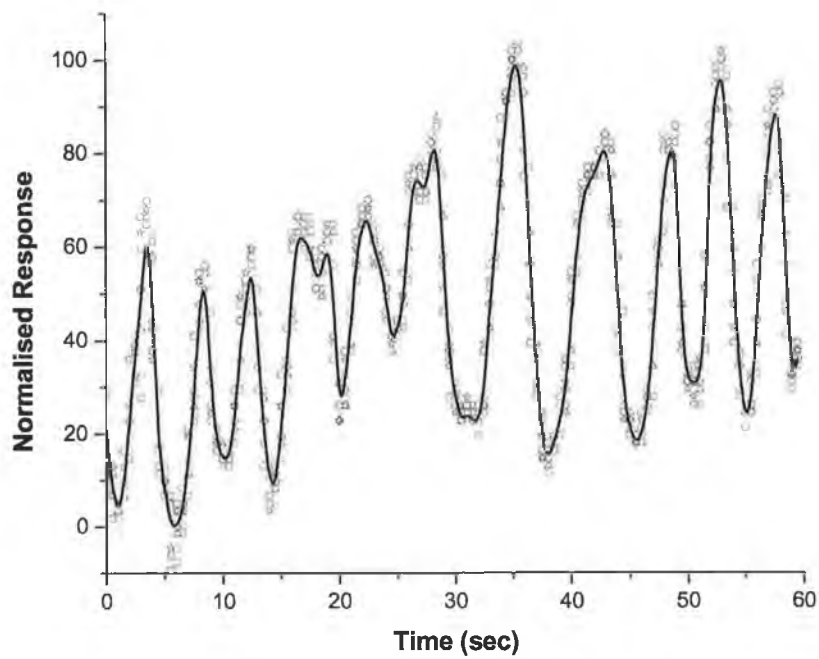


Fig. 5.17 Normalised response of the breathing sensor for normal breathing.



**Fig. 5.18** Normalised response of the breathing sensor for deep breathing.



**Fig. 5.19** Normalised response of the breathing sensor for paced breathing at 10BPM.

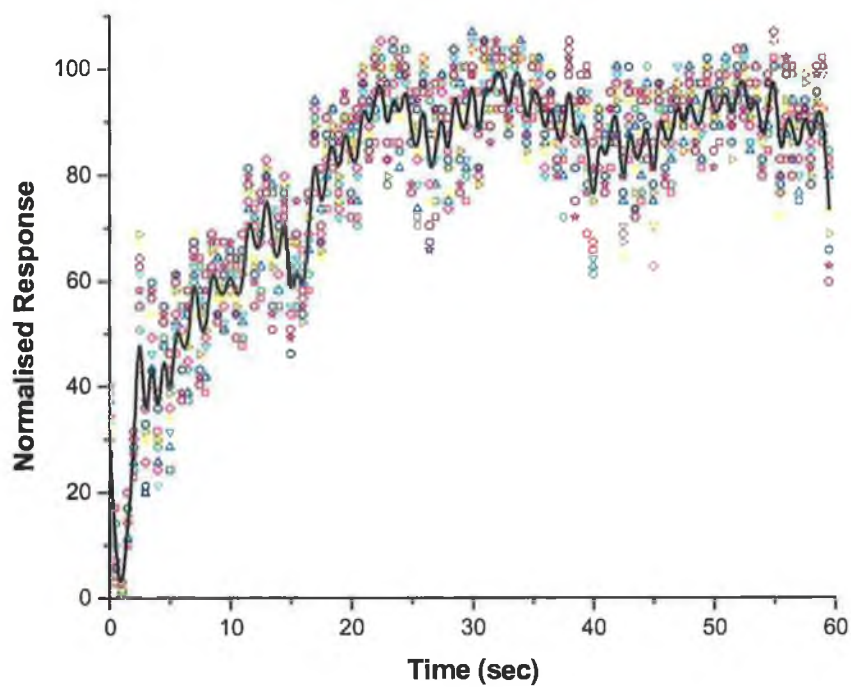


**Fig. 5.20** Normalised response of the breathing sensor for hyperventilation.

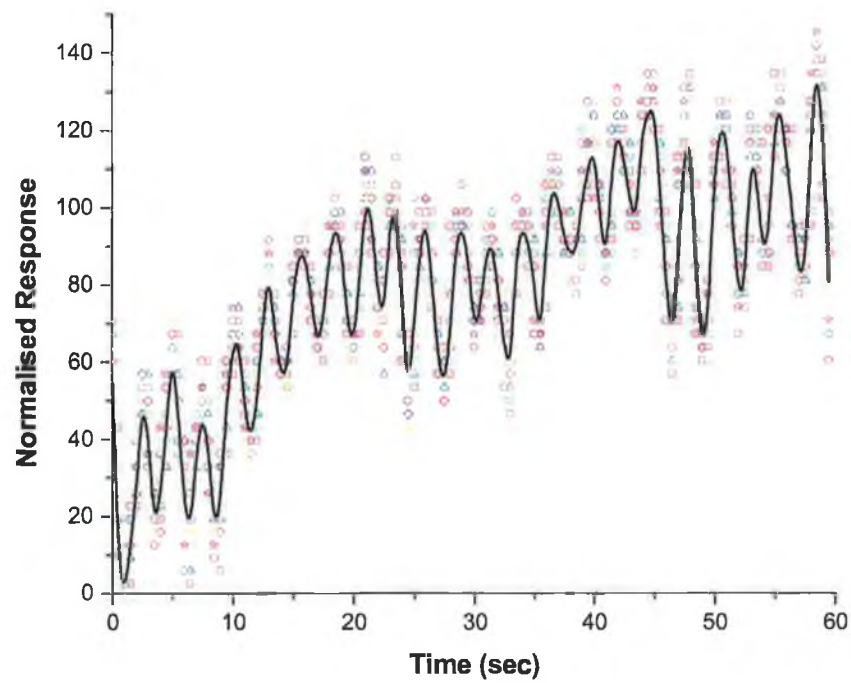


**Fig. 5.21** Normalised response of the breathing sensor for 25 seconds while the breath is being held.

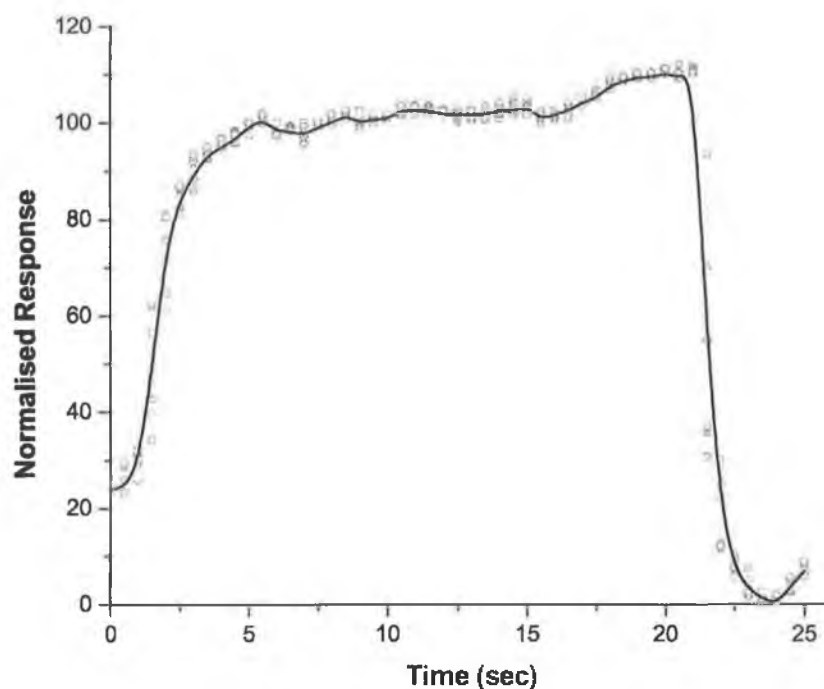


**Fig. 5.22** Normalised response of the breathing sensor for 25 seconds while the breath is being held.

As can be seen in the graphs, Fig. 5.17 - Fig. 5.21, the response from the PPy-PU foam sensor displayed a series of peaks and troughs that corresponded to the repetitive action caused during breathing. This response contrasted with the single large peak was observed in Fig. 5.22. This signified the large expansion of the lungs, as would be expected when a subject is asked to hold their breath for extended periods. From Fig. 5.22, it can be seen that the breath was held for approximately 23 seconds, at which point the lungs were emptied completely as indicated by the large decrease in the measured signal from the sensor.



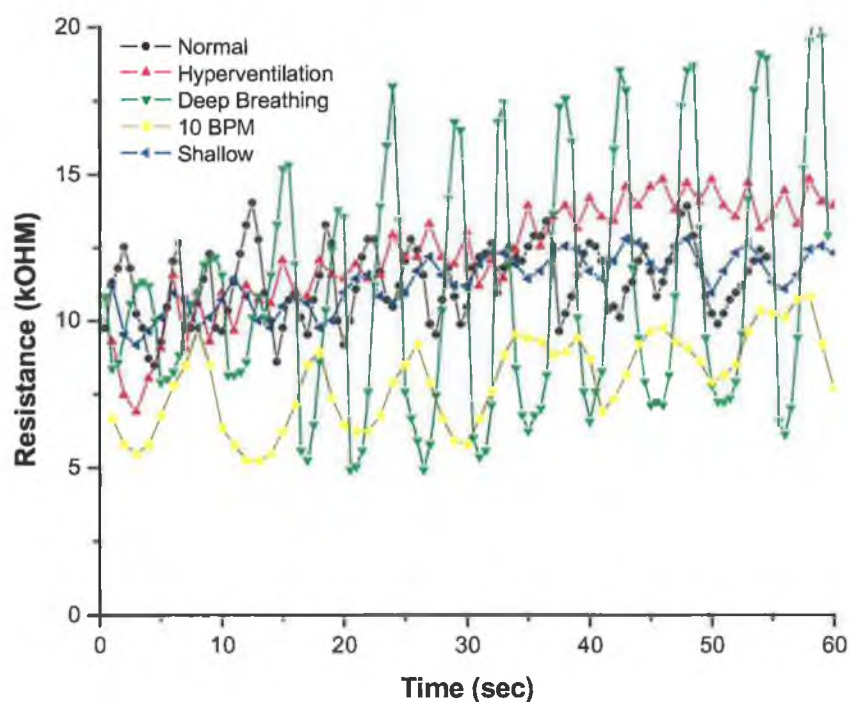


**Fig. 5.23** Average plots (n=10) for each breathing style used to assess the performance of the breathing frequency prototype monitor.

As can be seen in Fig. 5.23, the same PPy-PU foam sensor was clearly able to distinguish between these different styles of breathing and was able to register both the changes in frequency and depth of movement that occurred during testing.

When the peak counts recorded by the PPy-PU foam sensor were compared to the number of breaths registered by the metabolic system, shown graphically in Fig. 5.24, it was observed that there was no significant difference between the two datasets,  $p > 0.05$ ,  $df = 6$ . This statistical data is shown in Table 5.1. In this graph, Fig. 5.24, the height of each column represents the number of breaths recorded by the metabolic system (Vmax machine) and PPy-PU foam sensor, respectively. The error bars represent the standard deviation of both sets of data for the ten subjects.

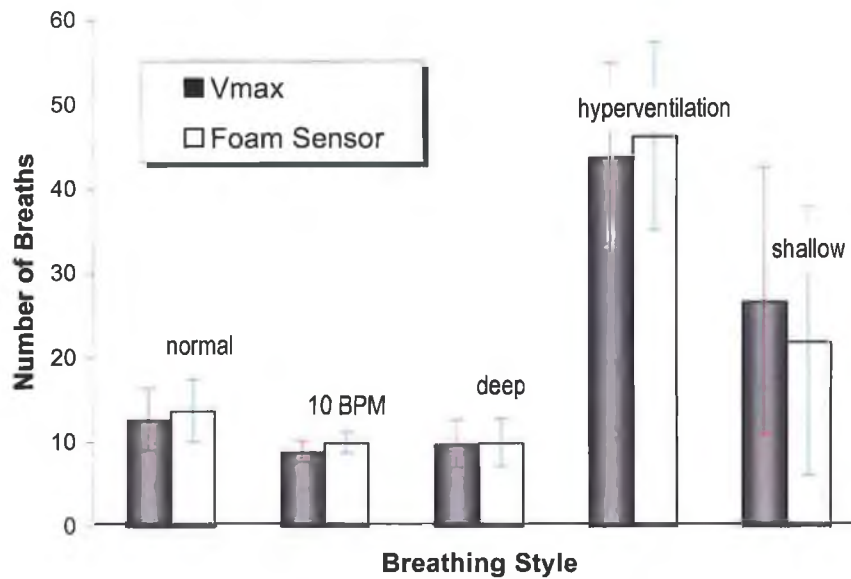


**Fig. 5.24** Comparison of peak counts from the foam sensor (column height) to the number of breaths registered by the Vmax (line) for all ten subjects. The error bars represent the standard deviation for each measurement protocol.

These results indicated that the output generated by the foam sensor was as good as the data recorded by the metabolic system and thus could yield a true reflection of the breathing activity of the wearer. The PPy-PU foam sensor was able to distinguish between the different modes of breathing. The number of breaths recorded by the PPy-PU foam sensor correlated very well with those picked up by the metabolic system, with no significant difference with 95% confidence. The statistical information for these results are listed in Table 5.1.

**Table 5.1** Statistical comparison of the data from the PPy-PU foam sensors (dataset A) and the metabolic system (dataset B) for 10 subjects.

Action	Mean A (Variance A)	Mean B (Variance B)	t	p	Significantly Different at 0.05 level?
Deep Breathing	9.5 (0.5)	9.5 (0.5)	-	-	No
Hyperventilation	43.75 (54.92)	41 (13.33)	-0.66575	0.53032	No
Shallow Breathing	25 (50)	26 (32)	0.15617	0.89024	No
Normal Breathing	14.5 (12.5)	14 (2)	-0.1857	0.86981	No
10 BPM	10 (0)	10 (0)	-	-	No
Holding Breath	1 (0)	1 (0)	-	-	No

The graph (Fig. 5.24), showed the average number of breaths recorded by all ten subjects who perform the different breathing styles for this experiment and the error bars represented the standard deviation of these measurements. It can be seen that the largest standard deviations occurred during shallow breathing and hyperventilation, both for the metabolic system and the foam system. Both of these breathing styles require minimum lung displacement, thus the foam sensor would be pushed to the limit to detect these movements. However, though the average breath counts for these two styles of breathing differed the most, it can be seen that they were still not significantly different from the number detected by the metabolic system. It was believed that the origin of this large standard error, shown in Fig. 5.24, was due to anthropometric variation, that is when each subject was asked to hyperventilate or to breath shallowly, the specific rate was not set and so what would be deemed fast or shallow for one person may not translate to the next. It can be seen that when the subjects were requested to breath at 10BPM, by watching the metabolic system, this standard error dramatically decreased.

The proto-type garment configuration used here did not appear to impede the subjects' movements during testing. Also the wireless connection afforded by the MicaMotes did not have any effect on the accuracy of the response of the foam sensor.

The use of the PPy-PU foam sensor in this configuration has been shown to successfully and reliably count the number of breaths under static conditions. Exercise was then introduced to see if the variable of body movement would have an effect on the performance of the smart shirt's ability to again count the number of breaths performed.

#### *Monitoring of breathing rates during exercise*

The subject, for the exercise experiment, was instructed to breathe normally while cycling at a constant rate of 75W. This intensity was chosen by the subject so that a constant RPM, as controlled by the cycling apparatus, could be maintained throughout the experiment. The intensity was increased twice by adding weights to the front of the bicycle. Therefore, there were three intensity ranges: 75 W, 150 W and 225 W. The subject cycled continuously for 3 minutes per intensity range

Fig. 5.25 shows the breathing profile recorded by the PPy-PU foam sensor during the first minute during the exercise programme at 75 W. Similar breathing profiles were recorded for the subsequent 8 minutes of the exercise programme. As for the non-exercise breathing experiments, data was collected at a rate of 20 Hz, which are indicated by the symbols in Fig. 5.25. The black line shows the average response for this data collected.

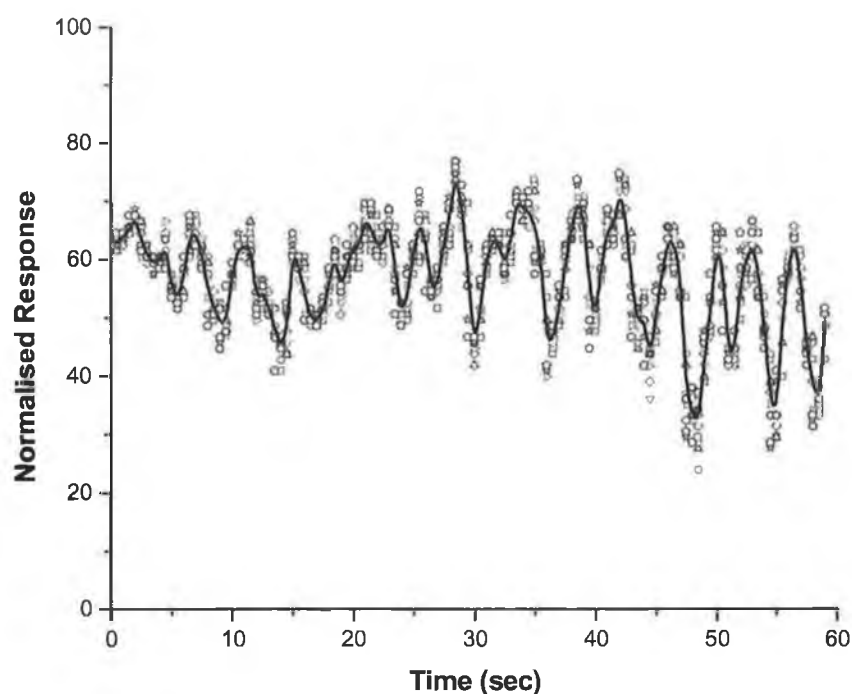


**Fig. 5.25** Normalised resistance response recorded by the base station for the first minute of exercise at 75 W.

Using the Origin software it is possible to count the number of peaks and pull information such as peak locations (x-values) and peak intensity (y-values).

During exercise the demand for energy increases, varying with the type, intensity and duration of the exercise. In most situations much of the body's ability to respond to the demand for more energy depends on the availability of oxygen. To provide this needed oxygen for aerobic energy production, the respiratory systems must respond. This response to short-term (5-10 min), light to moderate aerobic exercise has been described

in detail in physiology textbooks [26], but to summarise two characteristic changes to breathing are expected:

1. an increase in breathing rate/frequency is due to hyperpnea (increased pulmonary ventilation that matches an increased metabolic demand).
2. an increase in the tidal volume (depth of breath).

These two changes result in more air (L) being taken in per minute (minute ventilation,  $V_E$ ) to match the need of the muscle at the onset of exercise.  $V_E$  is the product result of both the breathing/respiratory rate and the tidal volume. Both tidal volume and frequency level off at a steady state that satisfies the requirements of the short aerobic activity.

In terms of the expected response for the breathing sensing system, these changes would expect to be observed as:

1. an increase in the number of peaks recorded, an indication of increased breathing rate / frequency.
2. an increase in the amplitude of the peaks, an indication of increased tidal volumes.

During the 9-minute exercise programme, both of these changes did occur. The following table, Table 5.2, summarises these features.

**Table 5.2** Summary of information recorded using the PPy-PU foam sensor.

<b>Time</b> ( $n^{\text{th}}$ minute)	<b>Intensity</b> (W)	<b>Peak Count</b>	<b>Ave.</b> <b>Peak Height</b>	<b>Std. Deviation</b> <b>Peak Height</b>	<b>%RSD</b> <b>Peak Height</b>
1	75	20	115.70	5.54	4.78
2	75	16	122.38	6.81	5.57
3	75	21	124.38	5.09	4.10
4	150	24	107.25	8.19	7.64
5	150	28	109.32	8.83	8.08
6	150	29	113.62	13.20	11.62
7	225	33	128.30	12.35	9.62
8	225	35	121.29	14.72	12.14
9	225	33	103.12	10.71	10.38

As can be seen from Table 5.2, the number of peak counts increased when the intensity of the exercise was increased from 75W to 150W to 225W. This would indicate that during the exercise programme the breathing frequency increased to match the metabolic demand of the increased exercise burden. During the exercise programme the amplitude of the peaks was also monitored. The amplitude was taken to be the difference from peak to trough of the outputted signal. These values are listed in Table 5.2 as average peak height, with the standard and % relative standard deviation also included.

As the intensity of the exercise increased from 75 W to 150 W, the recorded the amplitude of the peak decreased. This would indicate that the subject decreased the tidal volume, but increased their breathing frequency, that is took shallower breaths more frequently when the intensity of the exercise was increased. When the intensity of the exercise was increased to 225 W the number of breaths recorded was seen to increase again. The amplitude of the peak was also seen to increase. This would indicate that the subject took deeper breaths more frequently as would be expected when a subject is under aerobic stress. The exercise programme was terminated after minute 9 due to the subject becoming fatigued, however it can be seen that much information regarding the aerobic status of the subject can be obtained from using the PPy-PU foam sensor as a breathing monitor.

A comparison to the metabolic system was also carried out for the exercise programme. Table 5.3 shows the results for the statistical comparison of the two datasets. It can be seen with these values that the number of peaks counted by the PPy-PU foam sensor did not differ significantly from the number recorded by the metabolic system, even whilst exercising.

**Table 5.3** Statistical comparison of the data from the metabolic system (dataset A) and the PPy-PU foam sensors (dataset B) for 1 subject performing the exercise protocol.

Intensity (Watts)	Number of Peaks counts		Mean (Stdev)		t	p	Significantly Different at 0.05 level?
	A	B	A	B			
75	16	20	19.000 (3.606)	19.000 (2.646)	0.000	1.000	No
75	18	16					
75	23	21					
150	25	24	27.667 (2.517)	27.000 (2.646)	0.316	0.768	No
150	28	28					
150	30	29					
225	34	33	35.333 (1.527)	33.667 (1.155)	1.508	0.206	No
225	35	35					
225	37	33					

## **5.5 FURTHER STUDIES: LIMB MOVEMENT**

### **5.5.1 Synopsis**

Hitherto, the PPy-PU foam sensor has been successfully applied to monitoring biomimetic events such as breathing and plantar pressure. However, it is possible that this sensing technology can be applied to monitor biomimetic actions, such as limb (leg or arm) movement. A study was carried out [27] to track arm movements using the PPy-PU foam pressure sensors to record dynamic forces present in a worn garment structure in motion. The soft PPy-coated PU foam sensors were used in four discreet locations around the armseye, and resistance changes were recorded for all four sensors as the subject performed four arm movements. This study is explored the utility of PPy-PU foam-based sensors in the recording of body movements through garment response. The results presented though preliminary; do indicate that the responses of this sensor in these locations can adequately indicate upward, downward and forward arm positions. Further work, however would be required to model the more complex garment interaction experienced during backward arm movement, and the effect of garment structure on sensor response. This and future work will be carried out with our collaborating partners in UCD, whose focus it has been to take the information generated by the foam sensors to initiate artificial learning for automatic feedback of biomimetic movement to the wearer.

In brief, the experimental setup used four PPy-PU foam sensors integrated into a woman's cotton knit shirt. These sensors were located around the armseye to monitor the movement of the arm. Data was collected using a MicaMote at a rate of 10 Hz. The subject was instructed to move their arm to four specific locations to determine whether the responses from the PPy-PU foam sensors could distinguish between these movements.



## 5.5.2 Results & Discussion

The graphs of the average sensor resistance changes are depicted in Fig. 5.26. Note that in these graphs, a positive percent change represented a decrease in resistance. A negative percent change indicated an increase in resistance.

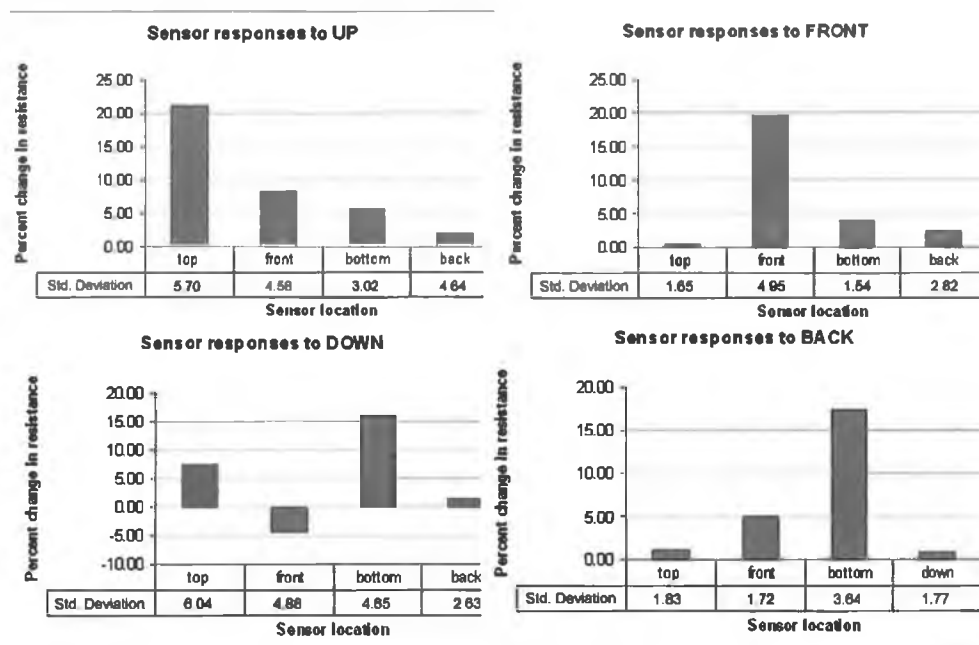


Fig. 5.26 Average sensor responses to 180 degree abduction.

As seen in Fig. 5.26, the hypothesized sensor exhibited the strongest response for the “up”, “down”, and “front” positions. The top, bottom, and front sensors respectively showed responses that were at least 8.7% stronger than any other sensor’s response. For example, in Fig. 5.26 (top right), it can be seen that the front sensor exhibited a percentage resistance change of almost 20%, compared to less than 5% for the next strongest response (for the bottom sensor). However, this was not the case with the “back” position, as seen in bottom right of Fig. 5.26. The bottom sensor in this case had the strongest response, and the back sensor (the hypothesized strongest response) had the weakest response. This response may be due to a combination of body anatomy, sensor location, and shirt construction. As the shoulder joint has significantly less range of motion to the dorsal side of the frontal plane than to the ventral, this can be

assumed to have decreased the amount of compressive force experienced by the back sensor during dorsal abduction. A further study comparing the response of the same sensors to the movements of an artificial ball-and-socket joint with a full 360 degree range of motion would be useful in evaluating the anatomical impact on sensor response. Also it may be possible that other garment constructions would result in different sensor response patterns. Thus further studies would be necessary to explore these variables. Ultimately it is envisaged that reliable movement prediction will be possible only by taking a combination of sensor readings rather than relying on a dominant response from any single sensor. In other words, it is likely that the most reliable predictions will come from understanding the characteristic responses of all 4 sensors to movement.

In future work these studies will enable the application of machine learning algorithms to predict movement from training examples that are generated from this raw data

### **5.5.3 Conclusion**

As demonstrated, soft garment-integrated pressure sensors show promise for sensing of upper arm position, especially in the more common joint directions (to the ventral side of the frontal plane). This work represented early investigation into the utility of this sensor in monitoring body movements through garment interactions. The results from this study will serve to inform future work, by identifying influencing variables that require further investigation. Specifically, further study is necessary to explore the consistency and specificity of the foam sensor, and to investigate the complicating factors of joint anatomy (range of motion), garment structure, and sensor placement. Additionally, research in the sensing of intermediate angles (other than the 0, 90, and 180 degree angles used in this study) would be of use in many wearable applications.

## 5.6 CONCLUSION

The PPy-coated PU foam which has previously been proven to be pressure sensitive has been used in a real application to monitor body movement. A number of PPy-PU foam sensors were cut and placed at strategic points on a custom-built garment. The change in compression of the foam corresponded to a movement at each sensor point. These changes in compression could be observed as changes in resistance as measured by a multimeter or the lighting of an LED, powered by a battery. Ideally the response of the foam would be channelled through an RF unit to a remote station for later data collection.

Based on these results, the PPy-coated PU foam showed considerable promise as a basic sensing technology, and for use in detecting body movements, physiological functions, and body state from body-garment interactions. Importantly, the sensor maintains the attractive structural properties of foam, consistent with the objectives of wearability, washability, and comfort in a smart garment. Integration of this kind of sensor into standard garments preserves wearability more than other forms of monitoring, but also presents more complex variables that influence the performance of the sensors, such as joint anatomy, garment construction, and sensor location. Also integration of this sensor into a wireless platform implied that the issue of interconnecting wires could be avoided. This approach successfully combined the benefits of soft textile-like sensors with the freedom of wireless sensors. These results showed that this simple system of using a single on-body sensor to obtain data about a single parameter such as breathing frequency was viable without having to compromise the users' physical activity or general comfort. Thus, the PPy-coated PU foam showed considerable promise as a sensor for medical, wearable, and ubiquitous computing applications.

Following this statistical analysis, it could be seen that there was no significant difference between the number of breaths measured by the metabolic system and the PPy-PU foam sensor, showing that this prototype can reliably detect the breath rate of the wearer both in a static position. The case-study of the exercise programme highlighted the potential of a wearable sensor for the monitoring of breathing rates during activities such as cycling.

These results highlight the possibility of integrating these sensors into other peripheral devices, such as seating or bedding to generate additional information depending on the aim of the application. Indeed results for shoulder blade pressure indicated that the PPy-PU foam sensors could be used to gather information relating to extended periods of pressure, which would be of vital importance for the care of bed-ridden patients at risk of bed-sores and ulcers. Alternatively the information could simply rely the suitability of the ergonomic design of the structures be they in the home, office or other situation such as driving, which over time could cause strain or injury to the subject. They may also be used to inadvertently track the activity of subjects, without disturbing them from their daily routine. Elderly or isolate patients may find use for such sensors, enabling them to maintain their lifestyle, while still gathering information, which maybe used to trigger a response if such a need arose.

It is our intent to generate more complex systems or on-body networks whereby information from multiple positions on the body can be brought together through the use of simple wearable sensors and a wireless communication platform.

Further study is necessary to fully understand the ability of the foam to serve as a reliable sensor over time and under the hostile conditions that garments must usually face. For instance, further work is required to understand and determine the effects of oxidation on baseline drift, the influence of variable conductance responses, calibrations of these responses and the optimal locations for sensors. In addition, processing algorithms for extraction of patterns from gathered data are required, as well as wearable and wireless hardware to allow the data to be used in real-time.

## 5.7 REFERENCES

1. Scilingo, E.P., Gemignani, A., Paradiso, R., Taccini, N., Ghelarducci, B., and De Rossi, D., *Performance evaluation of sensing fabrics for monitoring physiological and biomechanical variables*. IEEE Trans Inf Technol Biomed, 2005. **9**(3): p. 345-52.
2. Bonato, P., *Advances in wearable technology and applications in physical medicine and rehabilitation*. J Neuroengineering Rehabil, 2005. **2**(1): p. 2.
3. Paradiso, R., Loriga, G., and Taccini, N., *Wearable system for vital signs monitoring*. Stud Health Technol Inform, 2004. **108**: p. 253-9.
4. Binkley, P.F., *Predicting the Potential of Wearable Technology*. Ieee Engineering in Medicine and Biology Magazine, 2003. **22**(3): p. 23-24.
5. Farrington, J., Moore, A., Tilbury, N., Church, J., and Biemond, P. *Wearable Sensor Badge & Sensor Jacket for Context Awareness*. in *International Symposium of Wearable Computing*. 1999.
6. Seon-Woo, L. and Mase, K., *Activity and location recognition using wearable sensors*. Pervasive Computing, IEEE, 2002. **1**(3): p. 24-32.
7. Hertleer, C., Grabowska, M., Van Langenhove, L., Catrysse, M., Hermans, B., Puers, R., Kalmar, A., Van Egmond, H., and Mattys, D. *Towards a Smart Shirt*. in *Proceedings of Wearable Electronic and Smart Textiles*. 2004. Leeds, UK.
8. Scilingo, E.P., Lorussi, F., Mazzoldi, A., and De Rossi, D., *Strain-sensing fabrics for wearable kinaesthetic-like systems*. Ieee Sensors Journal, 2003. **3**(4): p. 460-467.
9. Spinks, G.M., Wallace, G.G., Liu, L., and Zhou, D., *Conducting polymers electromechanical actuators and strain sensors*. Macromolecular Symposia, 2003. **192**: p. 161-169.
10. Martin, T., Jones, M., Edmison, J., Sheikh, T., and Nakad, Z., *Modeling and simulating electronic textile applications*. Acm Sigplan Notices, 2004. **39**(7): p. 10-19.
11. Ishida, R., Yonezawa, Y., Maki, H., Ogawa, H., Ninomiya, I., Sada, K., Hamada, S., Hahn, A.W., and Caldwell, W.M., *A wearable, mobile phone-based respiration monitoring system for sleep apnea syndrome detection*. Biomed Sci Instrum, 2005. **41**: p. 289-293.
12. De Rossi, D., Carpi, F., Mazzoldi, A., Paradiso, R., Scilingo, E.P., and Tognetti, A., *Electroactive Fabrics and Wearable Biomonitoring Devices*. AUTEX Research Journal, 2003. **3**(4).

13. Akin, D. and Braden, J. *Neutral Buoyancy Technologies for Extended Performance Testing of Advanced Space Suits*. in *International Conference On Environmental Systems*. 2003. Vancouver, BC, CANAD.
14. Davies, M.L., Hamilton, C.J., Murphy, S.M., and Tighe, B.J., *Polymer membranes in clinical sensor applications: I. An overview of membrane function*. *Biomaterials*, 1992. **13**(14): p. 971-978.
15. Toney, A. *A novel method for joint sensing on a wearable computer*. in *International Symposium on Wearable Computers*. 2000. Boston.
16. Someya, T., Sekitani, T., Iba, S., Kato, Y., Kawaguchi, H., and Sakurai, T., *A large-area, flexible pressure sensor matrix with organic field-effect transistors for artificial skin applications*. *PNAS*, 2004. **101**(27): p. 9966-9970.
17. Chi, E.H., *Introducing wearable force sensors in martial arts*. *Pervasive Computing, IEEE*, 2005. **4**(3): p. 47-53.
18. Misawa, T., Kutsumi, Y., Tada, H., Kim, S.S., Nakai, T., Miyabo, S., Hamada, T., Arai, I., and Suzuki, T., *Noncontact and noninvasive microwave biological measurements*. *Journal of Cardiology*, 1990. **20**(1): p. 209-16.
19. Lorussi, F., Rocchia, W., Scilingo, E.P., Tognetti, A., and De Rossi, D., *Wearable, redundant fabric-based sensor arrays for reconstruction of body segment posture*. *Sensors Journal, IEEE*, 2004. **4**(6): p. 807-818.
20. Steele, J., Wallace, G.G., and Munro, B. *Intelligent Knee Sleeve: A valid and reliable device to combat ACL injuries*. in *Journal of Science and Medicine in Sport*. 2002. Australia.
21. De Rossi, D., Della Santa, A., and Mazzoldi, A., *Dressware: wearable hardware*. *Materials Science & Engineering C-Biomimetic and Supramolecular Systems*, 1999. **7**(1): p. 31-35.
22. Arzt, M., Young, T., Finn, L., Skatrud, J.B., and Bradley, T.D., *Association of Sleep-Disordered Breathing and the Occurrence of Stroke*. *Am J Respir Crit Care Med*, 2005. **172**(11): p. 1447-1451.
23. Rothenberg, M., *A new inverse-filtering technique for deriving the glottal air flow waveform during voicing*. *J Acoust Soc Am*, 1973. **53**(6): p. 1632-45.
24. Brady, S., Diamond, D., and Lau, K.-T., *Inherently conducting polymer modified polyurethane smart foam for pressure sensing*. *Sensors and Actuators A: Physical*, 2005. **119**(2): p. 398-404.
25. Thieblemont, J.C., Planche, M.F., Petrescu, C., Bouvier, J.M., and Bidan, G., *Stability of Chemically Synthesized Polypyrrole Films*. *Synthetic Metals*, 1993. **59**(1): p. 81-96.

26. Plowman, S.A. and Smith, D.L., *Exercise Physiology, for Health, Fitness & Performance*, San Francisco: Benjamin Cummings.
27. Dunne, L.E., Tynan, R., O'Hare, G.M.P., Brady, S., Diamond, D., and Smyth, B. *Coarse Sensing of Upper Arm Position Using Body-Garment Interactions*. in *International Forum on Applied Wearable Computing*, 2005. Zurich: Wear it at work.

## **Chapter 6    GENERAL CONCLUSION**



## 6.1 SUMMARY OF THIS THESIS

The aim of this thesis has been to investigate the interesting properties of conducting polymers, in particular polypyrrole, and to develop a sensing system using this material as the active sensing platform. Polypyrrole (PPy) by itself can be used to sense for chemical targets such as ammonia. Alternatively it can be combined into a composite, enabling an electrically conductive pathway to be formed between different sensing materials. This thesis investigated in detail the development of a wearable pressure sensing device using polypyrrole combined with polyurethane foam. The polypyrrole layer, being electroactive coated the entire polyurethane matrix, thus rendering the whole material conductive. Being conductive, it was possible to measure its resistance. It was found that if the PPy-coated PU material was compressed, the resistance of the material changed. The porous nature of the PU substrate was able to conform to these changes and could relax to its original size after compressions repeatable. The porosity of the PU also enabled air or other gaseous analytes to flow through the material which the result that a greater surface area of the PPy was exposed to the gaseous agent compared to a compact film. Thus, a sensing system was established. Throughout the research, certain aspects, outside the scope of the chemistry of the sensors, required modification, including the communication module. If the sensors could be wearable, then the communication module would also have to be wearable less the entire system would become redundant. Thus these considerations had to be met during the course of the studies. The aim of this thesis had been to present this material as one which could be used as a platform for further wearable sensors.

## 6.2 SUMMARY OF RESULTS

The PPy-coated PU foam presented in this thesis confirms the notion that textiles and other fabric-based materials can be made functional, for example to detect pressure events, without compromising the inherent properties of the material itself. The core sensing element depends on the conductivity of the conducting polymer (PPy) that was deposited on the PU substrate. If chemical analytes such as ammonia were present, then the conductivity of the PPy was altered, indicating the presence of such a reagent; if the area of PPy was increased, such as would occur if the substrate was compressed, then the conductivity of the substrate also changed to record that response.

Investigations into using different base materials were carried out during this thesis. Characterisation of coated materials, including resistance measurements, surface area estimates and SEM analysis were performed. Then integration of the PPy-PU material into working prototypes and assessment of their performance in various situations was performed. Alteration to the communication module to incorporate the wireless transmission of data led to the development of further sensing prototypes. Validation of these sensors was also performed, which showed that the data obtained using the wearable sensors were statistically indifferent results to those generated by the standard method. Thus, the foam substrate coated with PPy acted as a sensor to different stimuli.

### 6.3 COMPARISON WITH OTHER SENSING MATERIALS

This technology was simple to implement and did not compromise the handling of the material with the result that the coated substrates retained the characteristics of the original material. However, the shelf-life and stability of this material was a major limitation, as PPy is susceptible to oxygen attack which gradually decreases the conductivity of the sensor material. Alternative technologies which integrate different piezoresistive and conductive components into textiles do exist. These include carbon filled silicone rubber [1, 2] and metal-based yarns [3, 4]. Carbon filled rubbers (CFR) coated fabrics coat the textile substrates in a similar manner as CEP however CFR have been found to age much slower than CEP-textile and behave like low-pass filters with a bandwidth from dc to 8 Hz [5]. However extreme care is required when loading rubbers, such as silicone with carbons to achieve homogenous mixtures as variations in local carbon concentrations may result in regions of very high areas of conductivity (aggregations of carbon) or areas of very low conductivity. Metal-based yarns, made by twisting two steel wires around a viscose textile yarn, can be integrated into the garment using a knitting technique to achieve a conductive pathway that is insulated from the external environment [6]. However, in order to improve electrical signal quality in dynamic conditions, such as during body movements, a hydrogel membrane must be used to improve both adhesion of the electrode to the skin and to improve the signal quality output. However, the use of the membrane is limited to 5-8 hours as sweating results in swelling of the membrane [6].

#### 6.4 FUTURE WORK: DEVELOPMENT AND INTEGRATION OF CHEMO- AND BIO-SENSORS

It is unfortunate, from the wearable sensing perspective, that the best sample for on-body diagnostics is blood, as this implies that the chemo/bio-sensor must be implanted, or in direct contact with blood that is drawn to a wearable external device through a catheter or shunt sampling system. In practice, all existing chemo/bio-sensors suffer from a limited effective lifetime (at best weeks), and during this time, they must be regularly recalibrated to produce accurate results. Furthermore, direct contact with blood over extended periods of time invariably results in infection.

Other potential sample sources for wearable chemo/bio-sensors include faeces, urine, saliva, sweat, intracellular fluids, tears, and breath [7]. While some diagnostic tests have been developed for saliva, and many exist for urine, access to the sample remains a problem. The most easily accessible sample fluid is sweat, but there is limited knowledge of its diagnostic capabilities. Despite this limit, a wearable device, which utilises the diagnostic markers in sweat samples has been developed. The device, a Cystic Fibrosis 'watch-sensor'[8], is worn on the wrist in the normal manner over a region previously stimulated using pilocarpine iontophoresis to generate sweat. Sweat trapped between the base of the 'watch' and the skin is drawn into the device through a narrow flexible tube and within a few minutes comes in contact with electrochemical sensors embedded in the device which can monitor the electrolyte composition of the sweat. Sodium and chloride concentrations, which are diagnostic markers for Cystic Fibrosis (CF), are measured using this device. The benefit of this device is the reduction in testing time; testing time was reduced from half a day, to less than one hour (including the pilocarpine stimulation phase). Furthermore, the test can be performed at point of need, rather than at a specialist centre that has the complex bench-top instruments typically used for this test. In a limited clinical trial, the device successfully discriminated between CF positive and normal samples [8]. However, this device is inherently limited to short-term usage, since diagnosis of CF is a once-off activity.

While the use of wearable sensors for monitoring critical health indicators is a very active area of research, long-term use is currently beyond the current state-of-the-art technology.

The success of the CF study highlights many of the issues impeding the introduction of longer-term wearable diagnostics such as:

- Access to a sample fluid that contains diagnostic markers but does not lead to infection of the wearer during extended use, e.g. sweat test for CF diagnosis or urine for pregnancy testing.
- Calibration of the chemo/bio-sensing device – in the above case, the device initially contains a calibration solution, which is displaced by the sample. For long-term wearable chemo/bio-sensors, calibration will be a difficult issue as it implies regular access to standards.
- Stability and reliability of the sensor – chemo/bio-sensors invariably suffer from drift, as they depend on a chemo/bio-active surface whose characteristics change with time, and in many cases, malfunction or “biofouling” will happen within a relatively short period of time (typically days). This is avoided in the CF example by choosing a ‘single-shot’ application and discarding the sensor after use, a common practice in many clinical tests.

Thus, if advances are to be made into developing wearable chemo- and bio-sensors then these issues will have to be addressed. Until such time comes, we may have to rely on transducers and sensors that can detect physical events such as force and pressure.

## **6.5 ISSUES ARISING FROM THE DEVELOPMENT OF WEARABLE SENSOR TECHNOLOGY**

With the development of wearable sensors, such as the one presented in this thesis, a number of questions can arise as to the ethical issues surrounding the area of wearable sensing. The motive behind much of this research is about empowering the wearer by providing them with contextual information either regarding themselves or their immediate environment. Information is transferred from their sensors to a data-logging centre, where either they can or authorised personal, such as clinicians and physicians, may access this information. In seconds, doctors would have an instant read-out of body chemistry and general health of the sensor user / wearer. This approach is completely different from the tradition “western” method of a person looking after their health. Generally, a person tends not to change their life-style until symptoms arise and then the disease is treated. In contrast, his process of continuous self-monitoring could make the lengthy trips to the GP a thing of the past, where the patients would only require specialists’ attention when the diagnostic testing would indicate the need. However, there is the possibility that this information could be accessed by non-authorised persons. The intent of these persons may not be malicious; however, it is unnerving to think that someone might be able to access information personal and private. Situations may arise where other bodies may wish to obtain information a sensor user / wearer, for example an health insurance company may wish to know the continuous blood sugar readings of a registered diabetic or perhaps the activity or indeed the inactivity of a person classified as being obese. For both of these situations the insurance company may argue that the health status of the insurance customer, is dependent on the self-maintenance and so they may justify increasing premiums if the customers do not address these issues properly.

Thus, a situation arises as to whether knowledge is power or if ignorance is bliss.

Of course this is the users’ preference, but if these wearable sensors become more mainstream and commercially available, the public may be faced with the situation of using wearable sensors or facing premiums for not! This forcing of monitoring and self-measuring onto a user may not be financially driven. It may be socially pressed onto a

user; for example, an elderly relative who wishes to remain living independently, may have family members who are concerned with the possibility of falls or injuries which may occur. So we “ask” the elderly relative to use the wearable sensors so that we can be confident that they are safe. However, is this forcing of wearing sensors infringing on their rights to privacy?

So the choice remains; power or bliss???

Whatever the ethical issues, the science behind these wearable sensors is under constant development. New technologies are emerging, enabling detection of cancers, heart conditions to be performed in minutes. This is science. It can reveal many secrets to us. Question is, how much to you want to know?

THE END

## 6.6 REFERENCES

1. Mazzoldi, A., De Rossi, D., Lorussi, F., Scilingo, E.P., and Paradiso, R., *Smart Textiles for Wearable Motion Capture Systems*. AUTEX Research Journal, 2002. **2**(4): p. 199-2003.
2. Lorussi, F., Scilingo, E.P., Tesconi, M., Tognetti, A., and De Rossi, D., *Strain sensing fabric for hand posture and gesture monitoring*. IEEE Trans Inf Technol Biomed, 2005. **9**(3): p. 372-81.
3. Paradiso, R., Loriga, G., and Taccini, N., *Wearable system for vital signs monitoring*. Stud Health Technol Inform, 2004. **108**: p. 253-9.
4. Scilingo, E.P., Gemignani, A., Paradiso, R., Taccini, N., Ghelarducci, B., and De Rossi, D., *Performance evaluation of sensing fabrics for monitoring physiological and biomechanical variables*. IEEE Trans Inf Technol Biomed, 2005. **9**(3): p. 345-52.
5. Lorussi, F., Rocchia, W., Scilingo, E.P., Tognetti, A., and De Rossi, D., *Wearable, redundant fabric-based sensor arrays for reconstruction of body segment posture*. Sensors Journal, IEEE, 2004. **4**(6): p. 807-818.
6. Paradiso, R., Loriga, G., and Taccini, N., *A wearable health care system based on knitted integrated sensors*. IEEE Trans Inf Technol Biomed, 2005. **9**(3): p. 337-44.
7. Mitsubayashi, K., *Wearable chemical sensors and biochemical gas sensors (bio-sniffers) by a soft-mems approach*. Annales De Chimie-Science Des Materiaux, 2004. **29**(6): p. 103-114.
8. Lynch, A., Diamond, D., and Leader, M., *Point-of-need diagnosis of cystic fibrosis using a potentiometric ion-selective electrode array*. The Analyst, 2000. **125**(12): p. 2264-2267.



## APPENDIX

The following CV graphs were obtained for a series of PPy coated PU foam samples which were attached to the platinum working electrode and scanned at different scan rates in a solution of 5 mM  $\text{K}_3\text{Fe}(\text{CN})_6$  in 0.5M KCl. A potential window of 0.5 to -0.1V, together with a Ag/AgCl reference electrode and platinum spiral counter electrode were used in each experiment, which were carried out at room temperature.

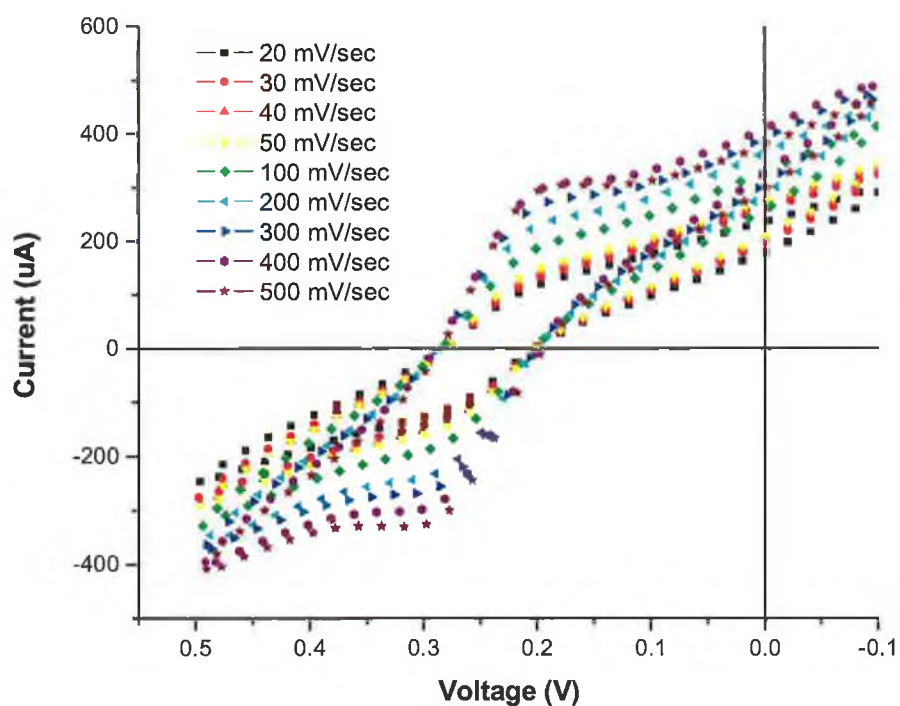


Fig. A.1 PPyNDSA deposited onto PU foam substrate and cycled at different scan rates in 0.05M  $\text{K}_3\text{Fe}(\text{CN})_6$  in 0.5M KCl

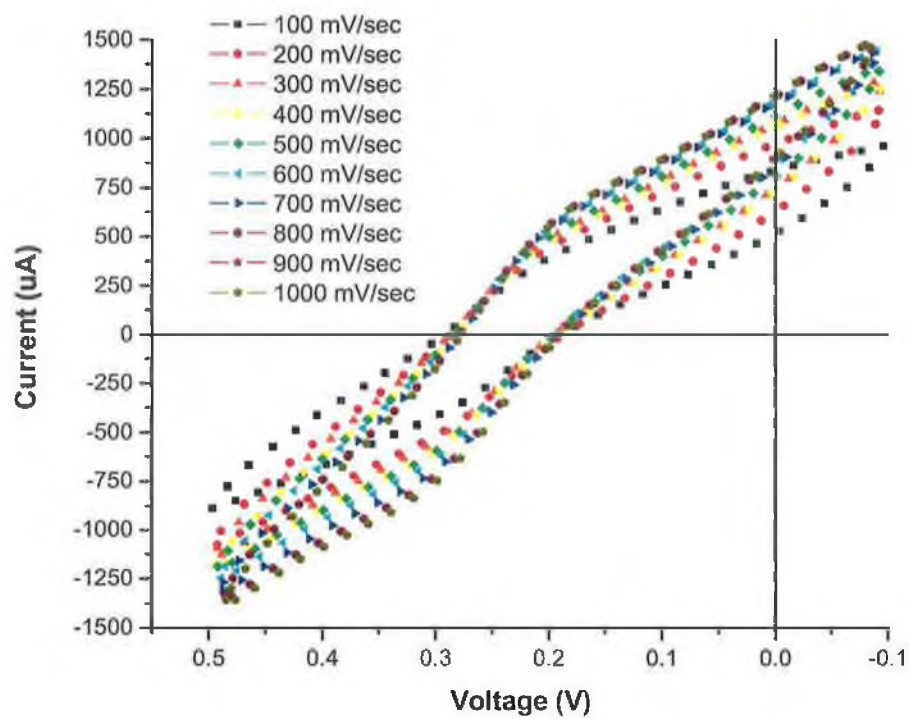
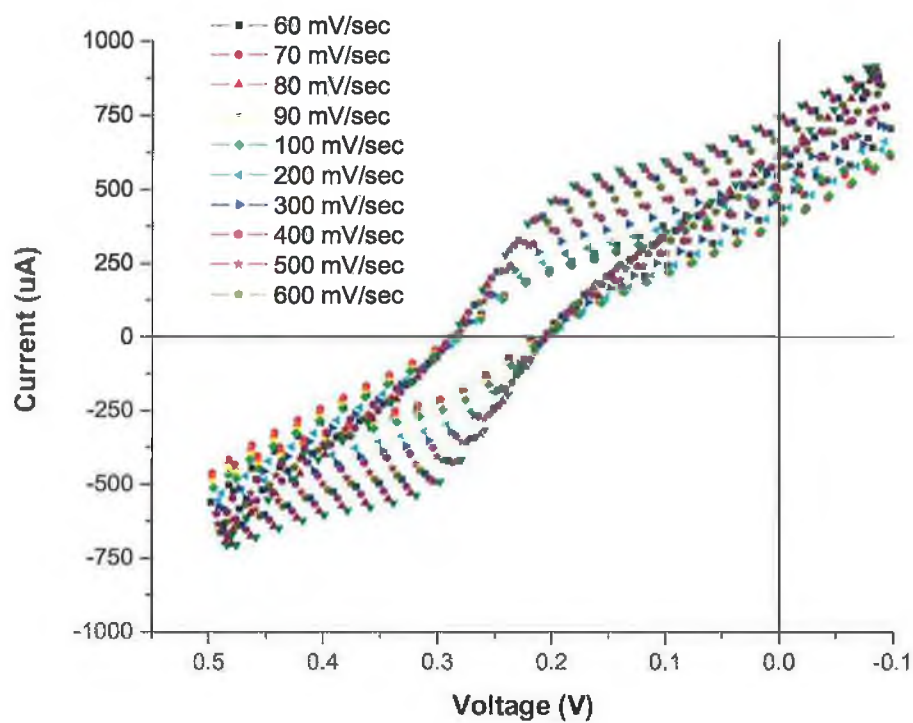


Fig. A.2 PPyNDSA x 2 deposited onto PU foam substrate and cycled at different scan rates in 0.05M  $K_3FeCN_6$  in 0.5M KCl



**Fig. A.3** PPyNDSA x 3 deposited onto PU foam substrate and cycled at different scan rates in 0.05M  $K_3FeCN_6$  in 0.5M KCl

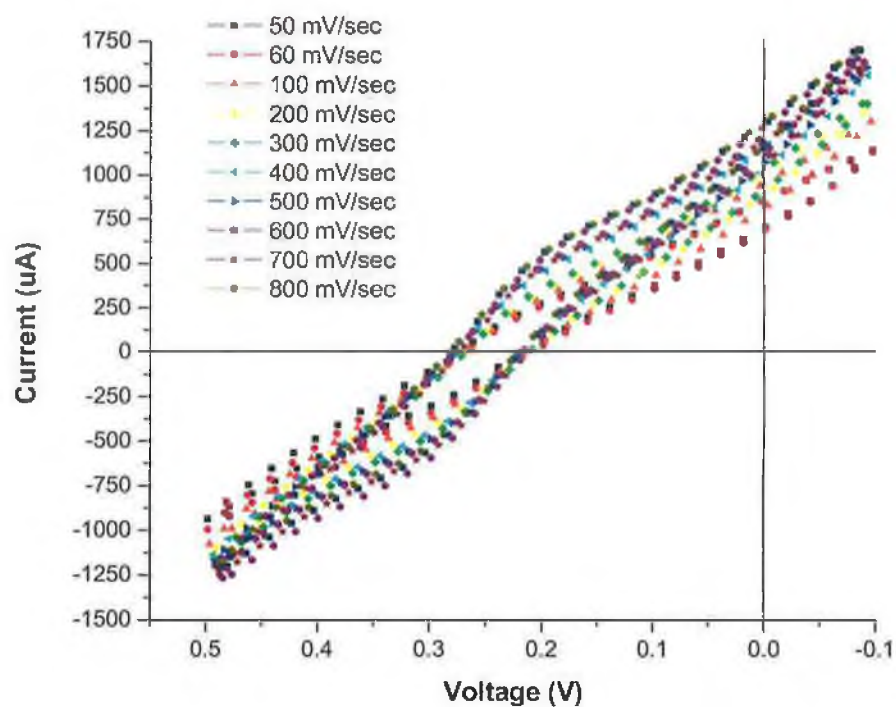


Fig. A.4 PPyNDSA x 4 deposited onto PU foam substrate and cycled at different scan rates in 0.05M  $K_3FeCN_6$  in 0.5M KCl